COMMONWEALTH OF AUSTRALIA
DEPARTMENT OF SUPPLY

AUSTRALIAN NATIONAL ANTARCTIC RESEARCH EXPEDITIONS

ANARE INTERIM REPORTS

SERIES A (IV) GLACIOLOGY

PUBLICATION No. 120

DERIVED PHYSICAL CHARACTERISTICS OF THE ANTARCTIC ICE SHEET

by

W. F. BUDD,* D. JENSSEN† and U. RADOK†

*Antarctic Division, Department of Supply
†Department of Meteorology, University of Melbourne

ISSUED BY THE ANTARCTIC DIVISION
DEPARTMENT OF SUPPLY, MELBOURNE
1971

PRINTED BY DEFENCE PRINTING ESTABLISHMENT, DEPARTMENT OF SUPPLY, BRUNSWICK, VICTORIA, 3056.

CONTENTS
(outline)

	Page
CONTENTS (outline)	i
CONTENTS (details)	ii
LIST OF MAPS	vi
LIST OF FIGURES	vii
LIST OF PROFILES	viii
LIST OF TABLES	viii
LIST OF SYMBOLS	ix
PREFACE	xii
ABSTRACT	xiv
CHAPTER 1. BACKGROUND - PURPOSE, AIMS AND PROBLEMS	1
CHAPTER 2. THE MEASUREMENTS AND DATA MAPS	6
CHAPTER 3. ICE SHEET DYNAMICS	22
CHAPTER 4. TEMPERATURE CALCULATIONS	47
CHAPTER 5. THE COMPUTER SOLUTION OF THE HEAT CONDUCTION EQUATION	90
CHAPTER 6. RESULTS OF TEMPERATURE CALCULATIONS	117
CHAPTER 7. VERTICAL PROFILES ALONG FLOWLINES	146
CHAPTER 8. FUTURE DEVELOPMENTS	166
REFERENCES	172

CONTENTS

(details)

		Page
1.	BACKGROUND-PURPOSE, AIMS AND PROBLEMS	1
	1.1. Philosophy of project	1
	1.2. Specific aims	4
2.	THE MEASUREMENTS AND DATA MAPS	6
	2.1. Traverse routes and data coverage	6
	2.2. Ice surface elevations	8
	2.3. Ice thickness	10
	2.4. Bedrock elevations	12
	2.5. Accumulation rate	15
	2.6. Ice surface mean temperatures	17
	2.7. Temperature-depth gradients near the ice surface	20
3.	ICE SHEET DYNAMICS	22
	3.1. General flow properties	22
	3.1.1 Direction of flow	22
	3.1.2 Magnitude of flow	23
	3.1.3 The flow law of ice	25
	3.2. Heat conduction equation	27
	3.3. Continuity and balance velocities	30
	3.4. Derived by-products of balance velocities	34
	3.4.1 Longitudinal strain rates	34
	3.4.2 Transverse strain rates	35
	3.4.3 Total horizontal and vertical strain rates	37
	3.4.4 Balance volume flow	39
	3.4.5 Particle paths	42
	3.4.6 Balance residence times	43
	3.4.7 The ages of the ice for balance	45
4.	TEMPERATURE CALCULATIONS	47
	4.1. Models used	47
	4.1.1 Steady-state column	49
	4.1.2 Non-deforming slab	50
	4.1.3 Constant strain rate	51

Page

4.1.4 Constant advection 51
4.1.5 Basal heating 52
4.1.6 Layer heating 53
4.1.7 Variable strain rate 55
4.1.8 Variable thermal parameters of ice 55
4.1.9 Non-steady state ice sheet 57
4.1.10 Flowline 59
4.1.11 Combined and general models 62
4.2. Additional input requirements for temperature calculations 63
4.2.1 Surface slopes 65
4.2.2 Basal shear stress 67
4.2.3 Geothermal heat flux 68
4.2.4 Basal temperature gradients 70
4.2.5 Surface temperature-elevation gradient 72
4.2.6 Surface warming rate 74
4.3. Analytical solution of heat conduction equation for simple column models 76
4.3.1 Graphical aids 79
4.3.2 Distribution of $y = \sqrt{\frac{AZ}{2\kappa}}$ 83
4.3.3 Distribution of surface advection gradient $\frac{V\alpha\lambda}{A}$ 84
4.4. Dielectric absorption 86

5. THE COMPUTER SOLUTION OF THE HEAT CONDUCTION EQUATION 90

5.1. Introduction 90
5.2. A new coordinate system 91
5.3. Vertical velocity in terms of the relative coordinate z 94
5.4. The heat equation for expanding, moving coordinates 96
5.5. Steady state computations 98
5.5.1 Finite differences 98
5.5.2 Boundary conditions 99
5.5.3 Solution of the steady state equation. Basal heating 100
5.5.4 Solution of the steady state equation. Layer heating 101
5.5.5 Output for steady states 102

Page

5.6. Transient state computations 106
5.6.1 The method 106
5.6.2 Boundary data 108
5.6.3 Lower boundary phase change 109
5.6.4 Computational stability 110
5.6.5 Additional computations 112
5.6.6 Output for transient states 114

6. RESULTS OF TEMPERATURE CALCULATIONS 117
6.1. Basal temperatures 117
6.1.1 Column model basal temperatures 118
6.1.2 Flowline model basal temperatures 120
6.1.3 High geothermal flux and melt rates 122
6.1.4 Half-balance velocities 124
6.2. Temperature-depth gradients at the surface 127
6.3. Depth of minimum temperatures 129
6.4. Mean column temperature 131
6.5. Dielectric absorption temperature 133
6.6. Total dielectric absorption 134
6.7. Partial dielectric absorption 136
6.8. Absorption per unit depth 138
6.9. Attenuation from absorption and dispersion 140
6.10. Dynamics velocity 142

7. VERTICAL PROFILES ALONG FLOWLINES 146
7.1. Particle trajectories 147
7.2. Ages of the ice 149
7.3. Isotherms 153
7.4. Temperature profiles 155
7.5. Dielectric absorptions 159
7.6. Dynamics velocity profiles 161

8. FUTURE DEVELOPMENTS 166
8.1. Up-dated versions 167
8.2. Grid coverage 167

Page

8.3. Three-dimensional treatment 168
8.4. Temperature-velocity feedback 169
8.5. Non-steady state 169
8.6. Incorporation of complex refinements 170
8.7. Use of measurements of output features 170
8.8. Use of primitive equations 171

REFERENCES 172

LIST OF MAPS

Map No.		Page
1/1	Traverse routes	6
1/2	Elevation of ice surface E m	8
1/3	Ice thickness Z km	10
1/4	Bedrock elevation b km	12
1/5	Accumulation rate A cm ice yr^{-1}	15
1/6	Temperature of ice surface θ_s $-^{o}C$	17
1/7	Observed temperature-depth gradients at the ice surface γs_{obs} $^{o}C/100$ m	20
2/1	Flowline spacing Y	22
2/2	Balance velocity V m yr^{-1}	32
2/3	Longitudinal strain rate $\dot{\varepsilon}_x$ $10^{-5}yr^{-1}$	34
2/4	Transverse strain rate $\dot{\varepsilon}_y$ $10^{-5}yr^{-1}$	36
2/5	Vertical strain rate $\dot{\varepsilon}_z$ $10^{-5}yr^{-1}$	38
2/6	Balance volume flow Φ $km^3/100$ km/yr	39
2/7	Balance residence time R 10^3yrs	44
2/8	Balance ages of the ice T 10^3yrs	46
2/1a	Flowlines used for calculations	48
3/1	Surface slope α 10^{-3}	66
3/2	Basal shear stress τ_b bars	67
3/3	Basal temperature gradient γ_b $^{o}C/100$ m	71
3/4	Surface temperature-elevation gradient λ $^{o}C/100$ m	73
3/5	Surface warming rate $S = V\alpha\lambda$ ^{o}C 10^{-3}yrs	75
3/6	Dimensionless thermal parameter $y = \sqrt{AZ/2\kappa}$	83
3/7	Surface advection gradient $\frac{V\alpha\lambda}{A}$ $^{o}C/100$ m	84
4/1a	Base temperatures for balance (column model) θ_{b_1} $-^{o}C$	118
4/1b	Basal temperatures from flowlines θ_{b_2} $-^{o}C$	121
4/1c	Basal temperature (column model, high geothermal flux) θ_{b_3} $-^{o}C$	123
4/1d	Basal temperatures (column model, ½ balance velocity) θ_{b_4} $-^{o}C$	125
4/2	Temperature-depth gradient at the surface (computed) γ_s $^{o}C/100$ m	127
4/3	Relative depth of minimum temperature $(\xi/Z)_{\theta_{min}}$	129
4/4	Mean temperature of ice column $\bar{\theta}$ $-^{o}C$	131
4/5	Dielectric absorption temperature θ_a $-^{o}C$	133
4/6	Total dielectric absorption (one-way) P dB	134
4/7	Partial dielectric absorption (0-1,000 m, one-way) $P_{1,000}$ dB	137
4/8	Absorption per unit depth (one-way) P/Z dB km^{-1}	139
4/9	Total radar signal attenuation (two-way) 2Π dB	141
4/10	Dynamics velocity (column model) V_d m yr^{-1}	143

LIST OF FIGURES

Fig. No.		Page
2.1	Variation of annual mean temperatures for several Antarctic stations	19
2.2	Temperature-depth profile in the ice at the summit of the Wilkes ice cap (Law Dome)	21
3.1	Coordinates used for shear stress in ice flowing down a slope	23
3.2	The flow law of ice (after Budd 1969)	25
3.3	Coordinates used for continuity relations	30
4.1	Coordinates used for temperature calculations	49
4.2	Effect of different model features on the temperature profile of an ice column (schematic)	53
4.3	The thermal properties of ice as functions of temperature (after Budd 1969)	56
4.4	Vertical section of an ice sheet showing parameters for flowline calculations (schematic)	59
4.5	Histograms of geothermal heat flux values over different geological regions(from Lee and Uyeda 1965)	69
4.6	Special functions associated with solutions of the heat conduction equation (after Budd 1969)	77
4.7	The function $G(y) = (\int_0^y e^{-x^2} dx)^{-1}$ used for determining the depth of the minimum temperature in the ice (after Budd 1969)	82
4.8	Dielectric absorption of ice as a function of temperature, from Westphal's measurements (after Robin et al. 1969)	86
5.1	The relation between the various parameters involved in the definition of the expanding coordinate system	92
5.2	A sample of the printout for a fixed-column temperature calculation.	103
5.3	A sample of the graphical printout for the fixed column calculation	105
5.4	A sample of the printout for a flowline calculation	115

LIST OF PROFILES

No.		Page
1	Trajectories and isochrones (Byrd flowline; Vostok - Wilkes flowline)	148
2	Trajectories and isochrones (flowline III to Mirny; flowline II to Dumont D'Urville)	150
3	Isotherms (flowline III to Mirny; flowline II to Dumont D'Urville)	152
4	Isotherms (flowline I; Byrd flowline)	154
5	Temperature-depth profiles (flowline III to Mirny; flowline I)	156
6	Trajectories, isochrones and temperature-depth profiles (Vostok-Wilkes flowline)	158
7	Temperature-relative depth profiles (Vostok-Wilkes flowline; Byrd flowline)	160
8	Dielectric absorption isolines (flowline I; flowline II to Dumont D'Urville)	162
9	Combined profiles (Vostok-Wilkes flowline)	164
10	Horizontal "dynamics velocity-depth profiles (flowline III to Mirny)	165

LIST OF TABLES

3.1	Flow law of ice used in programme computations for "dynamics velocities"	26
3.2	Total volume outflow for Antarctica	41
4.1	Geothermal heat flux	68
4.2	Graphical evaluation of temperature profiles	80
4.3	Estimation of depth of minimum temperature, from Fig. 4.6.	81

LIST OF SYMBOLS

1. LATIN ALPHABET		Introduced in section
A	Accumulation rate	2.5
a	Time component of error term	5.6.4
B	Amplitude of error term	5.6.4
b	1. Bedrock elevation	2.4
	2. Subscript "basal"	3.2
	3. Component of error term	5.6.4
C		
c	1. Thermal capacitance	3.2
	2. Subscript "coast", "computed"	3.4.6, 4.1.9.
D	Total derivative	4.1.9
d	Ordinary derivative	
E	1. Surface elevation	2.2
	2. Integral of Dawson's integral	4.3
e	Exponential function	
F	1. Dawson's integral	4.3
	2. Bedrock elevation	5.2
G	1. Subscript "Geothermal"	3.2
	2. Special integral of e^{t^2}	4.3.1
g	Gravitational acceleration	3.1
H		
h		
I	Subscript "Ice"	4.1.10
i	Arbitrary subscript (i=1,...3)	
J	Joule's equivalent	4.1.5
j	Arbitrary subscript (j=1,...3)	
K	Thermal conductivity	3.2
k		
L	Latent heat of fusion of ice	3.2
l		
M	Melt rate of ice	3.2
M	Integrated melt rate of ice	5.3
m	Subscript for "melt"	
N	Arbitrary integer	5.5,5.6
n	Index of power law for ice flow	4.1.7
O		
o		
P	Integrated dielectric absorption	4.4
p	Dielectric absorption per unit distance	4.4
Q	Internal heat production rate	4.1.8
q	Heat flux rate	4.2.4

		Introduced in section
R	Residence time	3.4.6
r	Arbitrary integer subscript	5.6.4
S	1. Surface area between flowlines	3.3
	2. Surface warming rate	4.1.5
s	1. Subscript "surface"	3.2
	2. Cross section area	5.3
T	Age of the ice	3.4.7
t	Time	3.2
U		
u	Horizontal velocity component	3.2
V	Downslope velocity	3.1.1
V	Velocity along flowline	5.
v		
W	Subscript "water"	4.1.10
w	Vertical velocity component	3.2
X	Total distance along flowline	
x	1. Distance along flowline	4.1.10
	2. Horizontal coordinate	3.
Y	Flowline spacing	3.1
y	1. Transverse coordinate	3.1
	2. Dimensionless parameter $\sqrt{\frac{AZ}{2\kappa}}$	4.3
Z	Ice thickness	
z	Height above base	3.1
ς	Relative depth ξ/Z	5.

2. GREEK ALPHABET		Introduced in section
A		
α	Surface slope	3.1
B		
β	Basal slope	4.1.10
Γ		
γ	Temperature depth gradient	3.2
Δ	1. Increment	5.
	2. Melt per unit time step	5.
δ	Basal layer increment	5.6.3
E		
ε	1. Strain ($\dot{\varepsilon}$ strain rate)	3.1
	2. Error term	5.6
Z		
ζ	Relative height above base z/Z	4.3
H		
η	Generalised viscosity	8.3
Θ		
θ	Temperature	3.1
I		
i		
K		
κ	Thermal diffusivity	3.2
Λ	Internal heating parameter	5.5.2
λ	Surface temperature elevation gradient	4.1.4
M		
μ	Generalised flow law parameter	3.1
N		
ν	Temperature index for flow law	4.1.6
Ξ		
ξ	Depth below surface Z-z	3.1.2
Π	Radar attenuation	4.4
π	Area of unit circle	
R		
ρ	Density (of ice)	3.1
Σ		
σ	Stress	3.1.2
T		
τ	Shear stress	3.1.2
T		
υ		
Φ	Total volume flow rate	3.4.4
ϕ		
X		
χ	Coordinate along flowline	5.2
Ψ		
ψ	Time stability factor	5.3
Ω		
ω	Relative vertical velocity	5.3

PREFACE

This report is mainly concerned with the temperatures in the Antarctic ice sheet, and with their consequences. The Antarctic Division's interest in this problem commenced with its collaboration with the Meteorology Department, Melbourne University during the IGY, when M. Mellor joined the Australian National Antarctic Research Expedition (ANARE) to Mawson and obtained the first extensive set of temperature-depth gradient measurements in the Antarctic. The theory of these gradients was extended by Radok and developed in collaboration with Jenssen into a series of computer studies, giving ice temperature profiles for various conditions. The results of this work were put to the test by further ANARE measurements inland of Wilkes (Casey), made early in the sixties by Budd and by A. Battye.

The problem received renewed consideration while Radok was working at the Scott Polar Research Institute, Cambridge, as a Visiting Fellow of Clare Hall in 1966. Theoretical developments by Budd and computer advances by Jenssen then led to a major combined attack on the problem. A summary of the first results was presented to the International Symposium on Antarctic Glaciological Exploration at Hanover, USA, in 1968. This meeting revealed a great interest in the many unknown physical characteristics of the Antarctic ice, and provided the incentive for continued collaboration between the Meteorology Department and the Antarctic Division, with the aim of determining the best estimates of these characteristics from all the available data.

Some preliminary results of this work have already been published, but this report presents the first full account of the project to date and gives an indication of the future programme. Its designation as "Mark I" is to indicate that updated versions may be produced, as new information becomes available. To facilitate such

updating, and also intercomparisons of the results, the principal maps are provided both in the text and as a larger-scale loose-leaf set attached to the report.

The extensive data reductions have involved a great deal of work for which we are indebted mainly to Françoise Jardel Boronkay, Jim Fletcher and Tim Jacka. We are equally appreciative of the drafting of Danka Dragosavlevic, who prepared the final version of the 36 maps, and of the typing of Susan Walker Moir. For their help, and for the support of many other members of the Meteorology Department and the Antarctic Division, we express our gratitude.

This report was published earlier as Publication No. 18 of the Meteorology Department of the University of Melbourne.

ANTARCTIC PENINSULA STATIONS

	Latitude	Longitude
DECEPTION ISLAND	62°59'S	60°34'W
STONINGTON ISLAND	68°11'S	67°00'W
ARGENTINE ISLANDS	65°15'S	64°16'W
ADELAIDE	67°46'S	68°55'W
NTINA		
IÓN"	62°59'S	60°43'W
NZA"	63°24'S	56°59'W
TE MATIENZO"	64°58'S	60°03'W
"ARTURO PRAT"	62°30'S	59°41'W
"GENERAL BERNADO O'HIGGINS"	63°19'S	57°54'W
"GABRIEL GONZALEZ VIDELA"	64°49'S	62°52'W
"PEDRO AGUIRRE CERDA"	62°56'S	60°36'W
D STATES OF AMERICA		
	64°46'S	64°05'W

ANTARCTICA

POLAR STEREOGRAPHIC PROJECTION

SCALE IN LATITUDE 71° 1:20,000,000

STATUTE MILES

100 0 100 200 300 400 500

KILOMETRES

100 0 100 200 300 400 500 600 700 800

LEGEND

- (definite)
- (approximate)
- (approximate)
- (conjectural)
- n ice, rock, in metres .2880 .3355
- ress in metres .(2190)
- station • MAWSON (AUST)
- Exposed rock
- Ice shelf and front
- Glacier
- Iceberg tongue
- Ice cliff or escarpment

Produced by the Division of National Mapping, Department of National Development, Canberra, Australia.

This map has been compiled from

ANTARC

POLAR STEREOGRAPHIC

SCALE IN LATITUDE 71°

STATUTE MILES 100 0 100 200

KILOMETRES 100 0 100 200 300 400

ANTARCTIC PENINSULA STATIONS

		Latitude	Longitude
BRITAIN			
Base B	DECEPTION ISLAND	62°59'S	60°34'W
Base E	STONINGTON ISLAND	68°11'S	67°00'W
Base F	ARGENTINE ISLANDS	65°15'S	64°16'W
Base T	ADELAIDE	67°46'S	68°55'W
ARGENTINA			
"DECEPCIÓN"		62°59'S	60°43'W
"ESPERANZA"		63°24'S	56°59'W
"TENIENTE MATIENZO"		64°58'S	60°03'W
CHILE			
Base A	"ARTURO PRAT"	62°30'S	59°41'W
Base B	"GENERAL BERNADO O'HIGGINS"	63°19'S	57°54'W
Base C	"GABRIEL GONZALEZ VIDELA"	64°49'S	62°52'W
Base D	"PEDRO AGUIRRE CERDA"	62°56'S	60°36'W
UNITED STATES OF AMERICA			
PALMER		64°46'S	64°05'W

LEGEND

Coastline (definite)
(approximate)
Contour (approximate)
(conjectural)
Height on ice, rock, in metres .2880 .3355
Ice thickness in metres (3190)

Exposed rock
Ice shelf and front
Glacier
Iceberg tongue

Produced by the Department Can

This map

ABSTRACT

A summary is presented of the results to date of a project aimed at calculating various unknown physical characteristics of the Antarctic Ice Sheet as a whole, from the data available. These characteristics include the temperature and velocity distributions, the age of the ice, the particle paths and patterns of flow, and the state of balance. The data used and the computed results are presented by a series of 36 plan maps of the Antarctic and a selection of vertical profiles along flowlines.

The velocity and temperature of the ice sheet are related through the flow law of ice. However, none of these three are well known for the Antarctic. Hence the first approach has been to examine the consequences of assuming the ice sheet is in a steady state with zero net balance.

The data includes measurements of the ice surface elevation, ice thickness, ice accumulation rate, and surface mean temperature.

The large scale dynamics and thermodynamics of ice sheets are discussed and procedures are given to determine first the balance velocity from continuity, then the temperature distribution from the heat conduction equation, and finally a "dynamics" velocity from the flow law, as a check on the assumed balance velocity. A number of results are determined directly from the balance velocities such as strain rates, particle paths, ages, residence times, and volume outflow.

The solution of the heat conduction equation is examined for a number of different models, approximating the Antarctic ice sheet to varying degrees of complexity. The two major models represent the solution for a vertical column and for a two-dimensional flowline section. The inputs for these require the heat flux at the lower boundary, which involves geothermal heat flux and frictional heating. Maps are therefore also presented of basal shear stress, and the calculated basal temperature gradient.

At the upper boundary the column warms as it moves outwards to the coast. Maps of this warming are given, along with other aids to allow quick approximate graphical computations of the temperature profiles.

The computer solutions of the heat conduction equations for both major models are explained in detail, and examples are presented of the computer's numerical output.

The output is examined for a number of complete coverages of the Antarctic with 300 fixed columns, using a range of different input data. The basal temperatures are compared with the output of the main coverage from 53 flowlines, for the "balance" input. The variation of the base temperatures and melt rates with the unknown input values of geothermal flux and the state of balance is examined.

Many by-products from the temperature profiles are mapped, such as: surface temperature-depth gradients, the depth of the minimum temperature, mean temperature of the column, dielectric absorption and radar attenuation, and the dynamics velocity.

A number of 2-dimensional sections along the flowlines are presented to show particle paths and ages (isochrones), isotherms, temperature-depth profiles, dielectric iso-absorption lines, and dynamics velocity profiles. These dynamics velocities show a reasonable agreement with the input balance velocities in form, but with some anomalies and somewhat lower magnitudes. The lower magnitudes support the conjecture of a positive mass budget for the Antarctic.

Finally an outline is given of the proposed updating of the present output, and of future programs which aim at providing improved output from more sophisticated calculations, based on a three dimensional grid system. A major aim of the future program is to relax the assumption of steady state, to follow the response of the ice sheet to long-term changes in the input data.

DERIVED PHYSICAL CHARACTERISTICS OF THE ANTARCTIC ICE SHEET

W. F. Budd, D. Jenssen and U. Radok

1. BACKGROUND - PURPOSE, AIMS AND PROBLEMS.

1.1. Philosophy of project.

One of the greatest problems of present-day analysis is to determine readily the most important implications of the ever increasing amount of measurement data. We must regard as a major capital investment the development of techniques for the rapid absorption of the data and the production of answers to specific questions about their implications. This allows the present status of the measurements to be readily assessed, and points the way to the most important measurements for the future.

Very little data was available for the physical characteristics of the Antarctic ice sheet prior to the IGY. Following this period of intensive measurements however there soon appeared for the first time a number of maps, although still partly blank, of valuable essential information: ice surface elevation, ice thickness, surface mean temperature, and accumulation rate, cf. Wexler et al., Eds.(1962), Bentley et al.(1964) and Odishaw, Ed.(1964). At that stage the data was still too sparse to determine any of the more complex implications of the measurements for the Antarctic ice sheet as a whole. Further traverses have since then provided additional information allowing reasonably complete data maps for the whole of the Antarctic to be constructed without resort to too drastic interpolation. The comprehensive Soviet Atlas of the Antarctic (Bakayev Ed. 1966) presents a valuable collection of these complete data maps to that stage. Over the same period advances have been made in computer technology which allow the absorption and analysis of this data on a scale compatible with the density of the measurements and in a reasonable time.

The analysis of ice temperatures by computer has progressed from the study of single vertical profiles (Jenssen and Radok 1961) and flow lines (Jenssen and Radok 1963) to the systematic exploration of solution

fields (Radok, Jenssen and Budd 1970) and a broad-scale flow line coverage of all of Antarctica with the simplest ice sheet model (Budd, Jenssen and Radok 1970). Theoretical investigations of the dynamics and thermodynamics of ice masses (Budd 1969) have reached the stage of successfully interpreting isolated key observations,such as the deep borehole measurements at Camp Century, Greenland (Weertman 1968) and Byrd station, Antarctica (Gow, Ueda and Garfield 1968) in terms of glaciological regime parameters (Budd et al., to be published). Thus it appears well worthwhile to attempt an analysis of all available data for the Antarctic ice sheet as a whole, even though there remain large gaps in the data coverage.

The questions raised concerning the Antarctic ice sheet include:
How much ice is there, and how is it distributed?
What is happening to it at present - is the ice sheet growing or shrinking?
What is the history and age distribution of the ice?
How did the changes in the ice sheet come about, and what were the associated changes in climate?

In order to answer these general questions we need to know the surface elevation, ice thickness and surface temperature of the ice, and the accumulation rate, plus the complete velocity distribution of the ice. To calculate the velocity distribution from the flow law of ice we need the stress and temperature distributions. Now the temperature distribution is in general time-dependent,which means that the history of the ice sheet must be known. Hence we require not only data for the existing ice sheet, but for the whole period of its history. This argument shows that it is impossible to answer the general questions from the present data. However it also highlights the point that with sufficient measured surface velocities it may become possible to determine the ice flow law with such precision,that by a combined process the temperature distribution can be calculated together with the velocity distribution. The history of change could then be studied from prescribed input data of climate,i.e. accumulation and surface temperature distributions as a function of time.

Alternatively an initial attack on the problem can be based on a special simplified model of the Antarctic ice sheet,providing a first set of results for comparison with reality. Then, provided the simplification has

not caused departures from reality in the calculated values to be too drastic, these departures may serve to show how much the hypothesised simplification departs from reality, and thus provide a guide to improved models.

This is the procedure adopted here. We shall examine the special case of a steady-state ice cap (leaving all data constant with time) with a steady-state temperature distribution. From this assumption and the available data we calculate the velocities for balance from mass continuity considerations. We then calculate the temperature distribution from the heat conduction equation, and finally examine this in terms of other data, such as measurements of velocity, the flow law of ice, and isolated observed temperature profiles.

This may be regarded as the first phase or "Mark I" of a comprehensive project on the Antarctic ice sheet. This first phase has been completed and is summarised in this report. A corresponding study for the Greenland ice sheet is under way.

With incomplete data one faces a large range of possible implications, worth considering, which follow from the various assumptions made about the unknown elements. This imposes the need for judicious selection of those implications for study which on present evidence seem most likely to lead nearest to reality. However the range of variation of the implications is also of interest and suggests consideration of an appropriate range of the unknown features. This leads to vast quantities of output, and again it is necessary to select just a few of the most important results, to illustrate the possible range of variation to be expected.

The aim here has been to present typical examples of the output obtained, in order to indicate the power of the techniques and the scope of the study. Many questions similar to those specifically answered here could be answered by other additional diagrams. Such questions will be discussed later. It is hoped this work will provide food for further thought about the purpose of the Antarctic measurements and the most important specific answers being sought.

1.2. Specific aims.

Starting with the basic assumption of a balanced ice cap in steady state we wish to determine a wide range of derived physical properties of such an ice sheet which will enable this assumption to be tested by many simple independent measurements.

Thus measurements of the surface velocity over the ice cap provide a direct check of the assumed velocity distribution, once borehole or other data has enabled the velocity profile, or average with depth, to be calculated. In the interior regions, where velocity measurements may be difficult to obtain because of their small magnitudes, "flux divergence calculations" (cf. Mellor 1968) together with direct measurements of strain rate provide a check on the balance and a determination of the elevation change with time.

It will be shown in section 4.1.9 that more sophisticated calculations allow measured temperature profiles to be used to interpret the present state of balance and history of the ice sheet more completely. Even the measurements of temperature in the top few hundred metres of the ice cap provide a valuable guide as to the present state of change.

Calculated age-depth relations can be checked by age determinations with the down-hole sampling techniques described by Oeschger et al (1967). Steady state particle paths and past accumulation rates can be checked by stable isotope analyses of the ice cores, cf. Lorius (1968) and Dansgaard and Johnsen (1969).

Once sufficient data of this kind have been obtained, to enable estimates to be made of how the accumulation and temperature have changed with time, it will become possible to use a more precise assumption than that of steady state for the input to the numerical ice sheet model. In the meantime we shall examine the consequences of the steady state assumption.

Our main objectives will be to determine the velocity and temperature distributions throughout the ice and their derivatives. From the velocity we can obtain the strain rates, the volume or mass flow, the particle paths, the ages of the ice and its residence time in the ice sheet. From the temperatures we can obtain the temperature gradients, the basal temperatures and

melt rates, the dielectric properties and the flow parameters of the ice. Many other general properties are derived as by-products of the above general task.

The following sections indicate the course of the calculations, but first we examine the available data required for the input.

2. THE MEASUREMENTS AND DATA MAPS.

2.1. Traverse routes and data coverage.

The routes of the major Antarctic traverses which have collected the basic data of ice surface elevation, ice thickness, surface temperature, and accumulation rate are indicated in Map (1/1).

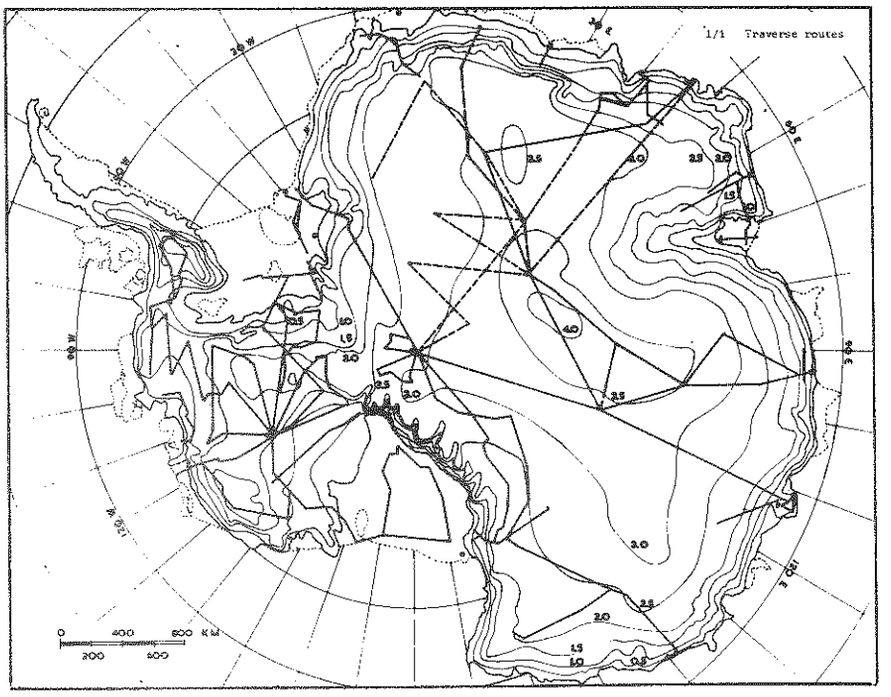

Map 1/1. Traverse routes.

The major Antarctic traverse lines to date up to 1970 are shown. Typically data on ice elevation, thickness, accumulation rate, and surface mean temperature have been obtained along these routes. The dotted lines indicate the more recent traverses for which all the data was not available at the commencement of this project.

The full lines represent the earlier traverses for which the data were available at the commencement of this project, while the broken lines indicate the more recent traverses for which some of the data was still unpublished. The coarseness of the spacing of the traverse lines gives some idea of the extent of extrapolation required for a complete coverage.

The largest gaps are about 1,000 km and exist in the regions of Wilkes Land and inland of the Lambert Glacier basin (for place names see frontispiece Map). In addition to the major traverse lines indicated here a number of aerial reconnaissance flights have provided additional data on ice surface elevations, which have allowed the detailed elevation contours to be extended to regions not covered by the traverses.

Since the ice surface topography is to some extent related to the bed topography, the ice thickness and bedrock structure have been extrapolated following surface trends. This is expected to be satisfactory for major large-scale variations, although the minor variations will all be smoothed over. The other two parameters, surface temperature and accumulation rate, seem to have more gradual large-scale variations which are also closely related to the large scale topography and geographical location. So again the broad scale extrapolation is expected to be satisfactory for the present study.

The major aims of current Antarctic field programmes is to fill in the large gaps in the present data, and as the new results become available, updated versions of both input data and output calculations will become possible. At the moment the coverage of West Antarctica is reasonably adequate for the coarse resolution of the present study, whereas by comparison the results for East Antarctica can only be expected to be accurate in the regions where data exist, and to be speculative in the others.

With this basic data coverage the aim of the present project is to obtain large scale regional variations and so for the present we consider regional averages smoothed over about 100 to 200 km. Variations on a smaller scale than this have been ignored. In particular, the high variations occurring as the coast and mountain regions are approached are avoided here by ceasing calculations when the ice thickness becomes less than 500 m.

2.2. Ice surface elevations.

The elevation contours used in this project are shown in Map (1.2). This is taken from the frontispiece, a 1:20 × 10^6 scale map published by the Australian Division of National Mapping with information received up to 1965. Since that time further data for East Antarctica have come from the U.S. Queen Maud Land traverses, from the Soviet 1966, 1967, 1968 traverses in Enderby and Queen Maud Lands, and from the Japanese 1968 traverse from Syowa to the South Pole. The main difference between the present map and the newer results appears to be that in the latter the 3,500 m contour in Queen Maud Land is continuous with that around the highest point in East Antarctica. Such an adjustment to the input data would cause corresponding deviations in the derived results which must be kept in mind in their evaluation.

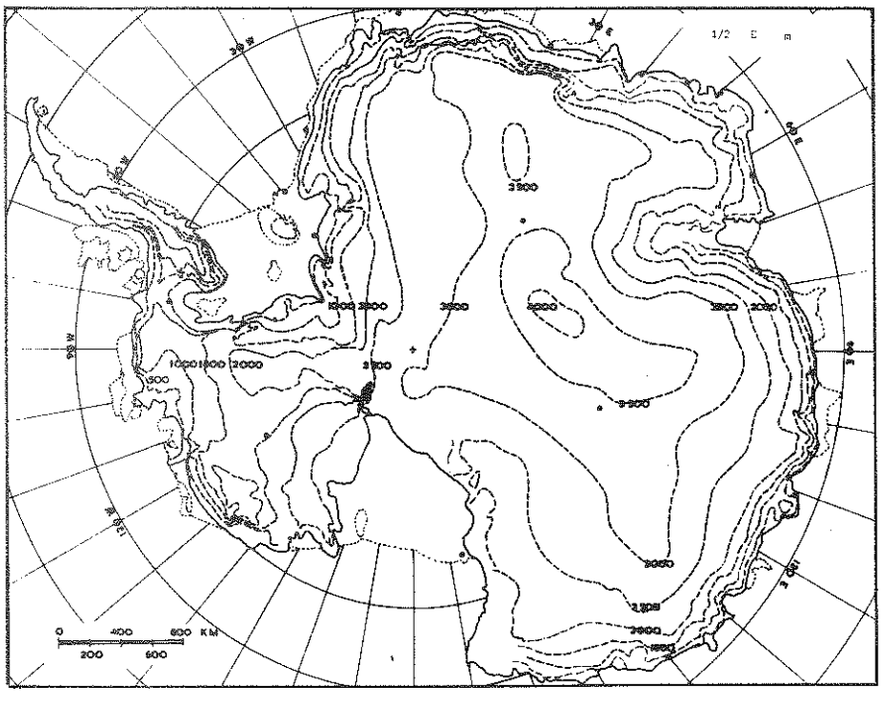

Map 1/2. Elevation of ice surface E *m*

The Australian Division of National Mapping 1:20,000,000 map of the Antarctic, 1965, has been used as basis for the ice surface elevations. This map is similar to the corresponding one in the Soviet Atlas of Antarctica, differing from it mainly in the 3,500 m contour for Dronning Maud Land. The more recent Japanese and Soviet traverses have now clarified the contours in this regions and introduced some changes here although the broader scale features remain unaffected.

For West Antarctica the 500 m contour spacing is somewhat coarse in comparison with the detail of the measurements available. Hence for our calculations in this region we have used more detailed elevation data such as those of Shimizu (1964, Fig. 8). Again the 100 km smoothing places the emphasis on the large scale variations to the exclusion of finer detail, provided only by larger scale maps. Since the object here is to provide, in a compact form, an indication of the major features of the Antarctic ice sheet as a whole, larger scale maps become somewhat unmanageable. For future studies, however, there will be a natural trend towards larger and more detailed maps as more data become available.

The main features of note in the elevation contours is the major high zone of about 4,000 m in central East Antarctica with the contour levels decreasing, at first slowly, then more rapidly towards the coast and the major ice shelf basins. In West Antarctica the average elevation of the ice surface is much lower. There are three separate major high regions over 2,500 m: one in the central region near the Whitmore Mountains, another near the coast close to the Executive Committee Range, and the third in Palmer Land. An interesting saddle point between two major high zones occurs in Byrd Land.

It will be seen in Map (1/3) that these surface contours to a large extent reflect the major bedrock features, and from Map (2/1) that they govern the major features of the ice flow patterns.

2.3. Ice thickness.

The distribution of ice thickness over the Antarctic used here is illustrated in Map (1/3). This map has been taken almost directly from the corresponding Map (94) in the Soviet Atlas of the Antarctic (Bakayev, Ed. 1966); however no attempt has been made to preserve detail on scales less than 100 km.

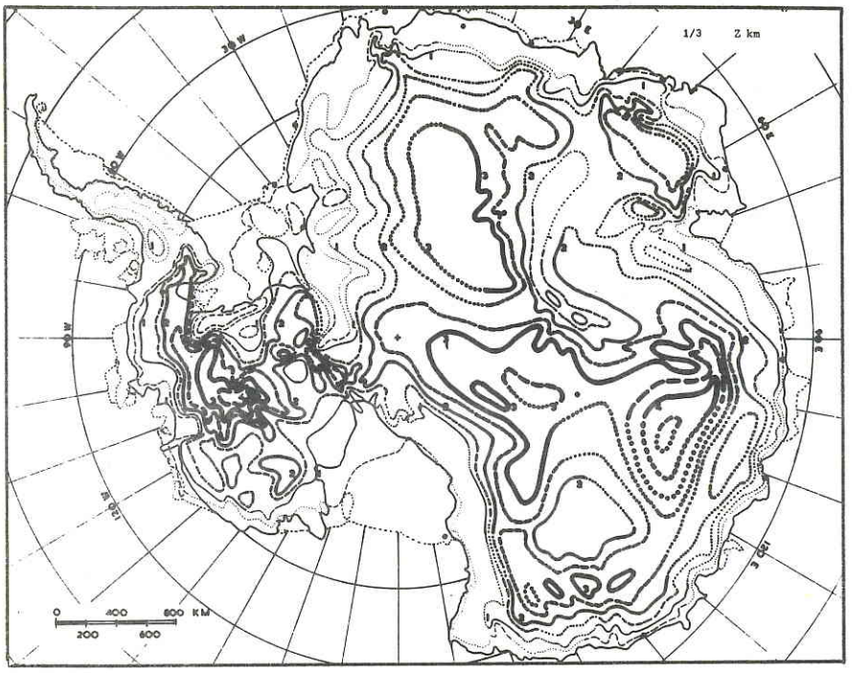

Map 1/3. Ice thickness Z km

The 1:20,000,000 ice thickness map in the Soviet Atlas of Antarctica has been the main source for this map. The major features include the especially thick ice (greater than 4,000 m) in central West Antarctica and the interior of Wilkes Land. The central east Antarctic ice sheet is comparitively thin over the Gamburtsev Mountains region.

The sources of the data for the map basically are the traverses (full lines) of Map (1/1) and have been discussed in detail by Kapitsa (1966). Again the later traverses and aerial radio soundings of ice thickness, e.g. Robin et al (1970), Bogorodskiy (1968), have provided additional

information to that used here; however, the major large scale features still retain their present form. West Antarctica has sufficient detail for the present purpose, but for East Antarctica only the large features on the scale of about 1,000 km and greater can be considered as reliable and accurate. The extrapolation and interpolation used here however provide a basis upon which later fine detail and deviations may be compared or superimposed.

The most notable features are the very thick ice (over 4,000 m) in East Antarctica inland of Casey (Wilkes) station and in central West Antarctica (Byrd Land). From these regions the ice thickness typically decreases towards the coast, the ice shelf basins and mountain ranges. An important additional feature is the thin ice zone which exists in central East Antarctica over the Gamburtsev Mountains. These major features of the ice thickness distribution tend to dominate many of the patterns of the distribution of the derived characteristics.

2.4. Bedrock elevations.

The broad scale bedrock elevations of the Antarctic are illustrated in Map (1/4). This in effect represents the subtraction of ice thickness (Map 1/3) from surface elevation (Map 1/2). The map used here has been largely taken from the equivalent Map (66) in the Soviet Antarctic Atlas (Bakayev, Ed. 1966). The full lines represent the regions above sea level, the line thickness increasing with the height, while the broken lines indicate similarly the regions below sea level. Where information is sparse the contours have been dotted.

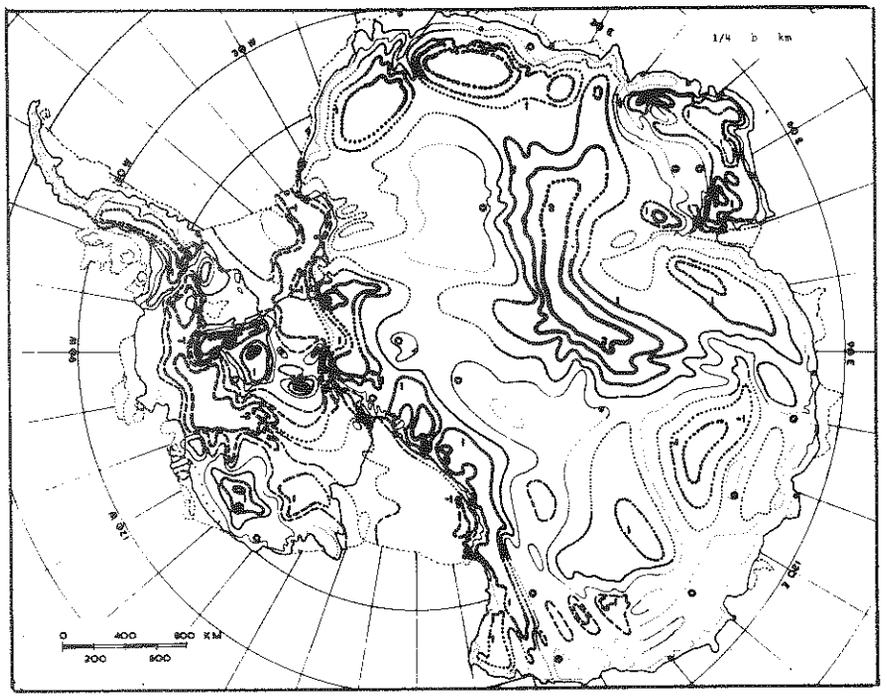

Map 1/4. Bedrock elevation b km.

The 1:20,000,000 map of bedrock elevations from the Soviet Atlas of Antarctica has been the main source for this map. The regions of major uncertainty are indicated by dotted lines. Data from the U.S. Queen Maud Land traverse, the Japanese South Pole traverse, and the Soviet Molodeznaya-Novolazarevskaya traverse have not been included here. Major features include the high regions of the Gamburtsev Mountains in East Antarctica and the Transantarctic Mountains, and depressions in Byrd Land and Wilkes Land as well as towards the coast and in the major ice shelf basins.

Kapitsa (1966) describes the basis for this map in detail. Since then additional information, not included in Map (1/4), has come from the U.S. Queen Maud Land traverses, the Soviet traverse from Molodezhnaya to Novolazarevskaya via the Pole of Inaccessibility, and the Japanese Syowa-South Pole traverse (Ishida 1970). More recent detailed radio echo sounding from the air has been carried out and described by Robin et al (1970) and by Bogorodskiy (1968). This important development suggests that in the not too distant future we may expect to have continuous profiles over the entire continent at about 100 km spacing. Such high detail will allow a more thorough investigation with the new analysis programmes to be described in Chapter 8. For the present however we take the bedrock elevations (Map 1/4) as the assumed input for this study and will refer the output results to it. Where this map departs from reality the output results can be expected to do the same. But again the representation should be quite sound for the large scale features.

These major features are very important since they largely determine where the original ice growth develops and thereafter dominate the whole pattern of ice flow. It will be seen in Chapter 6 that other derived features of the ice sheet are also closely related to the bedrock patterns. The loose maps attached to this report allow the various features to be superimposed on a light table so that the relations between them can be readily visualised.

One of the most striking features noticed from the bedrock map is the sharp contrast between East and West Antarctica, separated by the high ridge of the Transantarctic Mountains. East Antarctica shows the typical features of a large continental shield dominated by the Gamburtsev Mountains near its centre. The high Transantarctic Mountains and the coastal mountains of Queen Maud Land act as blocking features to the ice flow and thus cause high ice build up inland of them. The main low features include the Lambert Glacier basin and a deep trench in Wilkes Land.

West Antarctica by contrast represents a number of high peaks separated by deep basins descending below sea level. These result in a number of centres of ice flow and the interesting saddle point divergence over the very deep trough in central Byrd Land.

The bedrock features of the Antarctic continent give it its character. Their irregularity and the contrast between one region and another provide the main source of variability in the derived physical parameters. By contrast the other data parameters, such as ice elevation, accumulation rate and surface temperature, are much smoother on the scales considered here, but with dominant smooth trends from the inland to the coast.

2.5. Accumulation rate.

The pattern of the distribution of nourishment for the Antarctic ice sheet is illustrated in Map (1/5). The contours represent the measurements of the present-day mean annual snow accumulation rate in cm of ice equivalent per year. The bases for the map have been primarily the Soviet Atlas of Antarctica (Map 96I) and the accumulation map of Bentley et al.(1964). Additional information for East Antarctica has come from Cameron et al.(1968) and Battye (1964). For West Antarctica the detailed accumulation map of Vickers (1966) has also been used. The recent measurements of Gow (1970), Bentley et al.(1964), Picciotto et al.(1968), Ishida (personal communication) suggest some of the earlier estimates of inland accumulation rates to have been somewhat high, and adjustments for this have been made in the present map.

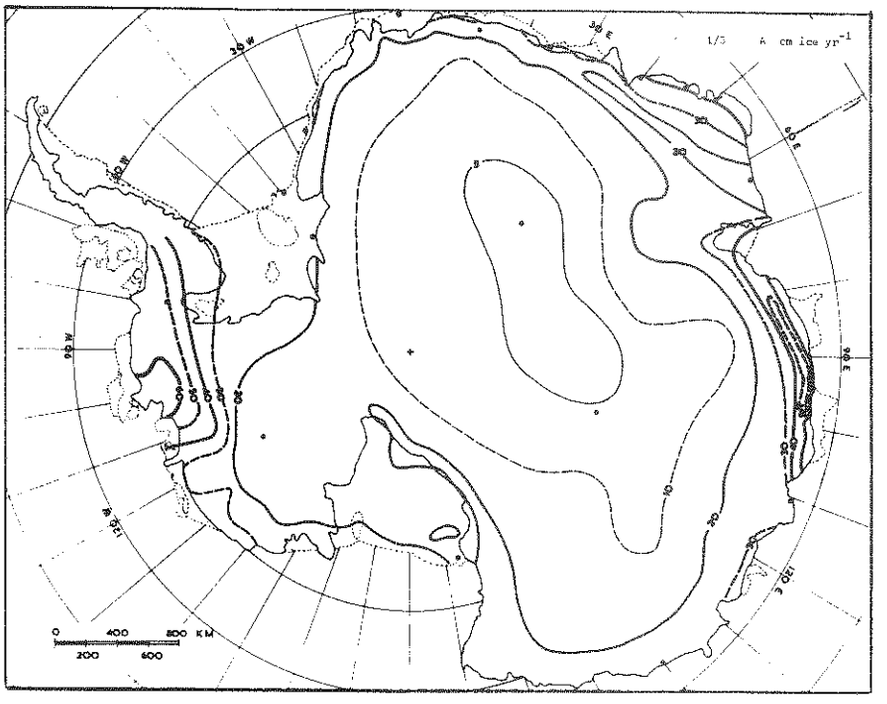

Map 1/5. Accumulation rate A cm ice/yr.

This accumulation map has been constructed from several sources including maps in the Soviet Atlas of Antarctica (96I), the American Geographical Society (Bentley et al 1964) and papers by Vickers (1966, p.171) and Cameron et al (1968). The values increase generally from low values of about 2-3 cm ice/yr in central East Antarctica to over 30 cm/yr near the coast.

Most of the results represented here come from relatively short-term measurements over a few years. There is much less longer term information available at this stage. Petrov and Barkov (1964) find a slight measure of variation over the last half century. The study of deep layers in the firn at South Pole (Giovinetto and Schwerdtfeger 1966), Wilkes S2 station (Cameron et al 1959) and the Byrd core (Bender and Gow 1961) suggest that over the last few hundred years the change on the average has been small. Much data of this kind is required however to build up a picture of not only the mean present-day accumulation rate distribution but also its pattern of variation in time.

The main features of the present smoothed accumulation pattern is a very low region in central East Antarctica with values down to 2.5 cm ice/year. A general, increasingly rapid, growth in accumulation rate occurs towards the coast reaching at least 20 cm/year, and, in some regions, up to 60 cm/year. For this study the high variability near the coast as well as the small regions of ablation have been smoothed over completely.

The general pattern of increasing accumulation towards the coast together with decreasing ice thickness plays an important role in the development of the temperature distribution in the ice, as will be shown in Chapters 4 and 6.

2.6. Ice surface mean temperatures.

The pattern of annual mean temperature over the surface of the Antarctic ice sheet is illustrated in Map (1/6). Most of the data for this map comes from measurements in the firn about 10 m below the surface. At this depth the temperature is generally within about one degree of the annual mean temperature there. Loewe (1970) discusses the relation between mean firn and mean air temperatures, which may differ by a degree or so from one region to another.

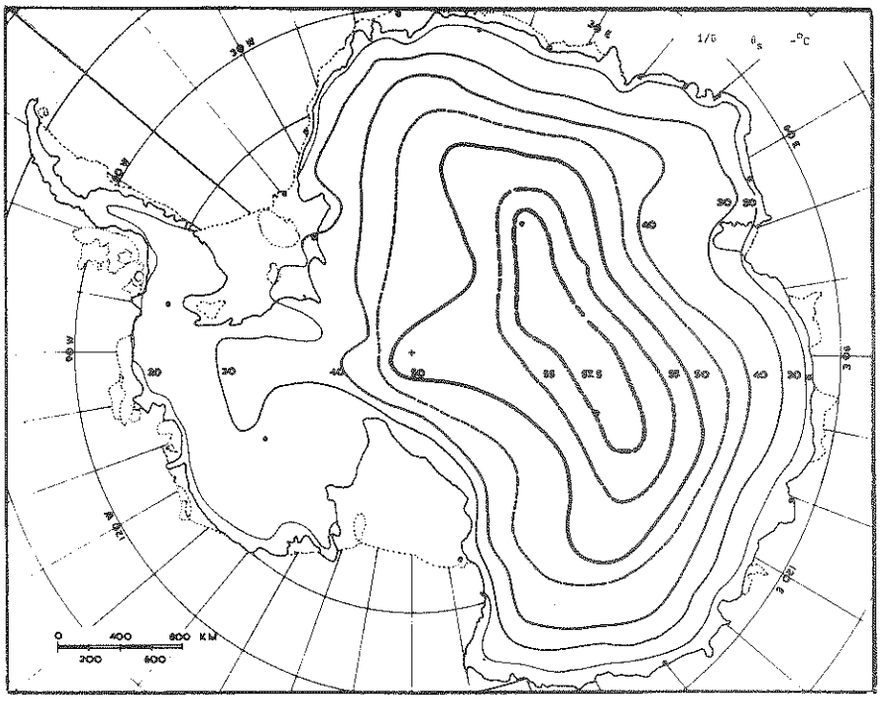

Map 1/6. Temperature of ice surface θ_s *-°C*

This surface mean temperature map has been constructed from several sources, including the maps of the Soviet Atlas of Antarctica (96III), the American Geographical Societ Map Folio (Bentley et al (1964)) and papers by Shimizu (1964), Cameron et al (1968). The values increase from about -60°C in central East Antarctica to about -20°C around 1,000 m elevation near the coast.

Many sources have been used for this map including Bentley et al. (1964), Bakayev, Ed. (1966, Fig. 96III), Shimizu (1964, Fig. 11), Cameron et al.(1968, Fig. 10), Kane (1970), Budd (1966a, 1969), Battye

(1964). The values have again been smoothed to bring out the main large scale features of the variation.

The general pattern of the temperature distribution is characterised by a cold core in central East Antarctica reaching about -60°C, and increasing temperatures outwards towards the coast, to about -20°C at the 1,000 m level, and further to about -10°C at sea level. This pattern of variation has largely been explained by the variation of temperature with elevation and latitude.

On top of this there are many anomalies, such as a zone several hundred kilometres inland where the temperature elevation gradient becomes large (cf. Map 3/4). Another large anomaly near the -50°C contour in Queen Maud Land has been described by Kane (1970) and linked with a region of small surface slope. Such variations are presumably associated with topographic, wind, and heat balance effects. For the present study they have been smoothed over. For future more detailed studies it may be possible to collect sufficient data to define them adequately and include them in the input data.

Like that of the accumulation rate, the temperature map represents conditions over a very short time period, largely since the IGY. Most of the values come from spot measurements at a single time of a particular traverse. The annual variability of the surface temperatures for a number of Antarctic stations is illustrated by Fig. 2.1. Although little data is available on the variation in temperatures over longer periods we may hope to derive some information on this from the analysis of the temperatures in the ice.

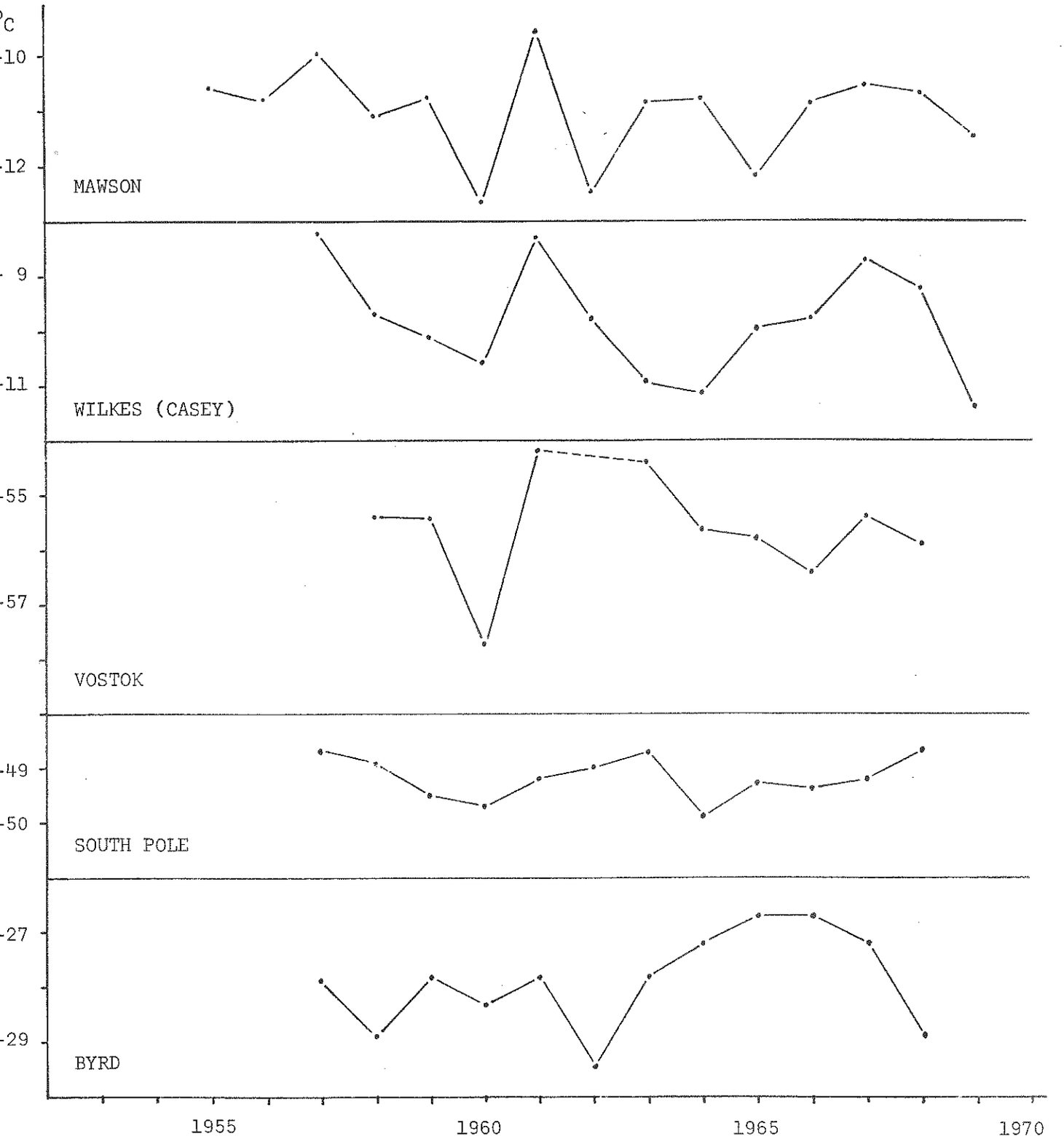

FIG. 2.1 Variation of annual mean temperatures for several Antarctic stations.

2.7. Temperature-depth gradients near the ice surface.

Although measurements of surface temperature-depth gradients in the ice are not sufficiently numerous to establish contour patterns over the ice sheet, those available are useful for a comparison with the results of the calculations to be described in section 6.2. Individual values of measured surface gradients have been plotted on Map (1/7) to illustrate what general trends are discernible. Most of the values come from boreholes less than 100 m deep. In this surface layer the density and diffusivity of the firn may differ markedly from

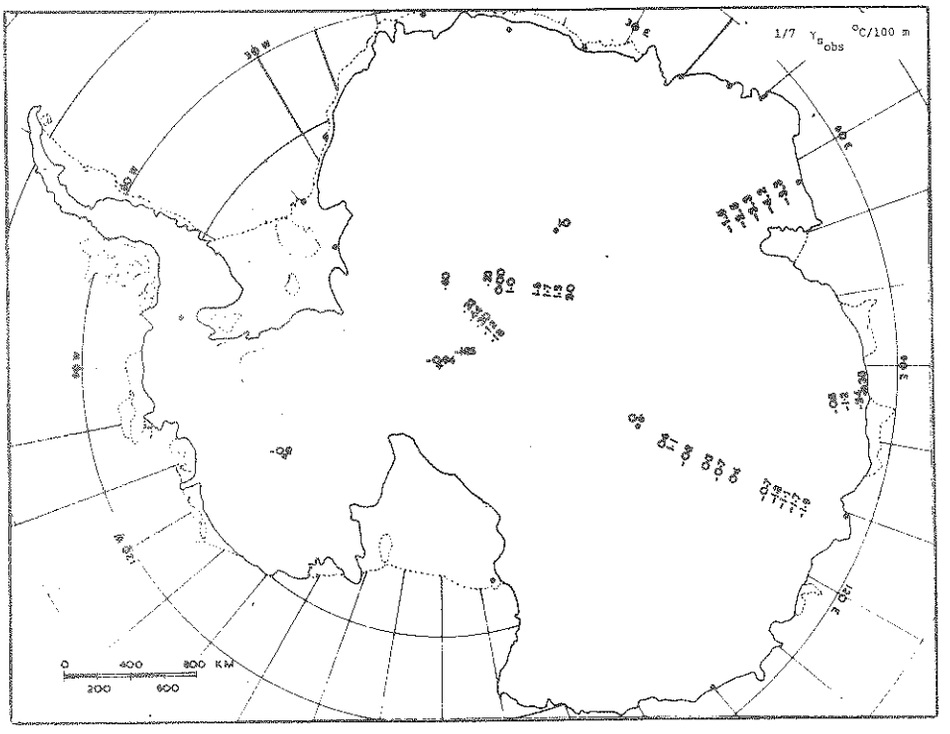

Map 1/7. Observed temperature-depth gradients at the ice surface $\gamma_{s_{obs}}$ *°C/100 m*

Only very few measured values of the temperature-depth gradient in the ice cap near the surface are available. The main values come from shallow holes (40-60 m deep) reported by Bogoslovskiy (1958), Battye (1964), Budd (1969) and Cameron et al (1968). The values generally suggest a trend from about +1°C/100 m in central East Antarctica to about -2°C/100 m near the coast.

that of ice. In addition shorter term temperature fluctuations at the surface may still have appreciable effects to these depths. Finally due to the small scale surface undulations of wavelength several times

the ice thickness (cf. Beitzel 1970, Budd and Carter, in press) we must expect a certain amount of local variation in shallow temperature gradients which are essentially spot values. The gradients inland of Mirny are from Bogoslovskiy (1958); those inland of Mawson from Mellor (1960); those inland of Wilkes from Battye (1964), and Budd (1966a and 1969); and those in Queen Maud Land from Cameron et al (1968). Finally several spot values are also available at such places as Byrd, South Pole and Pole of Inaccessability.

Of primary interest is the significant increase of negative gradients approaching the coast. If climatic change were thought to be the only cause of the surface gradient this systematic trend would be difficult to explain. It will be shown in Chapter 4 that this type of trend, as well as the magnitudes of the positive gradients inland and the negative gradients nearer the coast, are also what one would expect from the movement of the ice with constant climatic conditions.

The effects of recent climatic trends may be determined independently of the horizontal ice movement effects by measurements of the temperatures in boreholes at the summits of ice domes where the horizontal movement is zero. An example of such a temperature profile is given in Fig. (2.2) for the Summit of the Wilkes local ice cap (Law Dome), from data obtained by R. Anderson in 1969 (personal communication). The interpretation of such profiles however is dependent on whether or not the surface is remaining at the same elevation with time. Temperature changes associated with rising or sinking ice caps must be considered as well as those associated with climatic change. One of the objects of this study is to isolate such changes.

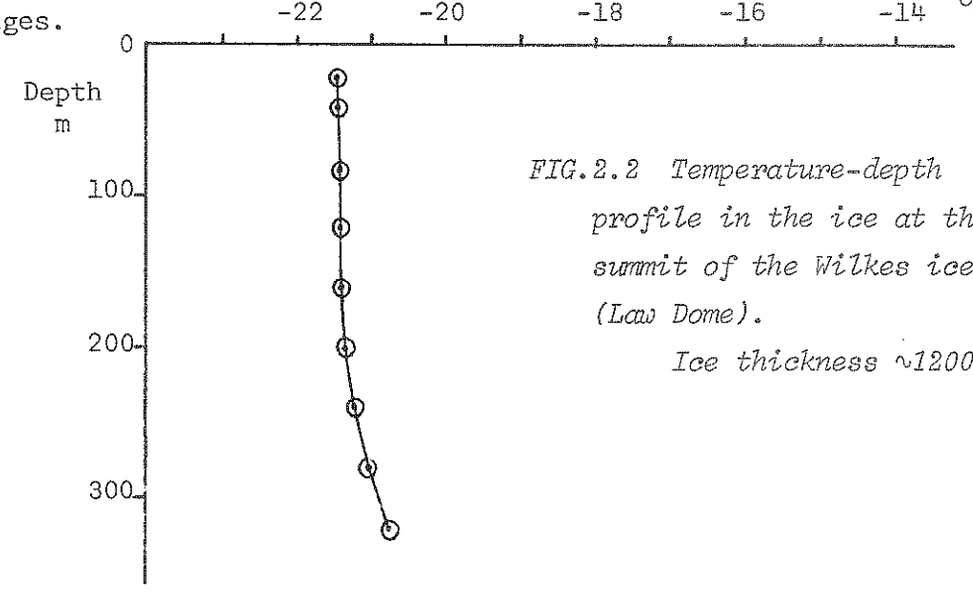

FIG. 2.2 Temperature-depth profile in the ice at the summit of the Wilkes ice cap (Law Dome). Ice thickness ~1200 m

3. ICE SHEET DYNAMICS.

3.1. General flow properties.

3.1.1. Direction of flow.

On the large scale (∿100 km) we may expect ice to flow downhill, in the direction perpendicular to the surface elevation contours. Budd (1970) showed that ice can travel uphill for distances of the order of several times the ice thickness; but for scales of 10 to 100 times the ice thickness the effect of the longitudinal stresses, causing such flow, becomes negligible. The flow vectors determined for the Wilkes local ice cap (cf. Budd 1969, Fig. 6.9) confirm the general relation between the flow direction and the orthogonals to the contours.

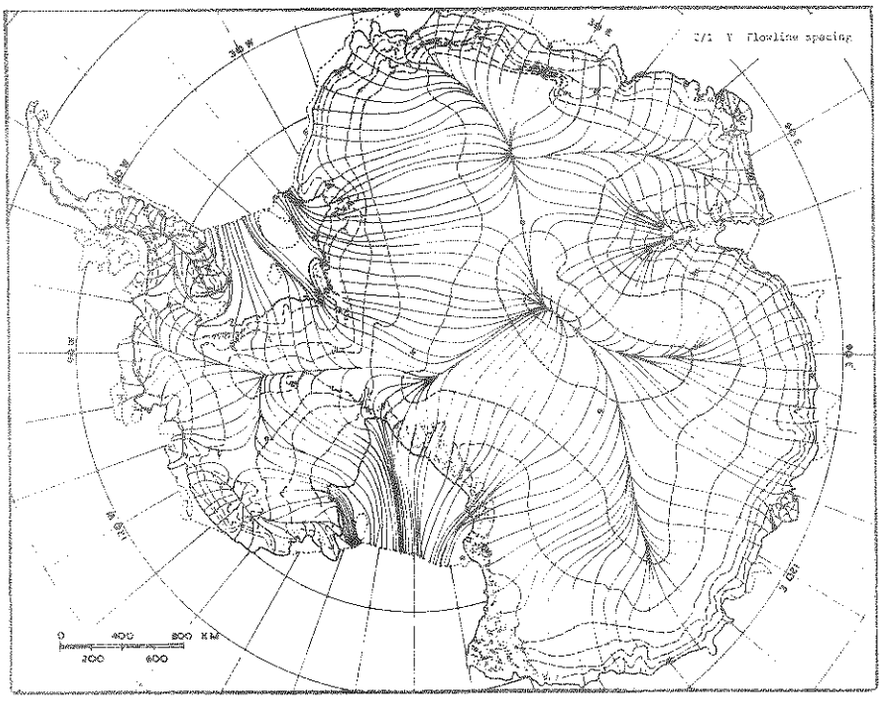

Map 2/1. Flowline spacing Y

The 500 m elevation contours for Antarctica from Map(1/2)have been used to construct orthogonal trajectories with about 100 km spacing and smoothing to represent the general ice flow directions and drainage patterns for the Antarctic ice cap. The major features include convergence of flow into the main ice shelf basins and divergence from the main ice divides.

Taking this as a general criterion we have constructed orthogonals to the surface elevation contours on the scale of about 100 km for the Antarctic ice sheet (cf. Map 1/2). Such a set of orthogonals is shown in Map (2/1) and serves to represent the large scale flow patterns. In this diagram the particular flow lines and spacings are arbitrary, the aim being simply to comply with about 100 km spacing and yet maintain individual flow lines continuous to the coast.

The resultant flow patterns may be used to delineate the main drainage basins, such as those of the three major ice shelves, and also the regions of divergence and convergence.

3.1.2. Magnitude of flow.

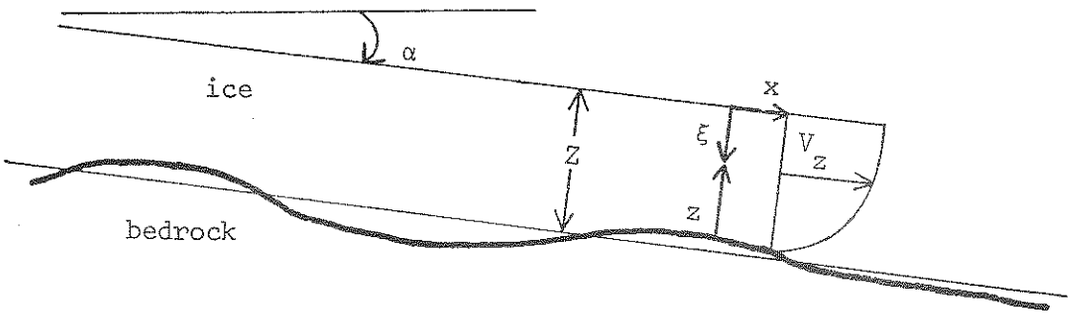

FIG. 3.1 Coordinates used for shear stress in ice flowing down a slope.

On the large scale we approximate the ice sheet by a uniform slab of ice of thickness Z, the mean thickness of the ice over the flowline interval, and slope α, the mean slope of the surface along the central flow line. With longitudinal and transverse stress gradients neglected the only effective stress gradient is the shear stress gradient perpendicular to the surface, $\frac{\partial \tau_{xz}}{\partial z}$, say.

We may write

$$\frac{\partial \tau_{xz}}{\partial z} = \rho g \alpha \tag{3.1}$$

where ρ is the density of the ice, and
g is the gravitational acceleration.

Now if we consider a flow law of the type

$$\dot{\varepsilon}_{ij} = \mu(\tau, \theta, \text{etc})\sigma'_{ij} \tag{3.2}$$

where $\dot{\varepsilon}_{ij}$ is the strain rate tensor
σ'_{ij} is the stress deviator tensor
μ is a scalar function of
τ, the octahedral shear stress
θ, the ice temperature (below pressure melting),
and other relevant properties of the ice (such as the crystal orientations) represented by "etc",

then we may take

$$\dot{\varepsilon}_{xz} = \frac{dV_z}{dz} = \mu \tau_{xz} \tag{3.3}$$

where V_z is the velocity at height z above the base of the ice.

Hence from (3.1) and (3.3)

$$V_Z - V_z = \rho g \alpha \int_z^Z \xi \mu dz$$

$$= \tfrac{1}{2} \rho g \alpha \xi^2 \bar{\mu}_\xi \tag{3.4}$$

where $\bar{\mu}_\xi = \frac{2}{\xi^2} \int_0^\xi \xi \mu d\xi$, and $\xi = Z - z$. (3.5)

In particular if the basal velocity is zero the surface velocity is given by

$$V_s = \tfrac{1}{2} \rho g \alpha Z \bar{\mu}_Z \tag{3.6}$$

3.1.3. The flow law of ice.

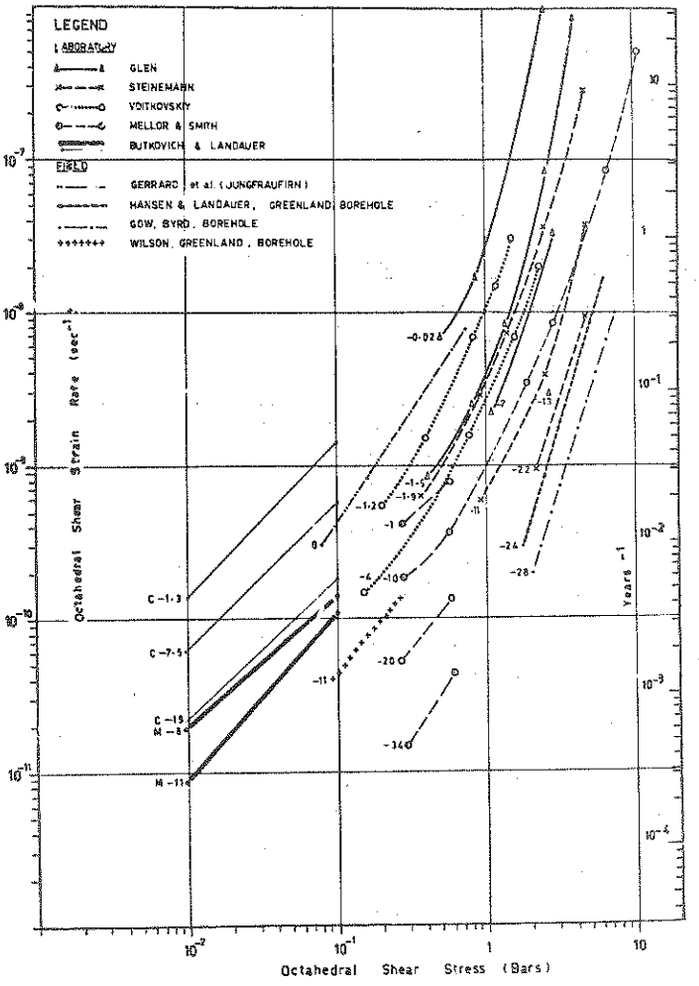

FIG. 3.2 The flow law of ice (after Budd 1969)

The nature of the flow law of ice is illustrated by Fig. (3.2) taken from Budd (1969). Here the strain rate is shown to increase very rapidly with stress and temperature, especially for the high stresses (greater than 1 bar). The majority of the measurements on which this diagram is based are for ice with small, randomly oriented crystals. So far there is insufficient information available on the direct effect of the crystal size and orientation fabric on the flow law. Hence for the present we consider just the stress and temperature effects and hope to obtain further information from future studies of flow rate measurements and core studies in the field and the laboratory.

Using an idealised flow parameter $\mu(\tau,\theta)$ which is a function of the octahedral shear stress and temperature alone and chosen to match the available measurements as near as possible we adopt Table (3.1) with appropriate interpolation as the flow law's numerical representation.

Table 3.1.

Flow law of ice used in programme computations for "dynamics velocities".

The table gives the value of the common logarithm of octahedral shear stress for given values of temperature and octahedral shear strain rate.

		$\log_{10}$ OF OCTAHEDRAL SHEAR STRAIN RATE							
		-1.0	-0.8	-0.6	-0.4	-0.2	0.0	0.2	0.4
TEMPERATURE (DEGREES CENTIGRADE)	0	-9.22	-8.96	-8.70	-8.43	-8.12	-7.69	-7.07	-6.23
	-5	-9.98	-9.78	-9.56	-9.28	-8.97	-8.62	-8.14	-7.66
	-10	-10.28	-10.08	-9.86	-9.63	-9.38	-9.10	-8.71	-8.29
	-20	-10.77	-10.56	-10.35	-10.12	-9.84	-9.56	-9.23	-8.82
	-30	-11.23	-11.00	-10.80	-10.59	-10.37	-10.12	-9.82	-9.42
	-40	-11.70	-11.50	-11.30	-11.10	-10.86	-10.60	-10.31	-10.00
	-50	-12.16	-11.96	-11.76	-11.56	-11.36	-11.16	-10.87	-10.53
	-60	-12.55	-12.35	-12.15	-11.95	-11.75	-11.55	-11.35	-11.00
	-70	-12.87	-12.67	-12.47	-12.27	-12.03	-11.77	-11.75	-11.41

Returning now to the expression for the velocity of the ice we see that with our assumption of a shear stress varying linearly with depth the remaining information required to calculate the flow is the vertical temperature distribution. The velocity calculated in this way is determined from the physics of the situation, viz. the dimensions and shape of the ice mass and the appropriate flow law of ice, which includes the effects of the temperature distribution. We shall here term this the "dynamics velocity". The whole problem of calculating the dynamics velocity reverts to that of calculating the temperature distribution. Hence we turn to the problem of heat conduction in a moving medium.

3.2. Heat conduction equation.

We consider the same large scale ice slab model as for section (3.1). We chose for the moment orthogonal axes x_i (or x, y, z with x along the line of flow, z vertically upward, and y transverse).

Now at the point x_i let θ be the temperature, u_i (or u, v, w) the velocity, $\dot{\varepsilon}_{ij}$ the strain rate, τ_{ij} the stress, ρ the ice density, K the conductivity, c the specific heat and κ the diffusivity of the ice. Then the heat conduction equation may be written

$$\frac{1}{\rho c}\left(\frac{\partial}{\partial x_i} K \frac{\partial \theta}{\partial x_i} + u_i \frac{\partial \theta}{\partial x_i} + \tau_{ij}\dot{\varepsilon}_{ij}\right) = \frac{\partial \theta}{\partial t} \qquad \theta < \theta_m \qquad (3.7)$$

$$= L \frac{\partial M}{\partial t} \qquad \theta = \theta_m$$

where θ_m is the pressure melting point where mechanical or heat units are understood throughout, and

M is the melt rate and

L is the latent heat of fusion.

With the model we are using the following terms may be neglected: $\frac{\partial^2\theta}{\partial y^2}$, $\frac{\partial^2\theta}{\partial x^2}$, $v\frac{\partial \theta}{\partial y}$, and all $\dot{\varepsilon}_{ij}$ except $\dot{\varepsilon}_{xz}$. This is suggested by typical values of these terms and moreover follows directly from the use of smoothed data.

Hence the heat conduction equation (taking K constant for the present) reduces to

$$\theta < \theta_m \qquad \kappa \frac{\partial^2\theta}{\partial z^2} + w_z \frac{\partial \theta}{\partial z} + u_z \frac{\partial \theta}{\partial x} + \tau_{xz}\dot{\varepsilon}_{xz} = \frac{\partial \theta}{\partial t} \qquad (3.8)$$

If we assume the vertical strain rate varies with depth proportionally to the horizontal velocity and if we neglect density variations, we may take for the vertical velocity w_z the relation

$$w_z = M_b + A\frac{zV_z}{ZV_s} \qquad (3.9)$$

where A is the ice accumulation rate at the surface,

M_b is the basal melt rate and

V_s the horizontal velocity at the surface

V_z the horizontal velocity at depth z.

It will be shown in Chapter 6 that for land-based ice the melt rate is usually small compared to the accumulation rate so for the moment M_b will be neglected.

Hence we write

$$w_z = \frac{Az}{Z} \frac{V_z}{V_s} \tag{3.10}$$

For the steady state situation in which the temperature distribution in the ice cap is constant with time, i.e. $\frac{\partial \theta}{\partial t} = 0$

$$\kappa \frac{\partial^2 \theta}{\partial z^2} + \frac{Azu_z}{Zu_s} \frac{\partial \theta}{\partial z} + \rho g \alpha \xi \frac{\partial u_z}{\partial z} = - u_z \frac{\partial \theta}{\partial x} \tag{3.11}$$

With the boundary conditions specifying the surface temperature θ_s and the basal temperature gradient $\gamma_b = \gamma_G$, where γ_G is the geothermal heat flux, the heat conduction equation (3.11) would be solvable over the two dimensional region (x,z) if the distribution of the horizontal velocity were known.

In section 3.1 we noted that we need the temperature distribution to calculate the velocity profile through the ice. One course out of this dilemma is to solve equations (3.6) and (3.11) for velocity and temperature simultaneously. This will be described for the single column model in section 4.1.6. However the result of such a procedure suffers from several major difficulties. First of all the flow law of ice is such that small errors in stress or temperature give rise to large errors in the strain rates and velocities. Secondly the flow law is still not sufficiently well known, especially for low temperatures, low stresses and strain rates and strong crystal fabrics, to allow more than coarse estimates to be made for the large range of values encountered in the Antarctic. Also any errors in the hypothesis of constant values with time of the ice cap elevation, surface temperature, and accumulation rate have an accentuated effect on the calculated velocity and temperature profiles.

Hence we take the following course of action. We shall consider the velocity distribution over the ice sheet which would exist if the ice cap were in a stationary state under the given existing accumulation rate.

On present estimates we may expect that such a "balance velocity" distribution may be correct within about a factor of two, whereas the estimated "dynamics velocity" may be out by an order of magnitude.

Having once calculated the "balance velocity" we can solve the heat conduction equation for steady-state to obtain the temperature profile. We may then use this temperature profile to calculate a dynamics velocity which can be compared with the initial balance velocity. This provides a basis for comparing the measured and computed values of temperatures and velocities, to throw light on our knowledge of (i) the flow law operating in practice and (ii) the variations from the steady state with time. Hence we next examine the velocity distribution required for balance.

3.3. Continuity and balance velocities.

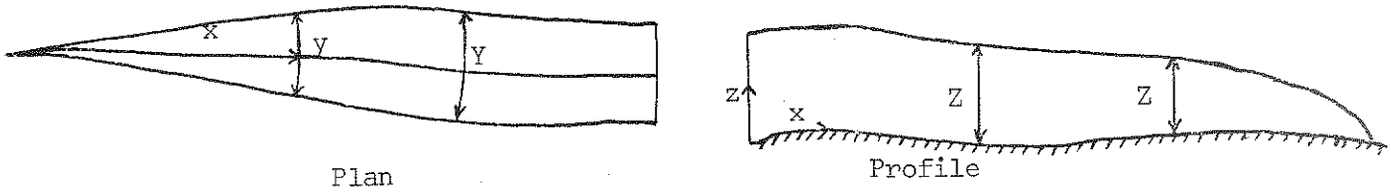

FIG. 3.3 Coordinates used for continuity relations.

In the present context we consider the steady state mass balance of the Antarctic for individual generalised sectors between flowlines such as those of Map (2/1). Consider one particular flowline and let x be the distance along it from its start. Take the neighbouring flowlines on each side at about 100 km distance at the midpoint of the central flow line and call Y the distance apart of these two flowlines at position x.

Let $\overline{Z}$ be the mean ice thickness across Y and let $\overline{V}$ be the mean velocity across this section. The total volume outflow at x is then given by

$$\Phi = \overline{V}\, Y\, \overline{Z} \tag{3.12}$$

If $\overline{A}_x$ is the mean accumulation rate (in cm of ice/year) over the sector to position x, and S_x the area of the sector then the total accumulation is given by $\overline{A}_x S_x$. A similar relation holds for the total melting at the base. However for the moment we disregard this melting until we have examined the calculated basal temperatures and melt rates in Chapter 6.

The condition for the steady-state balance of the sector then reduces to

$$\overline{V}\ Y\ \overline{Z} = \overline{A}_x\ S_x \tag{3.13}$$

from which we may find the mean velocity of the ice section at position x as

$$\overline{V} = \frac{\overline{A}_x S_x}{Y\overline{Z}} \tag{3.14}$$

Mathematically this velocity approaches the velocity of the ice column at position x in the limit as the flowlines come close together. Practically however the errors in measuring the areas usually increase as the area becomes smaller. Hence as a compromise we have taken for this study typical flowlines 200 km apart at the position in question.

The area S_x is given by

$$S_x = \int_0^x Y\ dx \tag{3.15}$$

and may be found by planimetry or numerical integration.

The mean accumulation is found similarly from the relation

$$\overline{A}_x = \frac{\int_0^x A_x Y\ dx}{S_x} \tag{3.16}$$

where A_x is the mean accumulation rate between the two flowlines at position x. By superimposing the accumulation rate Map (1/5) on to the flowline Map (2/1) this integration can be carried out numerically for small subintervals over each sector area. The mean sector width Y at position x is obtained directly from the flowline map and the mean thickness $\overline{Z}$ from the map of ice thickness (1/3). This then allows $\overline{V}$ to be calculated directly from an incremental form of equation (3.14).

The resultant balance velocity magnitudes ($\overline{V}$) have been plotted and contours drawn for the whole of the Antarctic ice sheet. These are shown in Map (2/2). The full velocity vectors are obtained by combining the flowline directions from Map (2/1) with the velocity magnitudes in Map (2/2).

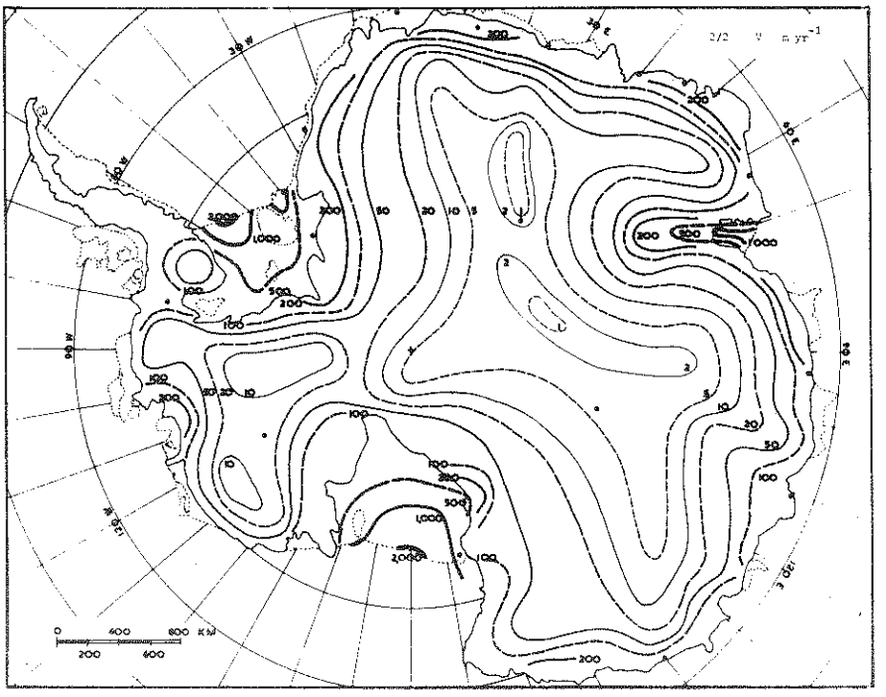

Map 2/2. Balance velocity V m/yr.

From the maps of ice thickness Z, accumulation rate A, and ice flow lines (distance apart Y at distance x) the average velocity V required for a balanced state has been calculated as $V = (\int\int AdYdx)/YZ$ *for sectors formed by the flowlines and 200 km segments of all the 500 m spacing elevation contours. Typically the velocities increase from about 1 m/yr inland to about 100 m/yr along most of the land-based ice margin and 1000-2000 m/yr at the major ice shelf fronts.*

These balance velocities are very useful in their own right. By comparing them with actual measured velocities (averaged over the appropriate range) a direct check can be made on the present state of balance. In particular the measurements across the fronts of the Ross Ice Shelf by Dorrer et al (1969), and across the Amery Ice Shelf by Corry (unpublished), suggest the balance velocities may be too high. However no basal melting has been included in the calculations of the balance velocities, and this could account for some of the discrepancies

if substantial melting under the ice shelves does exist. In fact the total melt required for balance could be calculated from the observed velocity and those shown in Map (2/2).

The general pattern of the balance velocity distribution is characterised by a region of slow ice moving only a few metres per year, in the central high regions of East and West Antarctica, and by velocities increasing somewhat exponentially to average values of 100 to 200 metres per year around most of the coast and the edges of the major ice shelf basins. This rapid increase is typical of the increasing longitudinal strain rates required by the increasing accumulation rates and the decreasing ice thickness towards the coast.

In regions nearer the coast than covered by the present calculations the flow is greatly broken up and divided into irregular sections of rapid ice streams (moving $\sim$ 500 m/year) and slow sheet flow ($\sim$ 50 m/year).

The prime reason for deriving the balance velocity distribution is to obtain a first guess for use in calculating the temperature distribution. This is followed up in Chapter 4. The velocity distribution however gives rise to many other direct and further indirect results of considerable importance. These include such features as mean strain rates of the ice, the volume flux, the residence times and the ages of the ice. These latter two require more involved and indirect two-dimensional calculations, and follow from the detailed flowline analysis to be described in Chapter 4. Here we next examine the direct consequences of the velocity distribution.

3.4. Derived by-products of balance velocities.

3.4.1. Longitudinal strain rates.

The "balance longitudinal strain rate" ($\dot{\varepsilon}_x$) distribution has been calculated as a mean through a column directly from the balance velocity distribution as

$$\dot{\varepsilon}_x = \frac{d\overline{V}}{dx} \qquad (3.17)$$

where x is taken along the flow line.

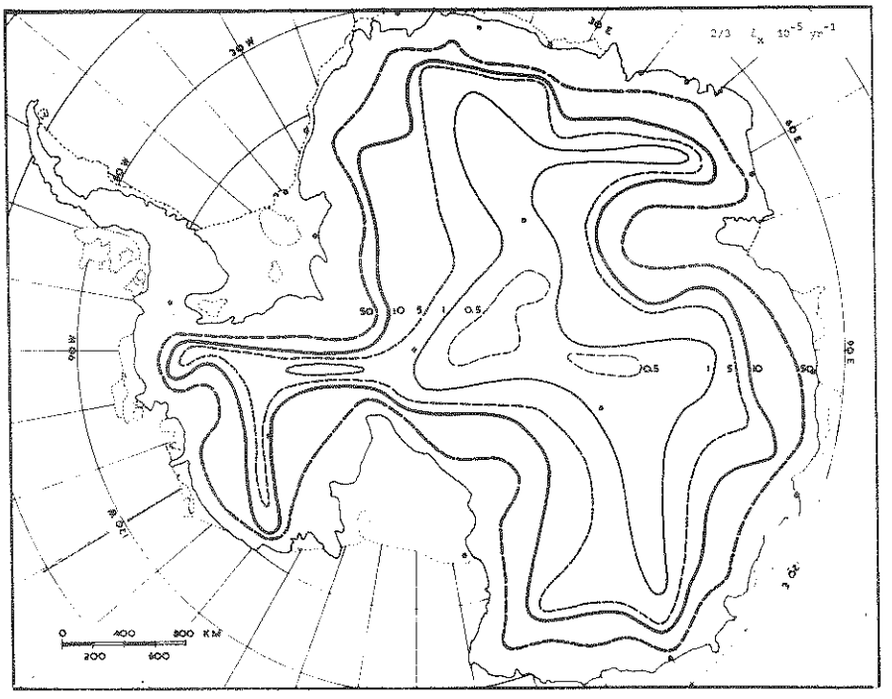

Map 2/3. Longitudinal strain rate $\dot{\varepsilon}_x$ $10^{-5}yr^{-1}$

The average longitudinal (balance) strain rate of the ice ($\dot{\varepsilon}_x$) has been calculated from the balance velocities (V), Map (2/2) along each flow-line as $\dot{\varepsilon}_x = \partial V/\partial x$. *These strain rates typically increase from* $0.5 \times 10^{-5}yr^{-1}$ *inland to over* $50 \times 10^{-5}yr^{-1}$ *towards the coast and the major ice shelf drainage basins.*

The values have been plotted and contoured over the ice sheet as shown in Map (2/3). The longitudinal strain rates are essentially positive on the large scales dealt with here. The magnitudes increase from low values of less than $1 \times 10^{-5}yr^{-1}$ in the inland regions to $50 \times 10^{-5}yr^{-1}$ near the coast and the edges of the major ice shelf basins. The increasing strain rate outwards is associated primarily with the increasing accumulation rate and decreasing ice thickness. The calculated strain rates can be compared with direct measurements of surface strain rates on the ice cap, provided sufficient is known of their variation with depth (cf. section 4.1), to make an assessment of the state of balance. However it is important to stress that because of the high irregularity of strain rates on the small scale (cf. Budd 1968) it is essential to obtain a wide observational coverage of large scale strain rates.

3.4.2. Transverse strain rates.

The mean "balance transverse strain rates" have been calculated from the velocity distribution $\overline{V}$ (2/2) and the flowline spacings Y (2/1) according to

$$\dot{\varepsilon}_y = \overline{V} \frac{1}{Y} \frac{dY}{dx} \qquad (3.18)$$

Again this relation has been approximated by taking flowlines about 100 km apart to determine the increments δY and δx in Y and x.

The resultant transverse strain rate contours are given as Map (2/4). Here the main features are the contrast between the positive divergence zones and the convergence (negative divergence) zones. The $\dot{\varepsilon}_y$ values in the central inland regions are typically positive and similar to the longitudinal strain rates (0.5 to $1.0 \times 10^{-5}yr^{-1}$). From here the lateral strain rates become more and more negative towards the major drainage basins and positive towards the major divergence regions between them. In both cases the magnitudes reach about $10^{-4}yr^{-1}$, which is about 1/5 of the longitudinal strain rates there.

Again we can expect a great deal of local variability so that only large-scale measured strain rates may be expected to be reliable indicators of the smooth patterns shown here.

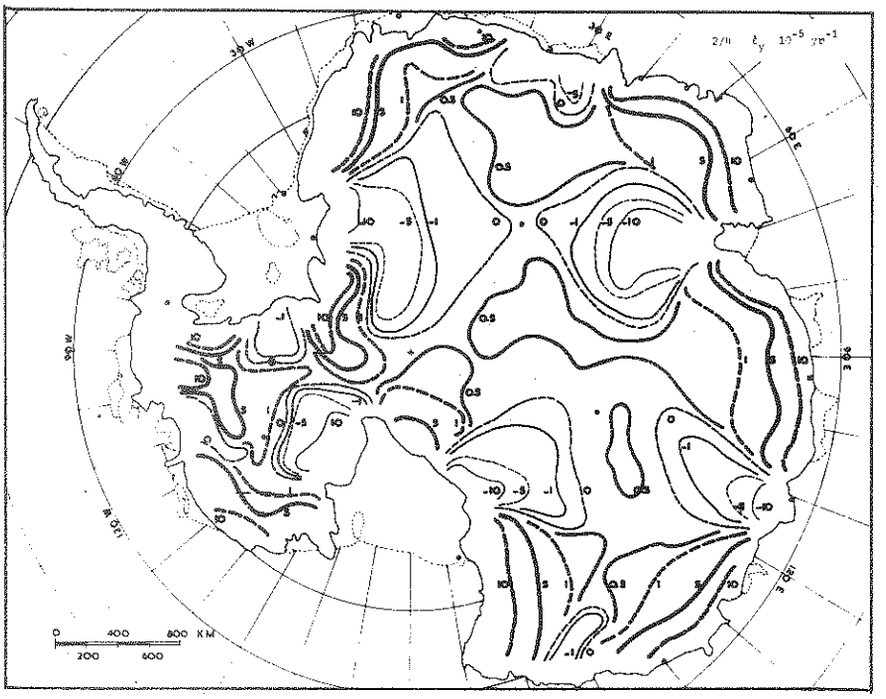

Map 2/4. Transverse strain rate $\dot{\varepsilon}_y$ $10^{-5}yr^{-1}$.

The transverse (balance) strain rate $\dot{\varepsilon}_y$ *has been calculated from the divergence of the flowlines* Y, *Map (2/1) and the balance velocities* V, *Map (2/2) as*

$$\dot{\varepsilon}_z = \frac{1}{Y}\frac{\partial Y}{\partial t} = \frac{1}{Y}\frac{\partial Y}{\partial x}\frac{\partial x}{\partial t} = \frac{1}{Y} V \frac{\partial Y}{\partial x}$$

where Y *is the distance between the flowlines at distance* x. *The contour pattern shows up the major regions of convergence (negative* $\dot{\varepsilon}_y$*) around the major drainage basins and divergence (positive* $\dot{\varepsilon}_y$*) along the ice divides. The strain rate magnitudes typically increase from* $0.5 \times 10^{-5}yr^{-1}$ *inland to over* $10 \times 10^{-5}yr^{-1}$ *near the coast.*

3.4.3. Total horizontal and vertical strain rates.

Regarding the ice density as constant a relation exists between the longitudinal ($\dot{\varepsilon}_x$), transverse ($\dot{\varepsilon}_y$) and vertical ($\dot{\varepsilon}_z$) strain rates, viz. the continuity equation

$$\varepsilon_{ii} = \dot{\varepsilon}_x + \dot{\varepsilon}_y + \dot{\varepsilon}_z = 0 \qquad (3.20)$$

Therefore

$$\dot{\varepsilon}_z = -(\dot{\varepsilon}_x + \dot{\varepsilon}_y) \qquad (3.21)$$

Thus the vertical strain rate has the magnitude and opposite sign of the sum of the two horizontal strain rates. In particular at the surface of an ice sheet in steady state balance the mean strain rate of a column over a fixed point of the bed is given by

$$\bar{\dot{\varepsilon}}_z = -\frac{A}{Z} \qquad (3.22)$$

where A is the ice accumulation rate and Z is the ice thickness. Hence

$$\dot{\varepsilon}_x + \dot{\varepsilon}_y = \frac{A}{Z} \qquad (3.23)$$

The values of $\dot{\varepsilon}_x + \dot{\varepsilon}_y = -\dot{\varepsilon}_z$ over the ice sheet have been calculated from (3.22), and are shown contoured in Map (2/5). They are in close agreement with the sum of $\dot{\varepsilon}_x$ and $\dot{\varepsilon}_y$ from Maps (2/3) and (2/4) and provide an additional check on the values of $\bar{V}$ and its derivatives. Since typically A increases and Z decreases towards the coast, $|\dot{\varepsilon}_z|$ also increases strongly. The major perturbations in ice thickness Z similarly show up in $\dot{\varepsilon}_z$.

The measurement of $\bar{\dot{\varepsilon}}_x + \bar{\dot{\varepsilon}}_y$ in the field is difficult. Even for the simple column model, in which the majority of the shear takes place at the base, such that the surface strain rate approximates the average value, it is difficult to measure the strain rate over a fixed point in the bed. This is because the surface markers used to measure the strain

rate travel with the ice. Hence it is necessary to make the strain grid large in comparison with its anticipated translation displacement.

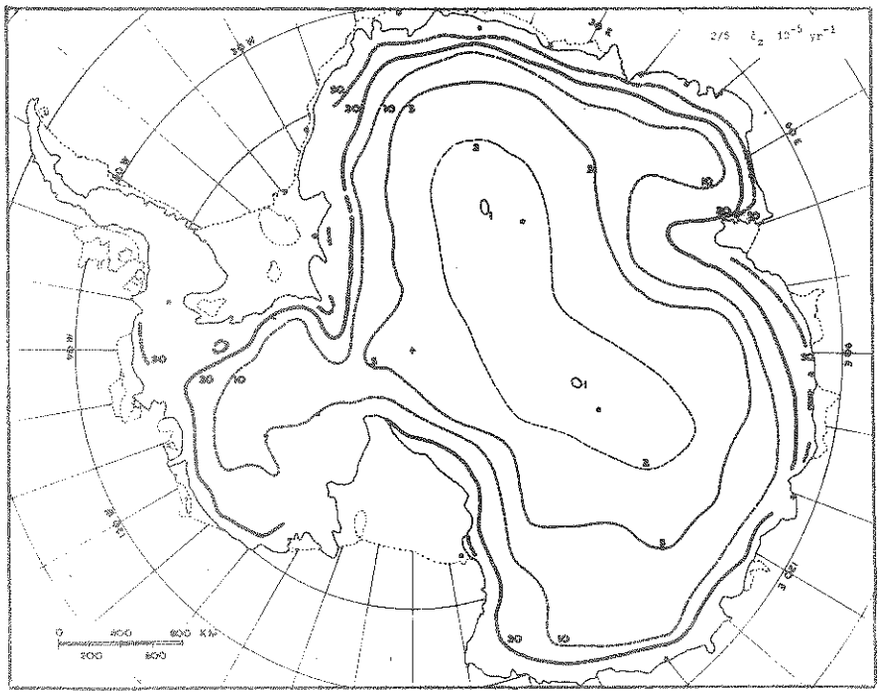

Map 2/5. Vertical strain rate $\dot{\varepsilon}_z$ $10^{-5}yr^{-1}$.

The average vertical strain rate through the ice for balance has been calculated from the ice thickness Z, *and accumulation rate* A *according to* $\dot{\varepsilon}_z = -A/Z$. *The magnitudes show a strong increase from* $1 \times 10^{-5}yr^{-1}$ *inland to about* $50 \times 10^{-5}yr^{-1}$ *near the coast. This is in reasonable agreement with the sum of the horizontal strain rates from Maps (2/3) and (2/4), viz.* $\dot{\varepsilon}_z = -(\dot{\varepsilon}_x + \dot{\varepsilon}_y)$.

One of the most promising ways of determining the vertical strain rate in regions of small slope and velocity is to measure the horizontal surface strain rates from grids, the vertical elevation change by gravity, and the accumulation rate. From these the balance of the ice sheet at that position can be obtained; in addition the relation between the mean vertical strain rate $\bar{\dot{\varepsilon}}_z = -A/Z$ and its surface value $-(\dot{\varepsilon}_x + \dot{\varepsilon}_y)$ can also be determined.

3.4.4. Balance volume flow.

The balance volume flow Φ has been calculated from the balance velocity $\overline{V}$ (2/2) and the ice thickness Z (1/3) according to

$$\Phi = \overline{V} Z \qquad (3.24)$$

Here the units are simply distance squared per unit time. However we are interested in the total outward volume flow, across unit distance of coastline say, so we have used the unit km^3/100 km/yr. This is then in line with the method of calculation using means over 100 km and flowlines a similar distance apart. The total mass flux rate is obtained simply by multiplying Φ by the density of ice ρ.

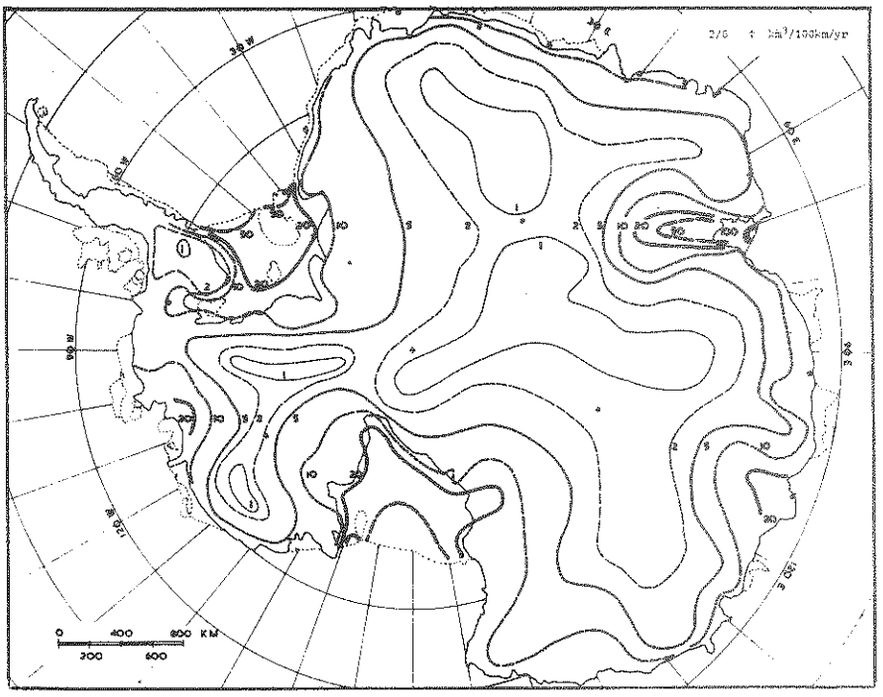

Map 2/6. Balance volume flow Φ km^3/100 km/yr.

The rate of outward ice flow along each flowline has been calculated from the ice thickness Z, Map (1/3) and balance velocity V, Map (2/2) as Φ = ZV. The volume flow increases typically from less than 1 km^3/100 km/yr inland to about 10 km^3/100 km/yr around most of the coast except for the three major ice shelf basins where the ice flow reaches 50-100 × 10^3km/100 km/yr and accounts for almost 50% of the total drainage.

The volume flow distribution is shown in Map (2/6) and represents at any position the integral of the surface accumulation rate from the centre. The values increase fairly smoothly from less than 1 km^3/100 km/yr inland to over 10 near the coast generally and the inland edges of the ice shelf basins, and over 50 km^3/100 km/yr at the major ice shelf fronts.

The total flow across the coast is given for the whole continent and its sub-sections in Table 3.2. The total outflow rate is $23.4 \times 10^2 km^3 yr^{-1}$; it may be seen that the three major ice shelf basins (segments 5-6, 11-13, 21-1) account for nearly 1/2 (45%) of the total outflow.

The volume flow depicted in Map (2/6) and in Table 3.2 (next page) provides one of the most direct means of assessing the balance of any particular region. The ice thickness and velocity need to be measured along a contour segment,and the accumulation rate over the generalised sector defined by that contour segment and the two flowlines through its end points. Again it is necessary to use large scales, and the most important task is to define the surface elevations with sufficient precision to determine the contours and the flowlines precisely.

Table 3.2.

Total volume outflow for Antarctica.

Segment boundary no.	Longitude at coast	Length of segment km	Mean flow rate km^3/100 km/yr	Total flow km^3/yr
1	166°E	2290	10	229
2	138°E	860	10	86
3	120°E	840	20	168
4	108°E	1700	10	170
5	73°E	160	100	160
6	90°E	160	10	16
7	66°E	540	5	27
8	53°E	1900	10	190
9	2°E	630	5	32
10	13°W	830	10	83
11	35°W	290	50	145
12	47°W	450	50	225
13	61°W	550	2	11
14	75°W	220	10	22
15	87°W	490	10	49
16	100°W	340	15	51
17	102°W	400	20	80
18	115°W	340	15	51
19	126°W	440	5	22
20	152°W	150	10	15
21	161°W	1020	50	510
	TOTALS	14,600		2,342

3.4.5. Particle paths.

For the simple mean column model considered so far, in which the ice moves outwards largely as a vertical column with the majority of the shear at the base, we also assume a constant vertical strain rate i.e. $\dot{\varepsilon}_z = \bar{\dot{\varepsilon}}_z = -A/Z$, a constant with depth. This gives for the vertical velocity at depth z

$$w_z = \frac{A}{Z} z \tag{3.25}$$

If we neglect for the moment the basal melting and also the low density firn at the surface, w_z varies linearly from A (the accumulation rate in cm ice/yr) at the surface to zero at the base. The particle paths of the ice for such a steady state ice sheet along a flowline may be calculated from the two velocities, $\bar{V}$ and w_z, which are in turn calculated from the accumulation and ice thickness distributions and the flowlines.

In particular the position of an ice particle at time t_1 from its arrival on the surface is given by the depth z_1

$$z_1 = \int_0^{t_1} \frac{A}{Z} z \, dt \tag{3.26}$$

and the distance X_1 from its start

$$X_1 = \int_0^{t_1} \bar{V} \, dt \tag{3.27}$$

Illustrations of the particle paths and ages of the ice will be discussed with the vertical section profiles in Chapter 7. Here we merely introduce the particle path concept to define the quantities "total residence time" and "age of the ice" which can be more readily illustrated by plan maps.

For cases in which we know the vertical profile of the horizontal velocity (e.g. from the temperature profile) it is possible to improve on the above "column" or "uniform strain" model by incorporating the variation of strain rate with depth. In this case if V_z is the velocity at

depth z and V_s the velocity at the surface, then the vertical strain rate may be taken as

$$\dot{\varepsilon}_z = \frac{V_z}{V_s}\frac{A}{Z} \tag{3.28}$$

Similarly

$$w_z = \frac{V_z}{V_s}\frac{A}{Z}\,z \tag{3.29}$$

and using these values for w_z and V_z the particle paths may be found as before.

3.4.6. Balance residence times.

The total time taken by a particle of snow deposited on the surface of an ice sheet to reach the coast represents the total time that ice spends in the ice sheet, so may be termed the "residence time". For a steady state ice sheet using the column model this time may be calculated from the balance mean velocity distribution $\overline{V}_x$ as follows: If t_1 is the time a particle is at the surface at position x_1 along a flowline, and t_c is the time it reaches the coast $x = x_c$, then the residence time is given by

$$T = t_c - t_1 = -\int_{x_1}^{x_c} \frac{1}{\overline{V}}\,dx \tag{3.30}$$

These residence times were actually calculated in the course of the flowline calculations described below (section 4.1.1) but could equally well have been derived directly from the velocity distribution of Map (2/2) and the flow lines of Map (2/1).

The resultant contours shown in Map (2/7) indicate that the snow deposited in the central zone of East Antarctica takes some five hundred thousand years to reach the coast, whereas the corresponding times for central West Antarctica are about fifty thousand years. As the coast is approached the residence time drops quickly to less than one thousand years.

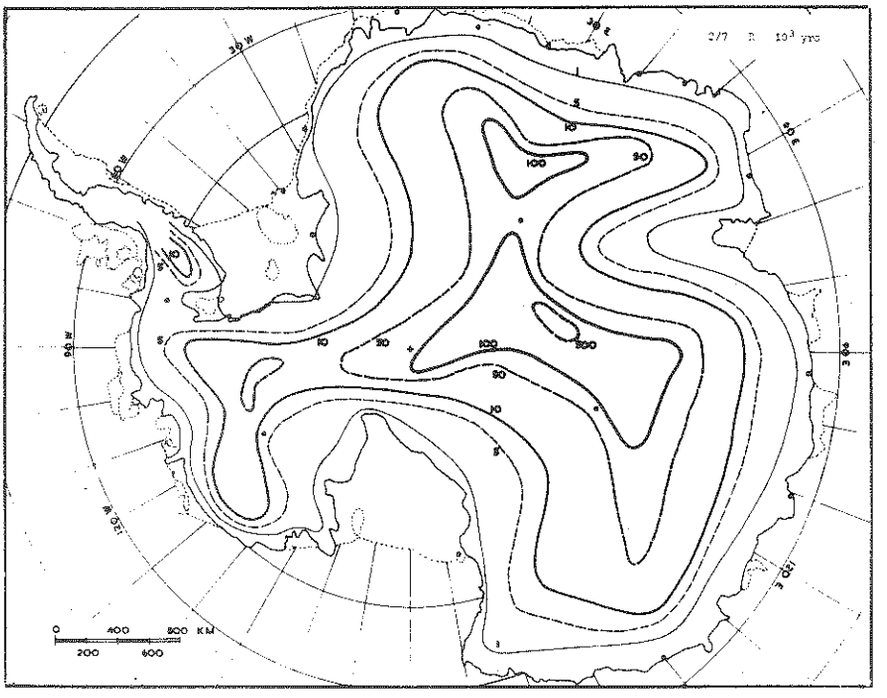

Map 2/7. Balance residence time R 10^3 *yrs.*

The balance residence times for the ice have been calculated from the balance velocities (2/2) and the flowlines (2/1) as the times taken for the ice accumulating at the surface to reach the coast. Residence times typically decrease from 500,000 yrs in central East Antarctica to less than 1,000 yrs near the coast.

For the non-constant strain model, incorporating the vertical profile of velocity, these large differences between the residence times of the inland and coastal ice become even more accentuated because of the older ice becoming concentrated into the low velocity layers near the base.

3.4.7. The ages of the ice for balance.

Using the balance values of the horizontal and vertical velocities of the ice, V_z and w_z, the age levels of the particles in the ice, counted from the time when they were deposited at the surface, can be constructed in a similar way to the particle paths. The time taken to travel each horizontal distance element δx is given by

$$\delta t = \frac{1}{V_x} \delta x \qquad (3.31)$$

and the vertical distance moved during this time is

$$\delta z = w_z \, \delta t \qquad (3.32)$$

In this way the particle paths and ages of the ice may be constructed simultaneously for a two-dimensional flowline profile. These ages have also been calculated in conjunction with the flowline calculations discussed in section 4.1.4 and also will be illustrated by profiles in Chapter 7. Here we just consider the plan map illustrating the age distribution of the ice over the whole ice sheet. To do this we have plotted the age of the ice at the depth of 90% of the ice thickness below the surface and at the 50% depth. These have been contoured and are illustrated in Map (2/8), with the 90% level a full line and the 50% level a broken line.

In the central regions of East Antarctica there is an old core with the 90% level older than 200,000 years and the half-depth older than 50,000 years. For West Antarctica the corresponding ages are less: 30,000 and 10,000 years respectively. These ages decrease markedly outward, approaching 20,000 and 5,000 years respectively near the coast.

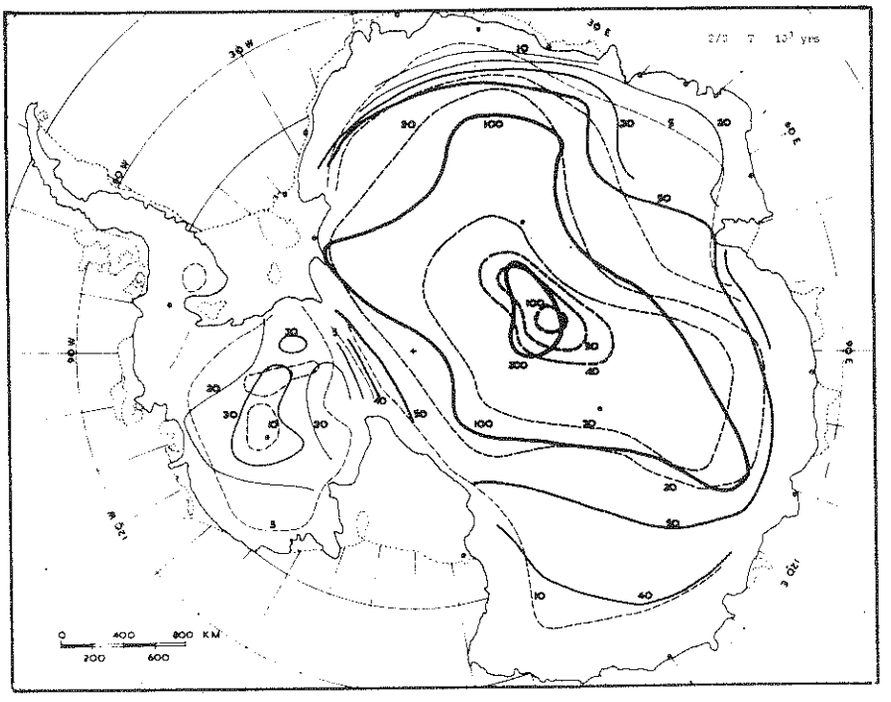

Map 2/8. Balance ages of the ice T 10^3 yrs.

The ages of the ice at the 90% depth level (full line) and at the 50% level (broken line) have been calculated from the steady state velocities, the accumulation, and the particle paths. In East Antarctica the ages of the 90% level vary typically from 200,000 yrs inland to 20,000 yrs near the coast. For West Antarctica the ice is typically much younger and the corresponding values range from about 30,000 to 10,000 yrs.

4. TEMPERATURE CALCULATIONS.

4.1. Models used.

Using the balance velocities we now consider the calculation of the temperature distribution throughout the ice sheet from the heat conduction equation (3.8). In choosing a method for this calculation one of the chief limitations is the speed of present computers. To carry out a complete three-dimensional analysis with fine grid-point spacing seems to be too large a job at present, but future programmes of this type are discussed in Chapter 8. For the present work we have considered a number of simplifications which allow a variety of models to be used, with computation times ranging from about one hour for a complete two-dimensional flowline to a few seconds for a single fixed column. The objective here is to obtain a complete coverage of Antarctica. Since the ice sheet is about 4,000 km in diameter, some 300 points are sufficient to cover Antarctica at about 200 km spacing with the fixed "column model" calculations. Hence a complete coverage output can be obtained in less than ½ hour computer time. By contrast some 50 flowlines are required to give a coverage to 200 km spacing. Hence over 50 hours computation time are required for a complete "flowline model" coverage.

It is a relatively simple matter to run through a number of complete column model coverages with different values of the input, e.g. geothermal flux, or a velocity field representing everywhere some fraction, say one half, of the balance velocity. In this way we can examine the effects on the output of a number of such variations. By contrast limitations of available computer time make it quite a formidable task to re-run a complete coverage of the flowline calculations.

The aim here has been to compare the outputs of the column and flowline models to examine their differences, then with the main coverage provided by the flowline calculations to study the variations resulting from different inputs by means of a number of column model coverages. The particular flowlines used for the main coverages are shown in Map (2/1a) below as heavy lines superimposed on the flowlines of Map (2/1).

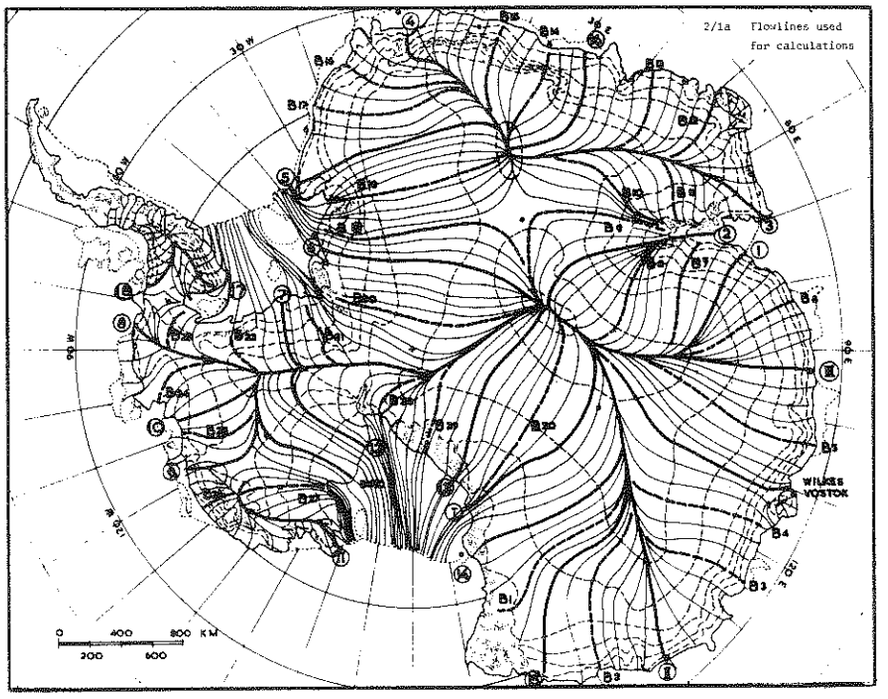

Map 2/1a. Flowlines used for calculations.

The full lines represent the flowlines used for the preliminary coverage discussed by Budd et al (1970). The broken lines with B numbers were added to make the density comparable to that of the fixed column coverage.

We now examine the main features of the different models.

4.1.1. Steady-state column.

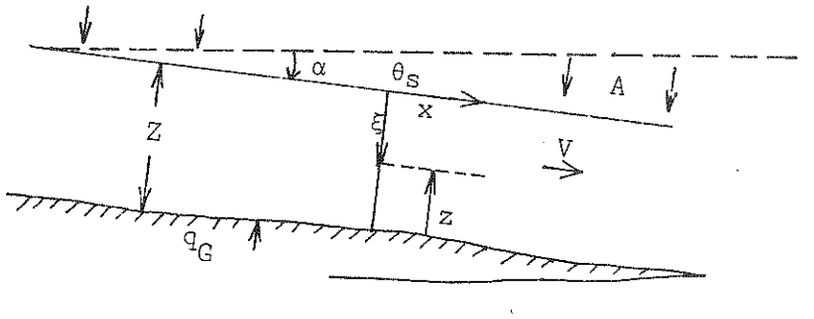

FIG. 4.1 Coordinates used for temperature calculations.

In section 3.2 we found the heat conduction equation (3.11) for a uniform slab of ice of thickness Z moving down an inclined slope α with average velocity $\bar{V}$ and velocity u_z at depth z, in the form

$$\kappa \frac{\partial^2\theta}{\partial z^2} + \frac{Az}{Z}\frac{u_z}{u_s}\frac{\partial\theta}{\partial z} + u_z\frac{\partial\theta}{\partial x} + \rho g\alpha\xi\frac{\partial u_z}{\partial z} = \frac{\partial\theta}{\partial t} \qquad (3.11)$$

For the small slopes encountered in Antarctica we can make the approximations

$$\sin\alpha \simeq \tan\alpha \simeq \alpha, \qquad \text{and} \qquad \cos\alpha \simeq 1.$$

Hence we need not distinguish between the magnitudes of the down-slope and horizontal velocities.

The essence of a column model is that the horizontal dimension does not appear explicitly as a variable in the equation. This may best be achieved, not by neglecting the variations with x, but by expressing them and all other terms of (3.11) as functions of z. A number of such one-dimensional models have been studied already e.g. Weertman (1968), Budd (1969), Dansgaard and Johnsen (1969), Radok et al. (1970). We begin with the simplest models and then progressively incorporate increasing complexity.

4.1.2. Non-deforming slab.

The simplest form of the heat conduction equation for a slab of thickness Z with surface temperature θ_s and basal gradient γ_G for no movement or accumulation is given by

$$\kappa \frac{\partial^2 \theta}{\partial z^2} = 0 \qquad (4.1)$$

with the boundary conditions

$$z = Z, \quad \theta = \theta_s; \qquad z = 0, \quad \frac{\partial \theta}{\partial z} = \gamma_b$$

The corresponding temperature profile is just a straight line determined solely by the surface and bed boundary conditions. As each additional parameter is considered the profile will be modified in a definite way. When the base reaches the pressure melting point (θ_m) the profile is determined by the surface and basal temperatures (θ_s and θ_m) and the remainder of the basal flux goes into melting according to

$$M = \frac{K(\gamma_G - \gamma_b)}{L} \qquad (4.2)$$

where γ_b is the computed base gradient
γ_G is the geothermal gradient
L is the latent heat of fusion.

4.1.3. Constant strain rate.

In this case we consider a profile through a uniform horizontal ice slab which is not moving horizontally but is staying in balance with accumulation rate A at the surface and uniform strain rate throughout the slab i.e.

$$\dot{\varepsilon}_{zz} = -\frac{A}{Z} \tag{4.3}$$

The boundary conditions are the same $\theta_Z = \theta_s$, $\gamma_b = \gamma_G$. The heat conduction equation becomes

$$\kappa \frac{\partial^2\theta}{\partial z^2} + \frac{Az}{Z}\frac{\partial\theta}{\partial z} = 0 \tag{4.4}$$

This model is useful for central regions of ice caps where flowlines start and the horizontal velocity is close to zero.

4.1.4. Constant advection.

We now consider the uniform slab moving down an inclined plane of slope α, sliding as a block with velocity V and remaining in a steady state of mass balance with accumulation rate A. The strain rate is constant as before, $\dot{\varepsilon}_{zz} = -\frac{A}{Z}$. Now let the surface temperature vary along the surface at a constant rate, say $\frac{\partial\theta_s}{\partial x} = \alpha\lambda$, where $\lambda = \frac{\partial\theta_s}{\partial z}$. Under these conditions we may expect the advection rate to be constant throughout the column viz.

$$V\frac{\partial\theta_s}{\partial x} = V\alpha\lambda \tag{4.5}$$

This defines the constant advection model.

4.1.5. Basal heating.

We note that in the case of advection there is additional heating $\tau_b V$ caused by the friction where τ_b is the basal stress. Hence we modify the lower boundary condition to

$$\gamma_b = \gamma_G + \frac{\tau_b V}{JK} \tag{4.6}$$

This defines the basal heating model. Incorporating this boundary condition with the constant advection model our equations now become

$$\kappa \frac{\partial^2 \theta}{\partial z^2} + \frac{Az}{Z} \frac{\partial \theta}{\partial z} = V\alpha\lambda \tag{4.7}$$

$$\theta_{z=Z} = \theta_s, \qquad \left.\frac{\partial \theta}{\partial z}\right)_{z=0} = \gamma_G + \frac{\tau_b V}{JK} \tag{4.8}$$

Equations (4.7) and (4.8) constitute the main "column model" which has been used to obtain large coverage and rapid output. It covers most of the essential features with the following five variables:

ice thickness Z

accumulation rate A

surface warming rate $S = V\alpha\lambda$

basal gradient $\gamma_b = \gamma_G + \tau_b V/JK$

surface temperature θ_s

Further modifications to this model may be considered as minor refinements, since typical variations of other effects produce only small deviations in the results, compared to the usual variations in these main five parameters. The power of this model is shown by the fact that it has enabled Budd et al (to be published) to fit the observed Camp Century temperature profile with an error standard deviation of .03°C and the Byrd profile to 0.4°C (cf. Fig. 5.3 and section 5.5.5).

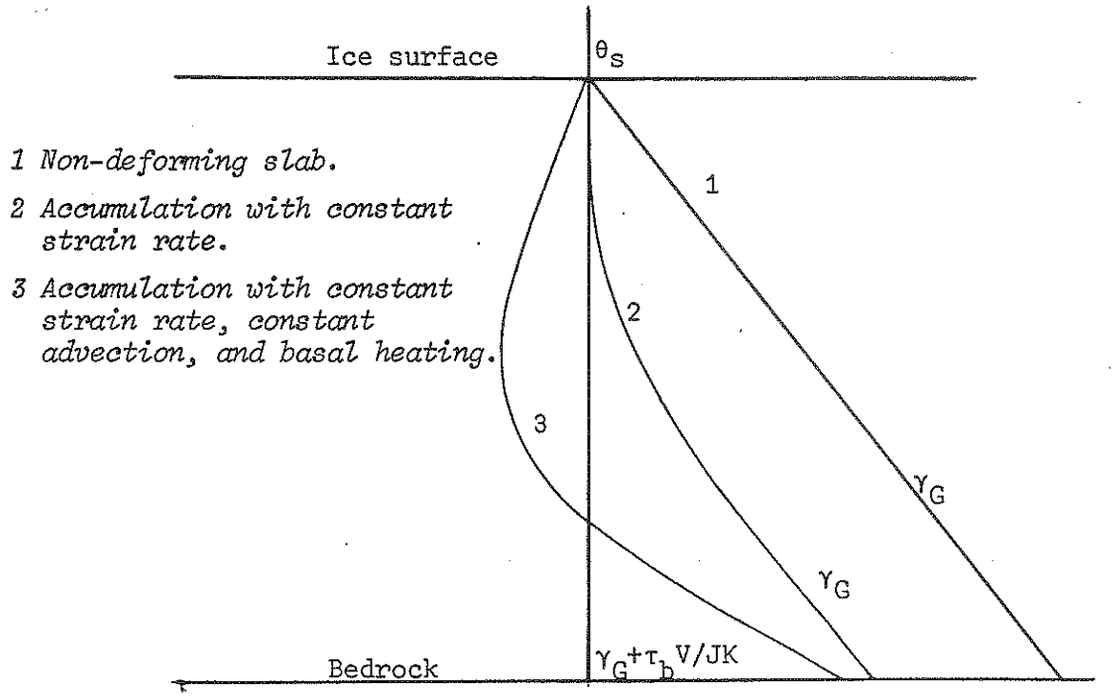

FIG. 4.2 Effect of different model features on the temperature profile of an ice column (schematic)

4.1.6. Layer heating.

In this case we consider the heat of friction as being distributed throughout the medium according to the values of stress τ_{xz} and strain rate $\dot{\varepsilon}_{zz}$ at all depths:

$$Q_z = \tau_{xz}\dot{\varepsilon}_{xz} \tag{4.9}$$

With a flow law of the type

$$\dot{\varepsilon}_{xz} = \mu' \tau^3_{xz} e^{\nu\theta} \tag{4.10}$$

where μ' and ν are given constants, the heat conduction equation becomes

$$\kappa \frac{\partial^2\theta}{\partial z^2} + \frac{Az}{Z}\frac{\partial\theta}{\partial z} + \mu'(\rho g\alpha\xi)^4 e^{\nu\theta} = V\alpha\lambda \qquad (4.11)$$

with

$$\frac{dV}{dz} = \mu'(\rho g\alpha\xi)^3 e^{\nu\theta} \qquad (4.12)$$

and boundary conditions

$$\theta_{z=Z} = \theta_s \qquad \left.\frac{\partial\theta}{\partial z}\right)_{z=0} = \gamma_G \qquad V_{z=0} = 0 \qquad (4.13)$$

Equations (4.11) and (4.12) have been solved simultaneously for the temperature θ and velocity V, with the numerical techniques described in Chapter 5. The effect of this internal heating on the temperature profile has been discussed by Budd (1969) and Radok et al (1970). The main effect is to create a slight upward convex curvature in the basal layer with a subsequent colder basal temperature. This effect becomes greater with the increase of internal heating.

An additional advantage of this model is that the surface velocity V_s or the average velocity $\overline{V}$, if known, can be used to determine the effective flow law constant μ compatible with the other conditions. A disadvantage of this model has been the problem that no solution appears to exist for certain values of the variables (cf. section 5.5.4). This has been discussed by Budd (1969); a similar feature was pointed out by Lliboutry (1968). A second disadvantage is the considerably greater computer time required for the solution of equations (4.11) to (4.13), in comparison to equations (4.7) and (4.8), which are for basal heating.

4.1.7. Variable strain rate.

Once we have the velocity profile u_z, either from the layer heating model, or simply from the temperature profile θ corresponding to some other model, and the relation

$$\frac{\partial u}{\partial z} = \mu'(\rho g \alpha \xi)^n e^{\nu\theta} \tag{4.14}$$

it becomes possible to improve on the constant strain rate and constant advection models by incorporating the variation of velocity with depth.

$$\dot{\varepsilon}_{zz} = \frac{A}{Z}\frac{u_z}{V} \qquad \frac{\partial \theta_z}{\partial t} = u_z \frac{\partial \theta_s}{\partial x} \tag{4.15}$$

The heat conduction equation then becomes

$$\kappa \frac{\partial^2 \theta}{\partial z^2} + \frac{Az}{Z}\frac{u_z}{V}\frac{\partial \theta}{\partial z} + \mu'(\rho g \alpha \xi)^n e^{\nu\theta} = u_z \alpha \lambda \tag{4.16}$$

with

$$\frac{\partial u}{\partial z} = \mu'(\rho g \alpha \xi)^n e^{\nu\theta} \tag{4.17}$$

4.1.8. Variable thermal parameters of ice.

If the ice properties (conductivity K, density ρ, specific heat c, or diffusivity κ) vary with position or temperature the heat conduction equation must be considered in its basic form (cf. Carslaw and Jaeger 1959).

$$\rho c \frac{\partial \theta}{\partial t} + \frac{\partial}{\partial x_i}\left(-K \frac{\partial \theta}{\partial x_i} + \rho c \theta u_i\right) + Q = 0 \tag{4.18}$$

where u_i is the velocity vector at x_i and Q is the rate of heat production per unit volume per unit time. For treatment of variable density and thermal properties with prescribed position in the ice the equation can be used as it stands. In the present context the important variation is that of the conductivity and specific heat with temperature. The variation of these thermal properties with temperature over the range we meet in Antarctica (0°C to -60°C) is illustrated in Fig. 4.3 (from Budd 1969), with data from several sources.

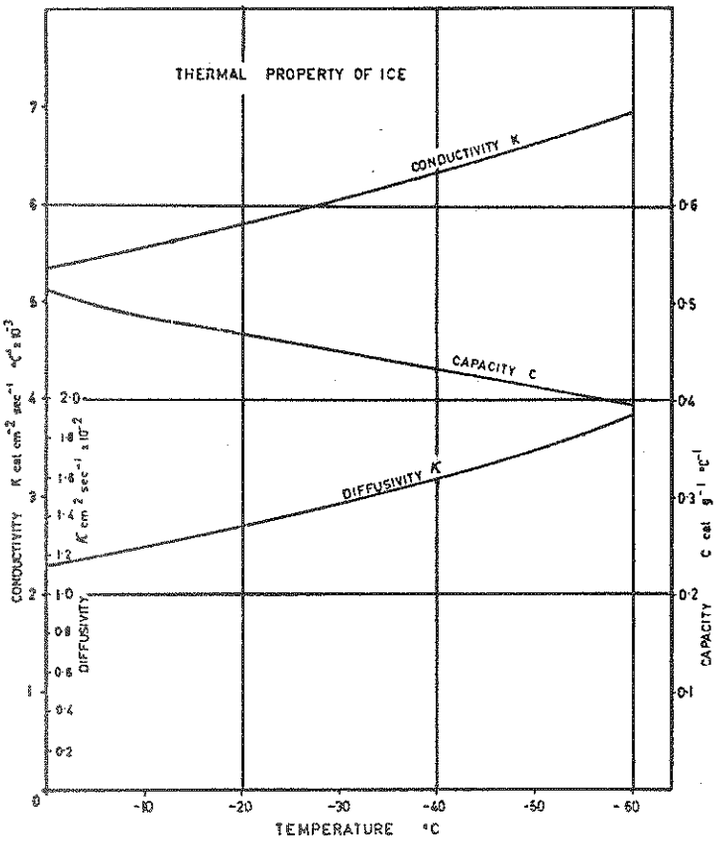

FIG. 4.3 The thermal properties of ice as functions of temperature (after Budd 1969)

Since $\frac{1}{K}\frac{\partial K}{\partial \theta}$ and $\frac{1}{c}\frac{\partial c}{\partial \theta}$ are small fractions the modifications to the temperature profile in typical cases is minor. A first approximation to the treatment of the variable thermal parameters is to use the constant parameter form of the heat conduction equation

$$\frac{\partial \theta}{\partial t} + \kappa \frac{\partial^2 \theta}{\partial x_i^2} + u_i \frac{\partial \theta}{\partial x_i} + \frac{Q}{K} = 0 \qquad (4.19)$$

but take for κ and K their proper values as functions of temperature.

The errors involved in this approximation can be assessed from the omitted terms

$$\frac{1}{K}\frac{\partial K}{\partial \theta}\frac{\partial \theta}{\partial x_i} + \frac{\rho c}{K}\left(u_i + \frac{1}{c}\frac{\partial c}{\partial \theta}\theta u_i\right) \qquad (4.20)$$

Operational solutions for variable parameters have been developed numerically from the solution with constant parameters by recycling with the variable parameters. In general only minor modifications of the temperature profiles have resulted.

4.1.9. Non-steady state ice sheet.

An ice sheet is in a non-steady state when it is undergoing local changes in any of its controlling parameters. Here we consider separately (a) climatic changes in temperature and (b) local changes in ice thickness.

(a) Temperature change with time (constant-shape temperature profile; steady-state gradient).

If we have a constant climatic change going on for a long time its effect may be incorporated into our model by simply adding a $\frac{\partial \theta}{\partial t}$ term. In fact any prescribed function of depth may be used for the warming (or cooling) rate and provided it were constant with time a form of steady-state temperature profile would be set up corresponding to the solution of

$$\kappa \frac{\partial^2 \theta}{\partial z^2} + w_z \frac{\partial \theta}{\partial z} + Q_z = -u_z \frac{\partial \theta}{\partial x} + \frac{\partial \theta}{\partial t} \qquad (4.21)$$

$$= \frac{D\theta}{Dt}$$

with

$$\theta_{z=Z} = \theta_s \qquad \text{and} \qquad \left.\frac{\partial \theta}{\partial z}\right)_{z=0} = \gamma_b \qquad (4.22)$$

In the interpretation of measured temperature profiles the $\frac{D\theta}{Dt}$ term represents the combined effects of advection and long term climatic change.

(b) Varying ice thickness.

By adopting for the vertical a variable relative coordinate (cf. Chapter 5)

$$\zeta = \frac{z}{Z} \tag{4.23}$$

the heat conduction equation can be made applicable to a rising or sinking ice sheet with the appropriate conditions for the moving boundaries. The solution of the equations

$$\kappa \frac{\partial^2 \theta}{\partial \zeta^2} + w_\zeta \frac{\partial \theta}{\partial \zeta} + Q_\zeta = \frac{D\theta}{Dt} \tag{4.24}$$

with

$$\theta_{\zeta=1} = \theta_s, \qquad \left.\frac{\partial \theta}{\partial \zeta}\right)_{\zeta=0} = \gamma_b \tag{4.25}$$

or

$$\theta_{\zeta=0} = \theta_m \tag{4.26}$$

may then be used to analyse the temperature in an ice sheet of varying thickness. This ice sheet is not in balance and

$$\frac{\partial Z}{\partial t} = A + \frac{\partial \bar{V} Z}{\partial x} \tag{4.27}$$

The changing surface elevation $\frac{\partial Z}{\partial t}$ is associated with a surface temperature change

$$\frac{\partial \theta_s}{\partial t} = \lambda \frac{\partial Z}{\partial t} \quad \text{say.} \tag{4.28}$$

which is then included in $\frac{D\theta}{Dt}$ in the same way as a climatic change.

These generalisations of the heat conduction equation to a non-steady state ice sheet greatly increase the power of the simple column model for analysing measured temperature profiles and in addition lead on to the even more powerful flowline model.

4.1.10. Flowline.

So far the equations used have all been one-dimensional - i.e. heat conduction has been considered in the vertical. The models of the "column" series are appropriate for situations in which conditions do not vary greatly along the line of flow i.e. A, Z, $\frac{D\theta}{Dt}$ vary but slowly along the flowline. In many cases this approximation is realistic but in other situations high gradients of ice thickness, accumulation or surface warming exist.

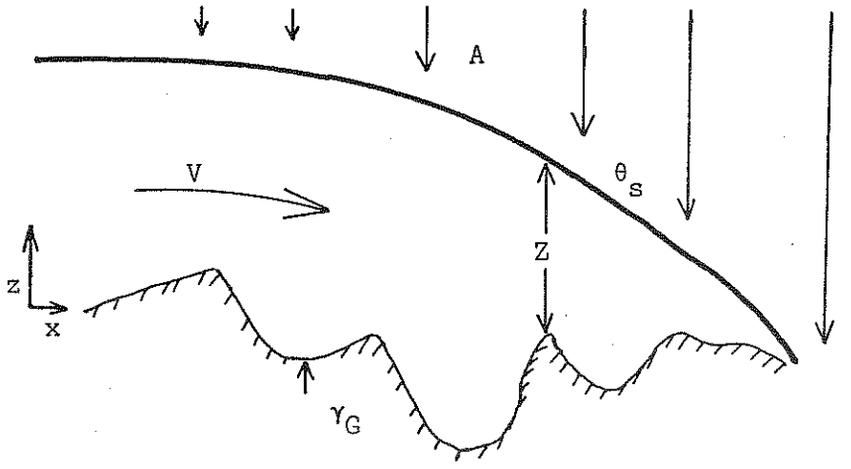

FIG. 4.4 Vertical section of an ice sheet showing parameters for flowline calculations (schematic)

Under these conditions the simple steady-state column model is unsatisfactory since it is difficult to express the term $\frac{\partial\theta}{\partial x}$ as a realistic function of z. A method suggested by Weertman (1968) was to solve the basic Robin (1955) steady state equation for several positions along a flowline and use these to calculate $\frac{\partial\theta}{\partial x}$. Obviously this method may be repeated to obtain better profiles and values of $\frac{\partial\theta}{\partial x}$.

However the model for a non-steady state ice cap with variable thickness and warming rate allows us to start with the steady state solution at the ice sheet centre and follow a column moving outwards along a flowline, using the prescribed values of ice thickness Z, accumulation rate A, surface temperature θ_s, and warming rate $\frac{\partial\theta_s}{\partial x}$

according to

$$\kappa \frac{\partial^2\theta}{\partial z^2} + w_z \frac{\partial\theta}{\partial z} + Q_z = \frac{D\theta}{Dt} \tag{4.29}$$

$$\theta_{z=Z} = \theta_s \qquad \left.\frac{\partial\theta}{\partial z}\right)_{z=0} = \gamma_b \tag{4.30}$$

By choosing time steps sufficiently small the variations of the parameters can be accommodated and the complete two-dimensional temperature field in x and z evaluated. Such a technique also makes it possible to keep a tab on the particle paths and ages of the ice in the course of the progress of the column towards the coast.

The condition of basal melting is treated similarly as for the fixed column model; where the base temperature reaches pressure melting point (θ_m) this becomes the basal boundary condition for the temperature profile instead of γ_b and the melting rate is found from

$$M = \frac{K(\gamma_b - \gamma_c)}{L} \tag{4.31}$$

where γ_c is the computed base gradient.

The problem of what happens to the meltwater has been difficult to solve with the flowline model, because the cases in which the meltwater flows back upstream could not easily be treated. The water flow for two dimensions in general is governed by the surface and bed slopes, α and β respectively, and by the ice and water densities, ρ_I and ρ_W, such that the flow is down the pressure gradient given by

$$\frac{dp}{dx} = \rho_I g \frac{\partial Z}{\partial x} + \rho_W g\beta \tag{4.32}$$

$$= \rho_I g(\alpha - \beta) + \rho_W g\beta$$

$$= \rho_I g + g\beta(\rho_W - \rho_I) \tag{4.33}$$

$$= \rho_I g\alpha\left(1 + \frac{\beta\Delta\rho}{\alpha\rho_I}\right) \tag{4.34}$$

Thus the water flow is in the direction of the surface slope unless the bedrock slope becomes $\frac{\rho_W-\rho_I}{\rho_I} \simeq 10$ times the surface slope in the opposite direction. This means we can expect to find the meltwater being trapped in any pockets of the bedrock blocked on the downstream side by reverse slopes greater than about 10 times the surface slope. In three dimensions slightly modified conditions apply but taking the components of the slopes we obtain a similar conclusion.

The flowline model has not been developed to cater explicitly for the water flow but it turns out (and will be shown in Chapter 6) that the basal temperatures of the ice sheet tend to be warmer in bedrock hollows, and that the melt production tends to occur there, or near the coast and the ice shelf borders. None of our calculations showed melt to set in on bedrock rises. This simplified the situation and allowed the following procedure to be adopted. The amount of basal melt was calculated at each time step and the computation proceeded with the total amount of meltwater at the base formed up to that time. In addition the basal water column was subjected to the same strain thinning or thickening as the column of ice above it. As the freezing point was reached the water was converted back into ice until it was used up. In this way the moving column would often come to a low bedrock zone where melting would set in; then after crossing it refreezing would commence until the meltwater was gone. The base temperature was then able to drop below pressure melting again. Thus some flowline calculations gave rise to regions of isolated meltwater at the base of the ice sheet in the interior of Antarctica, cf. Budd et al.(1970).

4.1.11. Combined and general models.

For the results presented later in this report we have made wide use of the simple column model with basal heating, constant strain rate and warming throughout at the surface rate. This provided a rapid coverage and yielded the most important features for the large scale. The flowline model, also with basal heating and constant strain rate, has been used for a complete coverage of the Antarctic. Individual column and flowline calculations have been carried out for a number of different cases to examine the effect of the different models on the output, particularly the basal temperatures.

Since many of the models designated above are independent they permit a large number of combinations such as flowline or column calculations with basal or layer heating, with constant or variable diffusivity, with constant or variable strain rates, etc.

The main conclusions of the comparisons between different models was that for the coarse data available refinements to the basic fixed column and flowline models produced variations small compared to those we may expect to result from typical changes in our input data. Such parameters as geothermal heat flux, the ice velocities, and the state of the ice sheet, are all in question and, as discussed below, have been examined by making quite large changes to the input. The variation in the output resulting from these major input changes has been one of the main objectives of the present study.

As more information becomes available, such as measured velocities and temperature profiles, the more refined models will be useful for a more detailed analysis. Already this has proved possible for the Byrd and Camp Century temperature profiles extending right through the ice to bedrock.

4.2. Additional input requirements for temperature calculations.

(a) Flowline model.

For the simple flowline column model with basal heating and constant strain rate and horizontal velocity with depth we have the equation

$$\kappa \frac{\partial^2\theta}{\partial z^2} + \frac{Az}{Z}\frac{\partial\theta}{\partial z} = \frac{D\theta}{Dt} \qquad (4.35)$$

where the warming rate $\frac{D\theta}{Dt}$ is a function of depth with

$$\theta_{z=Z} = \theta_s, \qquad \gamma_b = \gamma_G + \frac{\tau_b V}{JK} \qquad (4.36)$$

and

$$\left.\frac{D\theta_s}{Dt}\right)_{z=Z} = V\frac{\partial\theta_s}{\partial x} \qquad (4.37)$$

Initially the flowline column starts in the centre (highest point) of the ice sheet with a temperature distribution for the steady-state fixed column with zero velocity and zero surface warming. The column then moves outwards along the flowline according to a prescribed velocity V and surface temperature changes prescribed along the surface profile. Thus the input data required along the flowline are values of

1) ice surface and base elevations (E and b)
2) accumulation rate (A)
3) surface temperature (θ_s)
4) horizontal velocity (V)

Input constants include diffusivity κ, conductivity K, and geothermal heat flux gradient γ_G. The computer calculates from these

1) surface warming $\frac{D\theta_s}{Dt}$
2) base gradient $\gamma_b = \gamma_G + \frac{\tau_b V}{JK}$

where the base stress is calculated from $\tau_b = \rho g \alpha Z$ and $\alpha = \frac{\partial E}{\partial x}$ is the surface slope.

Additional information needed for special by-product calculations such as dielectric absorption, dynamics velocities, etc. will be described in the following sections.

(b) Column model.

For the simple column model with basal heating and constant strain rate and advection we have

$$\kappa \frac{\partial^2\theta}{\partial z^2} + \frac{Az}{Z}\frac{\partial\theta}{\partial z} = \frac{D\theta}{Dt} \tag{4.38}$$

and

$$\theta_{z=Z} = \theta_s \qquad \left.\frac{\partial\theta}{\partial z}\right)_{z=0} = \gamma_G + \frac{\tau_b V}{JK} = \gamma_b \tag{4.39}$$

In this case the warming rate is taken as a constant throughout the column and equal to the surface warming rate i.e.

$$\frac{D\theta}{Dt} = V\frac{\partial\theta_s}{\partial x} = V\alpha\lambda \equiv S, \text{ a constant with depth.} \tag{4.40}$$

The input data required are values of

1) ice thickness (Z)
2) accumulation rate (A)
3) surface warming rate (S)
4) surface temperature (θ_s)
5) base gradient (γ_b)

Of these five parameters we already have discussed Z, A, θ_s. The surface warming is calculated from

$$S = V\alpha\lambda = V\frac{\partial\theta_s}{\partial E}\frac{\partial E}{\partial x} \tag{4.41}$$

using the balance velocity V, the surface temperature θ_s, and the elevation E; the gradients are calculated along the flowlines x.

The base gradient is calculated from

$$\gamma_b = \gamma_G + \frac{\tau_b V}{JK} \tag{4.42}$$

with

$$\tau_b = \rho g \alpha Z \tag{4.43}$$

Here again we use the ice thickness Z, the surface slope α and the balance velocity V; as before the parameters γ_G, K, κ, ρ, g must be specified.

Because of the importance of the five major parameters Z, A, S, θ_s and γ_b we proceed to examine their variation over the ice sheet. Since the parameters α, λ, and τ_b are needed for the calculation of S and γ_b we present maps of these first.

4.2.1. Surface slopes.

Using the elevation contours of Map (1/2), E, and the flowlines Map (2/1), the maximum surface slopes have been calculated along the flowlines (i.e. perpendicular to the contours) as

$$\alpha = -\frac{\partial E}{\partial x} \qquad (4.44)$$

These slopes represent the mean over the intervals between the contours, as smoothed to the order of about 100 km. The resultant slopes have been contoured and are illustrated in Map (3/1).

The pattern is one of very small slopes, less than 10^{-3}, in the central inland regions of both East and West Antarctica. However the slopes generally increase strongly towards the coast to about 10^{-2} in the last 100 km. The basins of the major ice shelves are exceptions, with the ice flowing into them reaching slopes of about 5×10^{-3}, then flattening out on the ice shelves themselves.

One other region of low slope is that between the high central region of East Antarctica and the Filchner Ice Shelf. The reasons for the variations in surface slope are not completely understood, but since the slope strongly influences the basal stress, which in turn affects the velocity, we may expect some relation between the surface slope and the base temperature. This is inferred from the velocity Map (2/2) which shows a steady velocity increase outwards towards the Filchner Ice Shelf. Such anomalies will be referred to further in the discussion of the output results in Chapter 6.

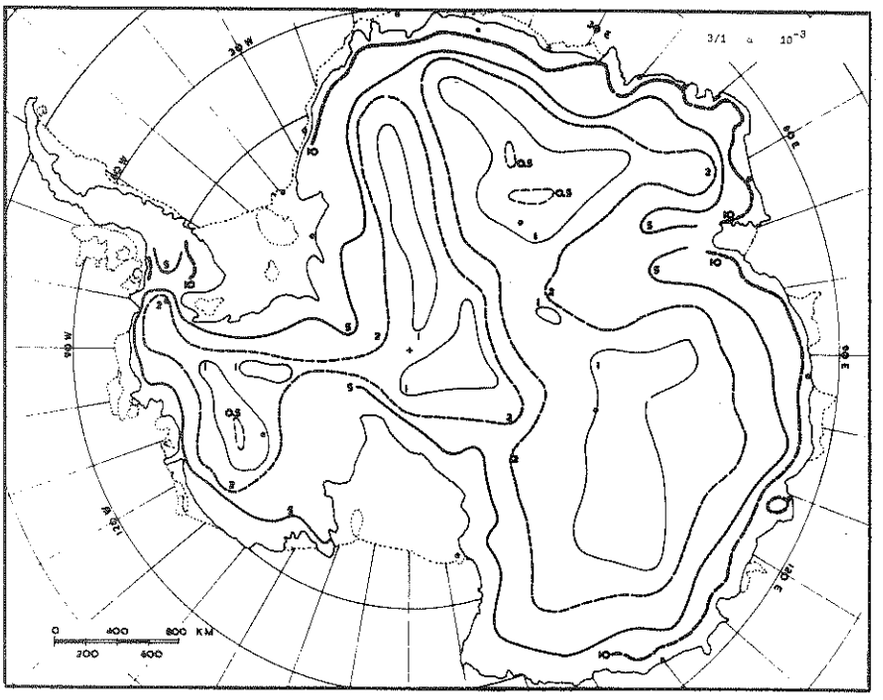

Map 3/1. Surface slope α 10^{-3}.

Regional surface slopes averaged over 100 km along the flowlines have been calculated from the flowline Map (2/1) and the ice surface elevations of Map (1/2). The general pattern shows a gradual increase from about 1 × 10^{-3} in the inland regions to about 1 × 10^{-2} near the coast. A region of anomalously low slopes appears between the East Antarctic summit and the Filchner Ice Shelf.

4.2.2. Basal shear stress.

From the maps for ice thickness, Z, and maximum surface slope α, the basal shear stress τ_b has been calculated as

$$\tau_b = \rho g \alpha Z \qquad (4.45)$$

where $\rho \simeq .91$ gm cm^{-2} has been taken as the mean density of the column and $g \simeq 982$ cm sec^{-2} as the gravitational acceleration.

The direction of τ_b is that of α i.e. along the flowlines. Again smoothing over 100 to 200 km has been adopted as for α and Z to derive contours, given in Map (3/2).

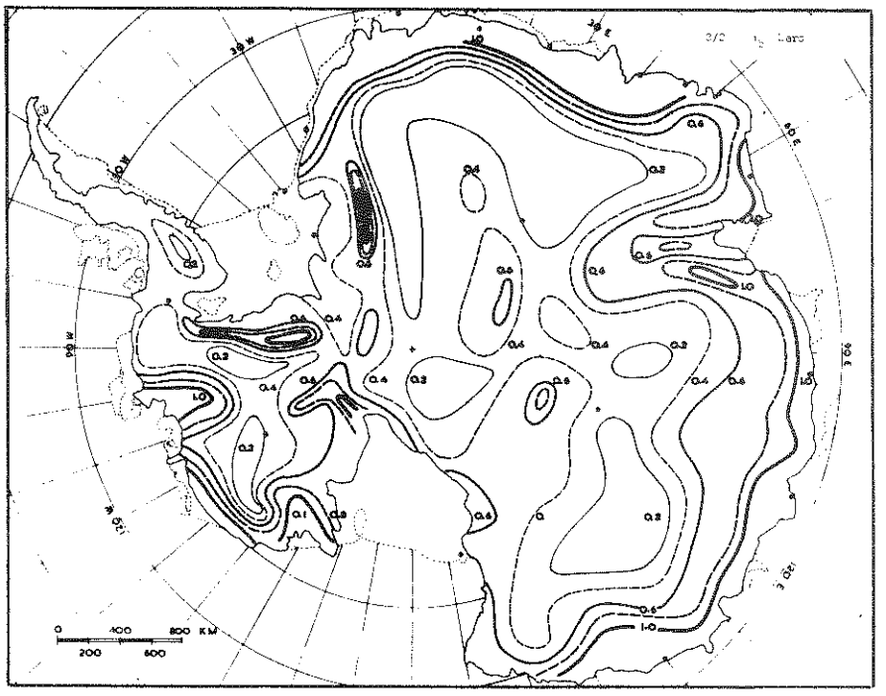

Map 3/2. Basal shear stress τ_b bars.

From the maps of ice thickness Z and surface slope α along the flowlines, smoothed over ~200 km, the basal stress (bars) has been calculated as $\tau_b = \rho g \alpha Z$ for each 200 km segment of the 500 m elevation contours. Typically the stress increase from 0.2 bars inland to about 1 bar near the coast. Local variations arise from the local variations in α and Z.

This map of base stresses is one of the most interesting of the present group. It shows the strong characteristics of the major ice thickness features and also the trend of increase towards the coast of the surface slopes, which more than compensates for the corresponding trend of decrease in ice thickness.

Overall the pattern can be described as a general increase in basal shear stress from about 0.2 bars inland to greater than 1 bar near the coast. Superimposed on top of this general trend are anomalies caused by the variations of ice thickness and surface slope associated with the bedrock features. The increase of basal stress towards the coast may be expected to be related to that of velocity. But it is necessary to consider the effects of the base temperature as well. We return to this in sections 6.1 and 6.10.

4.2.3. Geothermal heat flux.

So far very little is known of the value of geothermal heat flux in the Antarctic; hence we examine the information available in other areas. Lee and Uyeda (1965) have summarised measured heat flux values to that date; a more recent summary is given by Lee (1970). They concluded that the geological structure was the major parameter for which the heat flux values could be broadly grouped. Their mean values for these major groups from the existing data are indicated in the following table.

Table 4.1.

Geothermal heat flux.

Major geological feature	Geothermal heat flux Mean ± standard deviation $\mu cal\ cm^{-2} sec^{-1}$
Precambrian shield	0.98 ± .24
Paleozoic orogenic areas	1.43 ± .41
Post precambrian non-orogenic areas	1.49 ± .40
Mesozoic Cenozoic orogenic areas	1.76 ± .58
Ocean trenches	1.16 ± .70
Ocean basins	1.27 ± .53
Ocean ridges	1.90 ± 1.48

On the very large scale the Antarctic continent may be divided into two main geological provinces: East Antarctic, a typical Precambrian shield, and West Antarctica, a product of mountain building since Cambrian times. Hence although we may expect a great deal of smaller scale variation, we adopt for this study the classification of East Antarctica as in Lee and Uyeda's Precambrian shield category and West Antarctica as a Paleozoic orogenic area.

The histograms of geothermal flux measurements for these two types of regions are given in Fig. 4.5. For most of our studies we have taken the values 1.2 μcal $cm^{-2}sec^{-1}$ for East and Antarctica and 1.4 for West Antarctica, which lie near the mean values for the Precambrian shields and the Paleozoic orogenic areas, respectively.

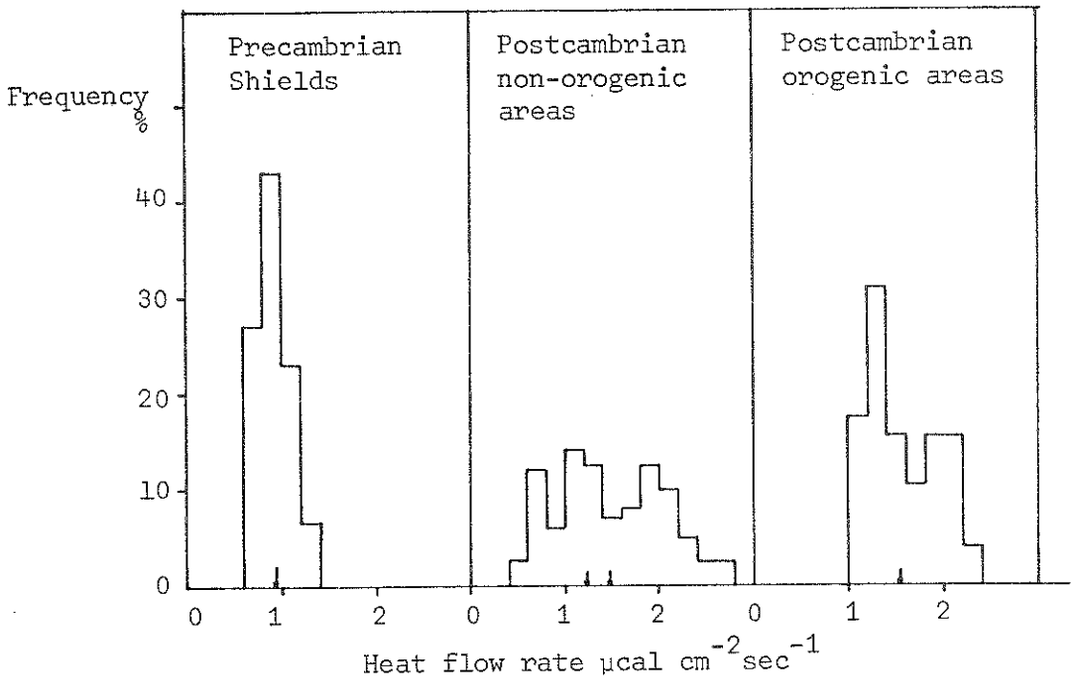

FIG. 4.5 Histograms of geothermal heat flux values over different geological regions (from Lee and Uyeda 1965)

In order to evaluate the effect of varying the geothermal heat flux values we also have run a complete coverage with higher values, 1.8 for East Antarctica and 2.1 for West Antarctica. In addition some flowline calculations, e.g., that through Byrd Station, have been run with different values of γ_G to study its effect on the basal melting features. Further developments will have to await some definite measurements of geothermal flux. These may be obtained by drilling into the rock below the ice; for regions with temperatures below pressure melting the basal gradient in the ice may be used if the ice velocity is also known. Of great importance here are those regions where the velocity is zero, such as dome summits or stagnation points. Here the geothermal flux could be obtained from the basal ice gradient alone, provided the temperature is below the pressure melting point.

4.2.4. Basal temperature gradients.

The contribution of the geothermal heat flux q_G to the temperature gradient at the base of the ice, when the temperature is below pressure melting is given by

$$\gamma_G = \frac{q_G}{K} \tag{4.46}$$

where K is the conductivity of ice.

As we have seen in section 4.1.8 the conductivity is dependent on temperature. Hence it is necessary to choose the value of K appropriate for the base temperature. Although this can be done in the course of a calculation, for the purpose of illustrating the variation in base gradient over the Antarctic we adopt a constant value of K, viz.

$$K = 5.4 \times 10^{-3} \text{ cal cm}^{-1}\text{sec}^{-1}{}^{o}\text{C}^{-1}$$

For the case of basal heating the base gradient is given by

$$\gamma_b = \gamma_G + \frac{\tau_b V}{JK} \tag{4.47}$$

where τ_b is the basal shear stress and V is the mean column velocity.

From the maps for velocity V (Map 2/2) and τ_b (Map 3/2) the values of γ_b have been calculated and contoured as shown in Map (3/3).

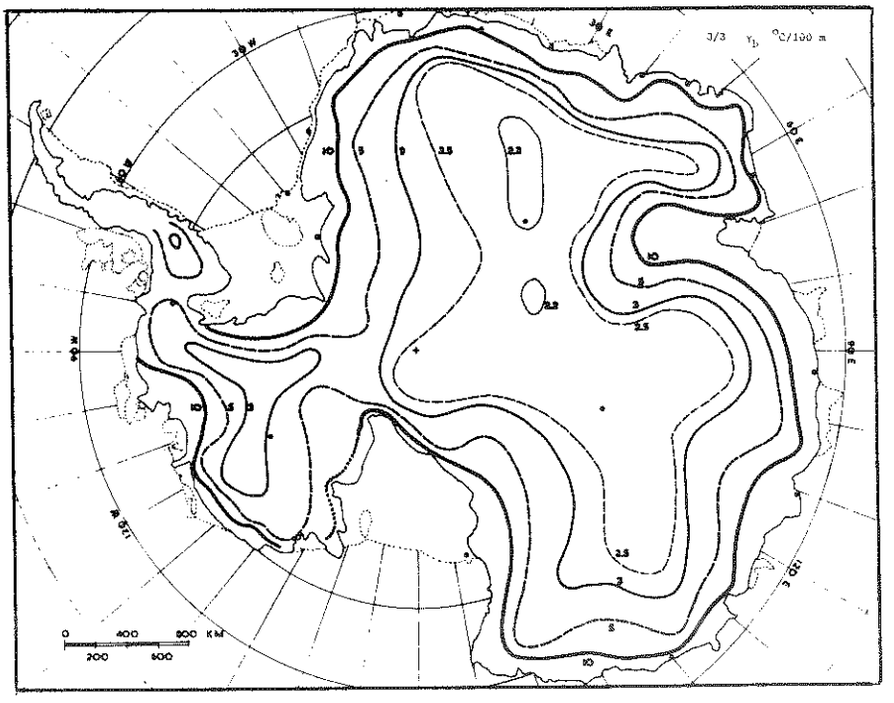

Map 3/3. Basal temperature gradient γ_b °C/100 m.

The temperature gradient near the base of the ice γ_b (in absence of melting) has been calculated for the simple 'basal heating' model as the sum of the geothermal heat flux gradient γ_G (taken as 2.2 and 2.6 °C/100 m in East and West Antarctica respectively) and the heat generated by the motion, assumed as being produced in a thin basal layer, $\gamma_b = \gamma_G + \tau_b V/JK$, where τ_b is the basal stress, V the average velocity, K the thermal conductivity, and J the mechanical equivalent of heat. The resulting gradients increase gradually at first then rapidly from γ_G near the centre to high values exceeding 10°C/100 m near the coast as the base stress and velocity become large.

The values of base gradient typically increase from 2.2°C/100 m in central East Antarctica and 2.6 in West Antarctica to values of about 10°C/100 m near the coast and the inland boundaries of the major ice shelves. The broad scale variation is comparatively smooth and greatly influenced by the strongly increasing trend the velocity distribution shows towards the

coast. Thus it is clear that the distribution of base gradient which would result from reducing the velocities to one half of the balance velocity would be a similar map to (3/3) with values ranging from 2.2 to 6.1 in East Antarctica where the values in (3/3) range from 2.2 to 10. Similarly the effect of systematic variation in the geothermal gradient γ_G can be readily assessed as an addition or subtraction to the values represented here.

4.2.5. Surface temperature-elevation gradient.

The vertical gradient (λ) of the surface temperature θ_s along the flowlines has been calculated from Map (1/6) for surface temperature (θ_s) and the elevations, Map (1/2), and flowlines, Map (2/1), according to

$$\lambda = \frac{\partial \theta_s}{\partial E} = \frac{\partial \theta_s}{\partial x} \Big/ \frac{\partial E}{\partial x} \qquad (4.48)$$

This vertical temperature gradient or "lapse rate" λ represents the total temperature change along the flowline at the surface and thus includes effects of elevation, latitude, continentality, surface heat budget etc. The calculation of λ is made difficult by the exaggeration of errors; i.e. small errors in θ_s or E lead to large errors in their gradients and their ratios. As a result of this the values have been smoothed over distances of about 200 km.

The resultant pattern of λ, as shown in Map (3/4) is quite complex. However several general trends are noticeable. Within about the first 500 km of the coast the λ values are about 1°C/100 m. Then in both East and West Antarctica there appears to be a definite zone of high gradients reaching over 2°C/100 m. This feature may be somewhat in the nature of a latitude effect but to a large extent occurs with a decreasing surface slope while the surface temperature continues to decrease inland more uniformly. Such a situation may be a result of a changing surface heat budget, reflecting the transition from strong katabatic winds in the coastal zone to lower windspeeds in the interior.

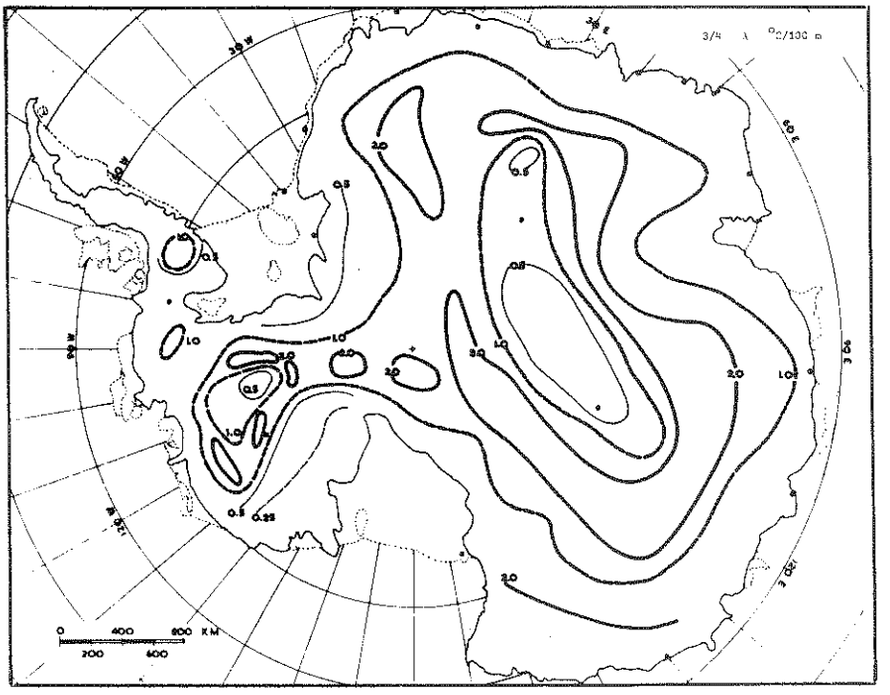

Map 3/4. Surface temperature-elevation gradient λ °C/100 m.

From the ice surface temperatures (θ_S) Map (1/6) and the elevations (E) Map (1/2) the vertical temperature gradient with distance along the flowlines has been calculated as $\partial\theta_S/\partial E = \partial\theta_S/\partial x \;/\; \partial E/\partial x$. *Obviously other effects such as latitude and continentality are also included. These temperature gradients typically increase from 0.5 °C/100 m far inland to maxima exceeding 2 °C/100 m several 100 km inland, then decrease to 1 °C/100 m near the coast.*

Further inland the gradients tend to decrease to values of about 0.5°C/100 m in the high central zones. Since the temperature data is still sparse it is difficult to assess any deviations from the general trends.

A number of workers have discussed the surface lapse rate λ over limited areas (Mellor 1960, Bogoslovskiy 1958, Crary 1961, Lorius 1964, Shimizu 1964). Kane (1970) noticed an anomolous zone of negative gradients in Queen Maud Land which he associated mainly with surface slope variations. For the present study we have smoothed over such irregularities in both the temperature and the temperature-elevation gradients.

For the flowline calculations values of surface temperature and surface elevation were taken at 100 km intervals along the flowlines and smooth curves fitted to them. From these smooth curves the gradient λ was calculated using equation (4.48). The general trends of the results showed a distribution similar to that shown in Map (3/4).

4.2.6. Surface warming rate.

The surface warming rate or horizontal temperature advection for a steady state ice sheet is calculated from

$$S = \frac{D\theta_s}{Dt} = V\frac{\partial\theta_s}{\partial x} = V\frac{\partial\theta_s}{\partial E}\frac{\partial E}{\partial x} = V\alpha\lambda \qquad (4.49)$$

Hence from the maps for balance velocity V, lapse λ, and slope α (2/2, 3/4, 3/1) we calculate their product S. The contours for the broad scale variation over the Antarctic are given in Map (3/5), in $°C/10^3yr$. Since the velocity and the surface slope both have trends of increase towards the coast (even though that in λ is not great), the resultant S values show a very strong increase over three orders of magnitude, from the inland to the coast. In the central zones of both East and West Antarctica low values of $0.05°C/10^3yr$ are typical. As the coast is approached S increases rapidly to over $5°C/10^3yr$ in West Antarctica and over $10°C/10^3yr$ in East Antarctica.

This map has a strong resemblance to the map for base gradients γ_b. Since both contain the surface velocity the similarity of pattern is not surprising. However, the order of magnitude increase towards the coast is also very similar and this has an important effect on the temperature calculations.

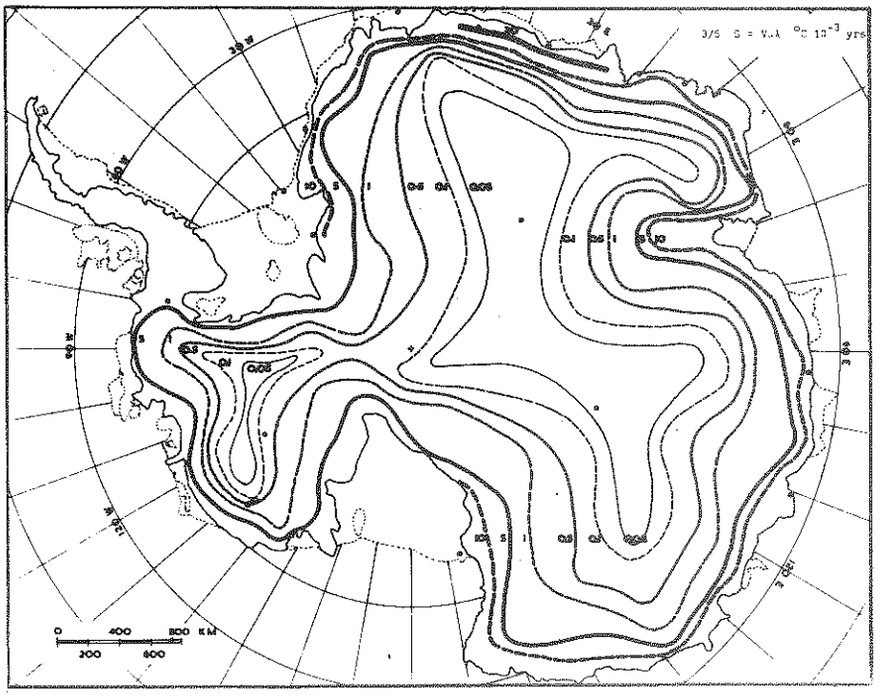

Map 3/5. Surface warming rate $S = V\alpha\lambda$ *°C* 10^{-3}*yrs.*

The rate at which the surface of a vertical column of the ice cap warms as it flows outwards to the coast is calculated from the surface temperatures θ_s *Map (1/6), balance velocities* V *Map (2/2), and elevations* E *Map (1/2) for each flowline as*

$$\frac{\partial\theta_s}{\partial t} = \frac{\partial\theta_s}{\partial x}\frac{dx}{dt} = V\frac{\partial\theta_s}{\partial x} = V\frac{\partial\theta_s}{\partial E}\frac{\partial E}{\partial x} = V\alpha\lambda$$

These warming rates typically increase from less than .05°C/10³yrs inland to over 10°C/10³yrs near the coast.

It is shown in section 4.3 that parameters S and γ_b tend to have opposing effects on the base temperature; i.e. large S tend to give low temperatures whereas large γ_b tend to give high temperatures. These effects of S are more clearly illustrated by Robin's (1955) parameter $\frac{\alpha V\lambda}{A}$ which has the same dimension as the base gradient, °C/100 m. This is discussed in section 4.3.3.

4.3. Analytical solution of the heat conduction equation for simple column models.

For the simple column model with basal heating, constant advection, diffusivity and strain rate equations (4.38) and (4.39) become, using (4.49)

$$\kappa \frac{\partial^2\theta}{\partial z^2} + \frac{Az}{Z}\frac{\partial\theta}{\partial z} = V\alpha\lambda \tag{4.50}$$

$$\theta_{z=Z} = \theta_s \qquad \gamma_b = \gamma_G + \frac{\tau_b V}{JK} \tag{4.51}$$

The solution of these for temperature gradient (cf. e.g. Budd 1969) is

$$\frac{\partial\theta}{\partial z} = \gamma_b e^{-(y\zeta)^2} + \frac{V\alpha\lambda}{A} 2yF(\zeta y) \tag{4.52}$$

where $\zeta = z/H$ is the relative height above the base,

$y = \sqrt{AZ/2\kappa}$ is a dimensionless parameter, and

$F(x)$ is the Dawson integral defined by

$$F(x) = e^{-x^2}\int_0^x e^{t^2}\,dt \tag{4.53}$$

which is tabulated in Abramowitz and Stegun (1965). In particular the temperature gradient at the surface is given by

$$\left.\frac{\partial\theta}{\partial z}\right)_s = \gamma_b e^{-y^2} + \frac{V\alpha\lambda}{A} 2yF(y) \tag{4.54}$$

It is apparent from these relations that the parameters γ_b, $y = \sqrt{AZ/2\kappa}$, $\frac{V\alpha\lambda}{A}$ are the crucial factors determining the temperature profile.

The ice temperatures are given by

$$\theta_z = \theta_s - Z[\gamma_b \frac{1}{y}(\text{erf } y - \text{erf } \zeta y) - \frac{V\alpha\lambda}{A} 2\{E(y) - E(\zeta y)\}] \tag{4.55}$$

where erf x is defined by

$$\text{erf } x = \int_0^x e^{-y^2}dy \tag{4.56}$$

and E(x) is the integral of the Dawson integral

$$E(x) = \int_0^x F(y)dy \tag{4.57}$$

In particular the base temperature is

$$\theta_b = \theta_s - Z[\gamma_b \frac{\text{erf } y}{y} - \frac{V\alpha\lambda}{A} 2E(y)] \tag{4.58}$$

Again we see that the base temperature depends critically on the values of γ_b and $\frac{V\alpha\lambda}{A}$. The functions $\frac{\text{erf } y}{y}$, 2E(y) are plotted over the range $0 \leq y \leq 4$ in Fig. 4.6. It will be seen below (Map 3/6) that the values of y lie essentially well within this range for the whole Antarctic ice sheet.

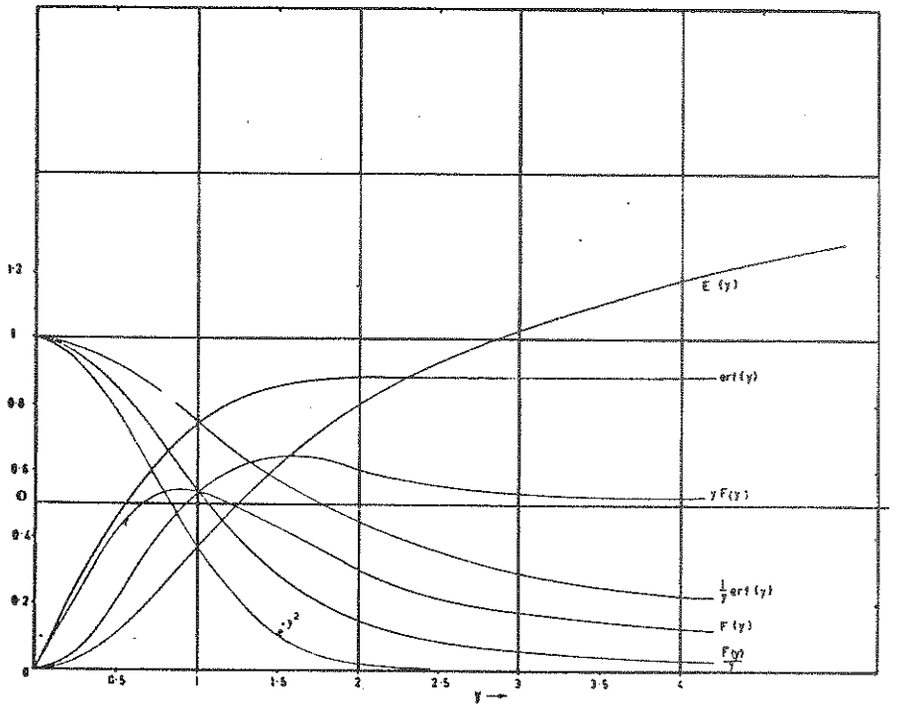

FIG. 4.6 Special functions associated with solutions of the heat conduction equation

(after Budd 1969)

Although Z is included in y, a small change in Z makes little difference to y. However equation (4.58) for the base temperature shows that the effect of a small increase in ice thickness is mainly to cause a proportional increase in the differences between the surface and base temperatures. Since the base is generally warmer than the surface this means that an increase in thickness typically causes higher basal temperatures. This accounts for the feature described in section 4.1, viz. that bedrock hollows in the interior of Antarctica may become associated with pockets of meltwater.

The effect of the five major parameters A, Z, S, θ_s, γ_b on the temperature profile has been discussed in detail by Radok et al (1970). Most of these features can be discerned from the formulas for base temperature (4.58) and surface gradient (4.54), together with Fig. 4.6 showing the graphs of e^{-y^2}, $2yF(y)$, $\frac{\text{erf } y}{y}$ and $2E(y)$.

It was pointed out by Budd (1969) that the expression for surface temperature gradient (4.54) is approximately the sum of the two "Robin terms", $\gamma_b e^{-y^2}$ for no horizontal motion, and $\frac{V\alpha\lambda}{A}$ for horizontal advection with no conduction (Robin 1955). This is because $2yF(y)$ differs only slightly from 1 for the typical values of y encountered in the Antarctic.

4.3.1. Graphical aids.

It is often useful to make a quick approximate estimate of a temperature profile for some given position. This can be done reasonably well if we know the surface and base temperatures and temperature gradients. An additional point of interest, in the case of profiles with a negative temperature-depth gradient at the surface, is the depth of the minimum temperature. The formulae of the last section together with the graphs of Fig. 4.6 allow a quick calculation of the base temperature and surface gradient from the five parameters A, Z, S, θ_s, γ_b entering the expression

$$\theta_b = \theta_s - Z[\gamma_b \frac{\text{erf } y}{y} - \frac{V\alpha\lambda}{A} 2E(y)] \tag{4.58}$$

For the Antarctic the maps of θ_s, Z, γ_b, $\frac{V\alpha\lambda}{A}$ together with the graphs for $\frac{\text{erf } y}{y}$ and E(y) allow θ_b to be estimated quickly. Table 4.2 gives an example of this calculation for the South Pole. However the error can be quite large when the two terms in the square brackets of (4.58) become large and their difference small.

A similar procedure may be used for the surface gradient from

$$\gamma_s = \gamma_b e^{-y^2} + \frac{V\alpha\lambda}{A} 2yF(y) \tag{4.59}$$

using the graphs for γ_b, y, e^{-y^2}, $\frac{V\alpha\lambda}{A}$, 2yF(y). Once more the errors may also be large if the two terms are large and their difference small.

Finally the depth of the minimum temperature was given by Budd (1969) as

$$\frac{z}{Z} = \frac{1}{y} G^{-1}(\frac{V\alpha\lambda}{A\gamma_b} 2y) \tag{4.60}$$

where

$$G(y) = (\int_0^y e^{t^2} dt)^{-1} \tag{4.61}$$

and is shown plotted in Fig. 4.7 (p.82). An example of its use is illustrated by Table 4.3.

Table 4.2.

Graphical evaluation of temperature profiles.

Quantity	Source	Values	
		South Pole	Byrd
Z m$\times 10^2$	Map 1/3	28	22
θ_s °C	Map 1/6	-51	-28
A m/yr	Map 1/5	0.08	0.15
$V\alpha\lambda$ °C/10^3yr	Map 3/5	0.15	0.25
$\frac{V\alpha\lambda}{A}$ °C/10^2m	Map 3/7	0.188	0.167
$y=\sqrt{AZ/2\kappa}$	Map 3/6	1.6	2.0
γ_b °C/10^2m	Map 3/3	2.5	3.1
$\frac{\text{erf } y}{y}$	Fig. 4.6	0.54	0.45
e^{-y^2}	Fig. 4.6	0.07	0.02
$2yF(y)$	Fig. 4.6	1.29	1.20
$2E(y)$	Fig. 4.6	1.31	1.6

1. Basal temperature $\theta_b - \theta_s = Z[\gamma_b \frac{\text{erf } y}{y} - \frac{V\alpha\lambda}{A} 2E(y)]$

$\theta_b-\theta_s$ °C	Z[1.35-.246]	Z[1.39-.27]
	28[1.1] ≃ 31	22[1.12] ≃ 25
θ_b °C	≃ -20	≃ -3

2. Surface gradient $\gamma_s = \gamma_b e^{-y^2} + \frac{V\alpha\lambda}{A} 2yE(y)$

$\gamma_b e^{-y}$	0.175	0.062
$\frac{V\alpha\lambda}{A} 2yE(y)$	-0.246	-0.532
γ_s °C/10^2m	-0.07	-0.47

Table 4.3.

Estimation of depth of minimum temperature, from Fig. 4.6.

Relative height above base $\frac{z}{Z}$

$$\left.\frac{z}{Z}\right)_{\theta_{min}} = \frac{1}{y} G^{-1}\left(\frac{V\alpha\lambda}{A\gamma_b} 2y\right)$$

Quantity	Value	
	South Pole	Byrd
Z m	2800	2200
$\frac{V\alpha\lambda}{A}$ °C/100 m	0.188	0.167
γ_b °C/100 m	2.5	3.1
y	1.6	2.0
$\frac{V\alpha\lambda}{A\gamma_b}$	0.075	0.054
$\frac{V\alpha\lambda}{A\gamma_b} 2y$	0.240	0.216
$G^{-1}[\frac{V\alpha\lambda}{A\gamma_b} 2y]$	1.48	1.52
$\left.\frac{z}{Z}\right)_{\theta_{min}}$	0.93	0.76
Depth ξ m	560	530

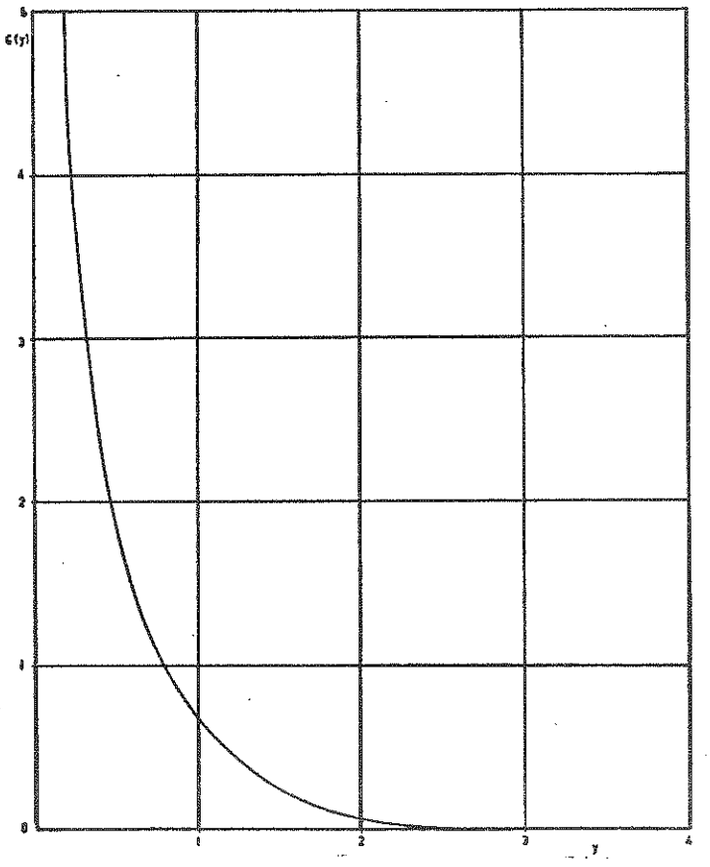

FIG. 4.7 *The function* $G(y) = (\int_0^y e^{-x^2} dx)^{-1}$ *used for determining the depth of the minimum temperature in the ice (after Budd 1969)*

4.3.2. Distribution of $y = \sqrt{AZ/2\kappa}$.

Because of its importance to the understanding of the temperature profile the variation of the dimensionless parameter $y = \sqrt{AZ/2\kappa}$ over the Antarctic has been calculated from the accumulation A (Map 1/5) and ice thickness Z (Map 1/3). The resultant contours are shown in Map (3/6).

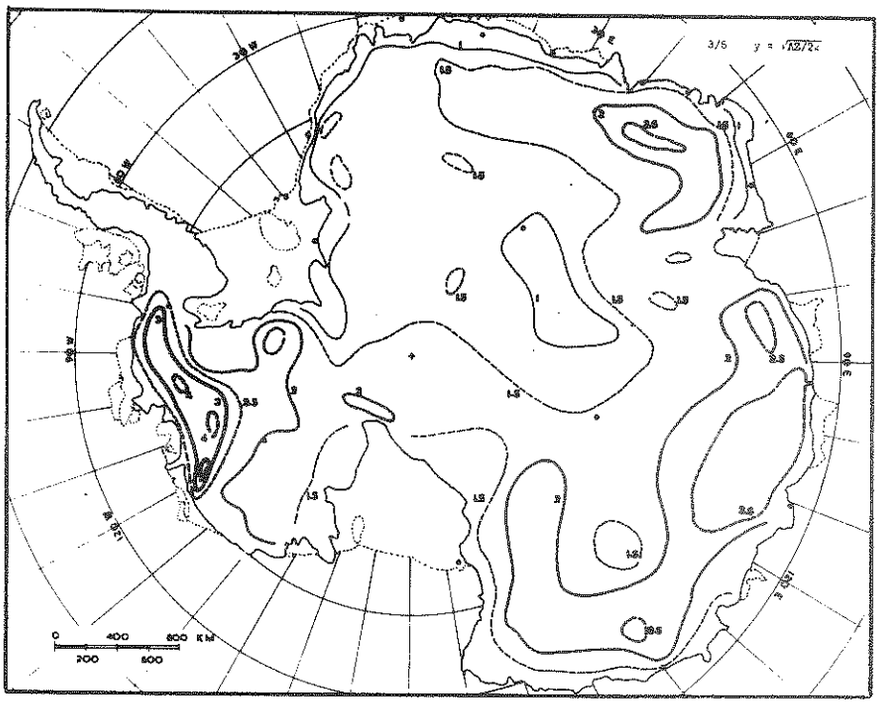

Map 3/6. Dimensionless thermal parameter $y = \sqrt{AZ/2\kappa}$.

From the maps for accumulation rate A *(1/5) and ice thickness* Z *(1/3) the dimensionless parameter* $y = \sqrt{AZ/2\kappa}$ *has been calculated using a constant value of* $\kappa = 1.4\ cm^{-2}\ sec^{-1}$.

The values show a general trend from 1 inland to about 2 to 2.5 near the coast in East and Antarctica, and over 3.5 in Ellsworth Land.

Since the accumulation tends to increase towards the coast, whereas the ice thickness tends to decrease, the product AZ and hence y on the average varies much less than either A or Z. However major perturbations from the general trend also show up in $\sqrt{AZ/2\kappa}$. The thin ice in central East Antarctica over the Gamburtzev Mountains has a low value of $y \sim 1$. High

values of y ~ 2.5 occur in the deep ice - high accumulation region inland of Mirny and Casey (Wilkes), and values of y > 3 occur in the region of deep ice and high accumulation between Byrd and Ellsworth Land in West Antarctica. This limited range of y values allows the graphs of Fig. 4.6 to be used over the entire ice sheet.

4.3.3. Distribution of surface advection gradient $V\alpha\lambda/A$.

The horizontal surface advection gradient $\frac{V\alpha\lambda}{A}$ has been calculated from the steady state surface warming $V \frac{\partial \theta_s}{\partial x} = V\alpha\lambda$ (Map 3/5) and the accumulation rate A (Map 1/5). The resultant values have been plotted and contoured as shown in Map (3/7) with units of °C/100 m.

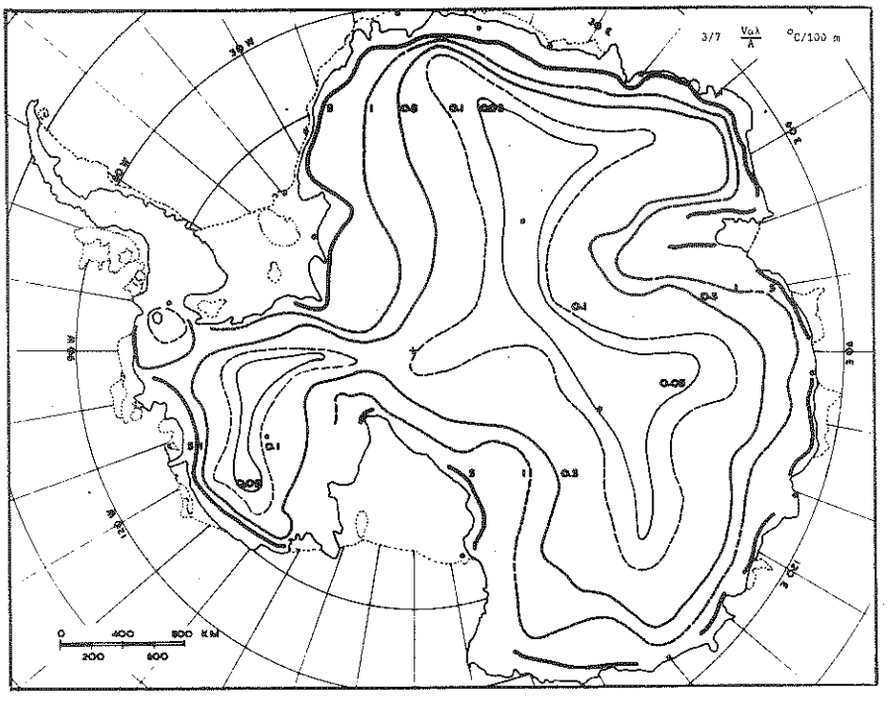

Map 3/7. Surface advection gradient $V\alpha\lambda/A$ °C/100 m.

From the maps of steady state surface warming $S = V\alpha\lambda$ *(3/5), and accumulation rate* A *(1/5), the surface horizontal advection gradient has been calculated as* $V\alpha\lambda/A$ *°C/100 m. The values show a decrease typically from -0.05°C/100 m inland to -5°C/100 m near the coast. These values are relevant to the computed values of surface gradient* γ_s*, Map (4/2) and the measured gradients of Map (1/7).*

The pattern of variation is very similar to that of surface warming ($V\alpha\lambda$) increasing strongly towards the coast; but since the accumulation also tends to increase outwards the trend in $\frac{V\alpha\lambda}{A}$ is reduced. The values vary from very small gradients inland, less than 0.05°C/100 m, to over 5°C/100 m near the coast. As shown in section 4.3 the advection gradient term is chiefly responsible for the negative temperature depth gradients at the surface. It will be seen in section 6.2 that the flowline output surface temperature gradients have similar values to $\frac{V\alpha\lambda}{A}$ near the coast, but are positive inland, roughly where the values of $\frac{V\alpha\lambda}{A}$ fall below 0.2°C/100 m. This is because the term of equation (4.52) which contributes to the positive part of the surface gradient (viz. $\gamma_b e^{-y^2}$, where $y = \sqrt{AZ/2\kappa}$) becomes dominant; typical values of y from Map (3/6) give $y \sim 1.5$, for which Fig. 4.6 shows $e^{-y^2} \sim 0.1$. Hence with a base gradient of $\gamma_b \sim 2.2$°C/100 m or greater we may expect the positive term to dominate, once $\frac{V\alpha\lambda}{A}$ fall below 0.2°C/100 m.

The measured values of surface gradient given in Map (1/7) also show the trend of negative temperature gradients near the coast and have about the same magnitude as $\frac{V\alpha\lambda}{A}$.

4.4. Dielectric absorption.

From the calculated temperature distribution through the ice sheet a number of other features that depend on the temperature may also be calculated. One of these, the "dynamics" velocity, was already discussed in section 4.3. Another feature has gained great interest in recent times with the advent of the radar ice thickness sounding, viz. the attenuation of the radar beam in the ice.

The basic quantity measured in radar ice thickness sounding is the strength of the return signal compared to the output strength. The details of the physics of the situation have been given by Robin, Evans and Bailey (1969). Here we note that the attenuation of the signal strength depends on several factors viz. the dispersion, which is primarily determined by the path length (ice thickness), the reflection coefficient from the bedrock, and the dielectric absorption in the ice. Other features such as internal reflections etc. are not considered at this stage. The most important feature in this context is the dielectric absorption in the ice which is temperature-dependent. Measurements of the dielectric absorption of ice have been discussed by Evans (1965).

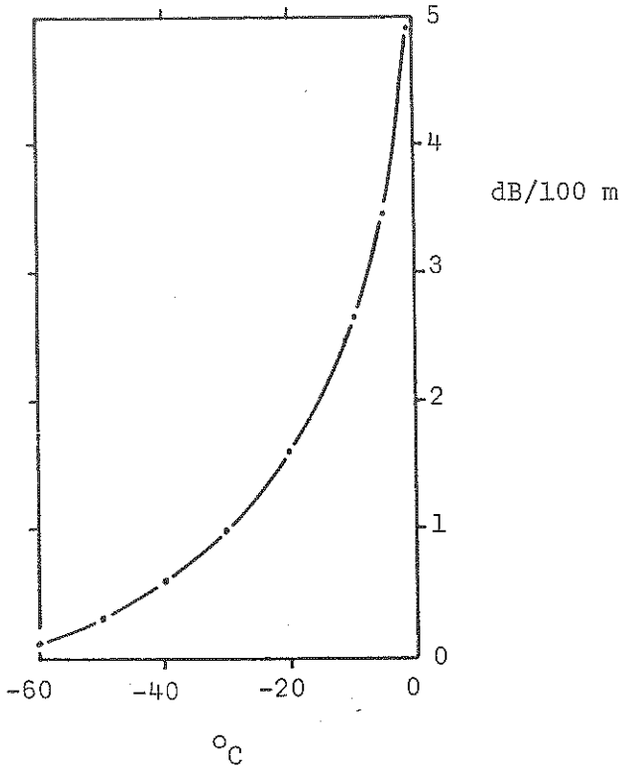

FIG. 4.8 Dielectric absorption of ice as a function of temperature, from Westphal's measurements (after Robin et al 1969)

Here we make use of Fig. 4.8, a curve taken from Robin et al (1969), based on Westphal's measurements of the dielectric absorption $p(\theta)$ in ice as a function of temperature (θ). It has been noted by Bogorodskiy (1968) that this curve is not greatly dependent on the radar frequency. Hence we take this curve as our data and compute from the temperature profile the integrated absorption

$$P_z = \int_0^z p(\theta_z)dz \tag{4.62}$$

In particular the total integrated absorption P_Z is the absorption right through the ice from surface to bed. In practice it is twice this absorption ($2P_Z$) which is relevant to the returned echo strength.

The value of the absorption calculations is twofold. Firstly, they provide a basic guide for the field operator measuring ice thickness of the regions for which great or little difficulty may be anticipated in obtaining echoes at this stage of our knowledge of the temperature distribution in different regions. Secondly, as more measurements of echo strength become available it may be possible to use these as a measure of the temperature structure in different areas.

A number of other quantities are of interest in this context such as

1) mean absorption or absorption per unit thickness

$$\frac{P}{Z} = \frac{1}{Z}\int_0^Z p(\theta)dz \tag{4.63}$$

This helps to eliminate the effect of ice thickness in comparing different absorptions.

2) absorption temperature $\overline{\theta}_a$, which is the temperature of an isothermal column of the same thickness with the same absorption as the given column

$$\overline{\theta}_a = p^{-1}\left(\frac{1}{Z}\int_0^Z p(\theta)dz\right) \tag{4.64}$$

3) attenuation from combined absorption and dispersion. Robin, Evans and Bailey (1969) give the dispersion as dependent on the square of the thickness Z. For simple calculations the following formula is used

$$\Pi = P_Z + 10 \log_{10} Z \qquad (4.65)$$

where Π is the attenuation in dB

P_Z is the dielectric absorption in dB

Z is the ice thickness in metres.

This leaves the variation in the bed reflection coefficient as the main remaining contributor to the variation in echo strength. Averaging over large areas overcomes some of the problems of local variation of the reflection coefficients, thus allowing Π to be used as an indicator of the temperature profile.

The calculation of these various parameters has been incorporated into the temperature calculation programme as set out in Table 4.4. The results of the calculation will be discussed in Chapter 6. In the next chapter we give an outline of the procedures and operations used in the present computer modelling of the Antarctic ice cap.

Table 4.4.

Calculation of derived characteristics.

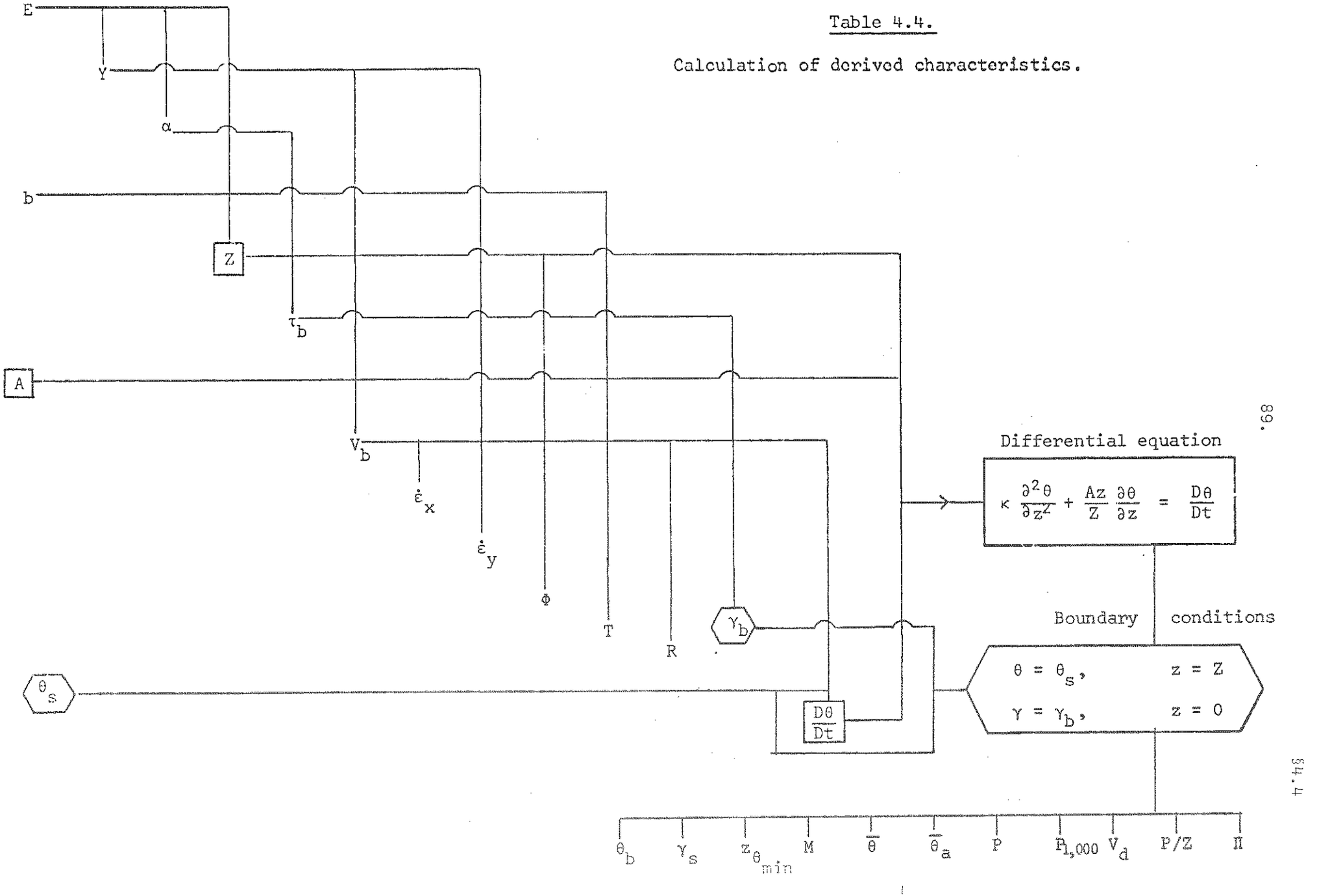

5. THE COMPUTER SOLUTION OF THE HEAT CONDUCTION EQUATION.

5.1. Introduction.

As discussed in Chapter 3, the full equation for heat conduction within an ice mass may be written (using vector notation) as

$$\frac{\partial\theta}{\partial t} + \underset{\rightarrow}{V}\cdot\nabla\theta = \frac{1}{\rho c}\nabla K\cdot\nabla\theta + \frac{K\nabla^2\theta}{\rho c} + Q \qquad (5.1)$$

where $\underset{\rightarrow}{V}$ is the velocity vector, and the thermal parameters have already been defined. Q, the heat input to the ice, is either confined solely to the base (basal heating) or spread throughout the ice (layer heating), and here has units of $^{\circ}C\ yr^{-1}$.

If it is assumed that transverse horizontal gradients and second derivatives of temperature are small, and that thermal conductivity (K) and specific heat (c) are constant, then equation (5.1) reduces to

$$\frac{\partial\theta}{\partial t} + V\frac{\partial\theta}{\partial x} + w_z\frac{\partial\theta}{\partial z} = \kappa\frac{\partial^2\theta}{\partial z^2} + Q \qquad (5.2)$$

in which κ is the thermal diffusivity.

This is the basic equation to be treated, and the problems of solving it for steady-state and transient effects will now be discussed.

5.2. A new coordinate system.

If equation (5.2) is employed in any computer programme to reduce the temperature profile of an arbitrary vertical section of the ice mass, certain problems are immediately apparent. In order to perform such calculations, the rate of temperature change at any depth ($\partial\theta/\partial t$) must be found; this in turn necessitates representing the local vertical by a number of discrete points, usually uniformly spaced and fixed at constant elevations above some arbitrary reference level. Unfortunately if the ice thickness is changing at the geographical location being examined, then the number of points in the vertical used to describe the column will also change, since the ice moves past the boundary points. Such motions introduce various errors into the calculations; the most serious are associated with computational stability (see section 5.6.4 below), and with sudden discontinuities in the temperature profiles, produced whenever a new grid point is added, or an old one lost, to the vertical grid. In order to correct for such errors, and to reduce boundary problems to a minimum, equation (5.2) will be reformulated in terms of a new coordinate system which expands or contracts as the ice grows or shrinks. In this new set of axes, the surface of the ice corresponds always to the vertical coordinate value zero, and the base to the value one. Any melt water is treated as lying outside the coordinates, but enters the calculations when continuity is considered.

The further simplifying assumption that the ice moves as a column is now made. This assumption has already been fully discussed in Chapter 4 and implies that the horizontal velocity of the ice along vertical is the same for all points in that vertical at a given time. This allows the new coordinate system to be further modified into one which moves with the ice column. In effect, then, two transformations must be made to the usual right-handed (x,y,z,t) system to produce the (χ,y,z,t) system to be employed:

(i) the new vertical coordinate z, is defined as

$$\mathit{z} = \frac{Z + M + F + z}{Z} \qquad (5.3)$$

where, as Fig. 5.1 shows, Z and M are the ice and melt water thicknesses respectively, and F is the bedrock elevation*: z has arbitrarily been chosen to be zero at the geoid surface.

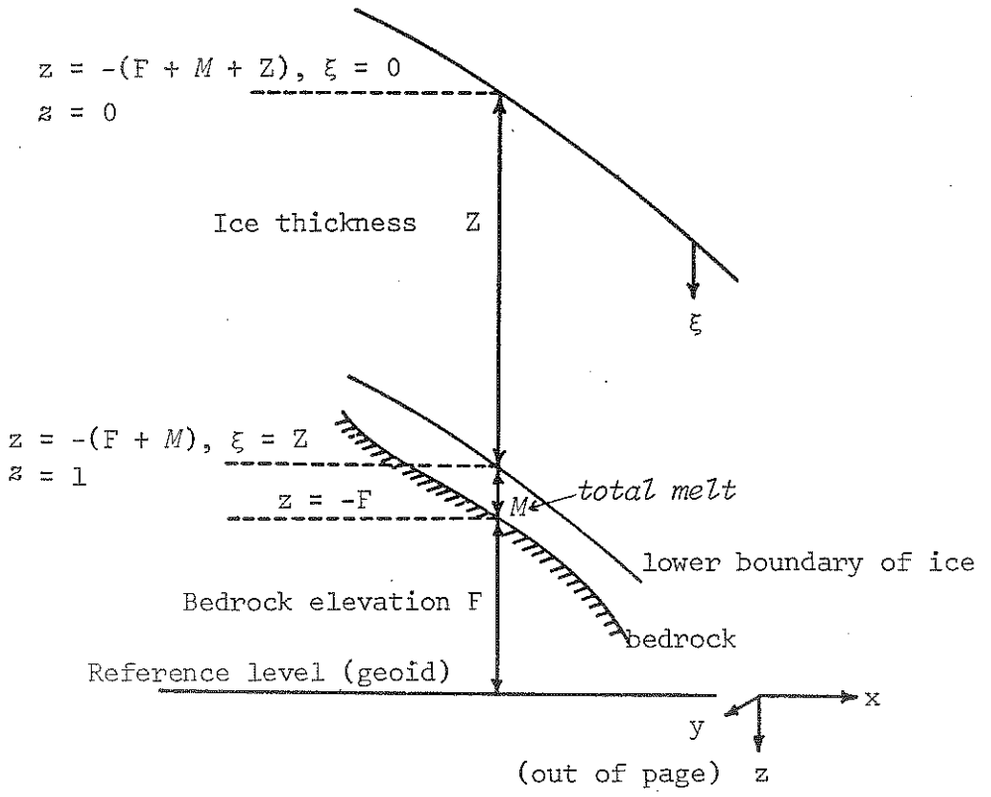

FIG. 5.1 The relation between the various parameters involved in the definition of the expanding coordinate system.

(ii) the new horizontal coordinate, χ, is defined simply by

$$\chi = x - \int_0^t V \, dt \tag{5.4}$$

To use equation (5.2) in this new system, it becomes necessary to transform the vertical derivatives and the vertical velocity into their z counterparts. The vertical derivatives are easily found from equation (5.3) to be

*In the presence of appreciable melt, the base of the ice (b) lies above the bedrock (F) by the amount M.

$$\frac{\partial}{\partial z} = \frac{1}{Z}\frac{\partial}{\partial z} \tag{5.5a}$$

$$\frac{\partial^2}{\partial z^2} = \frac{1}{Z^2}\frac{\partial^2}{\partial z^2} \tag{5.5b}$$

The vertical velocity is somewhat more complex and is considered in the next section.

5.3. Vertical velocity in terms of the relative coordinate z.

Differentiating (5.3) with respect to time yields

$$\omega = \frac{1}{Z}[w - \beta V + \frac{dM}{dt} + \frac{dZ}{dt}(1 - z)] \tag{5.6}$$

where ω is $\frac{dz}{dt}$ and β $(= -\frac{\partial F}{\partial x})$ is the bedrock slope. The quantity w $(= \frac{dz}{dt})$ is determined as follows. If the ice moves as a column, then with an accumulation of A m/yr and a melt rate of M metre of ice per year, the continuity equation for this column is

$$\frac{d}{dt}[(M + Z)s] = As \tag{5.7a}$$

where s is the cross-sectional area of the column. Just as for the derivation of equation (5.1), the ice medium has been assumed incompressible, and this together with columnar motion, requires that the total derivative of s be related to the horizontal divergence through

$$\frac{1}{s}\frac{ds}{dt} = \frac{\partial V}{\partial x} + \frac{\partial v}{\partial y} = -\frac{\partial w}{\partial z}$$

Use of this in equation (5.7a) yields

$$\frac{dZ}{dt} + \frac{dM}{dt} - A = (M + Z)\frac{\partial w}{\partial z} \tag{5.7b}$$

If the amount of melt is considered separately, it is clear that the mass change, $\frac{d}{dt}(M\rho s)$ must be balanced by the instantaneous melting, $M\rho s$. Thus

$$\frac{dM}{dt} = M + M\frac{\partial w}{\partial z} \tag{5.7c}$$

Substitution of this expression for $\frac{dM}{dt}$ into (5.7b) and integration with respect to depth from the ice/melt water interface, $z = -(M + F)$, to z gives the vertical velocity in the (x,y,z) framework as

$$w - w_I = \frac{1}{Z}\left(\frac{dZ}{dt} + M - A\right)(z + M + F) \tag{5.8}$$

where w_I is the vertical velocity at the ice/water interface: inasmuch as we have columnar motion, this clearly is

$$w_I = -V\left(\frac{\partial F}{\partial x} + \frac{\partial M}{\partial x}\right)$$

$$= \beta V - \frac{dM}{dt} + M$$

since $\frac{\partial M}{\partial t}$ is just M.

Substitution of this expression for w_I into equation (5.8) will yield an expression for w. When, in turn, that is used in equation (5.6), together with (5.3), we finally obtain

$$\omega = \frac{1}{Z}\left[A(1 - z) + Mz\right] \tag{5.9}$$

5.4. The heat equation for expanding, moving coordinates.

Equation (5.2) may be written more simply as

$$\frac{d\theta}{dt} = \kappa \frac{\partial^2 \theta}{\partial z^2} + Q \qquad (5.10)$$

where the total derivative on the left refers to the motion of a column remaining vertical as it moves. When transformed to the (χ,y,z,t) system, this total derivative does not change its form, but the physical interpretation of its various terms is altered. Making use of (5.5b), equation (5.10) becomes

$$\frac{d\theta}{dt} = \left(\frac{\partial \theta}{\partial t}\right)_z + V \frac{\partial \theta}{\partial \chi} + \omega \frac{\partial \theta}{\partial z} = \frac{\kappa}{Z^2} \frac{\partial^2 \theta}{\partial z^2} + Q$$

The subscript z indicates that the partial derivative is for the expanding, moving coordinates; V is the corresponding horizontal velocity. Substitution of (5.9) and use of (5.4) in the above finally yields

$$\left(\frac{\partial \theta}{\partial t}\right)_z = \frac{\kappa}{Z^2} \frac{\partial^2 \theta}{\partial z^2} - \frac{1}{Z} [A(1 - z) + Mz] \frac{\partial \theta}{\partial z} + Q \qquad (5.11)$$

This form of the heat equation has been used in the computation of transient state temperature distributions, with the method outlined in sections 5.5.3 and 5.5.4 below. It should be noted here that in the z-coordinate system the local derivative of temperature is interpreted physically as the change in temperature of a fictitious parcel of the ice which remains a fixed fraction of the depth below the surface, and moves with the column. The local derivative in the z system is closely, but not exactly, related to the total derivative in the (x,y,z) system.

As discussed in Chapter 4, there are many ways of defining a steady state for the temperatures; two examples are,either that the vertical temperature gradients in the ice flowing past a fixed vertical are constant with time, or that the temperature gradients in the expanding, moving column remain constant in time. These may be mathematically expressed as:

$$\left(\frac{\partial\theta}{\partial t}\right)_z = \text{constant} \qquad (5.12a)$$

$$\left(\frac{\partial\theta}{\partial t}\right)_z = \text{constant} \qquad (5.12b)$$

The latter of these two is more realistic, and equation (5.11) was derived partly in order to enable the corresponding steady states to be readily calculated. Clearly, if the gradients are to be preserved, while temperatures change with time, then there can be no melting at the lower boundary of the ice, since this implies a fixed temperature there. Inasmuch as the surface temperature is a known boundary condition, prescribing the boundary temperature gradient as well as the fixed base melt temperature is tantamount to overspecifying the problem since the solution of (5.11) for steady states can and must have only two boundary conditions. Thus if melting does take place, and temperatures or ice thickness change, the boundary temperature gradient must change, and hence there can be no steady state. Consequently equation (5.11) becomes

$$SZ^2 = \kappa \frac{\partial^2\theta}{\partial z^2} - Z[A(1 - z)] \frac{\partial\theta}{\partial z} + QZ^2 \qquad (5.13)$$

where S is the constant warming rate of equation (5.12b), the same for all z-points.

The difference between equations (5.11) and (5.13) must be clearly understood and emphasised. The former is used for transient computations and has $\left(\frac{\partial\theta}{\partial t}\right)_z$ as the unknown parameter, which must be found from the existing (known) temperatures and given boundary conditions. In equation (5.13), it is the temperatures which are to be determined, whilst $\left(\frac{\partial\theta}{\partial t}\right)_z$ is known (= S) and the boundary conditions are again predetermined. The entire computer approaches to these two equations are therefore fundamentally different and must of necessity be discussed separately.

5.5. Steady state computations.

5.5.1. Finite differences.

As mentioned in section 5.2 above, the vertical coordinate axis is divided into a number of points, and only at these points are values of the various parameters known or computed. It is necessary, therefore, to express the exact derivatives by inexact finite difference approximations. A large number of such analogues exist, and a comprehensive discussion of the determination of the most accurate ones possible can be found in Jenssen and Straede (1969). Since the temperatures are assumed to have no sharp discontinuities, it suffices to take for the present only those analogues which involve three, five or seven points of the vertical grid; these three different analogues will be referred to as low-, mid-, or high order, since their respective accuracies usually increase with the number of points involved. Near, and at the boundaries of the ice, forward or backward differences must be used, depending on whether one is dealing with the upper or lower boundary. All the analogues mentioned may be found in Abramowitz and Stegun (1965, p.914).

Preliminary tests showed significant differences between the results obtained with low- and mid-order finite difference schemes; but no such variations were found between mid- and high-order analogues, the temperatures agreeing in these two methods to five significant figures. Since the computation time is less for the mid-order analogues, they were chosen for all subsequent calculations. All three schemes were programmed, however, in case of a future need for either quick but slightly inaccurate, or slow but highly accurate, results.

5.5.2. Boundary conditions.

Two boundary conditions must be specified before equation (5.13) can be solved for temperatures.

(i) Upper boundary:

The surface temperature is given.

(ii) (a) Basal heating.

The lower temperature gradient is prescribed in terms of two effects - the geothermal heat flux into the ice (which can be expressed as a temperature gradient) plus frictional heating due to the motion of the column. All of the heat is applied at the lower boundary, and hence Q of equation (5.13) is zero. The temperature gradient is then

$$\left(\frac{\partial\theta}{\partial z}\right)_{\text{boundary}} = Z\left(\gamma_G + \frac{\tau_b V}{JK}\right) \qquad (5.14)$$

In the above γ_G is the geothermal heat flux, τ_b is the base stress and J is the mechanical equivalent of heat.

(b) Layer heating.

The heating produced within the ice is spread throughout its vertical extent, and Q is non-zero. This type of heating has been discussed in Chapter 4, section 4.1.6. It is easy to show that the expression for the internal heat Q (which is now in units of $^{o}C/yr$) is

$$Q = \frac{\kappa V \tau^4 e^{\nu\theta}}{JK \int_0^Z \tau^3 e^{\nu\theta} d\xi}$$

Here V is the surface velocity, which for the current model is the speed of the entire column, and ξ is the depth below the ice surface. It is now assumed that τ is a linear function, with depth, of the base stress τ_b ($\tau = \tau_b\ \xi/Z$). This enables the expression for Q to be written as the pair of equations:

$$Q = \frac{\kappa\Lambda\xi^4 e^{\nu\theta}}{K} \qquad (5.15)$$

and

$$\Lambda = \frac{V\tau_b}{JZ \int_0^Z \xi^3 \varepsilon^{\nu\theta} d\xi} \qquad (5.16)$$

Section 5.5.4 gives reasons for the introduction of the parameter Λ. The lower boundry condition is then that

$$\left(\frac{\partial\theta}{\partial z}\right)_{\text{boundary}} = Z\gamma_G \qquad (5.17)$$

Other parameters which must be given before (5.13) can be solved are the surface warming rate (S), the accumulation rate (A), the ice thickness (Z), the horizontal velocity (V), and the base stress (τ_b).

(c) Lower temperature is prescribed.

This, as stated in section 5.4,implies that the basal temperature gradient must change if the ice changes thickness, and is not therefore a "steady state" as previously defined.

5.5.3. Solution of the steady state equation. Basal heating.

Equation (5.13) when applied at the interior points of the N-point vertical grid, with some suitable finite difference scheme gives rise to N-2 simultaneous linear equations in the N unknowns (the temperatures). The two remaining equations are provided by the boundary conditions (i) and (ii)a or (ii)b. These N equations are then solved by a straightforward Gaussian elimination with partial pivot searching technique: the relevant program has been described by Flower (1964), and in detail by Carnahan et al.(1969). In order to avoid unreasonably lengthy computation times, N should be less than 100.

Occasionally the values of accumulation rate and surface warming selected may be so unreal so as to give an ill-conditioned set of equations. Such cases are detected by the program and a message is printed out to the effect that the resulting temperatures are unrealistic.

5.5.4. Solution of the steady state equation. Layer heating.

Since the heating term in this case is a function of temperature, equation (5.13) is no longer linear even when finite differences are applied, and the method of solution given above must be modified. Consequently the simple iterative scheme outlined below is employed. (Note that step (i) is only a preliminary manoeuver.)

(i) The heating Q is put to zero, and, with the given values of the parameters, (5.13) is solved as though it were a basal heating situation. The temperatures so produced are used as an initial guess to the final solution.

(ii) A is found from (5.16).

(iii) Q is then determined from (5.15).

(iv) This heating is shifted over to the left hand side of equation (5.13) and incorporated into the surface warming term SZ^2.

(v) The resulting equation is solved by the method of section 5.5.3 and a new temperature profile is produced.

(vi) The programme continually returns to (iii) until two sets of temperatures are produced which agree everywhere to within 10^{-3}°C. This constitutes a "minor" iteration.

(vii) The programme recycles back to step (ii) until two successive values of A differ by no more than 10^{-3}%. This cycle is a "major" iteration. This A value is chosen since it was found by experience to give temperatures on successive major iterations which agreed to five significant places.

The actual iterative procedure is somewhat more complex than the skeleton given above: in practice, the scheme may be speeded up by noting the way in which successive values of A change, and a good guess may be obtained directly, rather than through the currently computed temperatures. This method has the advantage of allowing divergent minor iterates to be quickly picked up. When this occurs a reversion to the last non-divergent A is effected and this value is then arbitrarily changed less rapidly than the method above would have it vary. If the new choice is minor convergent the scheme proceeds; if the A value still produces physically unreal temperatures a new selection is made from the last good value, which is now varied by an

even smaller amount. If unreal temperatures are produced even when Λ changes by only 10^{-3}%, then it is assumed that no minor convergence is possible, and that the value of the ice flow velocity (which was arbitrarily selected) is such that no steady states, as here defined, are physically possible.

This interpretation of non-convergence as being physical incompatibility of the parameters in equation (5.13) with a steady state is questionable, and should be investigated more thoroughly. It is conceivable that the iterative technique employed is never convergent for some boundary conditions, rather than that no steady state exists for the situation chosen. No such exhaustive theoretical study has yet been attempted, however.

5.5.5. Output for steady states.

An example of the output produced on the line printer by the steady states programme is given in Fig. 5.2. Much of this printout consists of internal checks on the input data and the current state of the computations, so that only the most salient features will be pointed out here. The present example is for Camp Century in Greenland.

The first line of data indicates that the grid consists of 34 points spaced 42 metres apart in the vertical: that the geothermal heat flux is 0.0264°C/metre; that accumulation is 0.3 metre/yr; and that the surface warming is -0.0001°C/year. The "loop data" are followed by information on the iterative procedure employed for layer heating. (If basal heating had been desired, the parameter "SURF.U", or surface horizontal velocity, would be negative.) It can be seen that the minor iterations required only three cycles, and that the major iteration also was three cycles long. In all, nine iterations were required to solve the very highly non-linear equation (5.13), a figure which attests to the powerful nature of the iterative scheme; it also supports the claim that in absence of convergence, no steady states are possible.

```
DATA
 N.PTS Z.INC ORDER WRITE  AUTO THERMLDIFF SURFCETEMP ACCUMULATN BASEGRAD.T BASETEMPTR LOCDERIV.T
    34    42     2     0     0 41.600000 -24.800000   0.3C0000   0.026400 -13.040000  -0.000100
LOOP DATA
 LOOP NUMBERS            INCREMENTS IN
 NZ NA NE          Z.INCRMNT ACCUMLATN LOCDERIVT                    PROGRESHN
  1  6  6                 0  0.100000 -0.000100                     0.000000
          M         NU      DELTB      NIOUT     SURF.U     BASE.TAU
   3.000000  0.100000  0.000010        300     3.0000       0.4500
LAMBDA =  0.4195E-12  DEG/YR/M(E4)
                                NUMBER OF ITERATIONS =   3
LAMBDA =  0.4157E-12  DEG/YR/M(E4)
LAMBDA =  0.5162E-12  DEG/YR/M(E4)
                                NUMBER OF ITERATIONS =   3
LAMBDA =  0.4148E-12  DEG/YR/M(E4)
LAMBDA =  0.4157E-12  DEG/YR/M(E4)
                                NUMBER OF ITERATIONS =   3
LAMBDA =  0.4157E-12  DEG/YR/M(E4)
  DEPTH   TEMPERATURE   T.VARIATION   OBSERVED T.    DEVIATION    T.GRADIENT     HORIZ.VEL
    0       -24.800        0.000         0.000         0.000     ***********       3.000
   42       -24.776        0.024         0.040        -0.016         0.060         3.000
   84       -24.750        0.050         0.080        -0.030         0.068         3.000
  126       -24.719        0.081         0.110        -0.029         0.078         2.999
  168       -24.684        0.116         0.140        -0.024         0.090         2.997
  210       -24.643        0.157         0.230        -0.073         0.106         2.995
  252       -24.595        0.205         0.330        -0.125         0.125         2.991
  294       -24.537        0.263         0.440        -0.177         0.148         2.985
  336       -24.470        0.330         0.540        -0.210         0.175         2.978
  378       -24.390        0.410         0.660        -0.250         0.208         2.969
  420       -24.294        0.506         0.780        -0.274         0.246         2.957
  462       -24.182        0.618         0.890        -0.272         0.291         2.942
  504       -24.049        0.751         1.030        -0.279         0.343         2.924
  546       -23.892        0.908         1.180        -0.272         0.403         2.903
  588       -23.709        1.091         1.370        -0.279         0.470         2.877
  630       -23.497        1.303         1.570        -0.267         0.545         2.847
  672       -23.251        1.549         1.810        -0.261         0.628         2.812
  714       -22.968        1.832         2.070        -0.238         0.718         2.772
  756       -22.647        2.153         2.390        -0.237         0.815         2.724
  798       -22.283        2.517         2.740        -0.223         0.918         2.670
  840       -21.875        2.925         3.130        -0.205         1.025         2.607
  882       -21.421        3.379         3.570        -0.191         1.136         2.534
  924       -20.921        3.879         4.050        -0.171         1.248         2.450
  966       -20.373        4.427         4.590        -0.163         1.359         2.354
 1008       -19.780        5.020         5.150        -0.130         1.467         2.242
 1050       -19.142        5.658         5.840        -0.182         1.568         2.113
 1092       -18.463        6.337         6.530        -0.193         1.662         1.963
 1134       -17.748        7.052         7.260        -0.208         1.744         1.790
 1176       -17.001        7.799         7.980        -0.181         1.812         1.589
 1218       -16.228        8.572         8.710        -0.138         1.864         1.357
 1260       -15.438        9.362         9.460        -0.098         1.898         1.088
 1302       -14.637       10.163        10.230        -0.067         1.912         0.776
 1344       -13.835       10.965        10.990        -0.025         1.901         0.415
 1386       -13.040       11.760        11.760        -0.000     ***********      -0.000

SURFACE GRADIENT OF COMPUTED TEMPERATURES =      0.053 DEGREES PER 100 METRES
   BASE GRADIENT OF COMPUTED TEMPERATURES =      1.875 DEGREES PER 100 METRES
LAMBDA =  0.4157E-12  DEG/YR/M(E4)

                                                 BASE HEATING =      0.204  DEG/100 M
                                                 LAYER HEATING =     0.165  DEG/100 M
```

FIG. 5.2 A sample of the printout for a fixed-column temperature calculation. The listed quantities are discussed at length on pp. 102 and 104

Once the major iteration has reached convergence, then the temperature profile is printed out, together with the corresponding depths. Also printed are the differences between the temperature at the current depth and the surface temperature, the observed temperature profile (where this has been determined in the field), the differences between these two profiles, the computed temperature gradients, and the "dynamics" velocity which would hold at the various (χ,y,z,t) points if the ice were not moving in a columnar manner, but shearing with no slip at the base. Section 5.6.5 below provides further details. Certain other programmed outputs (e.g. second derivatives of temperature) have been suppressed in this printout.

On the lower right of the output the total amount of heat supplied to the column by layer frictional heating is compared with the heat which would be supplied by basal heating for the given horizontal velocity (i.e. if Q were zero and equation (5.14) were used).

When an observed temperature profile is known and is to be compared with that computed, the programme user may, if he so desires, obtain a rough plot of these and of their differences. These are shown in Fig. 5.3 where the asterisks give the observed profile, the plus signs give the computed (both with origin on the left), and the zeros give the differences (computed temperature minus observed, with origin represented by the right column of dots). Scales are also given in the figure, but obviously only apply for the computer output and not for this reproduction. The standard deviation and variance of the difference between the two curves are also printed out at the lower left. The usefulness of graphs and data such as these has been discussed in section 4.1.5.

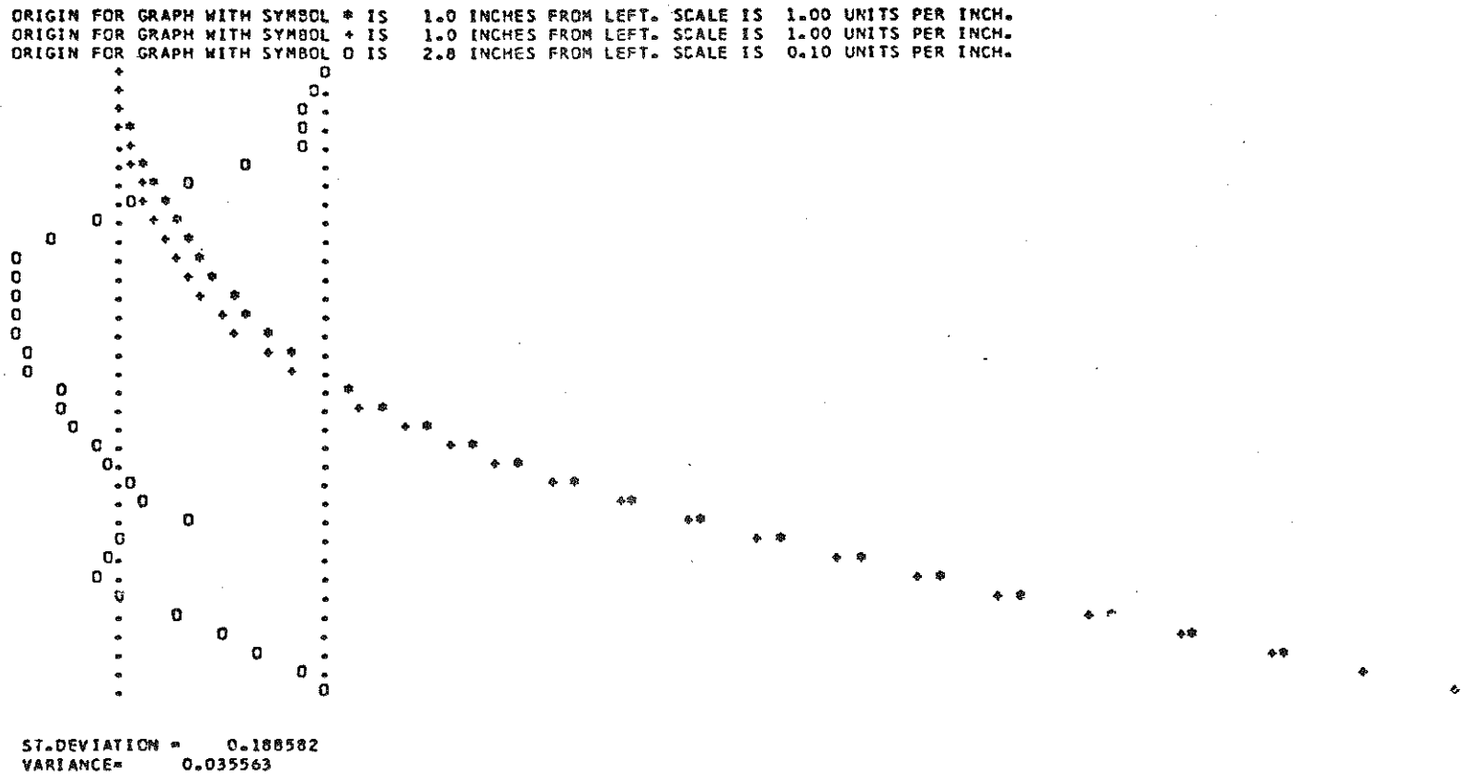

FIG. 5.3 A sample of the graphical printout for the fixed column calculation.
A detailed explanation is given on p. 104.

5.6. Transient state computations.

5.6.1. The method.

As emphasised in section 5.4 above, the transient state computations imply a totally different approach to the heat equation, which is now given by (5.11). The following procedure is now used:

(i) From an initially given temperature distribution with depth at position X^t and time t, the first and second derivatives are computed using the same finite difference analogues as in section 5.5.1. Using the known (computed) values of instantaneous melt, the terms of the right hand side of equation (5.11) may be evaluated, and $(\frac{\partial\theta}{\partial t})_z$ found.

(ii) The new temperatures at a time Δt later at each point of the grid are then determined through

$$\theta^{t+\Delta t} = \theta^t + \Delta t(\frac{\partial\theta}{\partial t})^t_z \tag{5.18}$$

(iii) The new position of the ice column is then found from the known velocity:

$$X^{t+\Delta t} = X^t + V\Delta t \tag{5.19}$$

(iv) Any melting is then found. This occurs whenever the basal temperature (for the computation of this quantity see the following section) is greater than the pressure melting point of the ice. If meltwater already exists, but the temperature is less than the pressure melting point, freezing must occur. As outlined in section 5.6.3 below, the amount of melt or freeze is:

$$M = \frac{K}{\rho LZ}\left[(\frac{\partial\theta}{\partial z})_{\text{prescribed}} - (\frac{\partial\theta}{\partial z})_{\text{computed}}\right] \tag{5.20}$$

where the gradients apply at the lower boundary point.

(v) Continuity is then used to determine the new ice thickness and amount of total melt. Equations (5.7b), (5.7c) and Figure (5.1) show that

$$Z^{t+\Delta t} = Z(1 - \Delta) + (A - M)\Delta t \qquad (5.21)$$

in which

$$\Delta = \frac{\Delta t}{M + Z}\left(A - \frac{dE}{dt} - \beta V\right) \qquad (5.22)$$

where E is the surface elevation, and quantities on the right hand side of the equations are for time t. This allows the new depths to be computed once M is found. The total melt is found directly from (5.7c) and (5.8) to be

$$M^{t+\Delta t} = M(1 - \Delta) + M\Delta t \qquad (5.23)$$

Again right hand quantities are current values.

(vi) The programme returns to (i) with the new temperatures and the integration continues for as long as desired.

This seems a much more straightforward procedure than the steady state computations, but there are attendant problems, the most exacerbating being that of computational stability. Before treating this, however, the quantities which must be supplied to the programme in order for steps (i) to (vi) to be effected will be discussed.

5.6.2. Boundary data.

Clearly, the initial temperature distribution must be prescribed. If the ice is slow-moving, or if the initial point lies close to a dome in the surface elevation, then the best temperatures that can be chosen (in the absence of a measured profile) are the fixed-column steady state distribution for the given surface warming, accumulation and thickness. Should the current computations start at a branch point from another flowline, then the computed temperatures for that point, found by previous use of the transient programme, can be utilised.

The flow line along which the computation is to provide temperatures is divided into a number of segments, which may be arbitrarily spaced apart: in general the segment end points have been taken at 100 km intervals. The values of accumulation, surface velocity and temperature, ice thickness, bedrock elevation and geothermal heat flux are determined at each of these points. A sub-programme then fits a quadratic to the two segment end points ahead, and the one behind, the current location along the flowline, and thereby interpolates values of all parameters to that location. Provision is made during this interpolation to insert a climatic variation into all of these quantities.

For temperatures the boundary conditions are:

Upper boundary: temperature prescribed and interpolated to the current location as just described.

Lower boundary:

(a) base temperature prescribed as a constant for the entire current segment. This is useful only when the ice is floating over an ocean. In most other cases it is too restrictive to be physically realistic;

(b) If melting or freezing occurs, the base temperature is set to the pressure melting point once the amount of melt or freeze has been determined;

(c) When basal heating occurs, equation (5.14) is used, the base stress being found from

$$\tau_b = - \rho g \frac{\partial E}{\partial x} Z \qquad (5.24)$$

Using a backward difference analogue for the bottom temperature gradient and equating this to the left hand side of (5.14), the unknown lower boundary temperature at time $t+\Delta t$ may be computed. For example, for the mid-order analogues, the gradient is approximated by

$$\frac{\partial\theta}{\partial z} = \frac{N}{12}(25\theta_N - 48\theta_{N-1} + 36\theta_{N-2} - 16\theta_{N-3} + 3\theta_{N-4})$$

and using (5.14) it is seen that

$$\theta_N = 0.04(\frac{12}{N}(\gamma_G + \frac{\tau_b V}{JK}) + 48\theta_{N-1} - 36\theta_{N-2} + 16\theta_{N-3} - 3\theta_{N-4}) \qquad (5.25)$$

Every term in this equation is for time $t+\Delta t$.

(d) When layer heating takes place the term $\tau_b V/JK$ is omitted in (5.25) above.

5.6.3. Lower boundary phase change.

If the lower temperature is greater than the pressure melting point, or if melt water already exists, then either melting or freezing must take place. The heat input at the base is prescribed and is given by equation (5.14). Should there be a phase change at the base, however, the lower temperature must be the pressure melting point, and the bottom temperature gradient thus calculated will differ from that prescribed. The amount of heat available for melting, or which must be accounted for in freezing, is in that case

$$\frac{sK}{Z}[(\frac{\partial\theta}{\partial z})_{\text{prescribed}} - (\frac{\partial\theta}{\partial z})_{\text{computed}}]$$

where s is the cross-sectional area of the ice column.

In order to raise the temperature of the lowest δ metres of the ice to melting, an amount of heat $\int_o^\delta \rho c\theta s dz$ cals must be supplied. Here θ is the temperature above the pressure melting point. By assuming that the temperatures in this small depth are approximately linear with depth,

the integral becomes $\frac{1}{2Z}\rho cs\delta^2(\frac{\partial\theta}{\partial z})_{prescribed}$ cals. To actually melt the δ metres of ice requires an additional $Ls\rho\delta$ cals, where L is the latent heat of fusion of ice. Comparison of this with the value of the integral shows that if δ is less than 100 metres (it is usually of the order of millimetres), the heat required to bring the ice to the pressure melting point is at least one order of magnitude less than that required to melt it. Hence the heat required to change the phase of the lowest δ metres is very closely $Ls\rho\delta$ cals. If this is equated to that available, then it is seen that

$$\delta = \frac{K}{Z\rho L}\left[(\frac{\partial\theta}{\partial z})_{prescribed} - (\frac{\partial\theta}{\partial z})_{computed}\right] \qquad (5.26)$$

If δ is positive then the phase change is from ice to water, if negative, ice is accreted at the lower boundary. Clearly, the melt rate M is just $\delta/\Delta t$ where Δt is the time step.

5.6.4. Computational stability.

As pointed out in section 5.6.1, the integration procedure used for temperatures is subject to certain stringent constraints. In particular, if errors in the computations due to machine round-off are not to amplify exponentially with time, the time and space increments must satisfy some inequality. The form of this inequality depends on the equation being integrated, so that it will change according to whether or not layer or basal heating is applicable. Only the inequality for the latter case will be dealt with here; the former case may be derived in an analogous manner. The following steps are first taken:

(i) Equation (5.11) is written using crude forward differences for the time derivative, and low-order centred ones for the vertical derivatives.

(ii) The temperature θ is replaced by $\theta^* + \varepsilon$ where θ^* is the exact value of temperature and ε is the corresponding error.

(iii) ε is assumed to be a function of time and space such that $\varepsilon = a(t)b(z)$.

(iv) b(z) is expressed by $\sum_{r=1}^{N-1} B_r \sin \frac{\pi r i}{N}$ where i = 1,2,3...N-1. Equation (5.11) then transforms into

$$\frac{a(t+\Delta t)}{a(t)} = 1 - \Delta t\left(\frac{4\kappa}{Z^2\Delta z^2} \sin\frac{\pi r}{2N} + \frac{A(1-z) + Mz}{Z\Delta z} \frac{\sin \pi r/N}{\tan \pi r i/N}\right) = 1 + \psi\Delta t$$

in which only one component b(z) has been considered. For the integration to be stable and ε not to increase with time we require $|a(t+\Delta t)/a(t)| < 1$. This is satisfied by (a) $\psi < 0$ and (b) $\Delta t < 1/|\psi|$. Inasmuch as the maximum value of $(\sin \pi r/N)/(\tan \pi r i/N) \simeq 1/\pi\Delta z$ criterion (a) requires $4\kappa > (A(1-z)+M)\frac{Z}{\pi}$. Since the melt is generally negligibly small this reduces to approximately $AZ < 4\pi\kappa \simeq 600\ m^2yr^{-1}$. Generally high accumulations are associated with small ice thicknesses, so that this criterion is almost invariably fulfilled. Certainly it has never been violated in any case treated so far. Criterion (b) requires that

$$\Delta t < \Delta z^2\left(4\kappa + [A(1 - z) + Mz]\frac{Z}{\pi}\right)^{-1}$$

or with

$$\kappa \simeq 50\ m^2yr^{-1} \quad \text{and} \quad z_{min} = 0$$

$$\Delta t < \frac{\Delta z^2}{200 + AZ/\pi} \quad \text{years} \qquad (5.27)$$

The programme allows the user to select his own value of the time step if he so desires, and so long as it satisfies the inequality (5.27) it will be used in preference to a more computationally efficient one. If, however, the time step becomes too large for the stability criterion to hold, it is immediately reset to 80% of the right hand side of (5.27). If the shortest possible computation time is desired, then the programme constantly revises the current value of the time step being used, so that the maximum possible Δt consistent with the stability criterion is employed. Computational instability has not been encountered in the present programme. Calculations in which (5.27) has been violated have been made, and instability has invariably resulted.

5.6.5. Additional computations.

Besides the calculations discussed above, certain ancillary computations are carried out, but only at the end of each segment. The more interesting of these are:

(i) One-way dielectric absorptions.

This has already been treated in sections 4.5 through 4.9. As regards the programme, the experimental data (Fig. 4.8, taken from Robin, Evans and Bailey 1969) is fitted by the polynomial:

$$p = 6.0 + 0.389714\theta + 0.01117540^2 + 0.14983\times10^{-3}\theta^3 + 0.736291\times10^{-4}\theta^4$$

where p is the absorption per unit distance (db/m), and θ is between 0 and -60°C. When θ lies between -60 and -100°C, the linear extrapolation

$$p = 0.00308(100 + \theta)$$

has been used to extend Fig. 4.8.

The absorption is taken as zero for temperatures below -100°C, and given an extremely high value (10^8) for temperatures above the pressure melting point.

The total one-way dielectric absorption in the vertical (P) is then

$$P = -Z\int_{z=1}^{z=0} p\,dz$$

(ii) Horizontal velocity.

The temperatures computed on the assumption of columnar flow may be used to determine the velocity along the flow line at any z-point, assuming no slip at the lower boundary and some predetermined flow law. These "dynamics" velocities will, of course, be inconsistent with the model calculations but are still valuable for the reasons given in section 3.3.

The current programme stores a table of the common logarithm of octahedral shear strain rate as a function of temperature and octahedral

shear stress (see Table 3.1). This table is used to determine the velocity-depth profile from the temperature and shear stress profiles in the following manner:

(a) Find the temperature at a given point.

(b) Determine the octahedral shear stress (given by $\sqrt{2/3}\ \rho g\ \frac{\partial E}{\partial x}\ \xi$) and hence its common log.

(c) Use values of (a) and (b) to look up the table for the corresponding entry, and then take the antilog - this gives shear strain rate when multiplied by $\sqrt{6}$ - and thus $\frac{1}{Z}(\frac{\partial V}{\partial z})$ at the point in question.

(d) Integrate this with respect to depth, from $z = 1$ to $z = 0$, with $V_b = 0$ to obtain the velocity at all points of the grid.

This method of determining the dynamics velocity from the temperature profile has also been used in the fixed column model.

(iii) The local rate of change of temperature at any point - $(\frac{\partial \theta}{\partial t})_z$.

This quantity allows a quick check to be made as to how closely the current transient profile approaches that of the fixed column with constant warming rate (cf. section 5.4). For close agreement $(\frac{\partial \theta}{\partial t})_z$ should vary only slightly with depth.

5.6.6. Output for transient states.

An example of the computer printout for a transient state calculation is given in Fig. 5.4. As with the steady state output, Fig. 5.2, only the most important features will be pointed out.

The first row of data gives the values of base stress as computed from the data, the instantaneous melt, M, and the total melt, M, in metre/year. The last quantity should be compared with the value near the bottom of Fig. 5.4 in the entry "integrated current melt" which is the total melt, uncorrected for the horizontal divergence of the column as it moves. The current melt is also repeated here, with a greater number of significant digits.

Current values of bedrock elevation, accumulation and other relevant parameters are then given, together with their climatic changes (here all zero), and the coefficients of the quadratic fitted to the segment data (see section 5.6.2 above). The quantities of the main table have already been fully discussed above.

At the right of the main table are given the depths of parcels of ice originally at the surface. In the example, parcel 1 was at the surface when the computation started and has now reached a depth 3017 metres; parcel 2 was at the surface at the beginning of the second segment and now is 2278 metres below that level; and so forth. The time taken for each segment is printed immediately below the main table, followed by the total distance moved. For the current example, the third segment is under computation, and the column has moved 220.115 km from the beginning of the flowline. That is, it has moved 20.115 km along the third segment, and has taken 1160 years to move that distance.

An interesting and important piece of information is given in the last line of the output. The time step at the beginning of the segment was 20.0 years (see second line of data under the heading "T.INC"), but during the computation (at 1780 years, to be precise) the ice has thinned sufficiently for the stability "criterion" (equation 5.27) to be in danger of being violated. The programme has detected this and has reset the time step to 17.98 years.

N.PTS	Z.INC	DEPTH	THRM.DIFF	BASE.TEMP	TAU	INST.MELT	TOTL.MELT	U.PICK
26	122.4718	3061.7961	42.8000	0.0000	0.8638	0.0018	1.9540	-2.0000

T.INC	TIME	T.PRINT	X.DIST	X.PRINT	T.EXIT	X.EXIT	PUNCH	SCALE
20.0000	1160.00**********		20.1146	40.0000**********		100.0000	0	-1.0000

VARIABLE		CURRENT VALUE	RATE OF CHANGE PER UNIT TIME	VARIATION COEFFICIENTS ALONG X LINEAR	QUADRATIC
BEDROCK HEIGHT	(METRE)	-0.37585E 03	0.	0.37500E-03	-0.32500E-07
ACCUMULATION	(M/YR)	0.48314E 00	0.	0.12150E-05	-0.63000E-11
SURFACE TEMPERATURE	(DEG)	-0.24211E 02	0.	0.28500E-04	0.30000E-10
GEOTHERMAL HEAT FLUX	(DEG/M)	0.22000E-01	0.	-0.	0.
HEIGHT ABOVE SEA LEVEL	(METRE)	0.26876E 04	0.	0.30000E-02	0.10000E-07
CONVERGENCE POINT	(METERS)	-0.	0.	-0.	0
HORIZONTAL VELOCITY	(M/YR)	0.18855E 02	0.	0.13500E-03	0.70000E-09

DEPTH	TEMPERATURE	TEMP.DIFF	TEMP.GRAD	2ND.DERIV.T	INTGD.ABSN	WARMING	HORIZ.VEL
0.	-24.211	-0.000	********	********	0.000	0.547	58.784
122.	-24.354	-0.143	-0.118	-0.251	1.523	0.535	58.737
245.	-24.500	-0.289	-0.121	-0.331	3.033	0.525	58.601
367.	-24.652	-0.441	-0.126	-0.399	4.532	0.518	58.381
490.	-24.809	-0.598	-0.131	-0.421	6.017	0.513	58.084
612.	-24.973	-0.762	-0.136	-0.380	7.490	0.509	57.844
735.	-25.142	-0.931	-0.140	-0.284	8.950	0.502	57.642
857.	-25.315	-1.104	-0.143	-0.149	10.395	0.493	57.415
980.	-25.491	-1.280	-0.144	0.030	11.828	0.473	57.157
1102.	-25.666	-1.455	-0.142	0.302	13.247	0.451	56.868
1225.	-25.836	-1.625	-0.136	0.762	14.653	0.425	56.549
1347.	-25.995	-1.784	-0.122	1.555	16.046	0.395	56.197
1470.	-26.129	-1.918	-0.095	2.875	17.429	0.362	55.814
1592.	-26.219	-2.008	-0.048	4.955	18.803	0.323	55.399
1715.	-26.234	-2.023	0.030	8.040	20.174	0.278	54.949
1837.	-26.127	-1.916	0.154	12.323	21.547	0.227	54.457
1960.	-25.833	-1.622	0.337	17.853	22.935	0.172	53.910
2082.	-25.271	-1.060	0.595	24.421	24.354	0.116	53.286
2204.	-24.341	-0.130	0.938	31.453	25.831	0.064	52.553
2327.	-22.940	1.270	1.364	37.953	27.406	0.023	51.649
2449.	-20.973	3.238	1.860	42.555	29.142	-0.003	50.470
2572.	-18.371	5.839	2.392	43.745	31.136	-0.014	48.854
2694.	-15.119	9.091	2.912	40.273	33.539	-0.011	46.550
2817.	-11.270	12.941	3.357	31.653	36.579	0.001	42.858
2939.	-6.951	17.260	3.669	18.557	40.589	0.021	34.960
3062.	-2.359	21.852	********	********	46.009	0.051	0.000
METRE	DEG.CENT	DEG.CENT	DEG/100M	DEG/KM/KM	DECIBEL	DEG/1000YR	M/YR

TRAJ.NO	TRAJ.DEPTH
1	3317.
2	2278.
3	497.
	METRE

TIME ELAPSED	=	1160.000	YEARS
DISTANCE MOVED	=	220.115	KILOMETERS
LATERAL DIVERGENCE	=	29.661	PER MILLION YR
STREAMLINES CONVERGE AT		-635.678	KILOMETERS DOWNSTREAM
CURRENT MELT	=	1839.862	MICRON/YR
INTEGRATED CURRENT MELT	=	2211.542	MILLIMETRE
COLUMN SURFACE WARMING	=	0.549	DEG/1000YR
COLUMN ELEVATION CHANGE	=	-60.356	METRE/1000YR
IMPLIED SURF. LAPSE RATE	=	0.909	DEG/100M
DIELECTRIC ABSORPTION	=	46.009	DECIBEL (ONE WAY)
ABSORPTION TEMPERATURE	=	-21.000	DEGREES
SURF GRADIENT OF COMPUTED TEMPERATURES	=	-0.115	DEGREES PER 100 METRES
BASE GRADIENT OF COMPUTED TEMPERATURES	=	3.794	DEGREES PER 100 METRES

TIME STEP RESET. NEW VALUE IS 17.97938 YEARS. TIME IS NOW 1180.000 YEARS.

FIG. 5.4 A sample of the printout for a flowline calculation.
The listed quantities are discussed on pp. 114 and 116.

The total one-way dielectric absorption is 46.009 db; that at any depth in the ice may be read from the main table. The absorption temperature (defined by equation (4.64)) is -21°C. These parameters were introduced and discussed in section 4.4.

The only parameter needing to be clarified is that labelled "implied surface lapse rate". This has been discussed in section 4.2.5, and is merely the quasi-horizontal gradient of surface temperature divided by the horizontal gradient of elevation along the flowline. Without climatic change in either variable, this ratio is the same as that of the total derivatives of these quantities, given in the two entries immediately above.

This completes the outline of the computer-modelling procedures and operations. We come now to the results obtained for the Antarctic ice cap.

6. RESULTS OF TEMPERATURE CALCULATIONS.

6.1. Basal temperatures.

A number of different maps of basal temperature have been constructed from different calculations. The column model steady state calculations have provided a coverage for some 300 independent points spread over the Antarctic area. The flowline calculations have provided a coverage for some 50 continuous flowlines. An additional column calculation has been carried out for high values of the geothermal heat flux. All these have been based on the balance velocity distribution. A further column calculation has been carried out with velocities one half of those needed for balance.

As was pointed out in section 4.3 the base temperature is extremely sensitive to the input data. In particular slight errors in the values of base gradient $\gamma_b = \gamma_G + \frac{\tau_b V}{JK}$, surface warming $S = \frac{V\alpha\lambda}{A}$, or ice thickness Z, make considerable errors in base temperature.

Because of these errors the output values have in most cases only been contoured to 10°C intervals. This shows the major trends and conforms with the input data smoothing. Minor differences of up to 5°C in basal temperature are not considered significant. It will be noticed that the large scale trends as well as the maps from different input data show changes much larger than this.

An earlier flowline output map was given by Budd, Jenssen and Radok (1970) in which only about half the present flowline density was achieved. The present density now brings the flowline output up to a density comparable to that of the column coverage.

6.1.1. Column model basal temperatures.

The results of the simple column model calculations are illustrated in Map (4/1a). The data used include: ice thickness Z (Map 1/3), accumulation A (Map 1/5), surface warming S (Map 2/5, assumed constant with depth), surface temperature θ_s (Map 1/6), and base gradient γ_b (Map 3/3).

The values of geothermal flux gradient used are

2.2 °C/100 m	East Antarctica	($q_G \sim 1.2$ μcal $cm^{-2}sec^{-1}$)
2.6 °C/100 m	West Antarctica	($q_G \sim 1.4$ μcal $cm^{-2}sec^{-1}$)

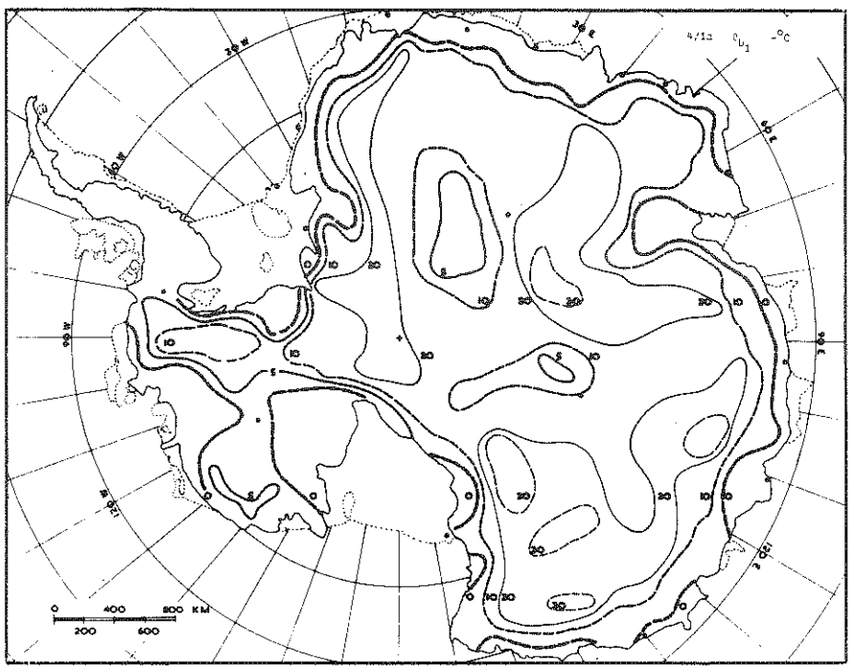

Map 4/1a. Base temperatures for balance (column model) θ_{b_1} *-°C.*

For each of 300 positions the basal temperature has been calculated from the heat conduction in a vertical column with a constant warming rate with depth, using the input data from the previous maps for ice thickness, accumulation rate, surface temperature, base gradient, and surface warming. These basal temperatures show similar cold areas inland and melt regions near the coast as the flowline results of Map (4/1b) but certain warmer regions inland tend to occur further upstream.

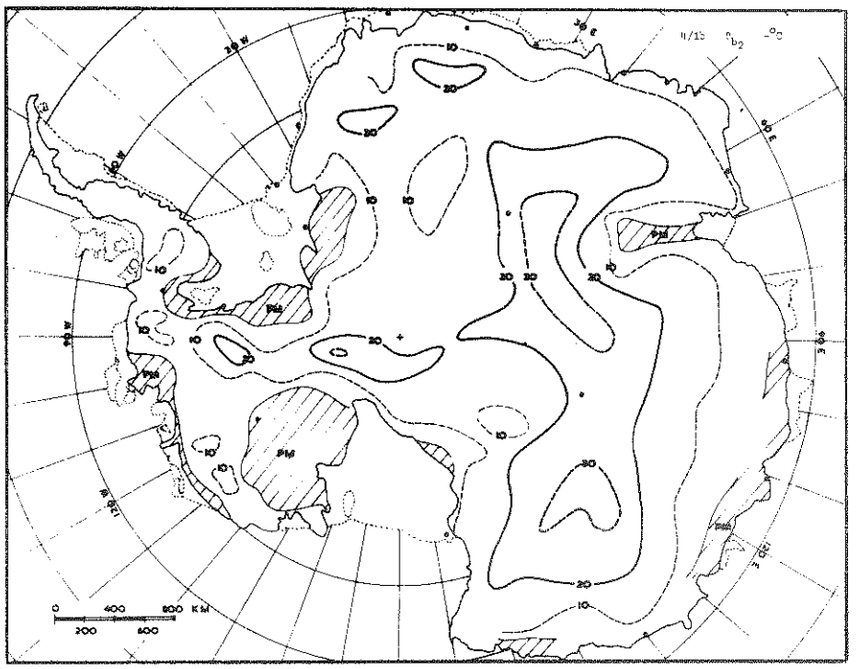

Map 4/1b. Basal temperatures from flowlines θ_{b_2} *-°C.*

From the maps of ice thickness, accumulation rate, surface temperature, velocity and basal stress, temperature depth profiles have been calculated following ice columns along 52 representative flowlines to the coast. The resulting basal temperatures have been contoured each -10°C and for pressure melting point (P.M.). The shaded areas indicate bottom melting or freezing. In general the inland areas of high bedrock tend to be coldest. The basal temperatures tend to rise to pressure melting towards the coast and ice shelf basins, and also in regions of low bedrock.

The resultant pattern is very expressive of the character of the major features of the Antarctic. Superimposition of this map on the map for bedrock elevation (1/4) or ice thickness (1/3) shows that the cold basal regions tend to occur on high bedrock, whereas the warm regions tend to occur in regions of low bedrock.

The predominant features in East Antarctica appear to be the cold areas with basal temperatures of about -30°C over the Gamburtsev Mountains and inland Oates Land and Terre Adelie. From there the temperatures tend to warm up to about pressure melting near the coast. Two anomalous warm regions (greater than -5°C) show up in thick ice near Vostok and between Plateau Station and the Filchner Ice Shelf. These regions are the areas in which we expect melting would most likely occur if large scale melting indeed exists in the interior of East Antarctica.

In West Antarctica two major cold regions exist in association with the thin ice of the two high regions (greater than 2,500 m) of the Whitmore Mountains, and the Executive Committee Range. From these areas the ice tends to warm up approaching the coast and the inland boundaries of the major ice shelves.

Thus on the large scale most of the melt regions appear to be connected to the sea. However it will be shown from the flowline profiles in Chapter 7 that small isolated melt regions may also occur.

6.1.2. Flowline model basal temperatures.

The flowline calculations use approximately the same data as those used for the column model calculations but incorporate more detail along the flowlines and less in between them. The other major difference is that the flowline calculations use as input the surface temperature along the flowline instead of the calculated warming rate (constant with depth) of the column calculations; for the flowline the warming rate is determined in the course of the calculations by the time integration and hence may vary with depth. This means that the flowline calculations should give a better representation in regions where marked changes occur along a line of flow. The flowline basal temperatures are therefore not as sensitive to changes in surface warming and base gradient as are the spot value column model temperatures. Hence the flowline calculations tend to smooth out or reduce small scale variations along the flow.

The results of some 50 flowlines have been contoured independently of the column results and are given in Map (4/1b). In spite of the differences in calculation procedure the maps for the two models are quite similar with respect to the major features. For minor features there appear to be general discrepancies of $\sim \pm 5^{\circ}C$ and displacements in position matching of $\sim \pm 200$ km. These are well within the expected limitations of either model.

The predominant cold interior (to $-30^{\circ}C$) with warming to pressure melting towards the coast and major ice shelf basins are common to both maps. The major regions of cold and warm also appear to correspond.

However the warm areas of the interior of East Antarctica appear to be somewhat downstream of the corresponding column model areas. This may be a feature of the smoothing and lagging of the basal temperatures behind surface changes in the flowline calculations.

Even though there are a number of dissimilarities the degree of agreement is strong enough to allow the confident use of the column model coverage as a powerful diagnostic tool to study deviations from this first balance-velocity model. The following two maps show examples of this.

6.1.3. High geothermal flux and melt rates.

The fixed column model coverage of section 6.1.1 has been repeated with high values of the geothermal flux in order to study the effect of this unknown parameter on the output. The values chosen are

γ_G = 3.3 °C/100 m East Antarctica ($q_G \sim 1.8$ μcal $cm^{-2}sec^{-1}$)

γ_G = 3.9 °C/100 m West Antarctica ($q_G \sim 2.1$ μcal $cm^{-2}sec^{-1}$)

From the histograms given in section 4.2.3 it appears that these values are well above the average for their expected types of geological background, and so we might expect the true conditions to lie between these and those used for Map(4/1a),but probably much closer to the latter.

The resultant basal temperature contours are given in Map(4/1c). The main effect of increasing the geothermal heat flux has been to increase the base temperatures and melt rates everywhere. This effect is most noticeable in the central zones where the base gradients are small whereas at the coast the temperature increase is proportionally much smaller.

The most noticeable change is the appearance of a large melt zone in East Antarctica. The warmer zones of the earlier Map (4/1a) have been extended and raised to pressure melting. However it is interesting to note that this melt zone is still surrounded by cold ice everywhere. The temperatures of the cold area have also been raised by about 10°C. In West Antarctica only small zones near the major mountain ranges have remained below melting. The melt rates are small, around 1 mm yr^{-1} in central East Antarctica, increasing to over 3 mm yr^{-1} near the coast and under parts of the thick ice in West Antarctica.

We notice that this map for high geothermal heat flux shows a pattern of interior melt similar to that given by Zotikov (1963). The values of basal flux used by Zotikov were chosen high to include the effect of basal friction. However we see from the base gradient (Map 3/3) that this effect strongly increases towards the coast. In addition the effect of horizontal advection, or surface warming, was

not included in Zotikov's model. Since both base gradient and surface warming are small inland and increase towards the coast, with opposite effects on the base temperature, the similarity of Map (4/1c) with Zotikov's may be regarded as a result of the two additional complexities somewhat cancelling each other's effects.

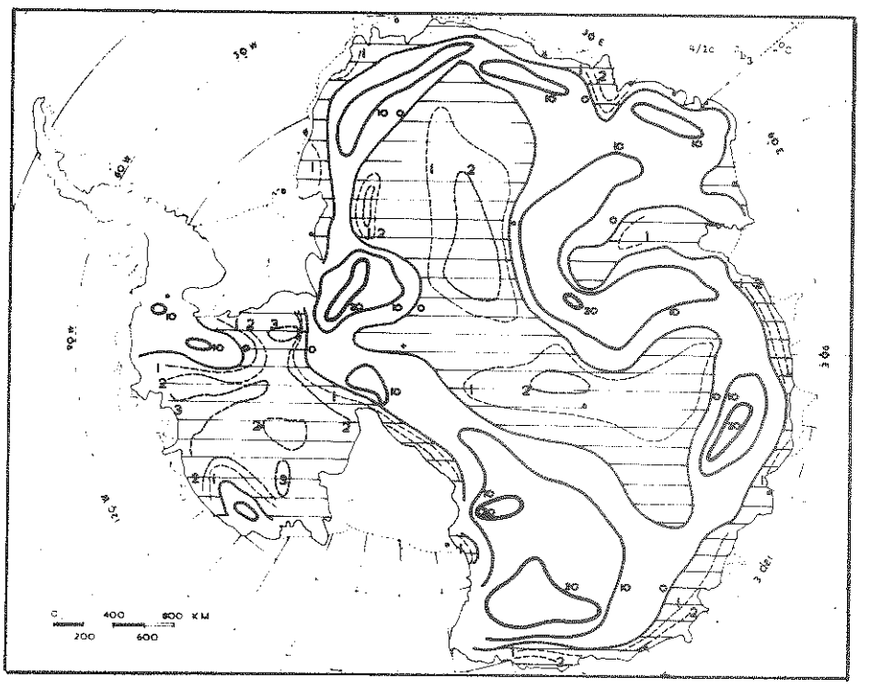

Map 4/1c. Basal temperature (column model, high geothermal flux) θ_{b_3} *°C.*

The basal temperatures have been calculated from the steady state column coverage for a balanced state as for those of Map (4/1a) except that the geothermal heat flux has been increased by 50% to 1.8 and 2.1 μcal cm^{-2}sec^{-1} for East and West Antarctica respectively. The main pattern features are similar to 4/1a but the temperatures on the average are about 10°C warmer inland causing wide areas of melting to develop in both East and West Antarctica (hatched zones). Melt rate contours (at 1 mm yr^{-1} intervals) are shown by the broken lines inside the melt zones.

6.1.4. Half-balance velocities.

In order to examine the importance of the assumption of balance velocities for the resultant base temperature distribution we turn to the formula (4.58) for base temperature

$$\theta_b = \theta_s - Z[\gamma_b \frac{\text{erf } y}{y} - \frac{V\alpha\lambda}{A} 2E(y)] \tag{6.1}$$

Since the velocity V also affects the base gradient according to

$$\gamma_b = \gamma_G + \frac{\tau_b V}{JK} \tag{6.2}$$

we may write (6.1) as

$$\theta_b = \theta_s - Z[(\gamma_G + \frac{\tau_b V}{JK}) \frac{\text{erf } y}{y} - \frac{V\alpha\lambda}{A} 2E(y)] \tag{6.3}$$

Inland where V is small the term $\gamma_G \frac{\text{erf } y}{y}$ dominates, so that unless V is increased greatly the base temperature is little affected. As the coast is approached the term

$$V[\frac{\tau_b}{JK} \frac{\text{erf } y}{y} - \frac{\alpha\lambda}{A} 2E(y)] \tag{6.4}$$

becomes important. Thus the effect of an increase in V is to accentuate the existing base temperature trend whereas a decrease in V reduces the existing trend.

The column model coverage of (4/1a) has been re-run using V = ½ V where V is the original balance valocity distribution of Map (2/2). This value has been chosen because a number of authors (Giovinetto et al 1966, Loewe 1967, Bardin and Suyetova 1967) have suggested that the total Antarctic ice sheet may be out of balance by as much as a factor of two - with an excess in gain over loss. This could occur if the actual velocities were around one half of the balance velocities.

The resultant basal temperature distribution is shown in Map (4/1d). The similarity with the earlier Map (4/1a) is quite apparent. The inland basal temperatures agree very closely.

However approaching the coast the temperatures are now not quite so warm; also the contrast between the various cold and warm regions is somewhat reduced.

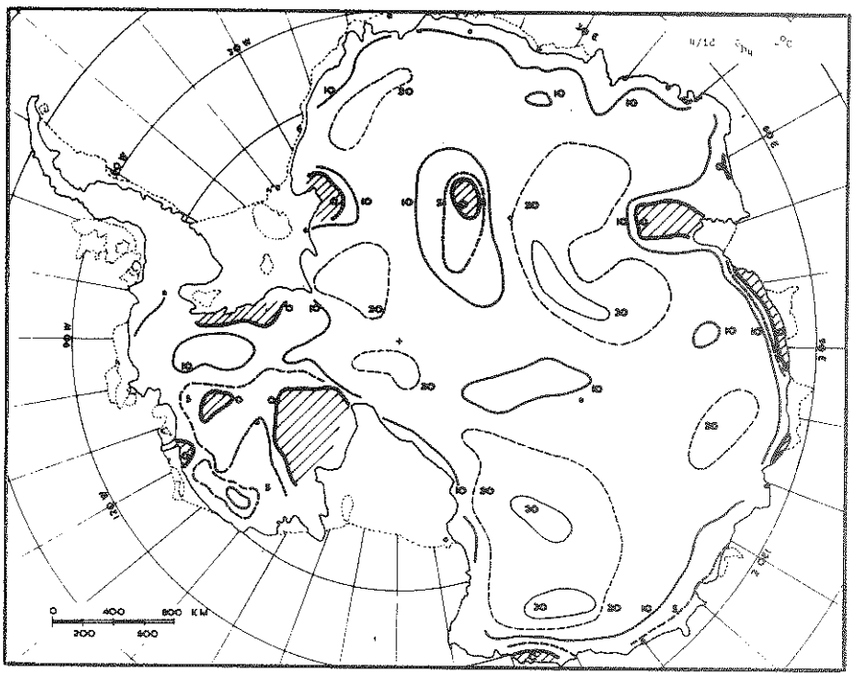

Map 4/1d. Basal temperatures (column model, ½ balance velocity) θ_{b_4} *-°C.*

The base temperatures here have been obtained from the first column coverage using the same data as for Map (4/1a) except that the velocities have been taken as half the balance velocities. This represents a considerable change in the state of balance yet because the velocity affects both the surface advection as well as the base gradient only comparatively minor changes result in the base temperatures.

The overall similarity between the two Maps(4/1a)and(4/1d)with quite different input velocities indicates that the assumption of balance velocities is not too critical as far as the basal temperatures are concerned. It must be realised however that near the coast the shapes of the temperature-depth profiles may have been altered much

more than the base temperatures by the change in the flow velocity. The profiles for higher velocities will have temperature gradients at the surface and the bed (near the coast) with almost double the gradients of the lower velocity temperature profiles. If we were to increase the input velocities rather than decrease them we could expect a greater effect on the basal temperatures inland because the friction heating there is only a small proportion of the basal heat flux. Such an increase in velocities would have a similar effect as the increase in geothermal flux discussed in section 6.1.3.

Since the restrictive balance assumption appears to have not too severe an effect on the base temperatures we now proceed to evaluate the many other features and consequences of the temperature distribution derived from the flowline calculations for conditions of zero mass balance.

6.2. Temperature-depth gradients at the surface.

The temperatures in the upper zones of the ice sheet are the easiest to measure. This makes the vertical temperature gradient in the surface layer, say below the firn layer of density less than 0.9 gm cm^{-3}, a useful guide to the temperature profile as a whole.

The output surface gradients from the flowline calculations are illustrated in Map (4/2). These may be compared with the few measured temperature-depth gradients in Map (1/7).

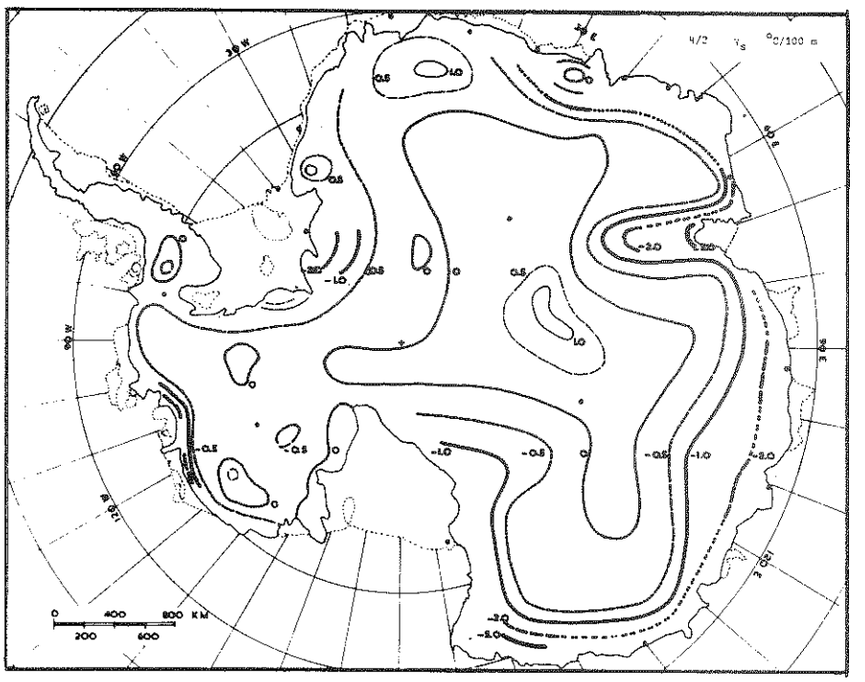

Map 4/2. Temperature-depth gradient at the surface (computed) γ_s °C/100 m.

The surface temperature-depth gradient of the temperature profiles obtained from the flowline calculations has been plotted and contoured. These gradients range typically from over +1°C/100 m inland to -2°C/100 m near the coast. A most interesting feature is the zero gradient line about half way separating an inner zone of positive from an outer belt of negative temperature-depth gradients. The few measured values available as shown in Map (1/7), show a similar general trend of variation.

The most important feature in Map (4/2) is the transition from positive to negative gradients about halfway out from the central inland regions to the coast. The values decrease typically from +1°C/100 m inland to less than -2°C/100 m near the coast. The positive values inland are associated with the small horizontal motion in areas with low values of $y = \sqrt{AZ/2\kappa}$. From equation (4.52) in this case the surface gradient is approximately $\gamma_G e^{-y^2}$. It can be seen from Map (3/6) for y, and from Fig. 4.6 for e^{-y^2}, that these high positive gradients are approximately 0.4 × 2.2 °C/100 m i.e. 40% of γ_b as expected.

The measured values of Map (1/7) show reasonable agreement in form with these results. The values along the Vostok-Casey line decrease from +0.6 to -2°C/100 m towards the coast, and the values inland of Mirny are quite similar.

In the inland region the shallow gradients of the U.S. Queen Maud Land traverse also show a weak trend from slightly negative near the South Pole to positive in the region of Plateau Station. Budd (1969) has pointed out that in absence of climatic change the rate of rise or fall of the ice sheet may be calculated from the surface temperature-depth gradient γ_s according to

$$\frac{\partial Z}{\partial t} = \frac{A\gamma_s}{\lambda} + \alpha V \qquad (6.5)$$

A much larger number of precise measurements of these surface gradients to greater depths will be required before they can be reliably used to thus diagnose the present state of balance of the ice sheet.

6.3. Depth of minimum temperatures.

From the flowline output of temperature profiles the relative depths ξ/Z of the temperature minima have been read off and are shown contoured in Map (4/3). In the central zone where the surface gradients are positive the minimum temperature occurs at the surface. However as the negative surface gradients develop the minimum temperature moves closer to the base. Hence its relative depth values increase typically from zero to up to 0.5 in some areas near the coast. It is of interest that the interpolated value for Byrd Station of between 0.3 and 0.4 agrees reasonably well with the value of 0.37 observed in the Byrd borehole.

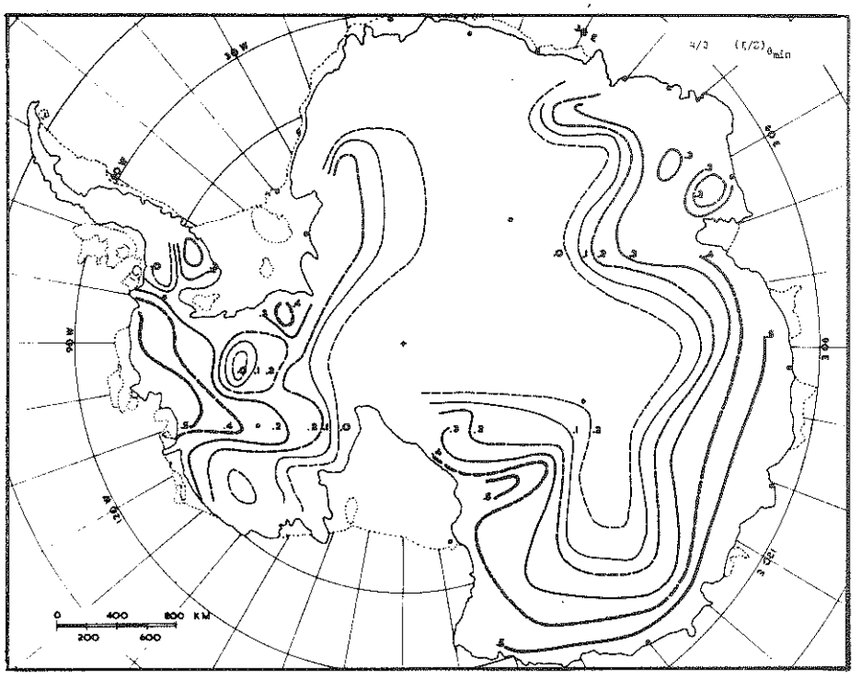

Map 4/3. Relative depth of minimum temperature $(\xi/Z)_{\theta_{min}}$.
The relative depth of the minimum temperature is shown as a fraction of the total ice thickness. Inland where the surface gradient is positive the minimum is at the surface. Approaching the coast where the gradients typically become negative and larger the depth of the minimum approaches half the ice thickness.

By using the surface temperature θ_s (Map 1/6), base gradient γ_b (Map 3/3), surface gradient γ_s (Map 4/2), base temperature θ_b (Map 4/1) and relative depth of the minimum temperature $(\xi/Z)_{\theta_{min}}$ (Map 4/3) a reasonably good approximation to the complete temperature profile at any position may be sketched.

6.4. Mean column temperature .

For many purposes, such as the study of longitudinal stresses and strain rates in the ice, the mean temperature through the column ($\bar{\theta}$) is a useful parameter. This value has been calculated from the flowline temperature profiles as

$$\bar{\theta} = \frac{1}{Z}\int_0^Z \theta \, dz \qquad (6.6)$$

The resultant distribution of mean column temperature is illustrated in Map (4/4).

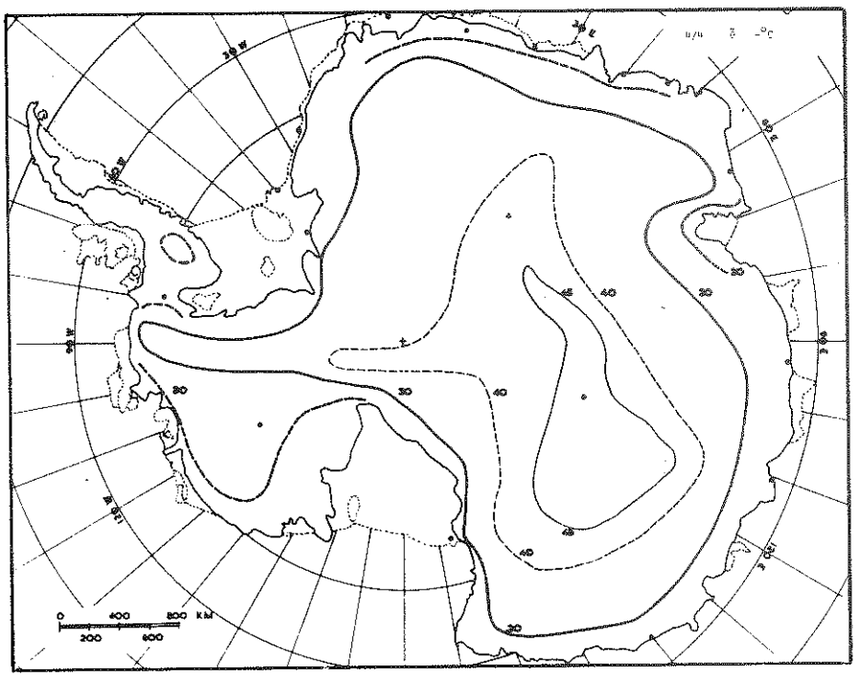

Map 4/4. Mean temperature of ice column $\bar{\theta}$ °C.

For many studies such as the longitudinal stress and strain rates in the ice it is desirable to know the mean temperatures through the thickness. Their pattern of variation is very similar to that of the surface temperature but inland, where the surface gradients are positive, the average temperature is significantly warmer than the surface temperature whereas towards the coast the average approaches the surface temperature.

Because the surface gradients are small the pattern shows great similarity to the pattern of surface temperatures. Where the surface gradients are positive the mean is generally considerably warmer than the surface whereas for negative surface gradients they are much closer. Thus the values of $\overline{\theta}$ increase typically from about -45°C in central East Antarctica to about -20°C near the coast.

6.5. Dielectric absorption temperature.

The results of the absorption temperature calculations as described in section 4.4 are shown in Map (4/5). Since the dielectric absorption increases greatly with temperature the absorption temperature is strongly influenced by the warm basal layers of the ice. Hence as we would expect the absorption temperatures tend to lie between the average column temperatures and the basal temperatures. In these circumstances it remains to be tested, by use of measured echo strength variations when they become available, whether this concept is a useful means of studying the variations in the temperature structure of the ice from one region to another.

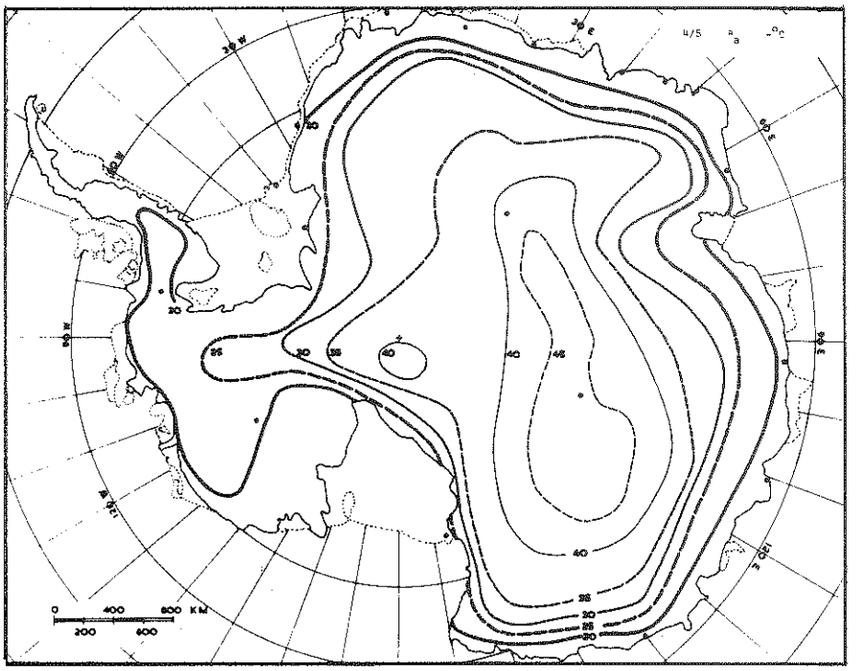

Map 4/5. Dielectric absorption temperature θ_a -°C.

The absorption temperatures have been calculated from the flowline temperature calculations as the temperature corresponding to an equal isothermal column of the same total absorption. The pattern is similar to that of the mean ice column temperature and shows an increase typically from -45°C in inland East Antarctica to about -20°C near the coast.

6.6. Total dielectric absorption.

The total one way dielectric absorption in the ice from top to bottom has been calculated from the flowline temperature profiles as indicated in sections 4.4 and 5.6.5. Its large scale variations are illustrated by contours in Map (4/6), with values in dB.

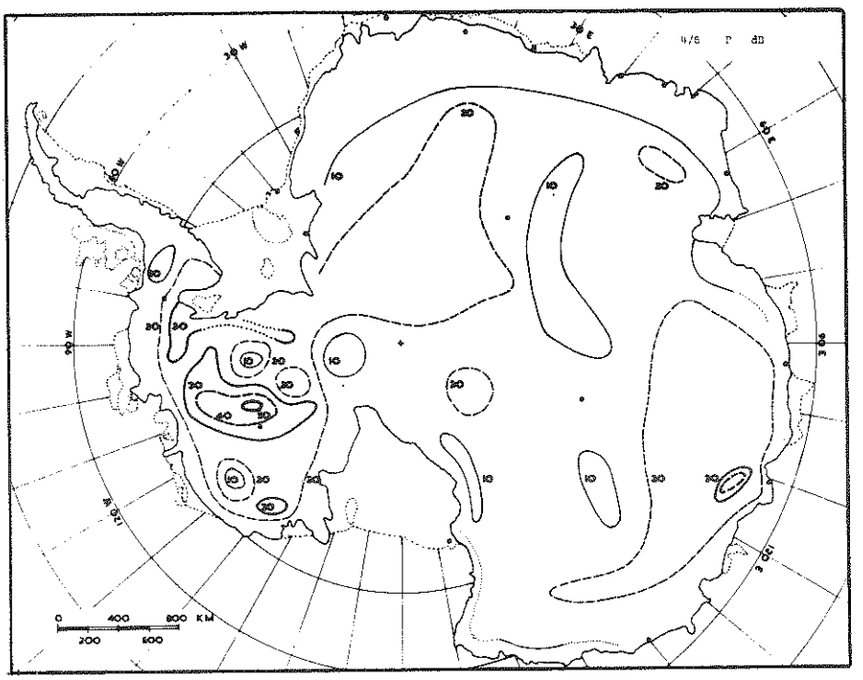

Map 4/6. Total dielectric absorption (one-way) P dB.

The total one-way dielectric absorption of radio waves in the ice has been calculated from the flowline temperature profiles and the absorption-temperature relation of Fig. 4.8 from Robin et al (1969). The absorption values show a marked dependence on surface temperature and ice thickness. Over the larger part of East Antarctica, the absorption is below 20 dB. The highest absorption occurs in West Antarctica where very low bedrock occurs with high ice thickness, and a relatively high surface temperature.

In order to appreciate the significance of Map (4/6) we consider the order of magnitude of typical echo strengths. For a radar sounding instrument with a systems performance of 165 dB we take a relatively high

reflection loss of 20 dB, leaving 145 dB. For a typical ice thickness of 3,000 m the dispersion loss is 20 $\log_{10}$ 3,000 = 95 dB.

This leaves only 50 dB. Hence if the one-way absorption in this case is greater than 25 dB we may expect the echo to be lost. Thus one-way absorptions less than say 20 dB may be termed "low", and those above 30 dB as "high".

With this terminology we notice that most of East Antarctica has comparatively low absorption, with the exception of a high zone inland of Casey. In contrast to that of East Antarctica, where the ice tends to get colder as it gets thicker, the thick ice in Byrd Land is associated with very low bedrock and surface elevations less than 2,500 m. In West Antarctica therefore we find a central zone of thick relatively warm ice with high absorptions, surrounded by thinner low absorption ice towards the coast, and the ice shelves and East Antarctica.

The difficulty of obtaining echoes in high absorption regions is not absolute, but depends on the systems performance of the instrument. At present it appears that the performance level will be below about 200 dB for some time yet. The possibility of covering the whole ice sheet is discussed further in connection with the combined absorption-dispersion map (section 6.9).

6.7. Partial dielectric absorption.

In order to assess the scope for receiving echoes from layers within the ice the absorption in the top 1,000 m of the ice has been calculated (see output example, Fig. 5.4). The detection of these internal echoes depends on many factors such as the wavelength of the radar, the readout system, etc. However for a given situation the variation from place to place is largely dependent on the absorption in the upper layers.

The one-way dielectric absorption to 1,000 m is shown in Map (4/7), with values in dB. The pattern is very similar to the pattern of surface temperature and the mean temperature of the column. This is because the small temperature gradients in the upper layers of the ice make the temperature in the top 1,000 m close to the surface temperature.

By comparison with the total absorption the values here are quite small. The trend is a smooth increase from about 3 dB in the centre of East Antarctica to 10 dB near the coast. In West Antarctica the values are somewhat higher, reaching about 14 dB near the coast. The subsurface layers generally have high reflection losses but even so the low values of absorption make this region especially suitable for studying internal echoes. Robin et al.(1970) have already shown a substantial set of records of continuous subsurface layers in this region.

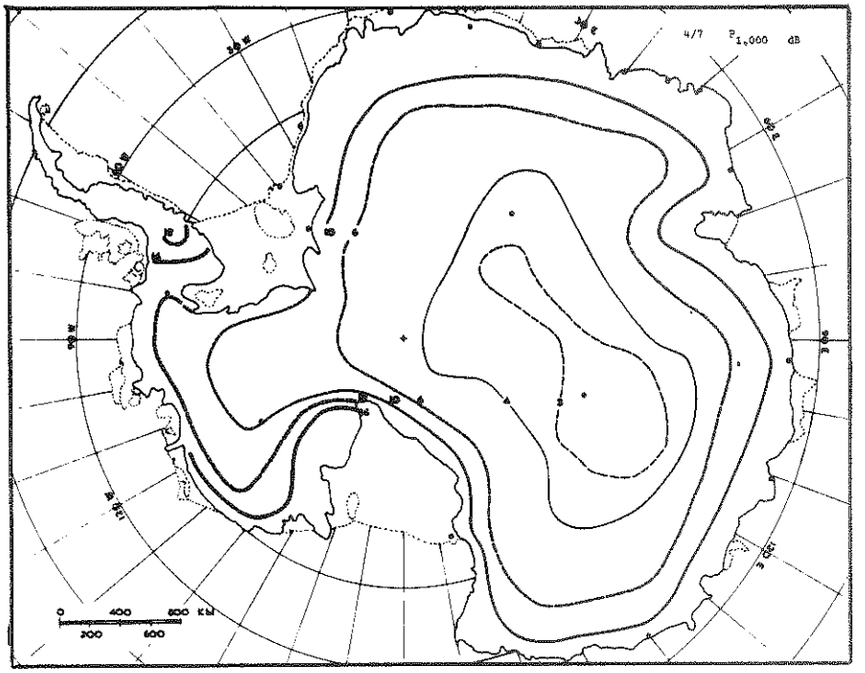

Map 4/7. Partial dielectric absorption (0-1,000 m, one-way) $P_{1,000}$ *dB.*

The one-way dielectric absorption to the 1,000 m depth in the ice has been contoured to indicate the ease of obtaining reflections from internal layers to that depth in the ice sheet. The pattern is similar to that of the surface temperature Map (1/6), with the additional variation expected from the surface temperature-depth gradient pattern Map (4/2).

6.8. Absorption per unit depth.

In order to indicate the temperature effect on the total absorption more clearly we divide the total absorption (P) by the ice thickness (Z) to give the absorption per unit depth (P/Z). This is equivalent to the mean absorption over the thickness. Although not as clear an indicator of the temperature of the ice as the absorption temperature, the mean absorption is much simpler to calculate and follows directly from the measured ice thickness and attenuation.

The output mean one-way absorptions from the flowline calculations are illustrated in Map (4/8) which shows contours in dB/km. There is a smooth trend of increase similar to that in temperature from the inland with values of 5 dB/km to the coast with values of about 15 dB/km. The irregularities of the total absorption (Map 4/6) associated with the regions of different ice thickness are now largely eliminated.

Again we need a large coverage of measured attenuation values to assess the usefulness of this parameter as an indicator of the temperature structure.

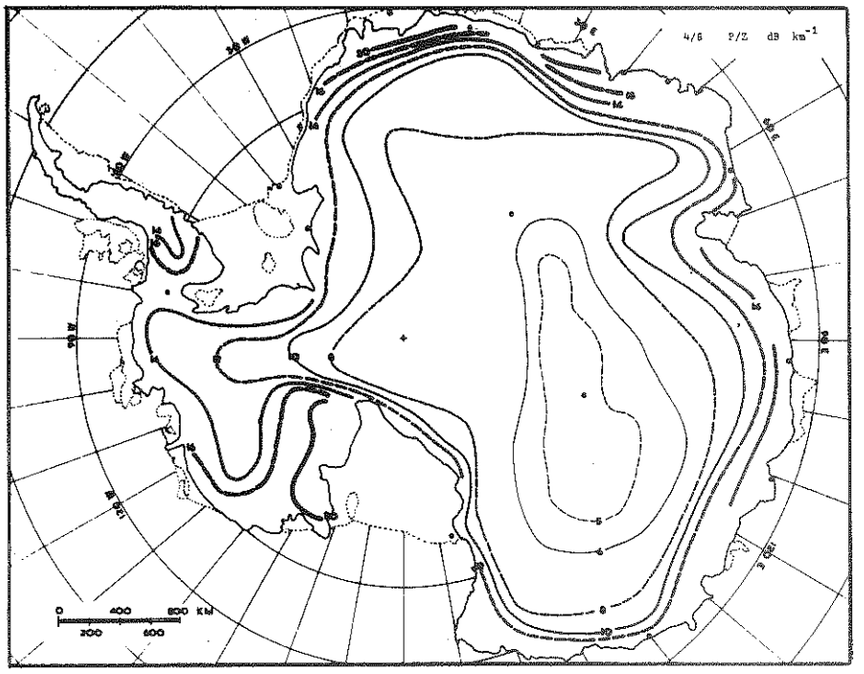

Map 4/8. Absorption per unit depth (one-way) P/Z dB km^{-1}.

By isolating the temperature effect in the attenuation of radar pulses this attenuation can serve as a guide to the temperature structure. The total one-way dielectric absorption (4/6) has been divided by the ice thickness to give the absorption per unit depth. These 'specific' absorptions show a marked similarity to the pattern of the average column temperatures (4/4) and hence may be a useful measure of that temperature.

6.9. Attenuation from absorption and dispersion.

The variation in radar sounding echo strength from place to place is more closely represented by combining the dielectric absorption and path length dispersion into a single map. This has been done by adding twice the dielectric absorption (2P) from Map (4/6) to 20 $\log_{10}$ Z where the ice thickness Z (Map 1/3) is in metres. The resultant two-way attenuation 2Π is shown in Map (4/9). This highlights the regions of thickest ice as the major zones of high attenuation: viz. central West Antarctica, and East Antarctica inland of Wilkes (Casey) and Mirny. The thick ice region in West Antarctica with its lower elevation and higher temperature has much the higher attenuation.

With a reflection loss of about 20 dB it appears that the ice thickness in most of East Antarctica should be measurable by the present systems performances available. For the highest attenuations in West Antarctica it appears that a systems performance in excess of 190 dB will have to be achieved to cover all large-scale areas.

Superimposed on the above broad scale coverage local anomalies may exist of up to about 100 km in extent with quite different attenuations from those shown by the map, without implying significant variations from the steady-state model. However any systematic large scale deviation of measured values from the computed ones would be a valuable guide for interpreting the temperature structure of the ice, and especially for filling in detail between measured temperature profiles at isolated locations.

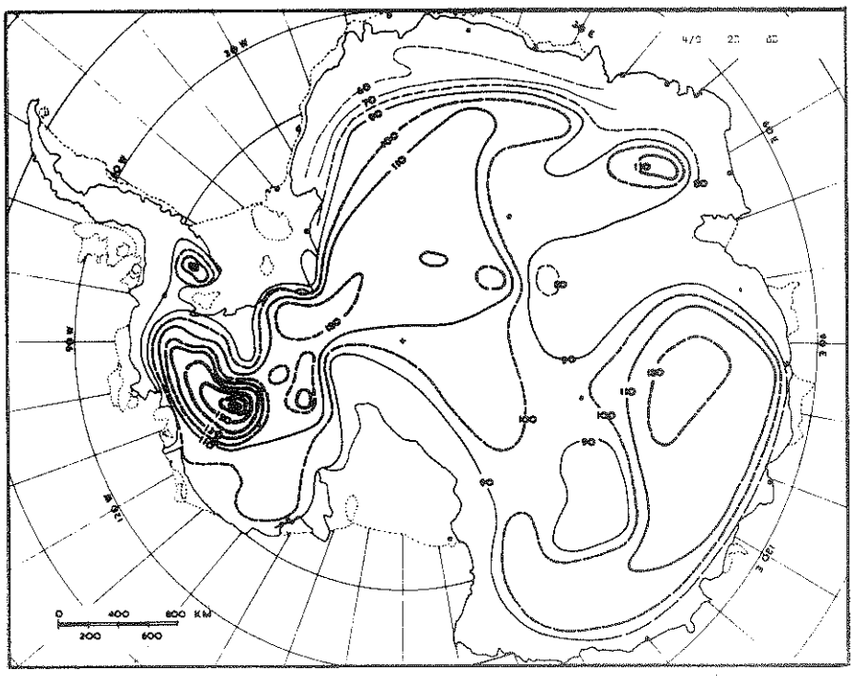

Map 4/9. Total radar signal attenuation (two-way) 2Π dB.

The total radar attenuation (2Π) in the ice has been calculated from the two-way dielectric absorption (2P) and the dispersion proportional the square of the ice thickness (Z) according to Robin et al 1969) by

$$\Pi = P + 10 \log_{10} Z$$

where Z is taken in metres, and Π, P in dB. In addition to these attenuation values the reflection coefficients (∿0-30 dB) have also to be included for calculating returned echo strength. On the whole echoes may be expected with present equipment over most of the Antarctic, on the average, except in Byrd Land and possibly inland of Mirny and Casey.

6.10. Dynamics velocity.

One of the major aims in calculating the temperature distribution throughout the ice sheet has been to use this temperature distribution to calculate the velocity distribution of the ice from the flow law of ice and the shear stress distribution. At this stage it seems fair to say that this aim is rather optimistic, because of three main reasons. Firstly, the assumptions on which the temperature calculations are based, such as the steady state condition and the geothermal flux values, may be considerably in error, thus giving rise to errors in the calculated temperatures. Secondly, the flow law of ice is not sufficiently well known, especially for strongly orientated ice, to allow accurate velocities to be calculated with confidence. Thirdly, the temperature distribution is very sensitive to some of the input data, and the velocity profile is very sensitive to the temperature distribution. Hence, rather than regarding the calculated dynamics velocities as realistic estimates, we consider them primarily as valuable diagnostic indicators of possible errors in the simplifying assumptions made for the temperature calculations.

With these limitations in mind we examine the distribution of dynamics velocities of Map (4/10) corresponding to the steady state temperatures of Map (4/1a) provided by the first column model. No corresponding values are given for the flowline calculations which were started before the dynamics velocity routine had been incorporated into the computer program. Although dynamics velocities are now available for a number of flowlines they do not yet suffice for the construction of reliable contours.

Considering the complex problems and assumptions involved, the output balance velocities in Map (4/10) have a reasonable measure of resemblance to the pattern of the input balance velocities, but with several large anomalies. The main similarity is the broad scale increase from about 2 m yr^{-1} in central East Antarctica to about 50 m yr^{-1} near the coast. This large scale variation shows the output dynamics velocity near the coast to differ from the balance velocity by a factor of about two, and in most cases to be lower than (i.e.

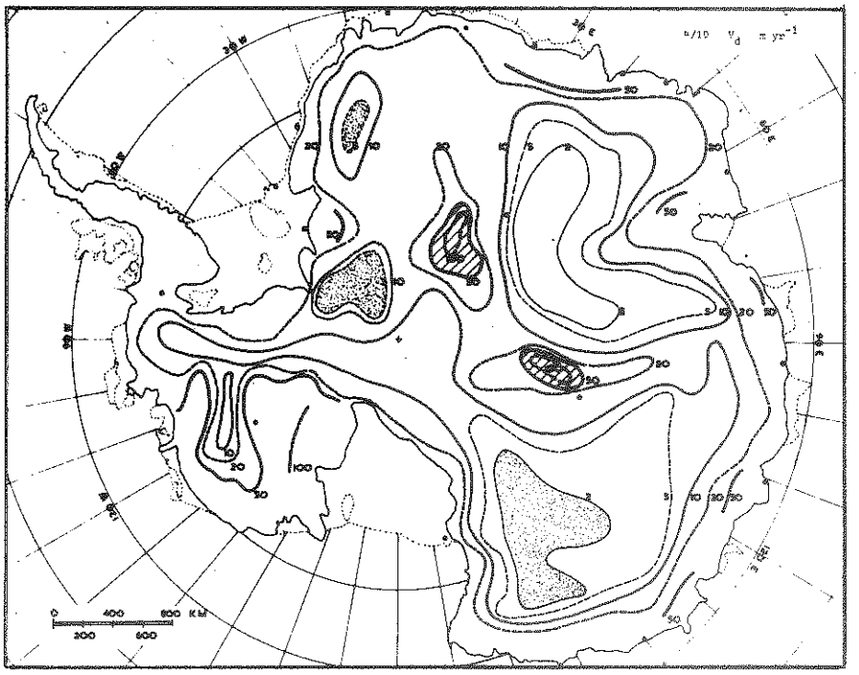

Map 4/10. Dynamics velocity (column model) V_d *m* yr^{-1}.

Velocity profiles have been calculated from the fixed column temperature profiles using the flow law of ice from Table 3.1 and the shear stress proportional to the surface slopes α, Map (3/1) times the depth below the surface ξ. The values show a general trend from 2 m/yr inland to about 50 m/yr near the coast, about half the balance velocities. Anomalous high and low velocity regions exist over regions with warm and cold base temperatures.

about half of) the balance velocity in Map (2/2). This agrees with the tenative conclusions reached about the balance velocity earlier (sections 3.3 and 6.1.4) but there are many other possible explanations, such as:

(i) the values chosen from Fig. 3.2 for the flow law parameter may be too low;

(ii) the actual temperature distribution may not be in steady state - i.e. long term climatic changes may not be negligible;

(iii) the ice sheet dimensions may not be in steady state;

(iv) the accumulation might not have been steady at the present rate;

(v) the geothermal flux may differ significantly from that assumed;

(vi) the relation between stress and velocity used for the dynamics calculations might not hold on the scales used here;

(vii) the fixed column model for temperatures might not be satisfactory.

Major anomalies to the general trend in the dynamics velocity are shown shaded and stippled in Map (4/10). They consist of two high velocity regions in central East Antarctica and three low velocity regions towards the Transantarctic Mountains of East Antarctica. It is obvious from the column model base temperatures (Map 4/1a) that the high velocity zones are associated with high basal temperatures and that the low velocity zones occur where the basal temperatures are low. The diagnostic conclusion here is that the calculated dynamics velocities point to base temperatures which are too high and too low in these respective zones.

It is interesting to note that the basal temperatures resulting from the flowline calculations (Map 4/1b) do not show these exaggerated high and low temperature zones as pronouncedly as the column model calculations. The limited dynamics velocity data available from flowline calculations suggests a broad scale trend similar to that obtained with the column model but without the severe anomalies of Map (4/10). This inspires more confidence in the accuracy of the flowline model method and suggests that point (vii) may be the major cause of the anomalies. However the general tendency of the dynamics velocities to be lower than input balance velocities needs some further comment.

As regards (i), the choice of the flow parameter, the most interesting difference between Antarctic ice and laboratory ice is the existence of strong crystal orientation fabrics, especially in the lower layers of the ice sheet. These however may be expected to enhance

the deformation rates of the Antarctic ice rather than lower them. Hence the use of ice flow parameters based on laboratory experiments is not thought to be the cause of the generally lower dynamics velocities.

The reasons (ii) and (iv) above involve some deviation from steady state. This is believed to be the major cause of the general discrepancy between dynamics and balance velocities and constituted one of the main points it was hoped this project would clarify.

Concerning the remaining factors (v) and (vi) it appears that little more of value can be done economically, other than experiments with a range of different input values, until further measurements become available. We note however that the dynamics velocities corresponding to the high geothermal flux values give velocities in East Antarctica which appear to be far too high ($\sim 10^2$ m/yr). This further supports the calculated base temperatures of Maps (4/1a) and (4/1b).

Since the distributions of velocity and temperature in the ice may both be measured independently, the true relations between them may be gradually worked out as measurements of them become available.

7. VERTICAL PROFILES ALONG FLOWLINES.

One of the most valuable features of the flowline model calculations is the ready access to output results in the form of two-dimensional profiles of all the various parameters as functions of depth and distance along the flowlines. The amount of information available is very large. For some fifty flowlines we can examine two-dimensional profiles of all output features, such as: temperatures, temperature gradients, particle trajectories, ages of the ice, warming rates following motion, radar absorption and attenuation. Moreover it is often useful to view this information in different presentations for different purposes: as a sequence of vertical profiles rather than isolines, or in relative rather than absolute coordinates. Given sufficient computer time and storage, much of this information could be presented as machine-output contoured plots. For the present project however we have concentrated on obtaining complete numerical outputs of detailed vertical profiles of the various parameters each 20 km along each flowline. From this basic data various parameters have been selected for several profiles drawn up for illustration. Thus, although the output data is readily accessible for the complete coverage of the flowlines of Map (2/1a), only a few typical examples will be given here to illustrate the main points of interest in the vertical profiles through the flowlines.

7.1. Particle trajectories.

From the printout of depths reached by different ice particles each successive 100 km along the flowline (see Fig. 5.4), smooth particle paths have been drawn for several flowline sections as shown in Profiles 1 and 2. A typical trajectory has a steep descent at the surface of the inland region, flattens out towards the base, and follows the basal contours to the coast. As the horizontal velocity increases towards the coast the trajectories start at a much flatter angle.

The trajectories crowd much closer together near the base. In fact the total vertical strain can be obtained directly from the vertical distances between the trajectories at different distances along the flowline. This feature is useful in the determination of the history of change of the crystals undergoing deformation.

Combined with the ages of the ice (cf. section 7.2) the trajectories give a clear picture of the history of the ice. The present trajectories calculated for steady state also correspond to the ice flowlines, but for non-steady state the two would differ. The use of stable isotope ratios e.g. O^{18}/O^{16} (cf. Lorius 1968, Dansgaard and and Johnsen 1969, Epstein, Gow, Sharp 1970) provide a valuable means of examining the course of the trajectories as well as the history of climatic change. The mean isotope ratio of the snow over a number of years has a strong dependence on the annual mean surface temperature (cf. Picciotto 1967) and thus on the geographical location. By determining these values on the ice cap surface along a flowline, and also their variation with depth in several boreholes along a flowline, the particle trajectories for steady state can be deduced. Their differences from calculated trajectories allows the variation from steady state and the course of any climatic change to be studied.

Finally the trajectories may be combined with the profiles of other parameters, such as the ages of the ice and the isotherms, to indicate the way various features of the ice have changed with time and the course of its travel. Examples of such combinations are shown in Profiles 6 and 9.

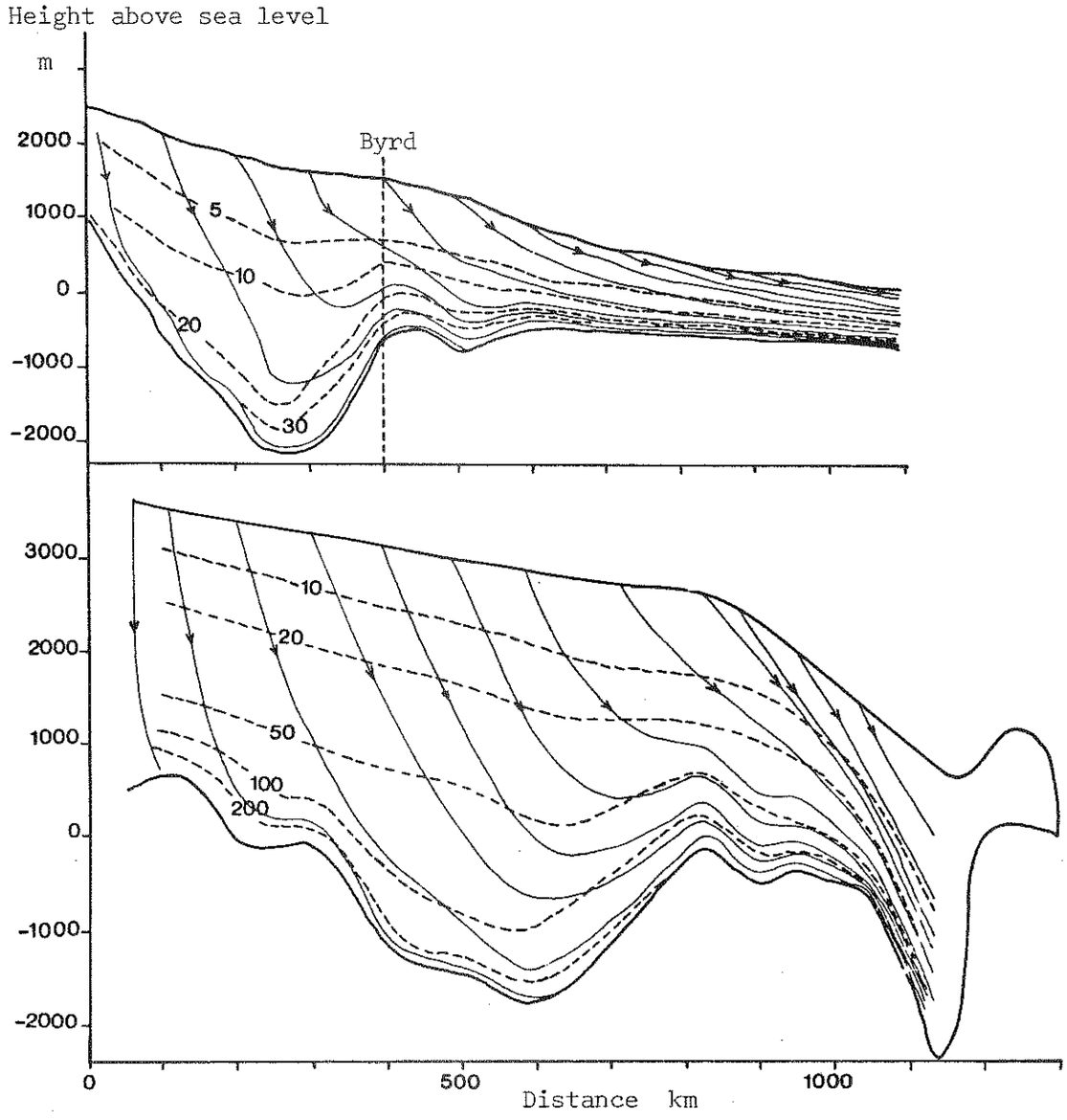

PROFILES 1 Trajectories (arrows) and isochrones (10^3 years, broken lines) for Byrd flowline (top) and Vostok-Wilkes flowline (bottom)

7.2. Ages of the ice.

From the flowline output the depths and ages of the ice particles since their deposition on the surface have been plotted at 100 km intervals along the flowlines and smooth lines drawn through points of equal ages. These have been labelled "isochrones" and several examples are shown in Profiles 1 and 2. In effect these lines represent the subsequent positions of the early surfaces of the ice at depth inside the ice sheet. Taken together with the particle trajectories these profiles also illustrate the horizontal strain and displacement in the ice.

Any features associated with the surface of the ice sheet at a particular time, for example volcanic ash and other fallout, become associated with such an isochrone within the ice sheet at a later period. Periods of melting or of different types of snow surface become stratified as depicted by the isochrones. This concept is particularly promising with regard to the recently observed subsurface echoes and "layers" in the ice obtained from the radar echo sounding cf. e.g. Robin (1969), Robin et al.(1970). The isochrones undergo a gradual transition from the shape of the surface to the shape of the bed as they descend through the ice sheet. This also seems to apply to many of the subsurface radar echoes.

The plan map of the ages of the ice for the whole of the Antarctic, Map 2/8, was obtained from these flowline values, by reading off the ages at the 50% and 90% depths at 100 km intervals along each flowline and plotting these over the whole ice sheet. In the lower layers the age lines crowd closely together and times beyond the 90% depth become very unreliable, especially when they extend beyond the major variations of the last ice age. Here the assumption of steady state is unlikely to be applicable. The two flowline Profiles 1, Vostok-Wilkes and through Byrd, illustrate the clear contrast in ages noted in Map(2/8)for East and West Antarctica.

The advent of downhole sampling techniques, cf. Oeschger et al (1967) and low carbon content counting techniques, cf. Oeschger et al (1966), promise valuable checks of these steady state ages - perhaps back as far as 50,000 years. Other unstable isotopes e.g. Cl^{36}, Al^{26},

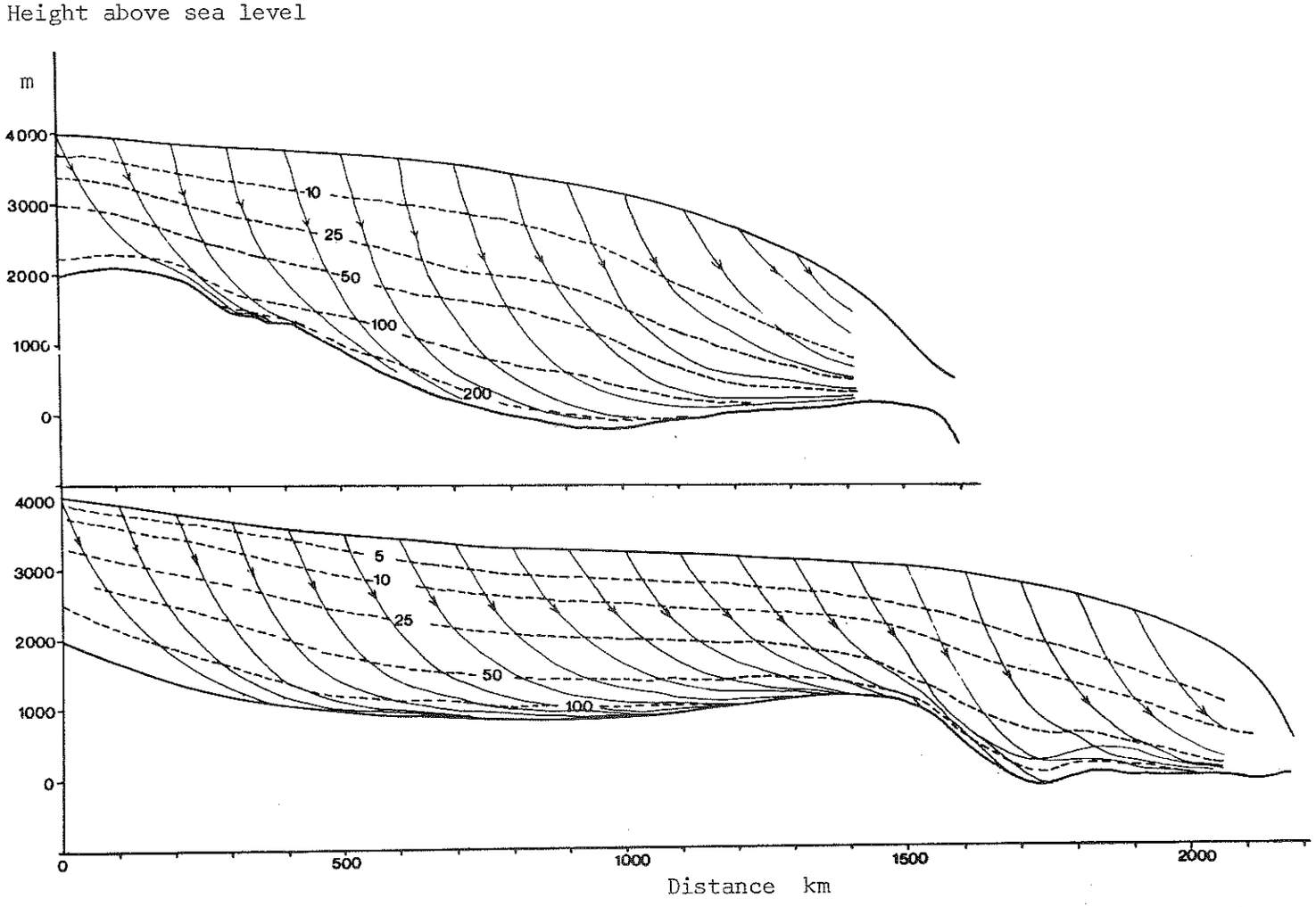

PROFILES 2 Trajectories (arrows) and isochrones (10^3 years, broken lines) for flowline III to Mirny (top) and flowline II to Dumont D'Urville (bottom). The results for the Mirny profile agree with that given by Shumsky (1968).

may be useful for greater ages. From such dating measurements with interpretation by flow models the true age distribution of the ice may be determined.

It is important to note that the age-depth relations here depicted, although calculated for steady state, still give a better representation than the simple formula for constant strain rate in a uniform slab viz.

$$\frac{dz}{dt} = \frac{A}{Z}$$

This is because the variations in A, Z, and V along the flowline have been incorporated naturally into the calculations.

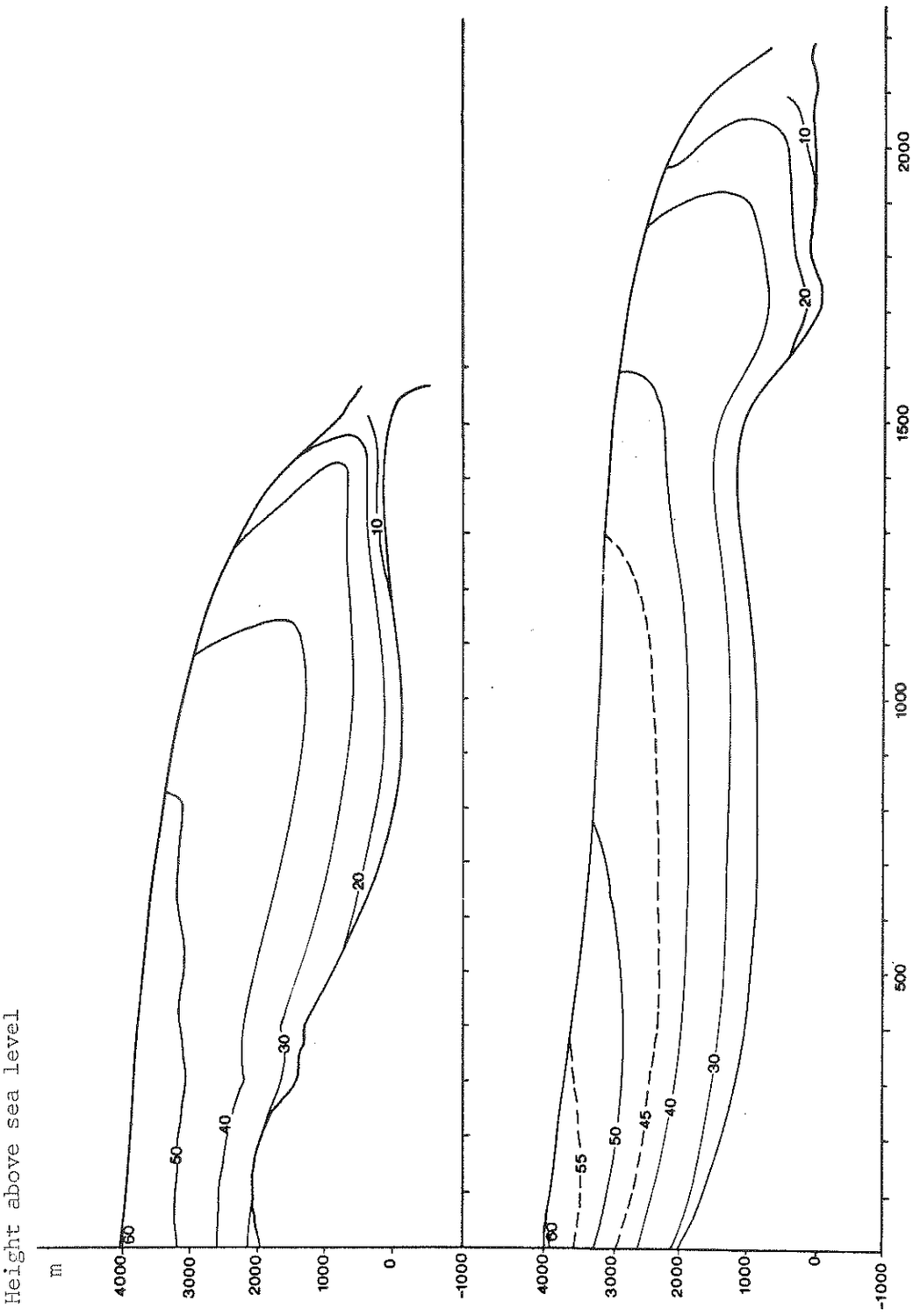

PROFILES 3 Isotherms (-°C) for flowline III to Mimy (top) and flowline II to Dumont D'Urville (bottom)

7.3. Isotherms.

The temperature profiles for the flowline output have been plotted at 100 km intervals along the route and smooth curves drawn through points of equal temperatures in the ice. These equal temperature curves are labelled "isotherms". Examples of the isotherm patterns along flowlines are shown in Profiles 3 and 4.

The general shape of the isotherms consists of trends to warming towards the base and towards the coast. An interesting feature is the line joining the most forward points of the isotherms. This line represents the depth of the minimum temperature of a vertical column along the route. This line first appears below the surface when the temperature-depth gradient at the surface becomes negative, cf. Map(4/2) and also Maps(1/7)and(4/3). From here the line generally moves deeper into the ice towards the coast.

The isotherms show up the trend from positive to negative surface gradient quite clearly by the reversal of slope approaching the surface. The way in which the cold surface temperatures inland become to some extent "fossilised" at depth in the coastal ice is well illustrated by the combined isotherm and trajectory Profiles 6 and 9.

The isotherms nearest the base tend to partly adopt the shape of the bed, but it should be noted how low bedrock depressions can also bring in new warmer isotherms. Similarly bedrock rises can penetrate up into colder isotherms.

Combined with the trajectories the isotherms show the rate of warming as the ice flows outwards to the coast.

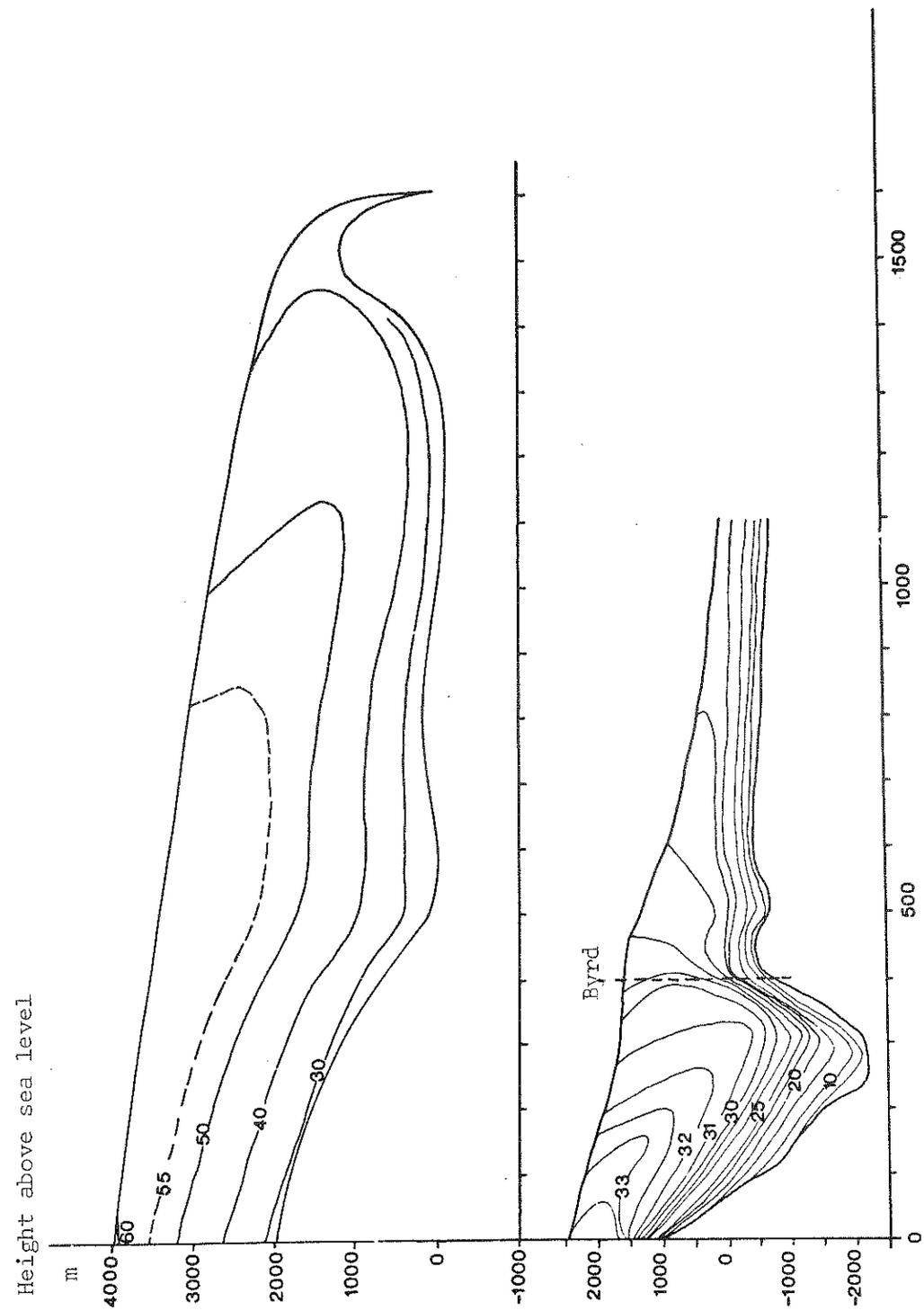

PROFILES 4 Isotherms (-^{o}C) for flowline I (top) and Byrd flowline (bottom).

7.4. Temperature profiles.

In addition to the isotherms illustrated above the temperatures in the ice can also be illustrated by a sequence of temperature-depth profiles along the flowline, as shown in Profiles 5 and 6, or with relative depth in Profiles 7. How the shape of a typical temperature distribution in an ice mass varies with the main parameters (ice thickness Z, accumulation rate A, surface warming rate S and base gradient γ_b) has been discussed by Radok et al (1970). The results of that general study are useful here for explaining how the temperature profiles vary along the line of flow. Some general comments follow.

(i) Increased ice thickness tends to increase the base temperature up to a certain depth, but if the surface warming rate is high, further increases in ice thickness lead to lowering of the base temperatures.

(ii) Increased accumulation rates tend to make the temperature profiles more isothermal.

(iii) Increased surface warming rates make the surface gradient more negative and base temperatures colder.

(iv) Increased base gradients make the base temperature warmer.

Now a striking feature is that as the ice column moves outward to the edge these variables tend to oppose one another in their action. Typically the ice thickness decreases and the accumulation rate increases so that the parameter $y = \sqrt{AZ/2\kappa}$ only varies slowly. The increasing warming rate and increasing base gradient also have opposing effects on the base temperature.

The general pattern of variation is for small positive surface gradients in the interior, such that deep ice has warm basal temperatures and shallow ice cold basal temperatures. As the coast is approached both negative surface and positive base gradients increase in magnitude so that the base temperatures only warm up slowly. Again in depressions the warming is enhanced while over rises the base becomes colder.

The diagram with relative depth coordinates shows more clearly the trend of increase in temperatures with time and distance. From these the warming rates at different depths can be deduced from the displacement of the profiles in the temperature field. The temperature gradient magnitudes however are distorted by this relative scale.

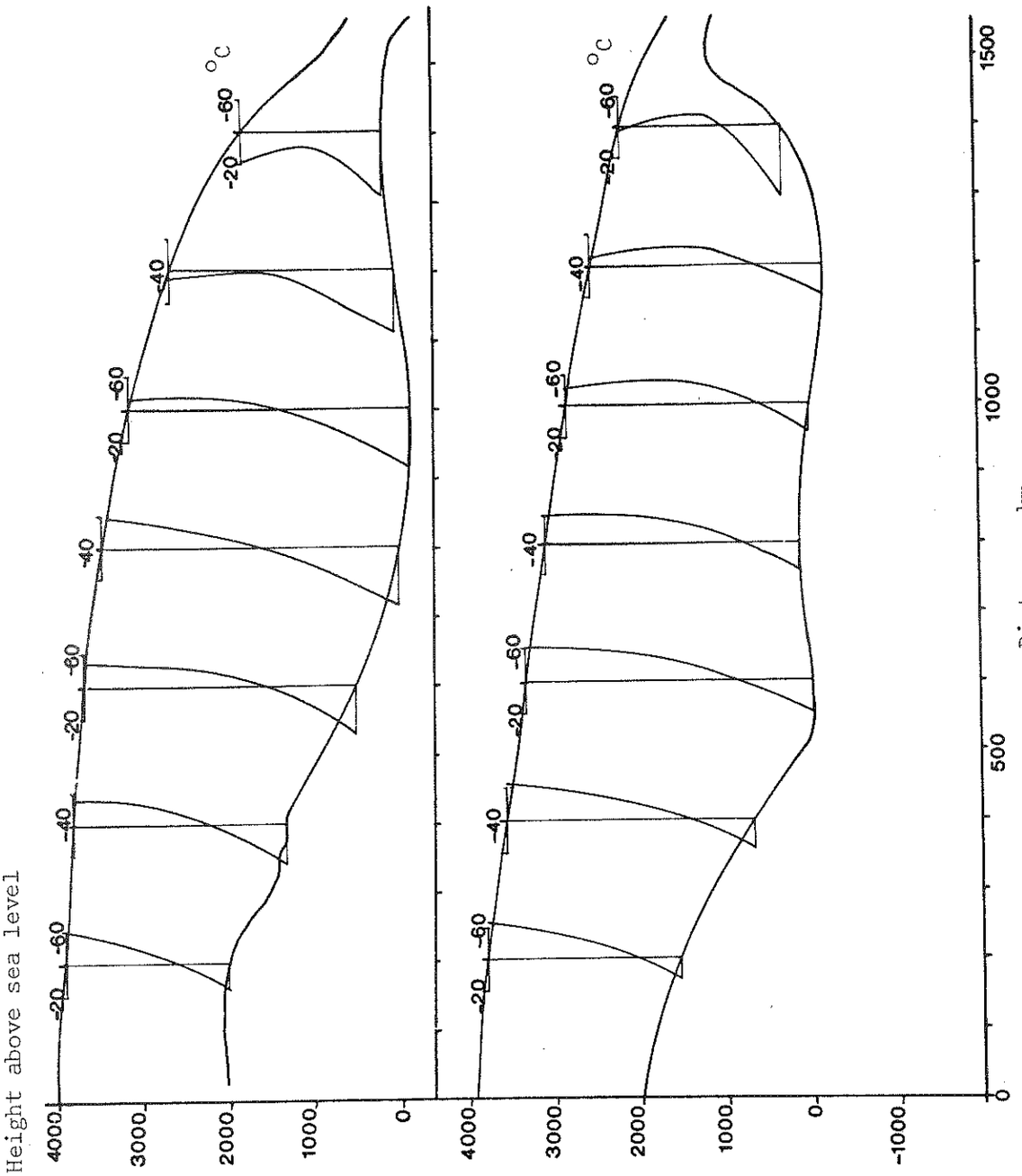

PROFILES 5 Temperature-depth profiles for flowline III to Mirny (top) and flowline I (bottom)

The theoretically convenient concept of constant warming rate with depth is rendered unrealistic by the lack of uniformity along the flowline. The magnitudes of the warming rates have been obtained from some of the flowline calculations. However a clearer understanding of how the warming rate of a column varies with depth and distance along a flowline may be obtained by reference to the relative depth temperatures of Profiles 7. It can be seen that in the upper layers the warming rate averaged over a large scale may be considered approximately constant. However in the basal layers there is a great deal of variation. Ice flowing into depressions tends to have high basal warming rates, while for ice flowing out of such depressions the warming rates may even turn negative. Finally it appears that a general improvement over the constant warming rate assumption could be achieved by adopting values which decrease with depth according to the horizontal velocity, as suggested in section 4.1.7.

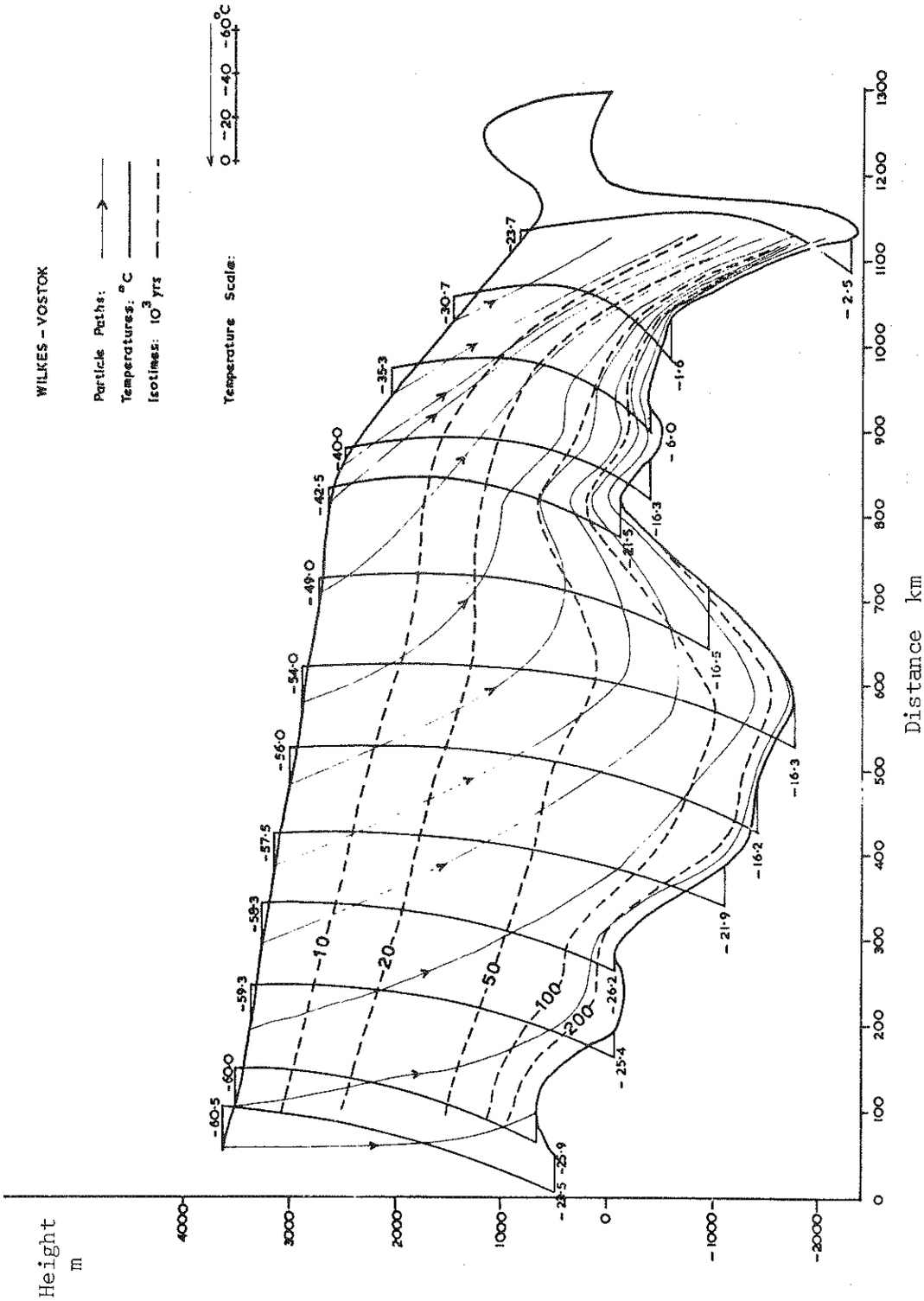

PROFILE 6 Trajectories (arrows), isochrones (10^3 years, broken lines), and temperature-depth profiles (full lines) for the Vostok-Wilkes flowline.

7.5. Dielectric absorption.

The dielectric absorption of radar waves from the surface to various depths (one way), as calculated according to section 5.6.5 has been plotted at 100 km intervals along a number of flowlines. The isolines of absorption in dB have been constructed from these and some examples are shown in Profiles 8 and 9.

The general pattern is that of an increase of absorption with depth; the rate of increase also becomes greater at the base. There is moreover a trend of increase of absorption at the same depth with increasing distance towards the coast. Both these effects are associated with the increase in temperature.

It is interesting to note that the iso-absorption lines near the bed tend to some extent to follow the configuration of the bed i.e., at the same depth lower absorption is found in deep ice than in shallow ice. However the deep layers introduce new high absorption levels which make the total absorption to the bed much greater. In fact the patterns of Profiles 8 and 9 clearly show how echoes are lost in troughs due to the very high absorption values in the basal layers. This assumes other factors, such as the reflection coefficient, remain constant. In some cases of depressions the increase of basal temperature may result in pressure melting being reached, with the consequence of a meltpool being formed in the depression. Such pools could account for stronger echoes received from a deep trench which would otherwise have caused a loss of echo, cf. Robin et al.(1970).

The total attenuation due to both absorption and dispersion is even more greatly affected by ice thickness and thus enhances the trend of loss of echo strength in bedrock depressions.

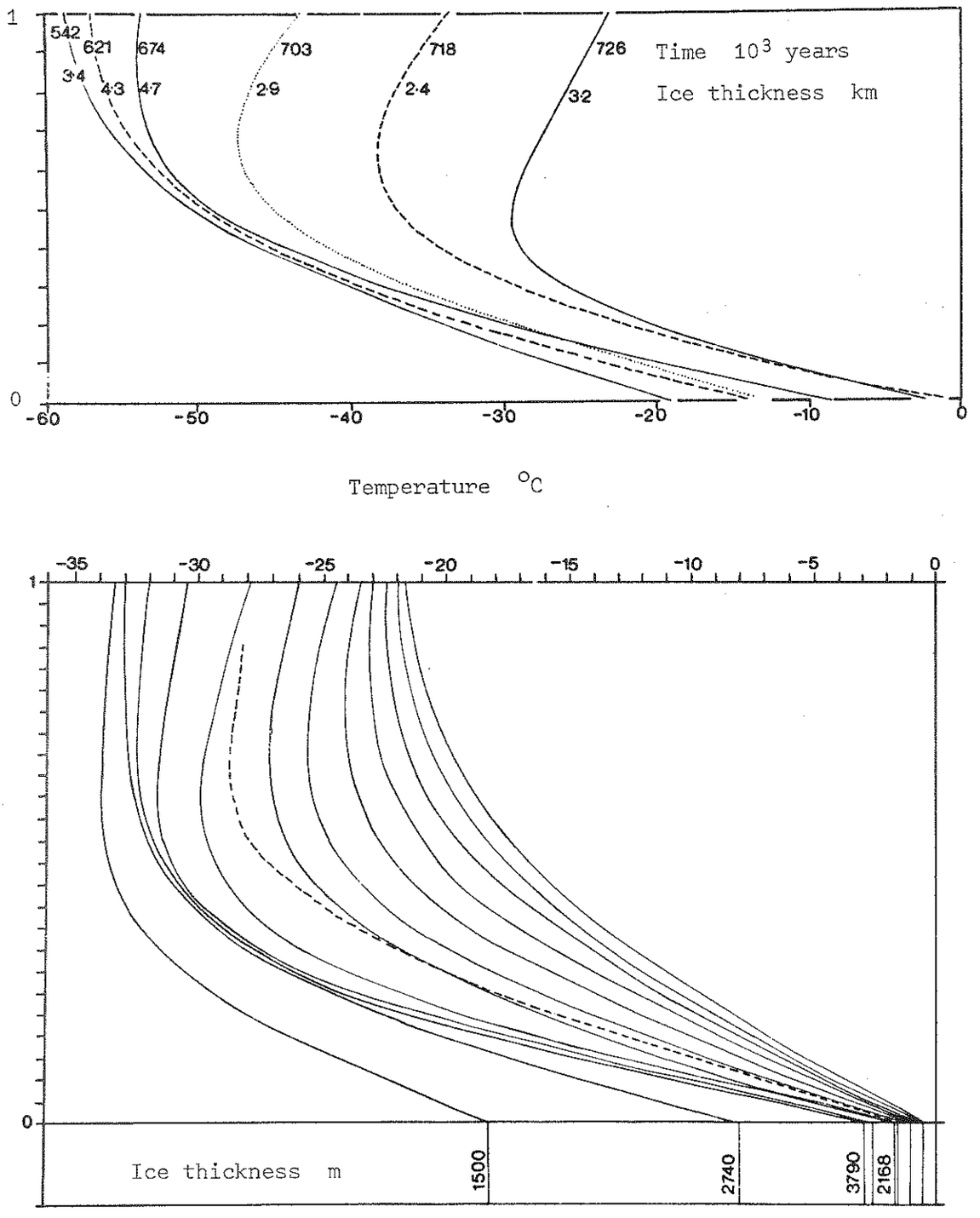

PROFILES 7 *Temperature-relative depth profiles at different distances along the Byrd flowline (top) and the Vostok-Wilkes flowline (bottom; broken curve gives the temperatures measured in the Byrd borehole, after Gow et al (1968))*

7.6. Dynamics velocity profiles.

The profile output information is very valuable for studying the variation of horizontal velocity with depth in the ice and with distance along a flowline. The dynamics velocity as discussed in sections 3.1 and 6.10, has been calculated directly from the flow law of ice, using the calculated profiles of temperature and shear stress through the ice. These dynamics velocities are therefore not directly related to the input balance velocities. For the present flowline model the input balance velocity has been taken as constant with depth. The calculated dynamics velocity profiles allow an assessment of this simplification.

As an example of the dynamics velocity distribution a series of velocity depth profiles on a relative depth scale are shown for 200 km intervals along the flowline to Mirny in Profiles 10. The increasing distances between the profiles over short time intervals represents the increasing strain rates towards the coast. The magnitudes of both the velocity and the strain rate along the line are remarkably similar to the corresponding balance values given in Maps(2/2)and(2/3).

The shapes of the profiles show the comparatively uniform velocity in the upper part, with most of the shear concentrated near the base. This is more clearly brought out by the relative-velocity/relative-depth profiles also shown in Profiles 10. The concentration of the shear towards the base increases towards the coast as the basal shear stress and basal temperature both increase.

The ratio of the average velocity through the column to the surface velocity increases from $\sim$ 85% at 100 km to $\sim$ 92% at 1300 km. This high concentration of the shear into the basal layers indicates that several of the simplifying assumptions used here become reasonable approximations. The longitudinal and vertical strain rates as well as the velocity are all nearly constant with depth in the upper layers. The horizontal heat advection tends to be fairly uniform with depth. The basal heating is a reasonable approximation; e.g., in the 1300 km position of the Mirny line 88.7% of the total frictional heating is produced in the lowest 10% of the thickness. These features make the

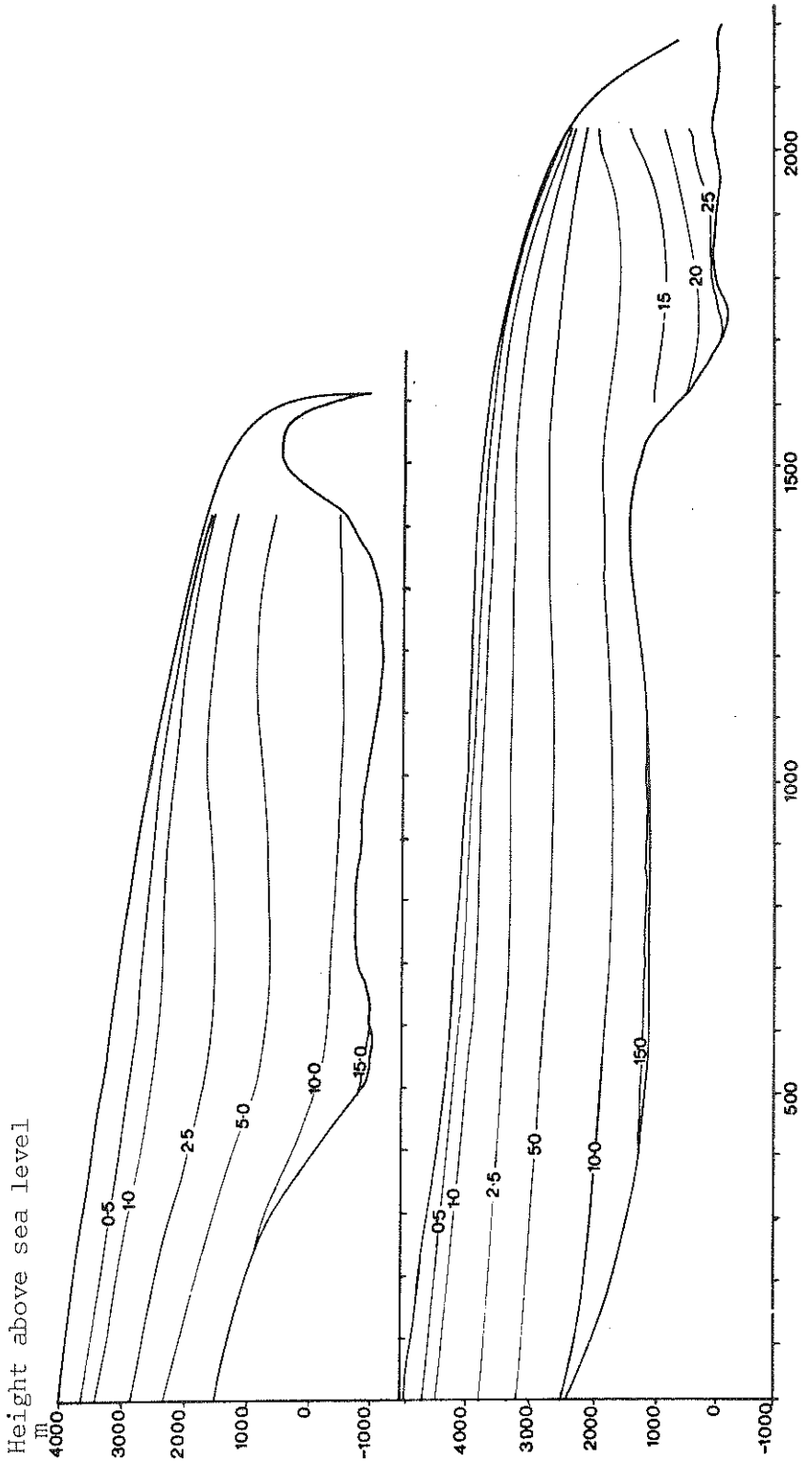

PROFILES 8 Integrated one-way dielectric absorption isolines (dB) flowline I (top) and flowline II to Dumont D'Urville (bottom)

velocity profile not greatly different from ideal basal sliding. Consequently our simple flowline model becomes a good approximation for the temperature calculations.

The success in obtaining reasonable results for the dynamics velocities gives us confidence for using them as an indication of the present state of balance of the ice sheet, and points the way to the future course of the project. This will be to use the dynamics velocities with feedback, instead of assumed velocity values, to govern the motion. A guide to such future schemes is given in the final chapter.

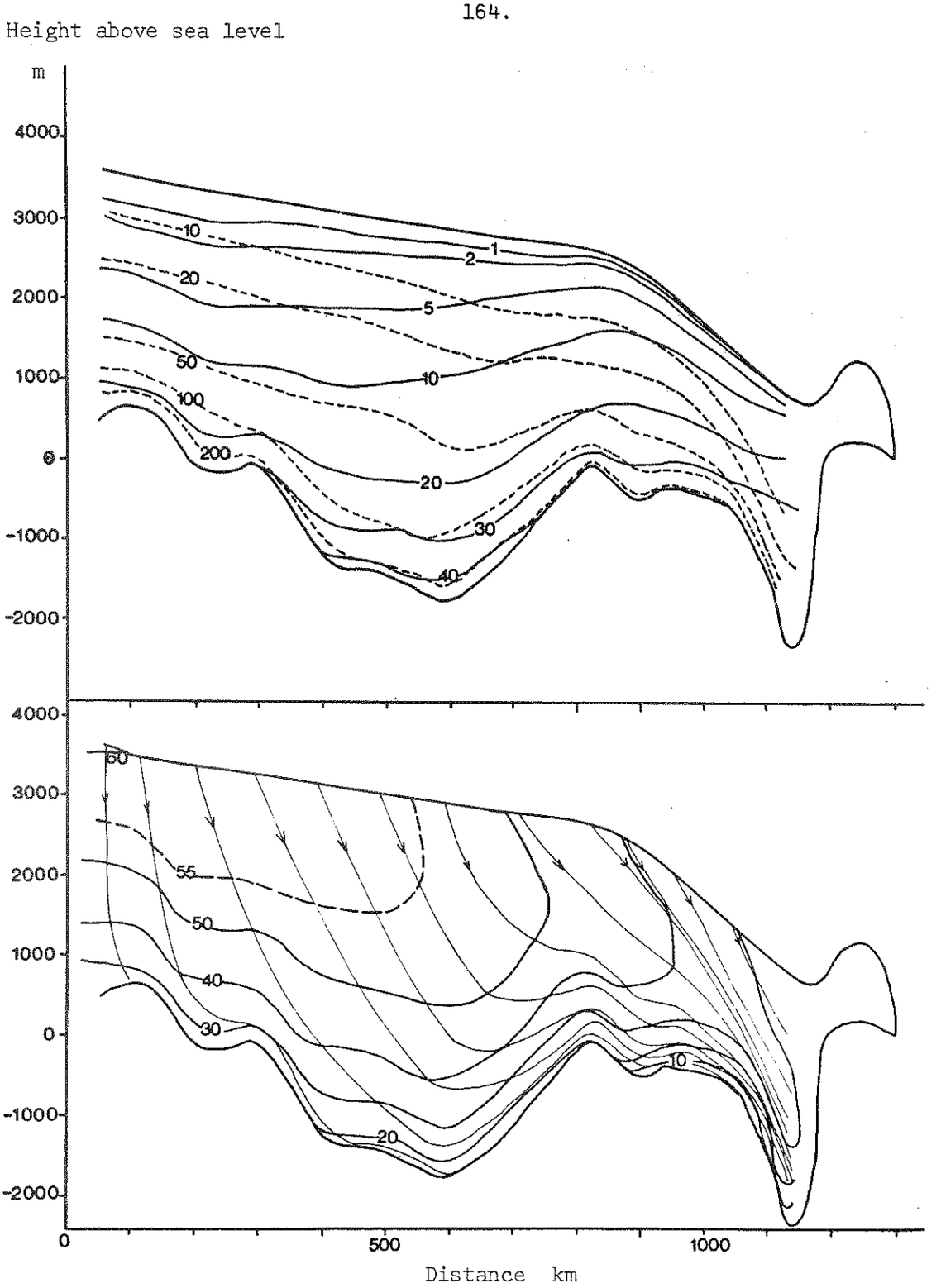

PROFILES 9 Combined profiles for the Vostok-Wilkes flowline showing top: Isochrones (10^3 years, broken lines) and integrated one-way dielectric absorption isolines (dB, full lines), bottom: Trajectories (arrows) and isotherms ($-^{o}C$)

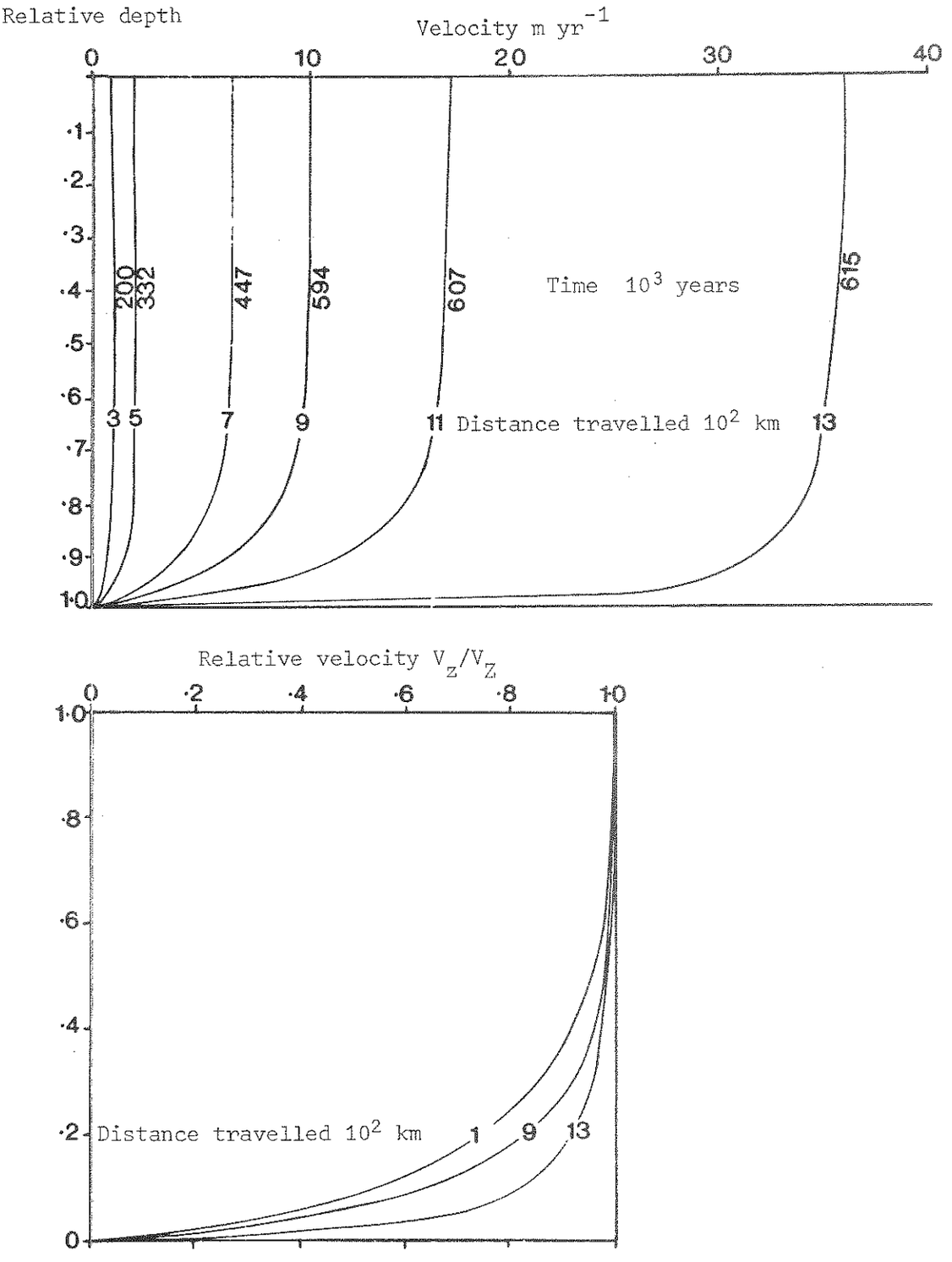

PROFILES 10 Horizontal "dynamics" velocity-depth profiles for flowline III to Mirny
top: absolute velocity-relative depth coordinates
bottom: relative velocity-relative depth coordinates

8. FUTURE DEVELOPMENTS.

Although the results obtained in the first stages of this project have suffered from a number of drawbacks, they do give a preliminary indication of the orders of magnitude to be expected for the various features, and their patterns of broadscale variation over the ice sheet. This must be regarded as merely a glimpse to highlight special features and regions of interest for special future study. The work of providing a detailed realistic picture of the physical characteristics of the ice sheet, well supported by actual measurements and not tied to restrictive assumptions such as steady state, is just commencing. Already a large quantity of new measurements have become available, which to some extent makes the present study obsolete. The designation MARK I attached to this particular report is to indicate that updated versions are planned. However in addition to these updated versions new developments are underway to generalise and automate the study and relax many of the simplifying restrictions used here. The following sections give an indication of the main points of this programme.

8.1. Updated versions.

In order to obtain a rapid turnover from new data to new results, a stream-lined system of data collection, evaluation, compilation, and distribution has to be developed. This is essentially a multinational task and is assisted greatly by the World Data Centres. Frequent exchanges of numerical data as well as updated versions of compilation maps are very valuable to other compilers. Some stream-lining may be possible by building up data banks of numerical data as functions of longitude and latitude in fine detail, to allow ready large scale machine plotting, smoothing, contouring, etc. at any pre-assigned scale. At present the data of importance for the present purpose include surface elevation, ice thickness, accumulation rate, and surface temperature. At a later stage information on the longer term variations of these parameters with time will also become necessary, for dealing with the non-steady state changes. In addition to such input data, measurements of some of the output features, such as surface velocity, will also become available and may be used to remove some of the restrictive input assumptions. The existing computer programmes enable the corresponding new output to be calculated, as new data compilations become available and new inputs are prepared.

8.2. Grid coverage.

In order to cope with continually changing input data, the use of a regular rectangular coordinate grid has a number of advantages over the flowline coverage. Firstly, the flowlines change as new elevation data become available, whereas the specified grid can be kept constant and if necessary more finely divided. This allows simple machine plotting and smoothing at any convenient scale. Secondly, the grid coverage allows a relatively simple progression from the two-dimensional flowline calculations to three-dimensional space variation. Any data specified in latitude and longitude can be simply transformed into mean grid values as required. But it will be necessary to have much more machine storage and greater speeds to handle the complete three-dimensional information and calculations.

8.3. Three-dimensional treatment.

Many features of the flow and temperature fields are essentially three-dimensional in character. Although the flowlines are satisfactory for the steady state assumption, a three-dimensional treatment is necessary in order to treat growth and decay of ice thickness and flow rates.

A numerical scheme is being devised at present for the three-dimensional extension of this study. The basic features of this scheme include flow in the direction of maximum slope of the surface, with the magnitude of the velocity V_z at depth z related to the dimensions of the ice sheet at that position by

$$\frac{dV_z}{dz} = \frac{\rho g \alpha z}{\eta} \qquad (8.1)$$

where α is the surface slope and η a generalised flow parameter, dependent on stress, temperature, etc, and obtained from a numerical table by interpolation.

The heat conduction equation is solved in three dimensions over the grid incorporating the effects of the velocity distribution calculated from equation (8.1) above. The flow law parameter is calculated from the temperature distribution by feedback with the velocity distribution. The continuity equation is used to track the change in shape and size of the ice sheet with time. By cycling the program the velocity and temperature distribution are also followed with time.

8.4. Temperature velocity feedback.

Although the present study introduces temperature and velocity feedback in the layer heating model, and calculates dynamics velocities which result from those temperatures and the flow parameters, no attempt has been made here to use the dynamics velocity to control the change of the ice sheet with time.

By tying the velocity and temperature distributions together it becomes possible to calculate such changes with time. In this way the state of balance of the ice sheet at any time will come out as a result, rather than being used as an assumption. Given a constant climate, i.e. constant temperature and accumulation distributions (in three dimensions), the equilibrium state may always be found simply by running the calculations for long enough.

8.5. Non-steady state.

The non-steady state model as described above promises to be a powerful new tool for future ice sheet calculations. Already a certain amount of evidence of climatic variations is available from other sources e.g. Epstein,Gow, Sharp (1970), Dansgaard et al.(1969), Emiliani (1970). Such estimates of climatic change (temperature and accumulation) may be used as input data and incorporated with the time variations into the calculations of the variation of the ice sheet and its features with time. This will provide realistic estimates for the response of the Antarctic to the climatic changes of the ice ages to be evaluated. In addition it may be possible to work backwards from the present situation to several earlier ice sheet configurations.

8.6 Incorporation of complex refinements.

With larger and faster computers it will become possible to include all the detailed complex refinements to the heat conduction model described in section 4.1. Such refinements include internal layer heating, variation of thermal parameters with temperature, variation of flow parameters with history, and variable strain rates with depth.

In addition several new features can be introduced which were difficult to incorporate into the present flowline calculations. One of the most important of these is the flow and distribution of the meltwater produced at the base of the ice sheet. By adding the equations of the flow of the water to the system its motion can be calculated from the ice sheet dimensions. The modifications to the heat conduction equation due to the refreezing produced can be readily treated with a grid system coverage.

The addition of a scheme for allowing the flow law parameters to vary with time makes it possible to study the growth and development of the ice crystal fabrics throughout the ice sheet and their subsequent feedback effect on the flow and history of the ice.

8.7. Use of measurements of output features.

As measurements of fundamental features, such as the velocity or temperature distribution, become available these may be used to determine other unknown parameters more accurately, or with fewer assumptions. This will be achieved by running a variety of input values through the program and varying them in such a way as to approach as near as possible to the measured output values. This then establishes the "best fit" input values for that model.

On the other hand, if the input values are quite well known, the model itself may be varied in such a way as to produce the measured output. This type of continual modification allows the model to be gradually improved as new information becomes available.

8.8. Use of primitive equations.

Beyond the immediate future an even more general approach than that proposed above, but requiring even better computer technology for a complete coverage, consists of direct use of the full or "primitive" equations of equilibrium. An outline of this procedure is given by Budd and Radok (to be published).

The main point is to use the complete equations of equilibrium for stress rather than the simple velocity gradient relation (8.1). Together with a generalised flow law, the heat conduction equation, the equation of continuity and the water flow equation, the problem of the velocity, stress and temperature distributions in the ice sheet may be solved. The equation of continuity then allows the time variation to be calculated as before.

Such generalisations are not expected to yield much more at this stage where we are dealing only with large scale average variations, i.e. with horizontal scales large compared to the ice thickness. As more detailed information becomes available however the effect of longitudinal and transverse strain rates must be considered because they become very important at scales of several times the ice thickness (Budd 1970). In this case the three-dimensional stress equations will become needed for determining the local variations in strain rates and velocity. With present techniques however it is unlikely that such a detailed coverage of the entire ice sheet will become available for some time yet.

REFERENCES.

Abramowitz, M. and Stegun, I.A. 1965. Handbook of mathematical functions. New York: Dover.

Bakayev, U.G. (Ed.) 1966. Soviet Antarctic Expedition Atlas of Antarctica. Main Administration of Geodesy and Cartography of the Ministry of Geology, USSR. Text translated in Soviet Geography: Review and Translation 8 (5/6) 261-507.

Bardin, V.I. and Suetova, I.A. 1967. Basic morphometric characteristics for Antarctica and budget of the Antarctic ice cover. Proc. Symposium on Pacific-Antarctic Science, 11th Pacific Science Congress, Tokyo: Department of Polar Research, National Science Museum.

Battye, A.C. 1964. Glaciological studies made at Wilkes Base and on the Antarctic ice cap between Wilkes and Vostok, in 1962. Unpublished M.Sc. thesis, Meteorology Department, University of Melbourne.

Bauer, A. and Lorius, C. 1964. The polar ice caps. Impact 14, 223-238.

Beitzel, J.E. 1970 The relationship of ice thicknesses and surface slopes in Dronning Maud Land. International Association of Scientific Hydrology Publ. no. 86, 191-203.

Bender, J.A. and Gow, A.J. 1961. Deep drilling in Antarctica. International Association of Scientific Hydrology Publ. no. 55, 132-141.

Bentley, C.R., Cameron, R.L., Bull, C., Kojima, K. and Gow, A.J. 1964. Physical characteristics of the Antarctic ice sheet. Antarctic Map Folio Series, Folio 2. New York: Americal Geographical Society.

Bogorodskiy, V.V. 1968. Fizitcheskie metody issledovaniya lednikov. Leningrad: Gidrometecizdat.

_____ 1970. Fizika l'da. Arctic and Antarctic Research Institute, Trudy no. 295.

Bogoslovskiy, U. N. 1958. The temperature conditions (regime) and movement of the Antarctic glacial shield. International Association of Scientific Hydrology Publ. no. 47, 287-305.

Budd, W. F. 1966a. Glaciological studies in the region of Wilkes, Eastern Antarctica, 1961. Australian National Antarctic Research Expeditions Scientific Reports Series A(IV) Publ. no. 88.

_____ 1966b. The dynamics of the Amery ice shelf. J. Glaciology 6 (45) 335-358.

_____ 1968. The longitudinal velocity profile of large ice masses. International Association of Scientific Hydrology Publ. no. 79, 58-75.

_____ 1969. The dynamics of ice masses. Australian National Antarctic Research Expeditions Scientific Reports Series A(IV) Publ. no. 108.

_____ 1970. Ice flow over bedrock perturbations. J. Glaciology 9 (55) 29-48.

Budd, W. F. and Carter, D. B. 1971. An analysis of the relation between surface and bedrock profiles of ice caps and ice sheets. J. Glaciology 9 (59) June 1971 (in press).

Budd, W. F., Jenssen, D. and Radok, U. 1970 The extent of basal melting in Antarctica. Polarforschung Bd. VI, 39, 293-306.

Budd, W. F., Jenssen, D. and Radok, U. 1971. A re-interpretation of deep ice temperatures. Submitted for publication in Nature.

Budd, W. F. and Radok, U. (to be published). Glaciers and other large ice masses. Submitted for publication in Reviews of Progress in Physics.

Cameron, R. L., Løken, O. H. and Molholm, J.R.T. 1959 Wilkes Station. Glaciological data 1957-1958. Report 825-1-Part III. IGY Project no. 4.10. Institute of Polar Studies, Ohio State University.

Cameron, R.L., Picciotto, E., Kane, H.S. and Gliozzi, J. 1968. Glaciology on the Queen Maud Land Traverse 1964-1965 South Pole - Pole of Relative Inaccessibility. Report no. 23. Institute of Polar Studies, Ohio State University.

Carnahan, B., Luther, H.A. and Wilkes, J.O. 1969. Applied numerical methods. New York: Wiley.

Carslaw, H.S. and Jaeger, J.C. 1959. Conduction of heat in solids, 2nd ed. Oxfoed: Clarendon.

Corry, M. unpublished Report on the 1968/69 Amery Ice Shelf Survey Programme.

Crary, A.P. 1961 Glaciological studies at Little America Station, Antarctica 1957 and 1958. IGY Glaciological Report no. 5. World Data Center A: Glaciology. American Geographical Society.

Dansgaard, W. and Johnsen, J.S. 1969. A flow model and a time scale for the ice core from Camp Century, Greenland. J.Glaciology 8 (53) 215-223.

Dansgaard, W., Johnsen, S.J., Møller, J. and Langway, C.C.Jr. 1969 One thousand centuries of climatic record from Camp Century on the Greenland ice sheet. Science 166, 377-381.

Dorrer, E., Hofmann, W. and Seufert, W. 1969. Geodetic results of the Ross Ice Shelf survey expeditions, 1962-63 and 1965-66. J. Glaciology 8 (52) 67-90.

Emiliani, C. 1970 Pleistocene temperatures. Science 168, 822-825.

Epstein, S., Gow, A.J. and Sharp, R.P. 1970. Antarctic ice sheet: stable isotope analyses of Byrd Station cores and interhemispheric climatic implications. Science 168, 1570-1572.

Evans, S. 1965. Dielectric properties of ice and snow - a review. J. Glaciology 5 (42)773-792.

Flower, W. 1964. LINEQ. Computer Department, University of Melbourne. Tech. Note no. 3.

Giovinetto, M.B., Robinson, E.S. and Swithinbank, C.W.M. 1966. The regime of the western part of the Ross Ice Shelf drainage system. J. Glaciology 6 (43) 55-68.

Giovinetto, M.B. and Schwerdtfeger, W. 1966. Analysis of a 200 year snow accumulation series from the South Pole. Archiv für Meteorologie, Geophysik, and Bioklimatologie A 15 (2) 227-250.

Gow, A.J. 1970 Preliminary results of studies of ice cores from the 2164 m-deep drill hole, Byrd Station, Antarctica. International Association of Scientific Hydrology Publ. no. 86, 78-90.

Gow, A.J., Ueda, H.T. and Garfield, D.E. 1968. Antarctic ice sheet: preliminary results of first core hole to bedrock. Science 161, 1011-1013.

Ishida, T. 1970. Glaciological research on the inland traverse of the 8th Japanese Antarctic Research Expedition. International Association of Scientific Hydrology Publ. no. 86, 130-140.

Jenssen, D. and Radok, U. 1961. Transient temperature distributions in ice caps and ice shelves. International Association of Scientific Hydrology Publ. no. 55, 112-122.

Jenssen, D. and Radok, U. 1963. Heat conduction in thinning ice sheets. J. Glaciology 4 (34) 387-398.

Jenssen, D. and Straede, J. 1969. The accuracy of finite difference analogues of simple differential operators. Proc. of the W.M.O./I.U.G.G. Symposium on Numerical Weather Prediction, Tokyo. VII, pp.59 - VII, pp.76.

Kane, H.S. 1970. A study of 10 m firn temperatures in central East Antarctica. International Association of Scientific Hydrology Publ. no. 86, 165-176.

Kapitsa, A.P. 1966. Glacial and subglacial relief of Antarctica. Soviet Antarctic Expedition Information Bulletin no. 58. American Geophysical Union Transl. 6 (2) 143-150.

Lee, W.H.K. 1970. On the global variations of terrestrial heat flow. Physics of the Earth and Planetary Interiors 2 (5) 332-341.

Lee, W.H.K. and Uyeda, S. 1965. Review of heat flow data. In: Lee, W.H.K. Ed. Terrestrial heat flow. Geophysical Monograph no. 8, 87-190. American Geophysical Union.

Lliboutry, L. 1968. Steady-state temperatures at the bottom of ice sheets and computation of the bottom ice flow law from the surface profile. J. Glaciology 7 (51) 363-376.

Loewe, F. 1967. The water budget in Antarctica. Proc. Symposium on Pacific-Antarctic Sciences, 11th Pacific Science Congress. Tokyo: Department of Polar Research, National Science Museum.

_____ 1970. Screen temperatures and 10 m temperatures. J. Glaciology 9 (56) 263-268.

Lorius, C. 1964. Glaciologie en Terre Adelia (1956-1959). Centre National de la recherche scientifique, Année Géophysique Internationale, Participation Francaise, Série IX, Fascicule 1.

_____ 1968. A physical and chemical study of the coastal ice sampled from a core drilling in Antarctica. International Association of Scientific Hydrology Publ. no. 79, 141-150.

Mellor, M. 1960. Temperature gradients in the Antarctic ice sheet. J. Glaciology 3 (28) 773-782.

_____ 1968. The Greenland mass balance - flux divergence considerations. International Association of Scientific Hydrology Publ. no. 79, 275-281.

Odishaw, H. Ed. 1964. Solid earth and interface phenomena. Research in Geophysics 2 Vol. 2. Cambridge, Mass.: MIT Press.

Oeschger, H., Alder, B., Loosli, H. and Langway, C.C.Jr. 1966. Radiocarbon dating of ice. Earth and Planetary Science 1 (2) 49-54.

Oeschger, H., Langway, C.C.Jr. and Alder, B. 1967. An in situ gas extraction system for radiocarbon dating glacier ice. Res. Rep. 236, US Army Cold Regions Research and Engineering Laboratory.

Petrov, V.N. and Barkov, N.I. 1964. The cyclical character of snow accumulation on the ice shelves of Antarctica. Soviet Antarctic Expedition Information Bulletin no. 48. American Geophysical Union Transl. 5 (3) 200-203.

Picciotto, E.E. 1966. The South Pole - Queen Maud Land Traverse II, 1965-1966. Antarctic Journal of the United States. 1 (4) 127-131.

_____ 1967 Geochemical investigations of snow and firn samples from East Antarctica. Antarctic Journal of the U.S. 2 (6) 236-240.

Picciotto, E., Cameron, R., Crozaz, G., Deutsch, S. and Wilgain, S. 1968. Determination of the rate of snow accumulation at the Pole of Relative Inaccessibility, Eastern Antarctica: a comparison of glaciological and isotropic method. J. Glaciology 7 (50) 273-287.

Radok, U., Jenssen, D. and Budd, W.F. 1970. Steady-state temperature profiles in ice sheets. International Association of Scientific Hydrology Publ. no. 86, 151-165.

Robin, G. de Q. 1955. Ice movement and temperature distribution in glaciers and ice sheets. J.Glaciology 2 (18) 523-532.

_____ 1969. Long range radio echo flights over the Antarctic ice sheet. Geogr. Journal 135 (4) 557-559.

Robin, G. de Q., Evans, S. and Bailey, J. T. 1969. Interpretation of radio echo sounding in polar ice sheets. Phil. Trans. R. Soc. A 265, 437-505.

Robin, G. de Q., Swithinbank, C. and Smith, B.M.E. 1970. Radio echo exploration of the Antarctic ice sheet. International Association of Scientific Hydrology Publ. no. 86, 97-115.

Shimizu, H. 1964 Glaciological studies in West Antarctica, 1960-1962. In: Mellor, M. Ed. Antarctic Snow and Ice Studies. Antarctic Research Series 2, 37-64. American Geophysical Union.

Shumsky, P.A. 1970. The Antarctic ice sheet. In Bugaev, V.A. (Ed) Soviet Antarctic Research, 1956-1966. Israel Program for Scientific Translations. Washington: NSF.

Vickers, W.W. 1966. A study of ice accumulation and tropospheric circulation in Western Antarctica. In: Rubin, M.J. Ed. Studies in Antarctic Meteorology. Antarctic Research Series 9 135-176. American Geophysical Union.

Weertman, J. 1968. Comparison between the measured and theoretical temperature profiles of the Camp Century, Greenland, borehole. J. Geophys. Research 73 (8) 2691-2700.

Wexler, H., Rubin, M.J. and Caskey, J.E.J. Eds. 1962. Antarctic Research. (Maury Symposium, 10th Pacific Science Congress). Geophysical Monographs no. 7. American Geophysical Union.

Zotikov, I.A. 1963. Bottom melting in the central zone of the ice shield on the Antarctic continent and its influence upon the present balance of the ice mass. International Association of Scientific Hydrology Bulletin 8, 36-44.

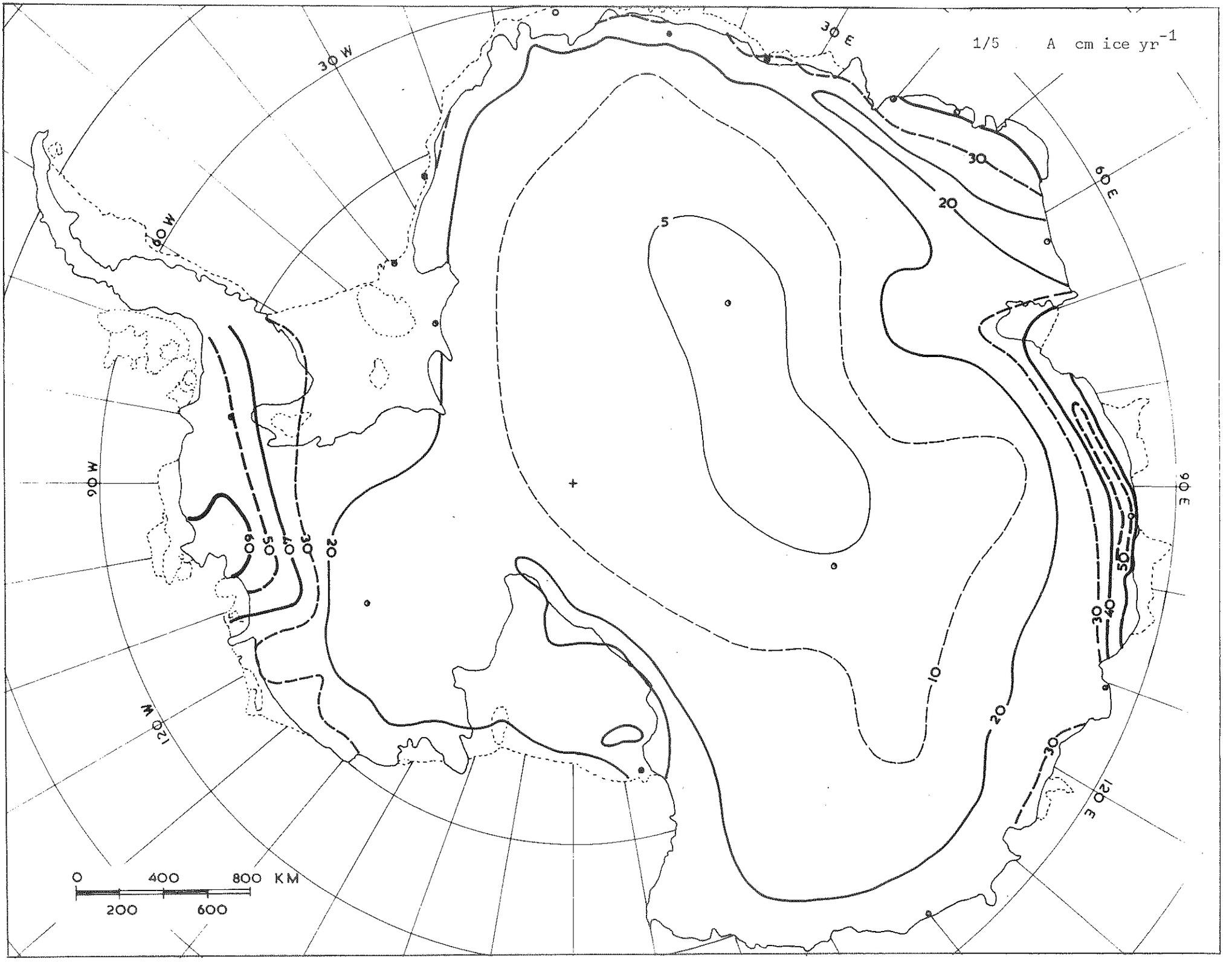
1/5 A cm ice yr^{-1}
0
30 W
60 W
90 W
120 W
30 E
60 E
90 E
120 E
5
10
20
30
40
50
60
0 400 800 KM
200 600

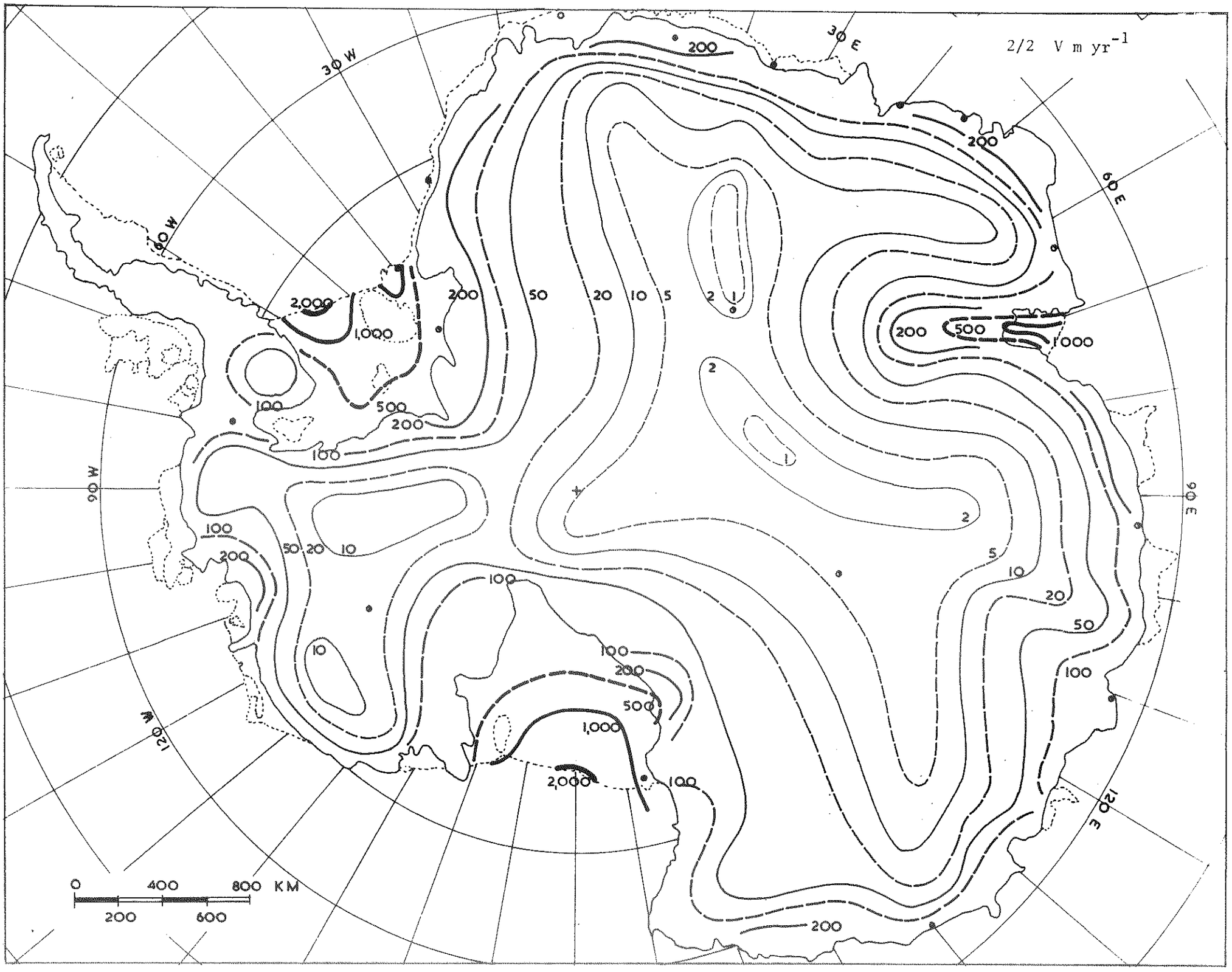
2/2 V m yr^{-1}
30 W
30 E
60 W
60 E
90 W
90 E
120 W
120 E
200
2,000
1,000
500
100
50
20
10
5
2
1
0 400 800 KM
200 600

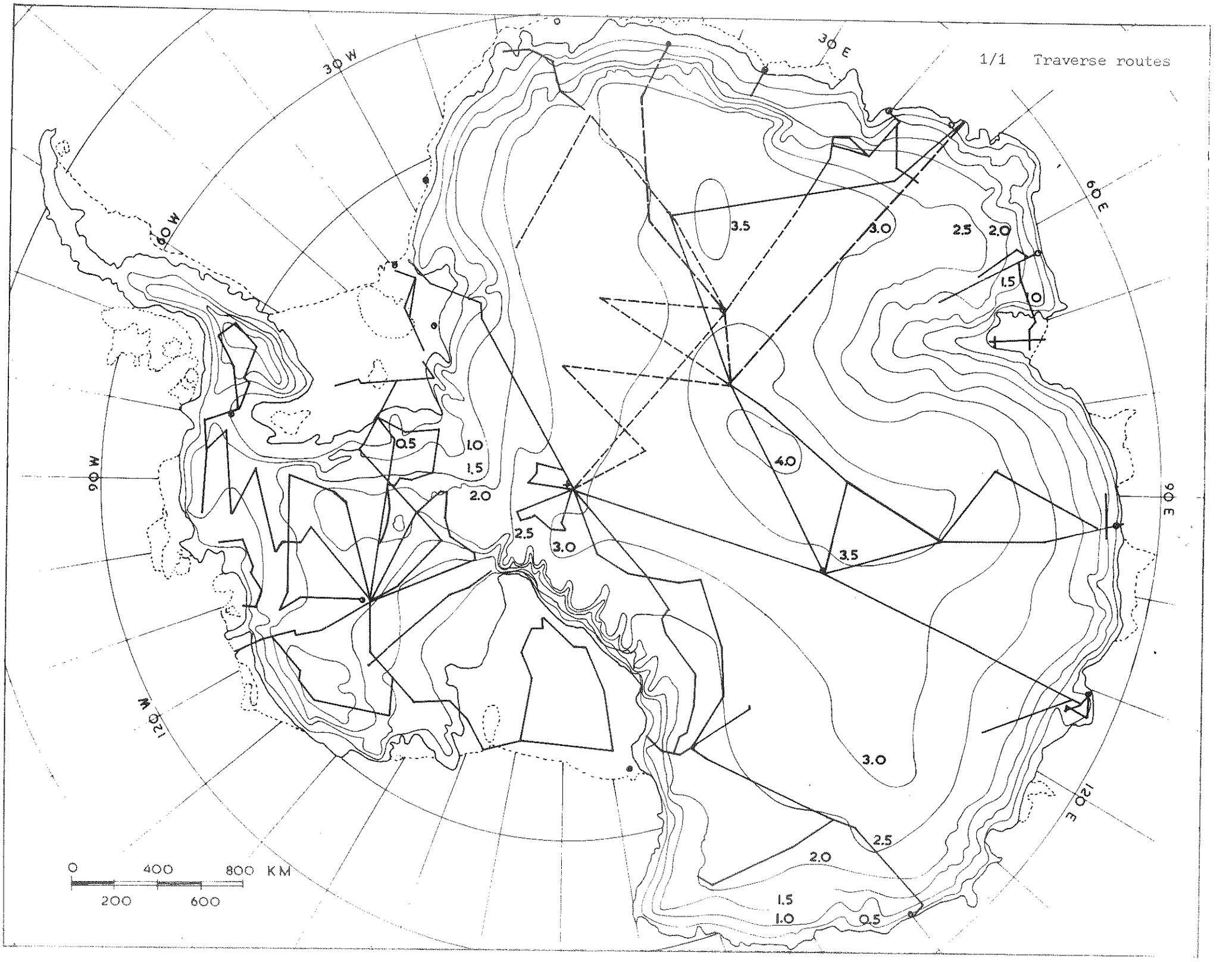
1/1 Traverse routes
0
30 W
30 E
60 W
60 E
90 W
90 E
120 W
120 E
0.5
1.0
1.5
2.0
2.5
3.0
3.5
4.0
0 400 800 KM
200 600

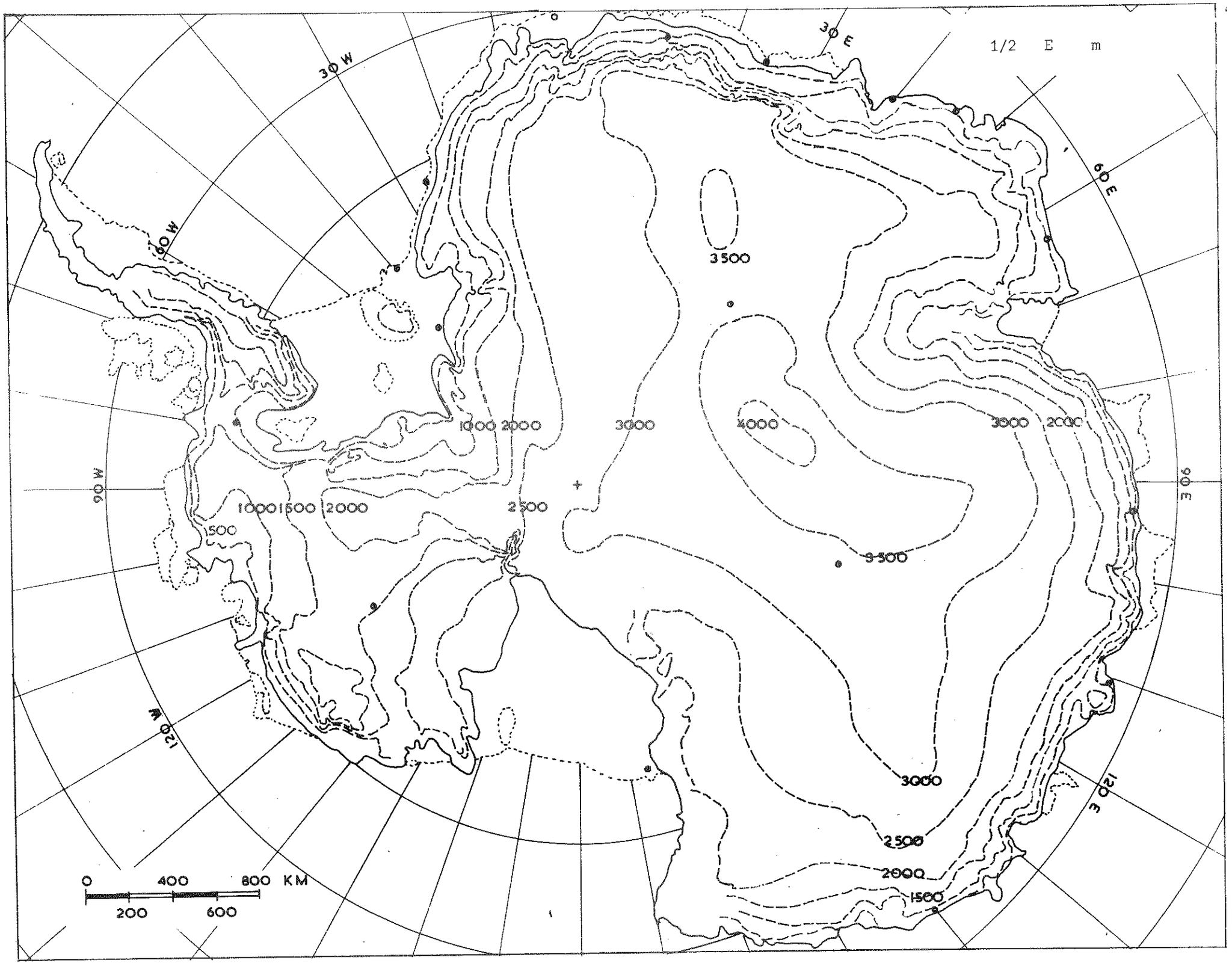
1/2 E m
30 W
30 E
60 W
60 E
90 W
90 E
120 W
120 E
3500
1000 2000
3000
4000
3000 2000
1000 1500 2000
2500
500
3500
3000
2500
2000
1500
0 400 800 KM
200 600

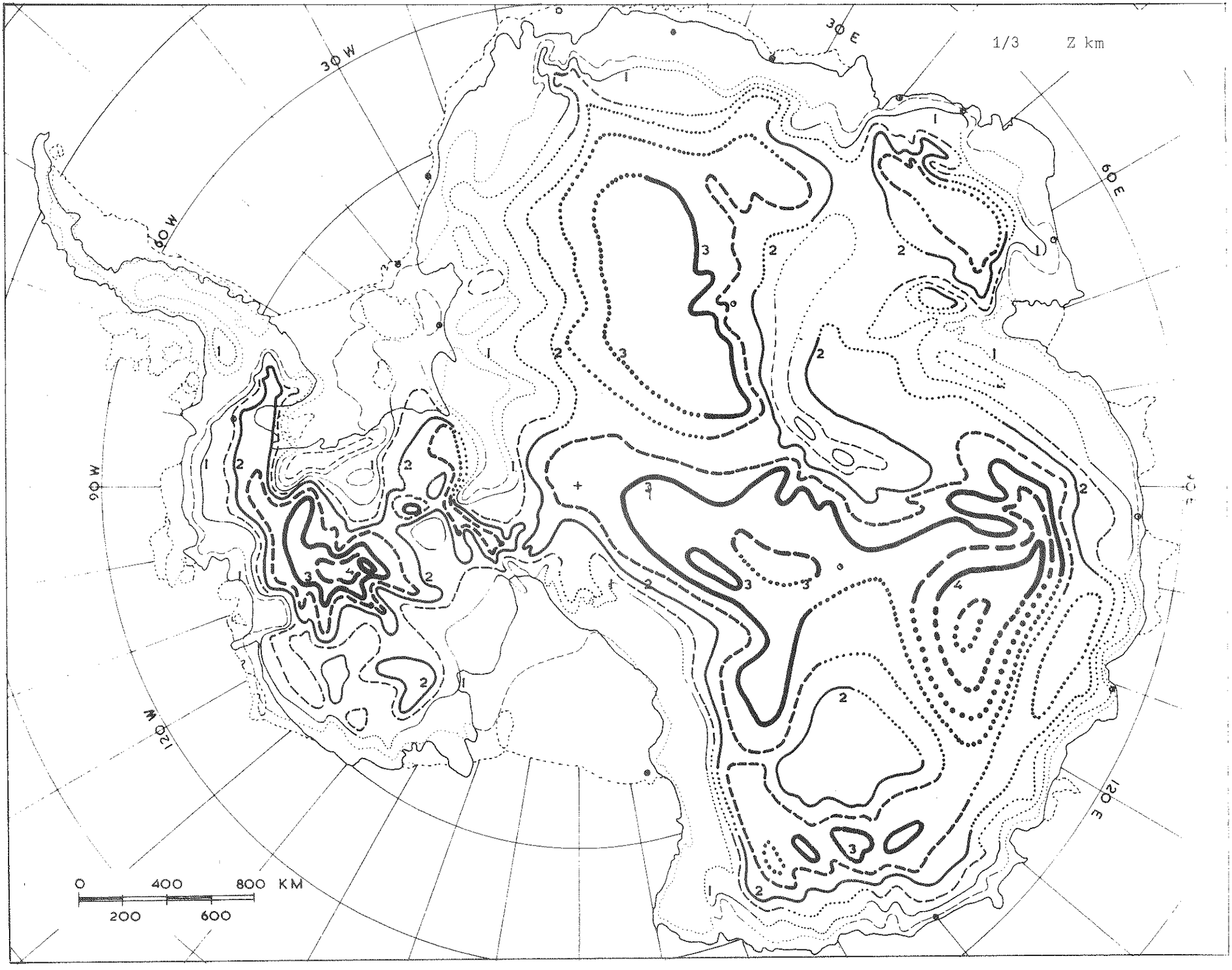
1/3 Z km
30 W
30 E
60 W
60 E
90 W
90 E
120 W
120 E
0 400 800 KM
200 600

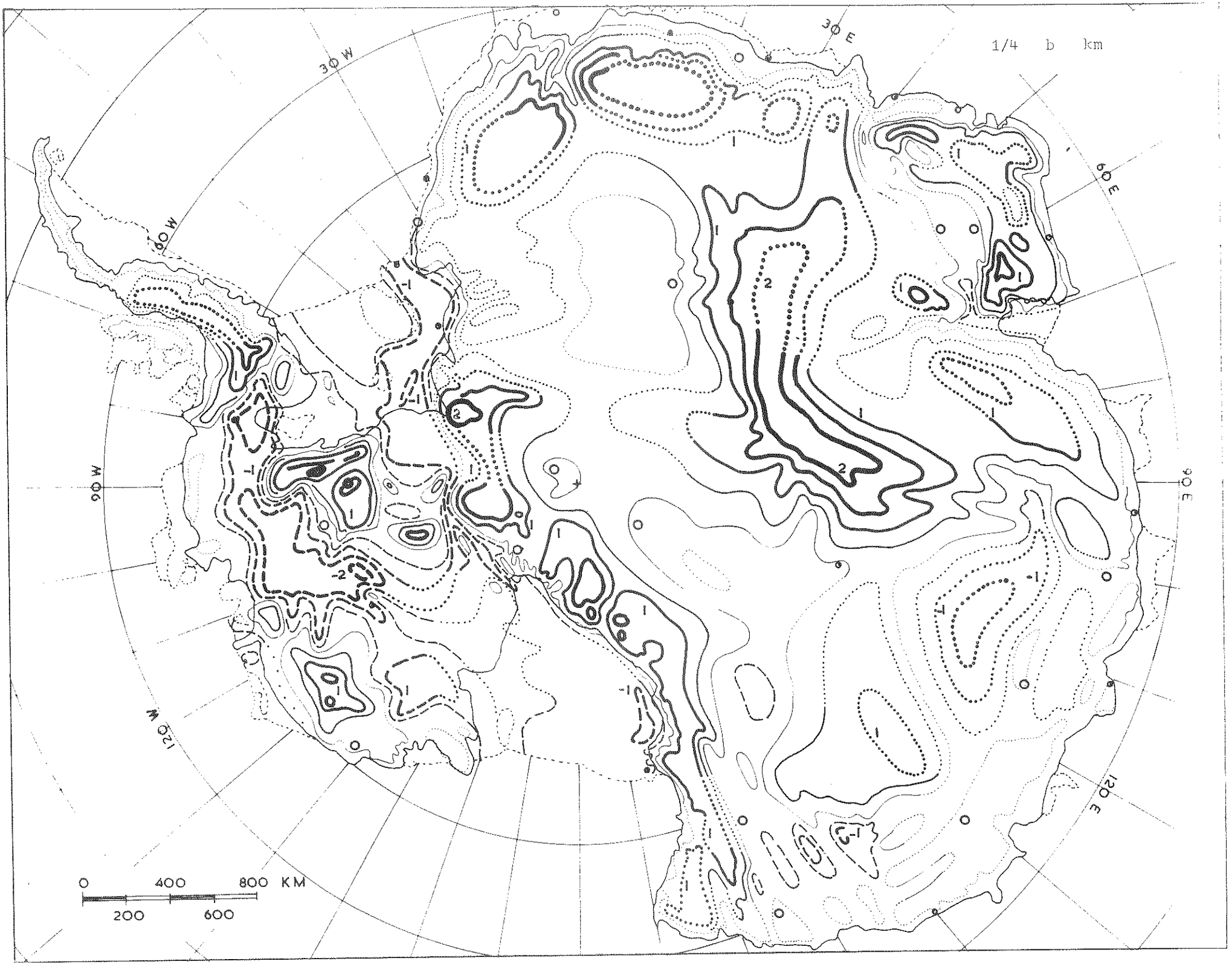
1/4 b km
30 W
30 E
60 W
60 E
90 W
90 E
120 W
120 E
0 400 800 KM
200 600

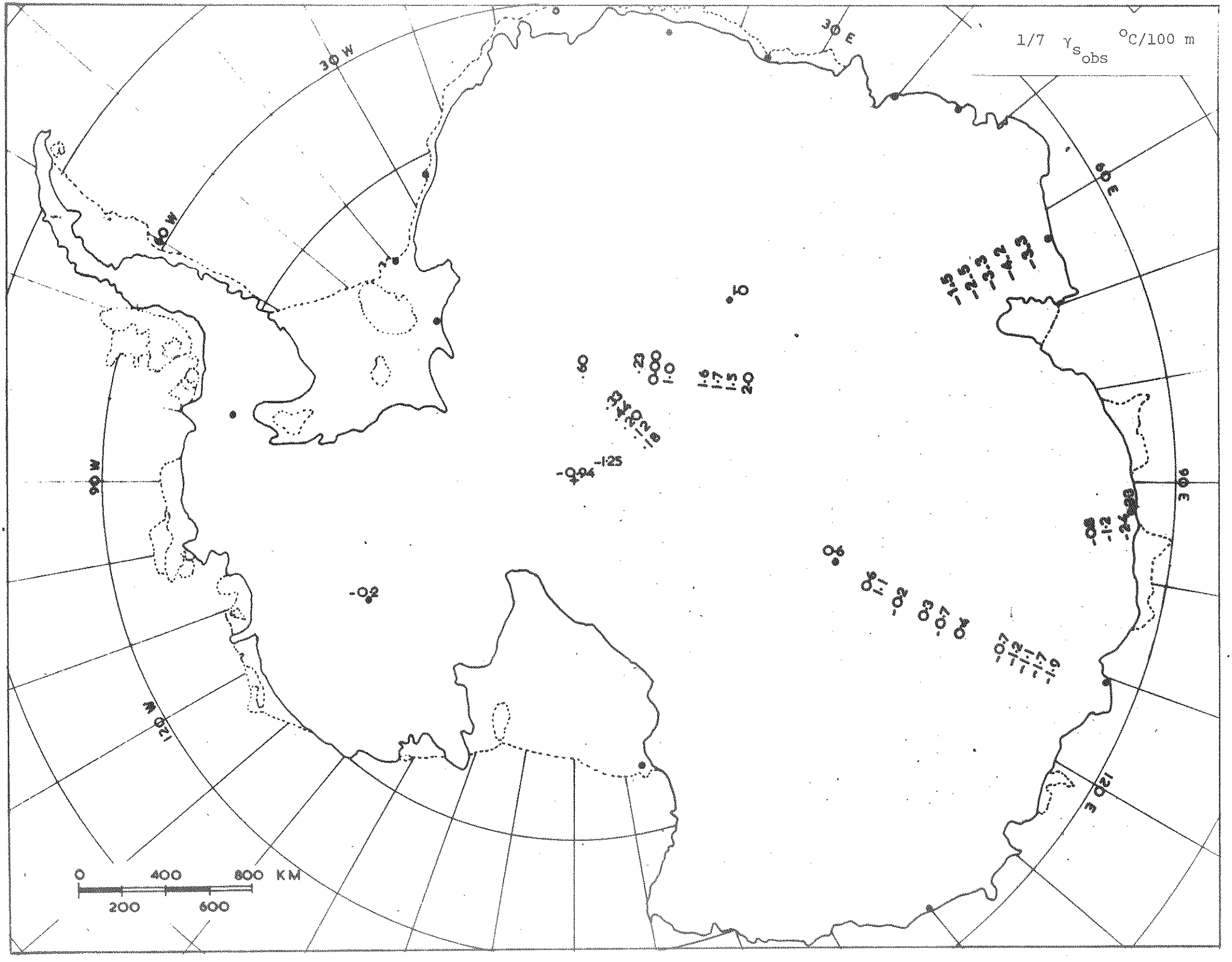
1/7 $\gamma_{s_{obs}}$ °C/100 m
30 W
30 E
0
60 W
60 E
90 W
90 E
120 W
120 E
-0.94
-1.25
-0.2
0 400 800 KM
200 600

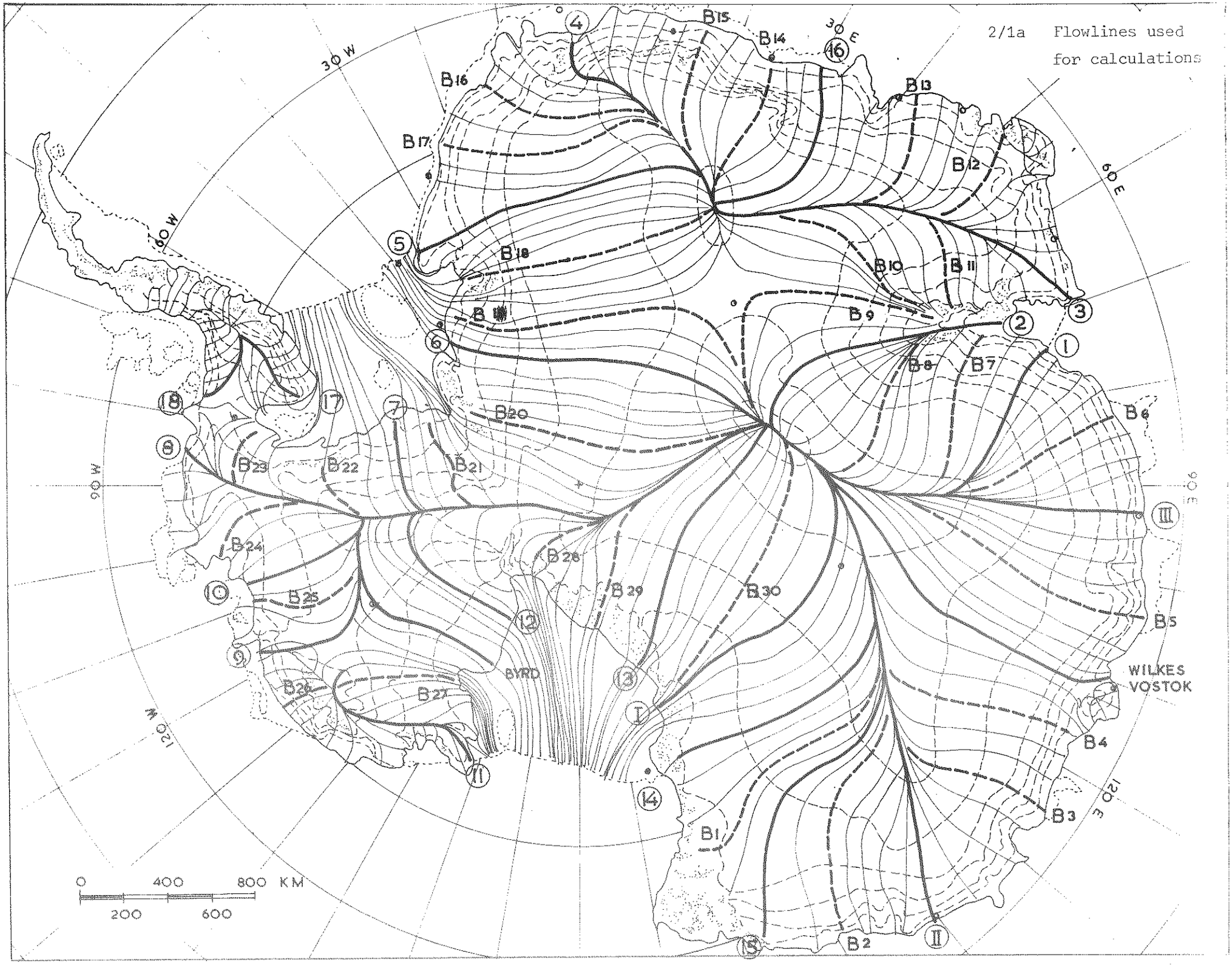
2/1a Flowlines used for calculations
30 W
60 W
90 W
120 W
30 E
60 E
90 E
120 E
B1
B2
B3
B4
B5
B6
B7
B8
B9
B10
B11
B12
B13
B14
B15
B16
B17
B18
B19
B20
B21
B22
B23
B24
B25
B26
B27
B28
B29
B30
BYRD
WILKES
VOSTOK
0 400 800 KM
200 600

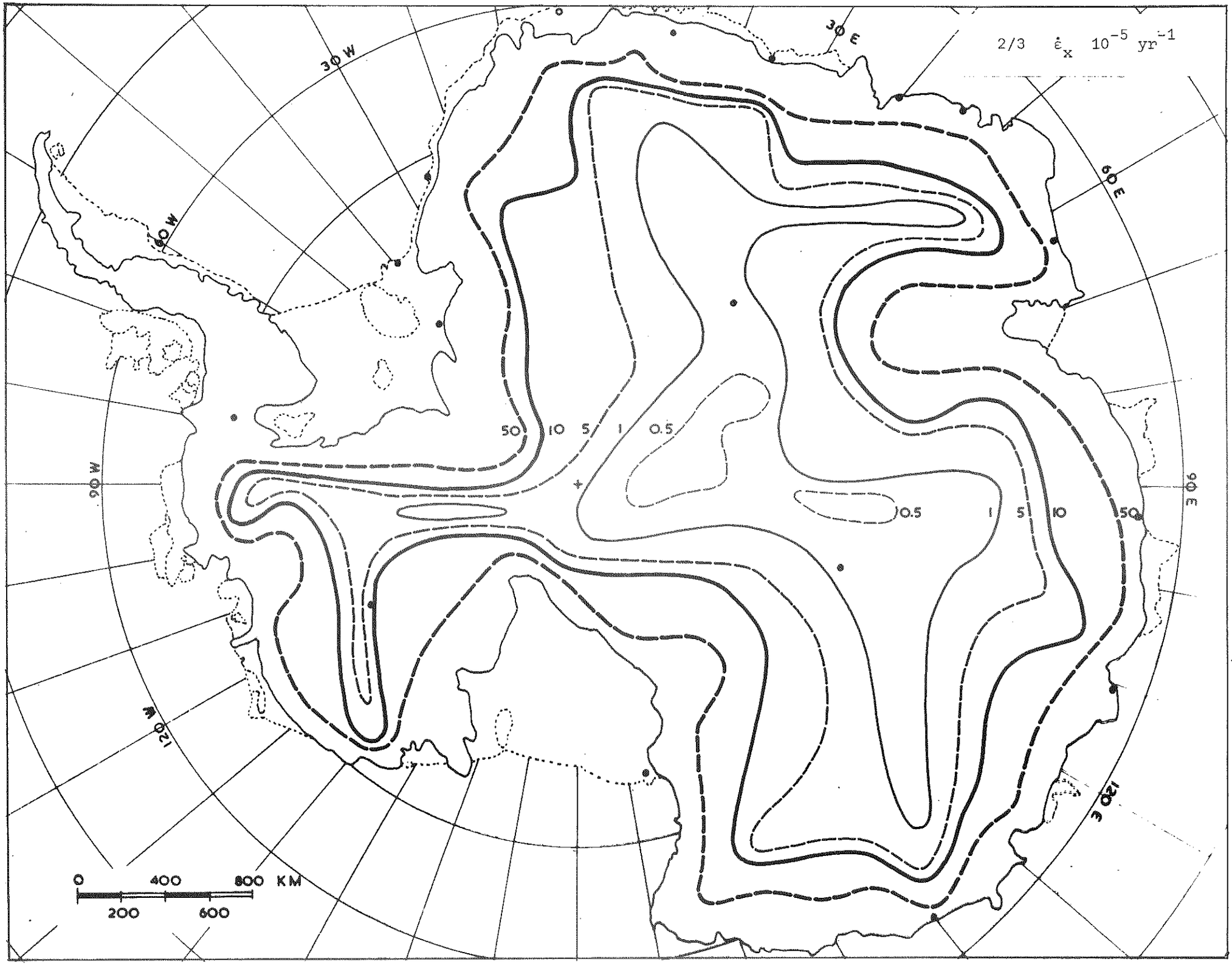
2/3 $\dot{\varepsilon}_x$ 10^{-5} yr^{-1}
30 W
30 E
60 W
60 E
90 W
90 E
120 W
120 E
50
10
5
1
0.5
0.5
1
5
10
50
0
400
800 KM
200
600

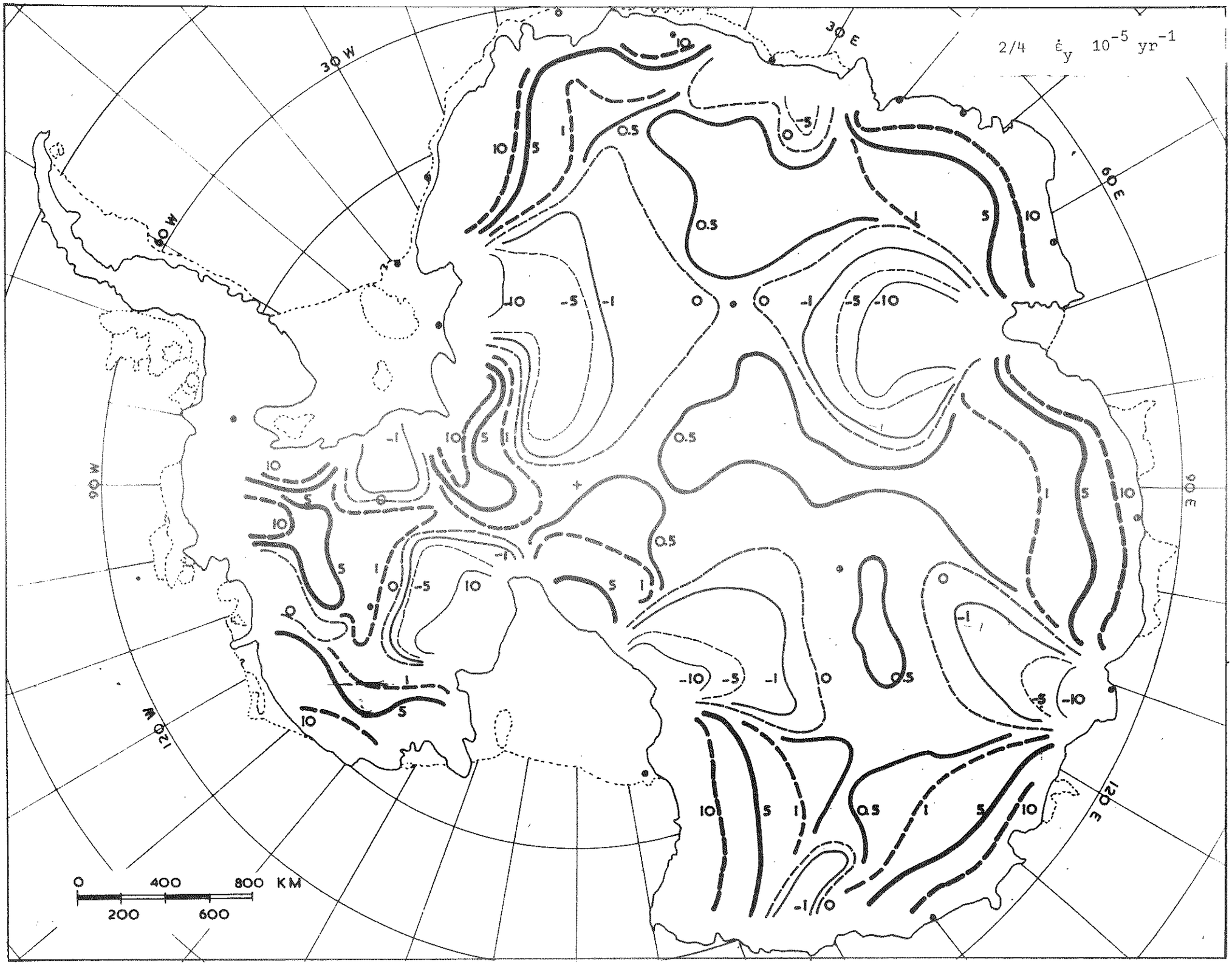
2/4 $\dot{\epsilon}_y$ 10^{-5} yr^{-1}
30 W
30 E
60 W
60 E
90 W
90 E
120 W
120 E
0 400 800 KM
200 600

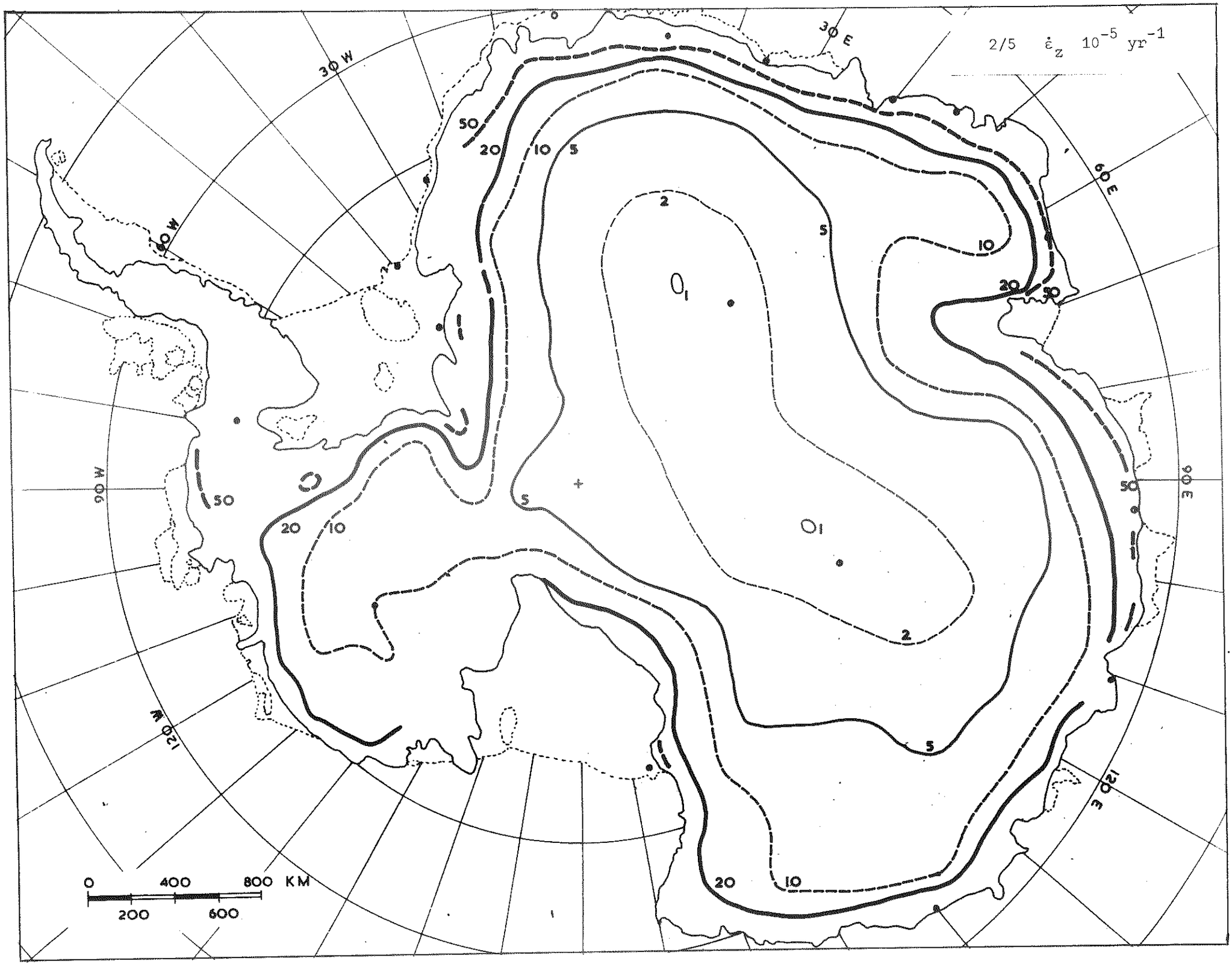
2/5 $\dot{\varepsilon}_z$ 10^{-5} yr^{-1}
30 W
30 E
60 W
60 E
90 W
90 E
120 W
120 E
50
20
10
5
2
1
0
0 400 800 KM
200 600

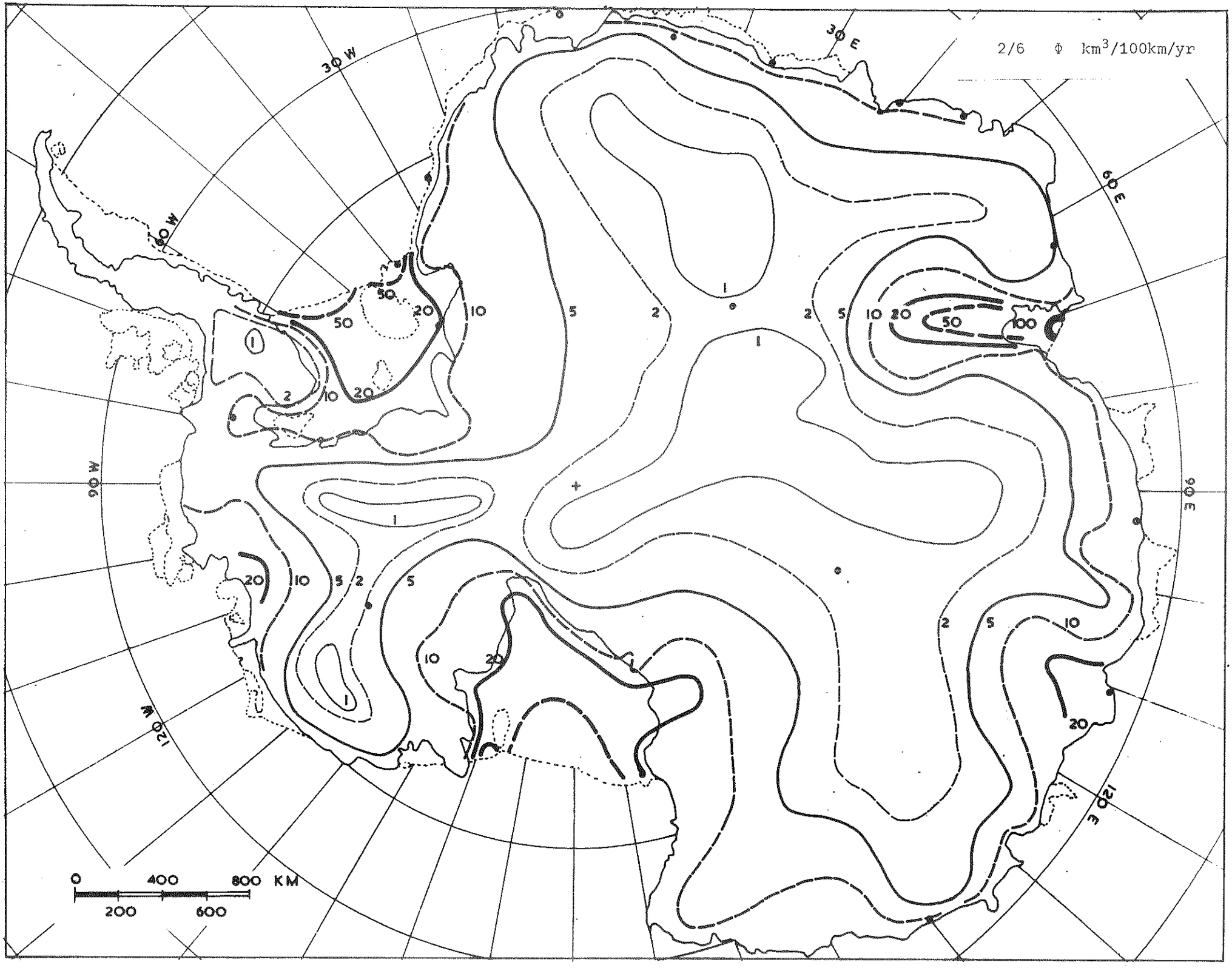
2/6 Φ km³/100km/yr
0
30 W
30 E
60 W
60 E
90 W
90 E
120 W
120 E
0 400 800 KM
200 600

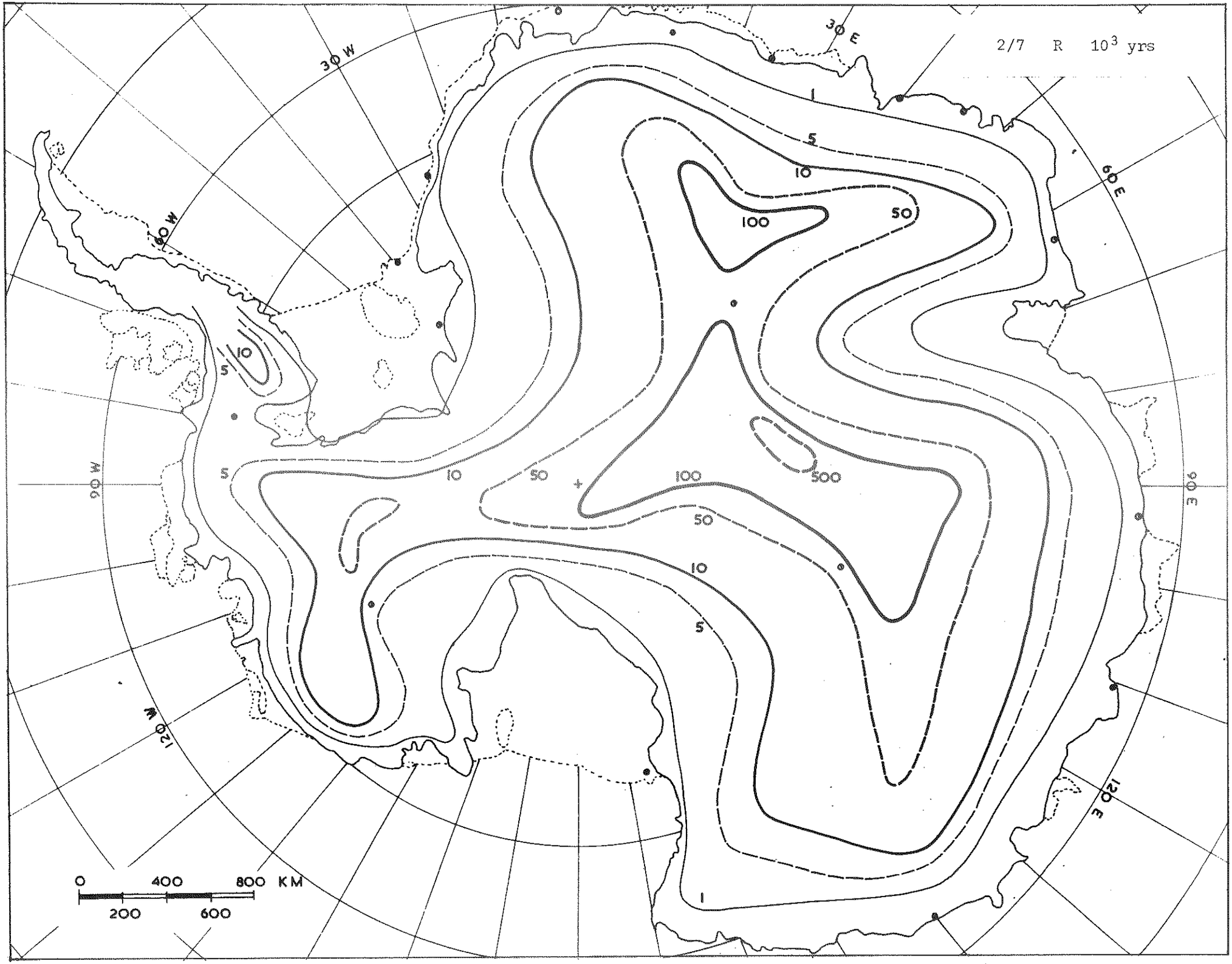
2/7 R 10^3 yrs
30 W
30 E
60 W
60 E
90 W
90 E
120 W
120 E
1
5
10
50
100
500
0 400 800 KM
200 600

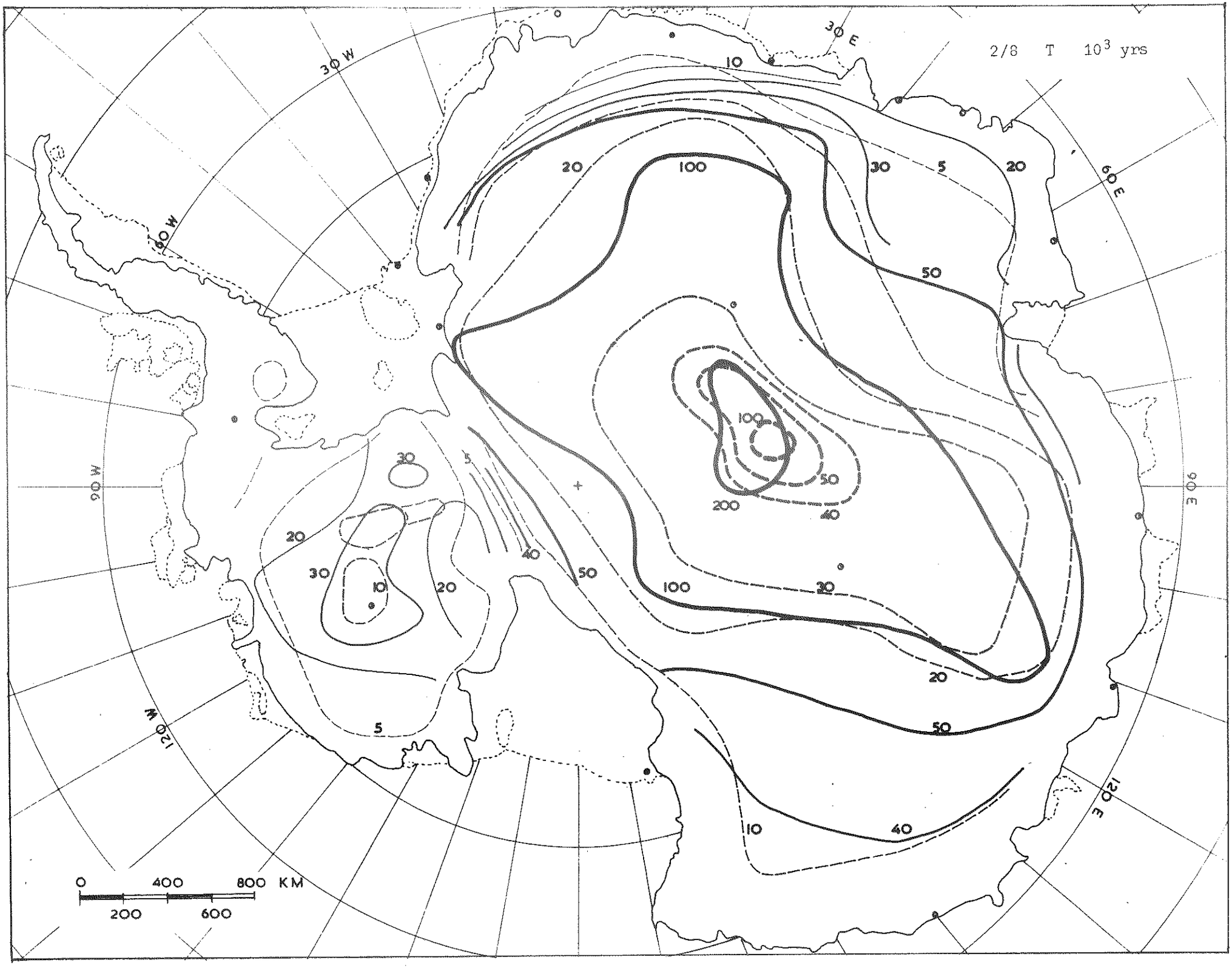
2/8 T 10³ yrs
30 W
60 W
90 W
120 W
30 E
60 E
90 E
120 E
10
20
30
40
50
100
200
5
0 400 800 KM
200 600

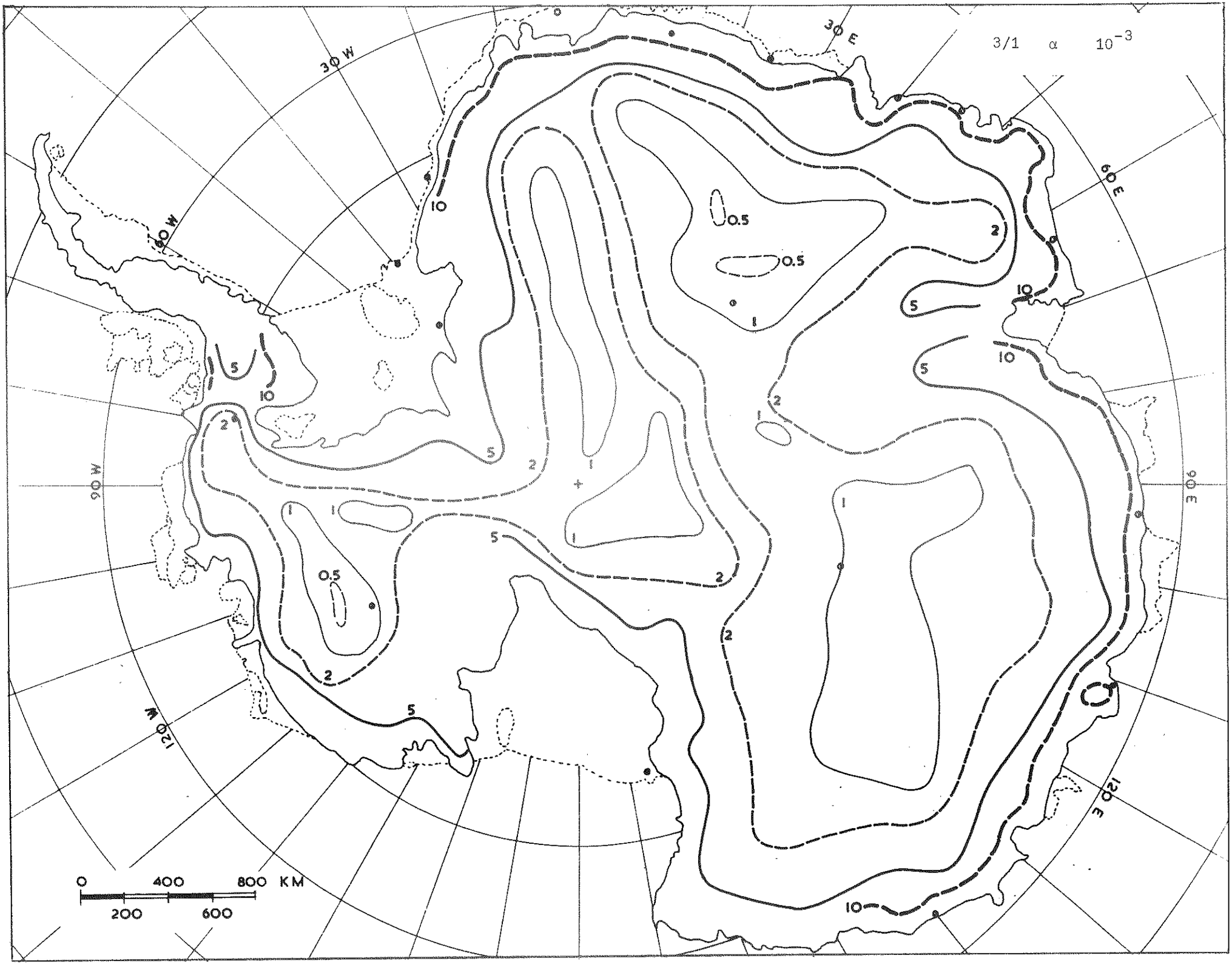
3/1 α 10⁻³
30 W
30 E
60 W
60 E
90 W
90 E
120 W
120 E
0
0.5
1
2
5
10
0 400 800 KM
200 600

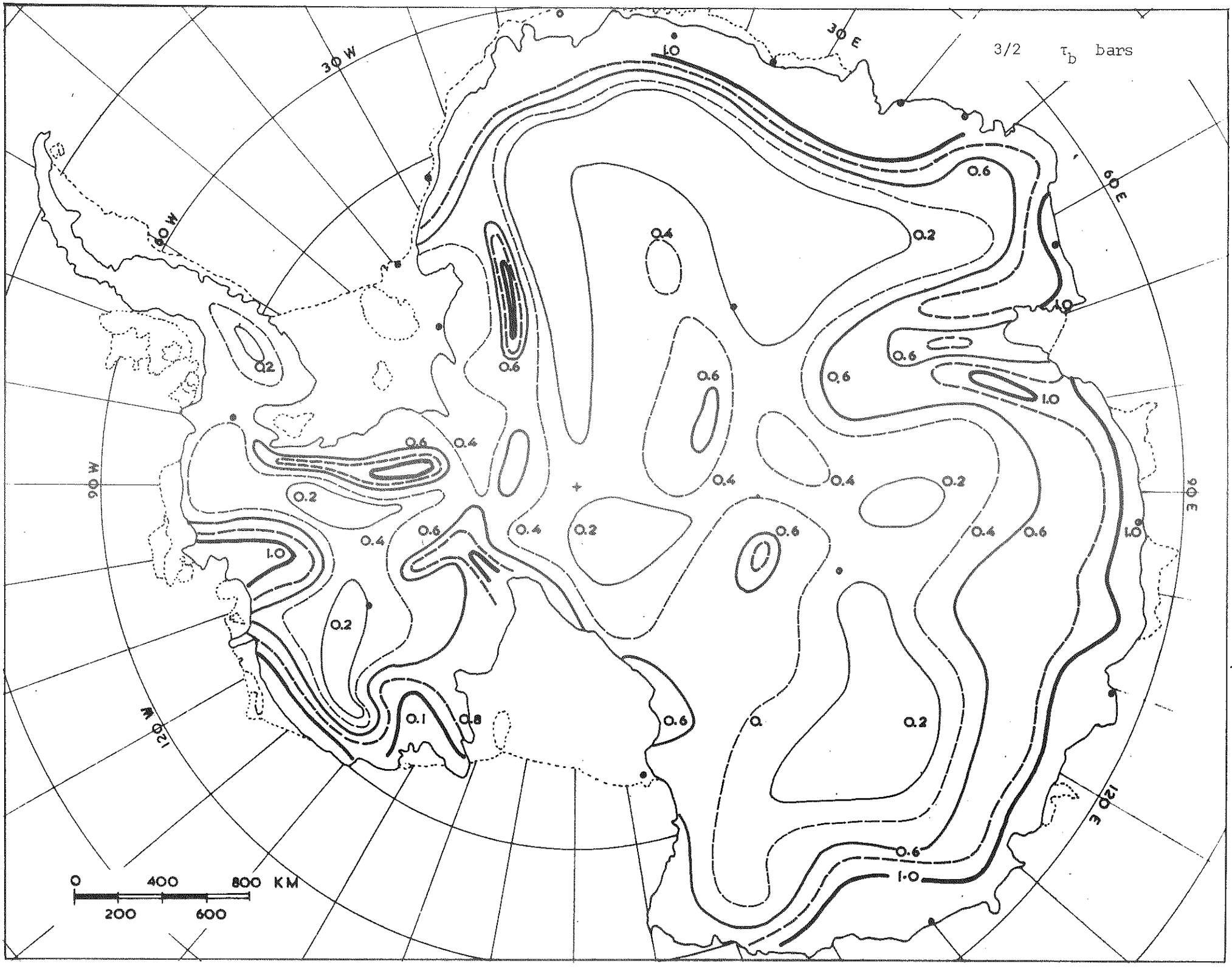
3/2 τ_b bars
30 W
30 E
60 W
60 E
90 W
90 E
120 W
120 E
1.0
0.6
0.4
0.2
0.1
0
0 400 800 KM
200 600

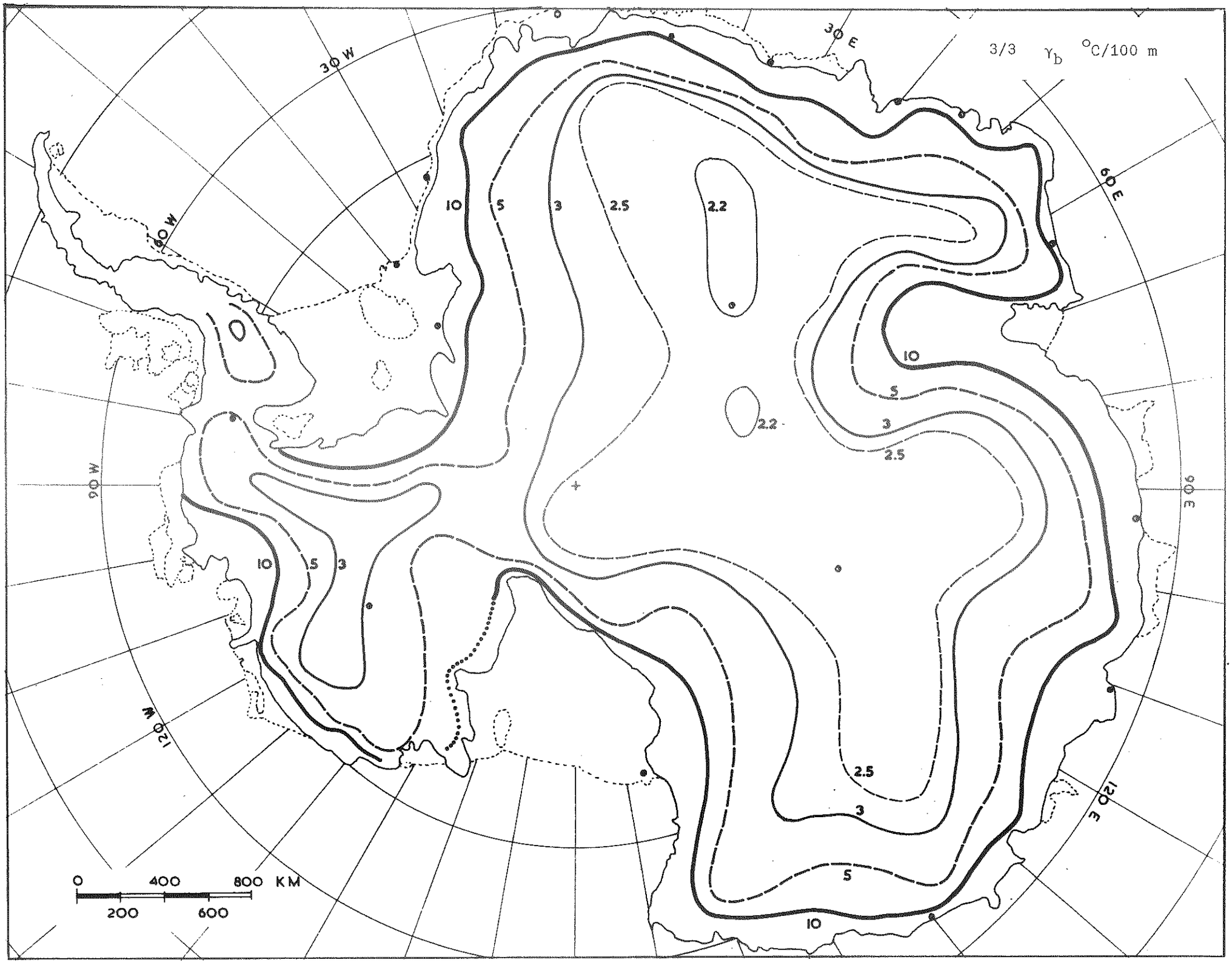
3/3 γ_b °C/100 m
30 W
30 E
60 W
60 E
90 W
90 E
120 W
120 E
10
5
3
2.5
2.2
0
400
800 KM
200
600

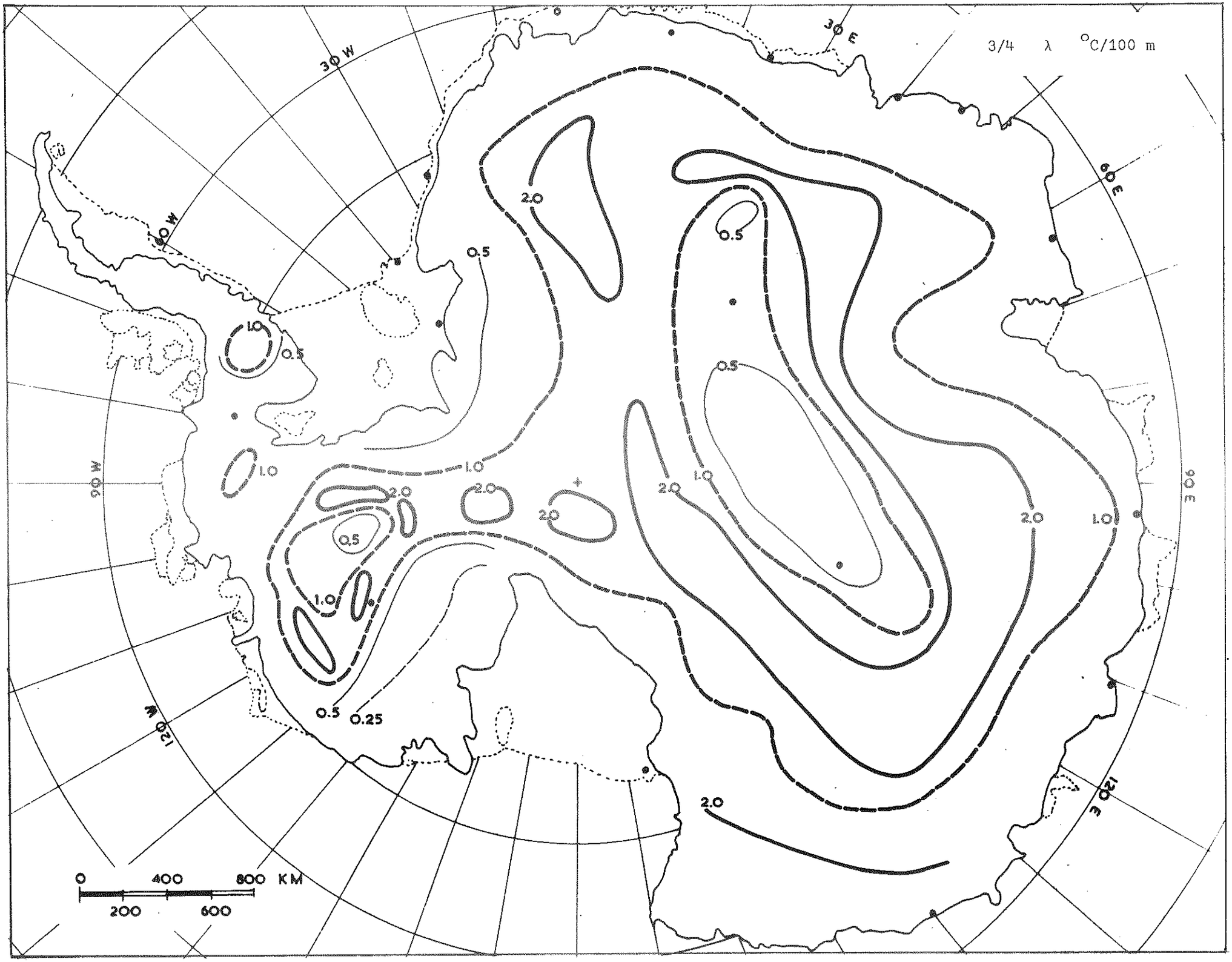
3/4 λ °C/100 m
30 W
30 E
60 W
60 E
90 W
90 E
120 W
120 E
0.5
1.0
2.0
0.25
0 400 800 KM
200 600

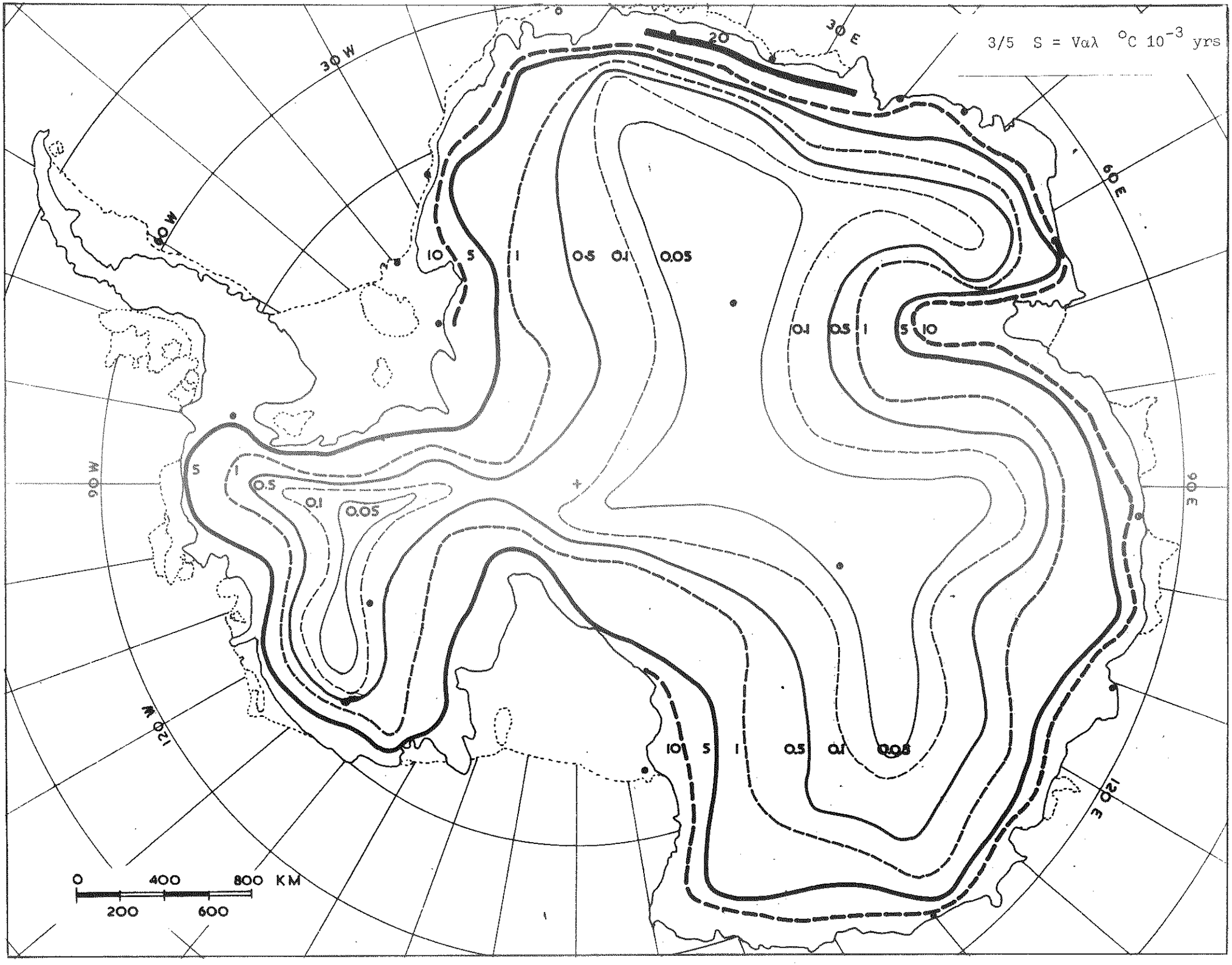
3/5 S = Vαλ °C 10⁻³ yrs
30 W
30 E
60 W
60 E
90 W
90 E
120 W
120 E
20
10
5
1
0.5
0.1
0.05
0 400 800 KM
200 600

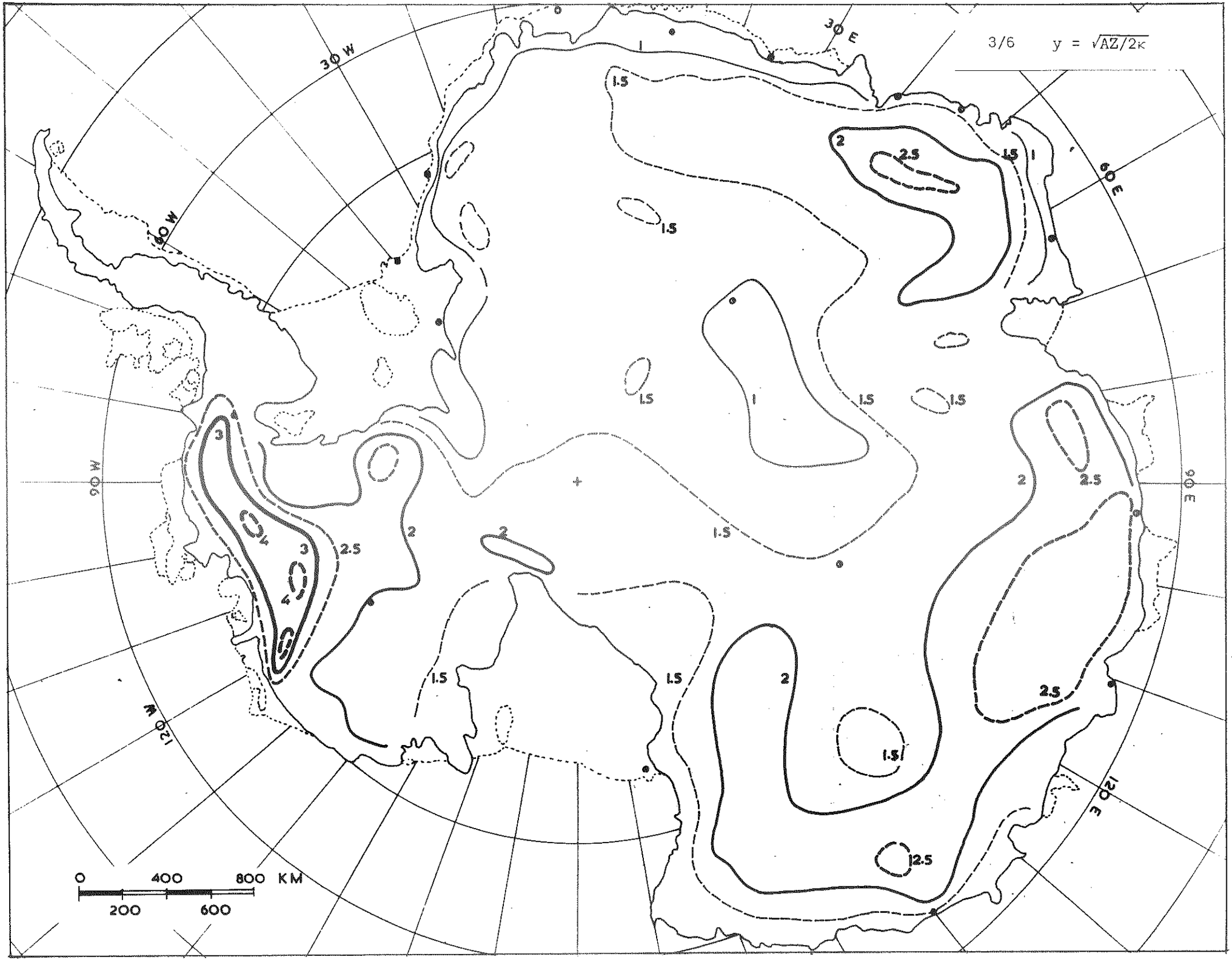
3/6 y = √AZ/2κ
30 W
30 E
60 W
60 E
90 W
90 E
120 W
120 E
0 400 800 KM
200 600

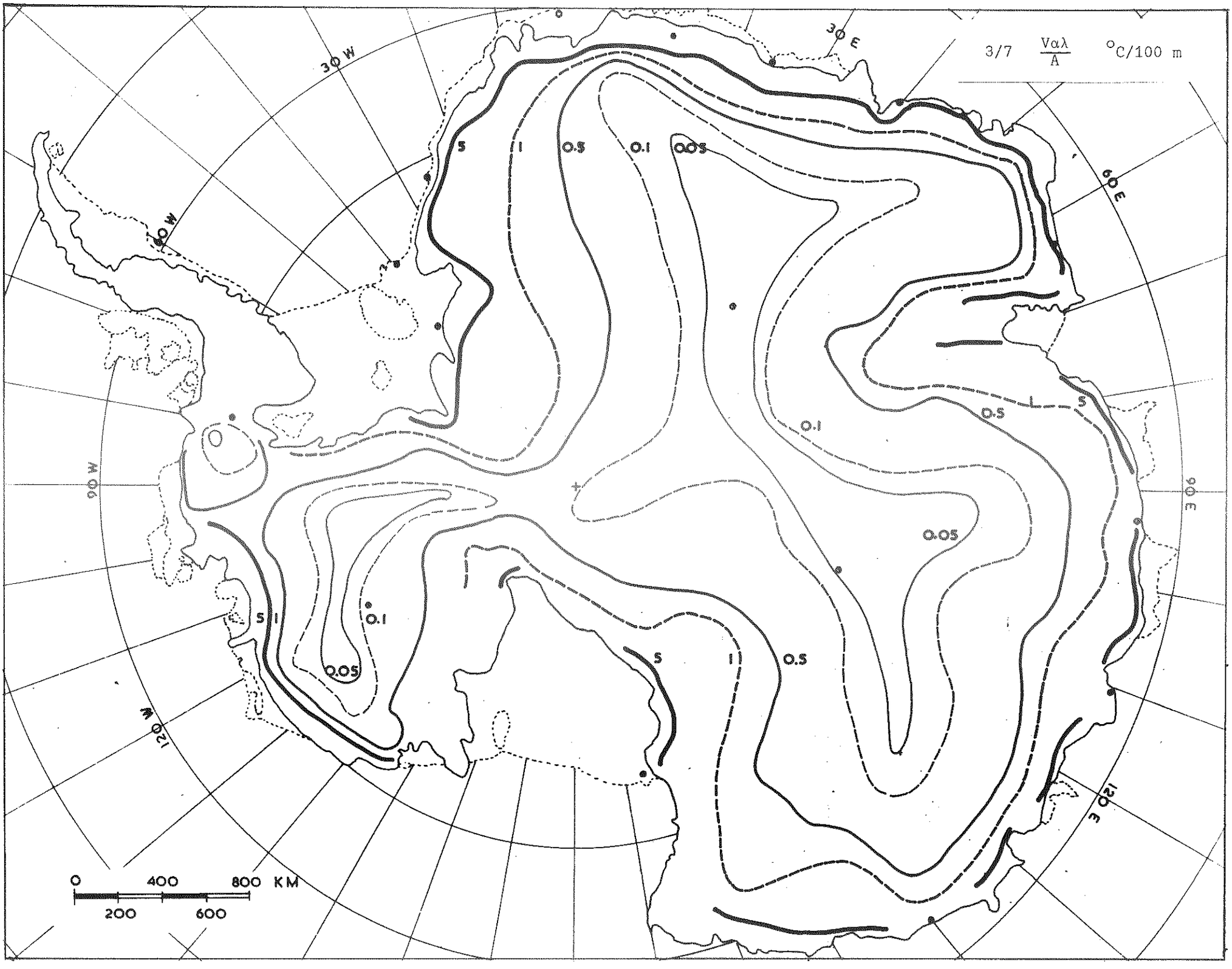
3/7 Vαλ/A °C/100 m
30 W
30 E
60 W
60 E
90 W
90 E
120 W
120 E
5
1
0.5
0.1
0.05
0 400 800 KM
200 600

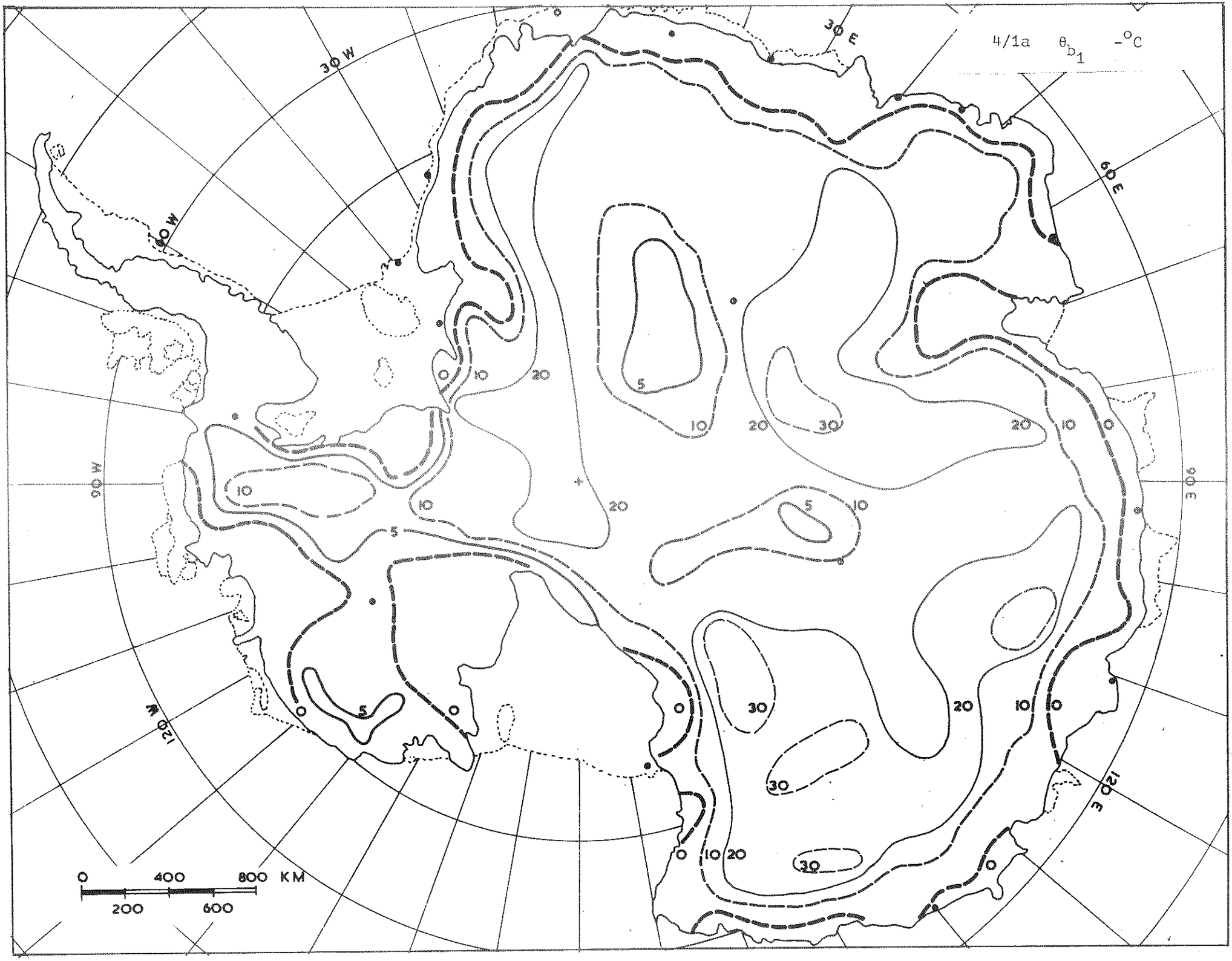
4/1a θ_{b_1} -°C
30 W
30 E
60 W
60 E
90 W
90 E
120 W
120 E
0
5
10
20
30
0 400 800 KM
200 600

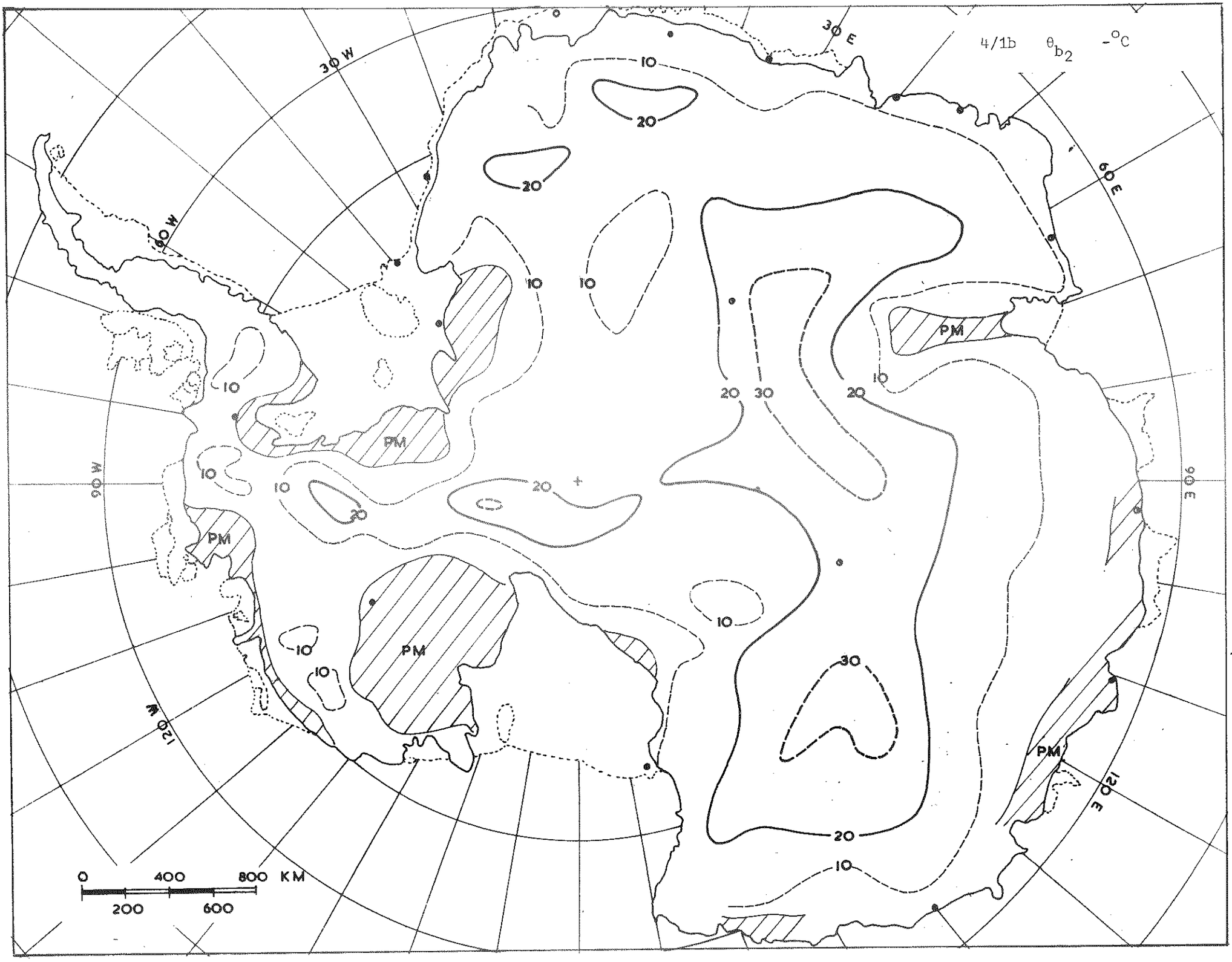
4/1b θ_{b_2} -°C
30 W
30 E
60 W
60 E
90 W
90 E
120 W
120 E
PM
10
20
30
0 400 800 KM
200 600

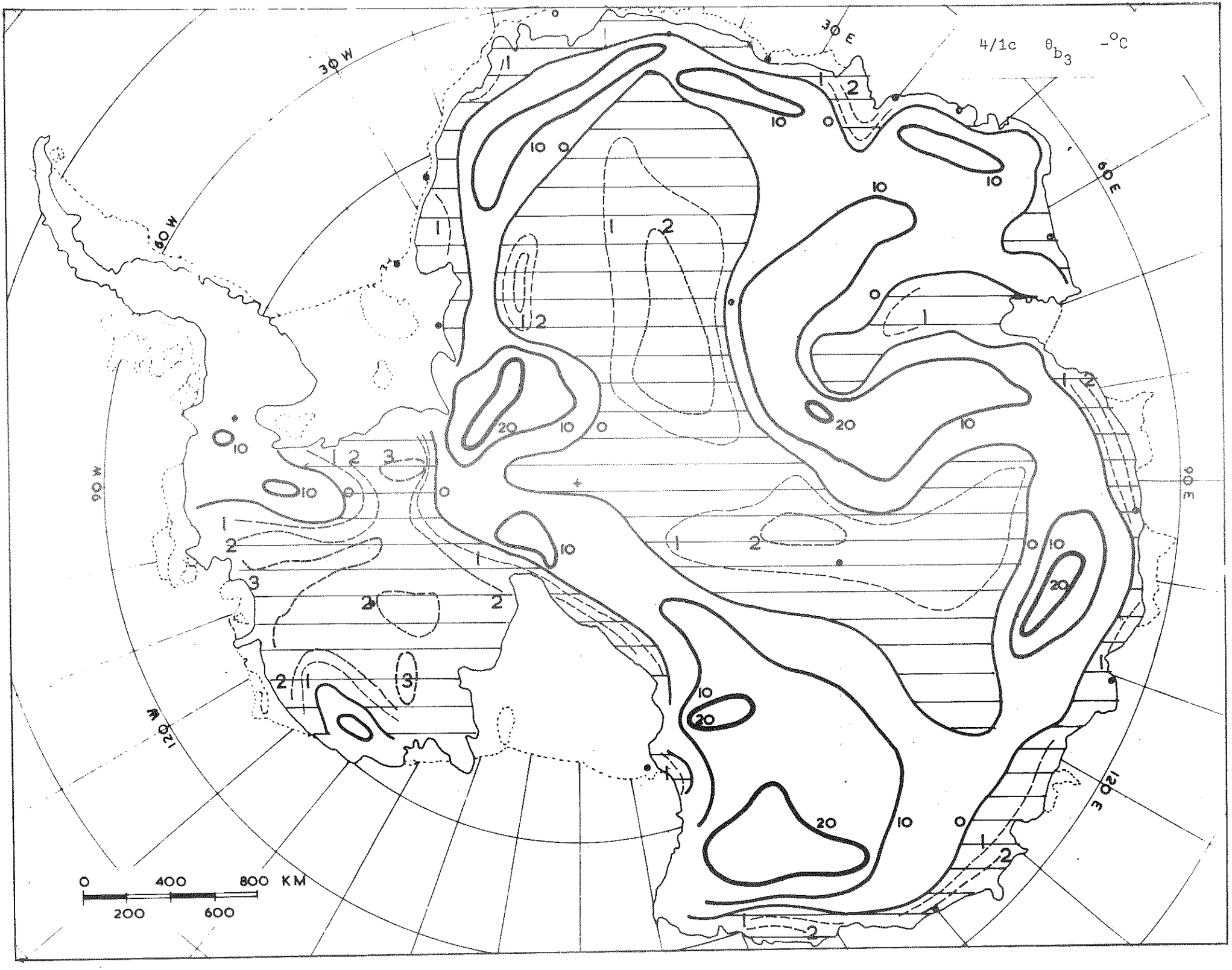
4/1c θ$_{D_3}$ -°C
30 W
30 E
60 W
60 E
90 W
90 E
120 W
120 E
0 400 800 KM
200 600

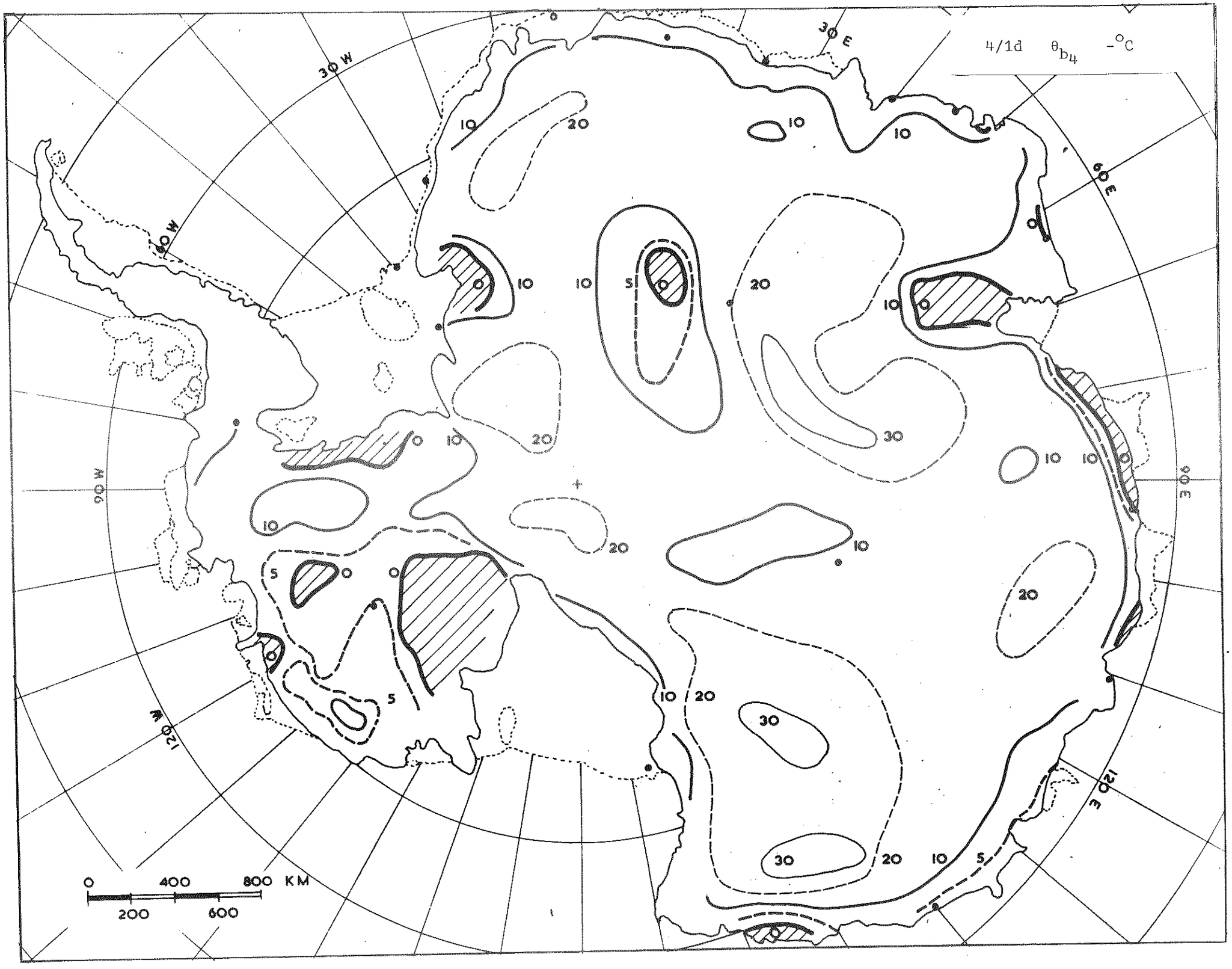
4/1d θ_{b_4} -°C
30 W
30 E
60 W
60 E
90 W
90 E
120 W
120 E
0
10
20
5
30
0 400 800 KM
200 600

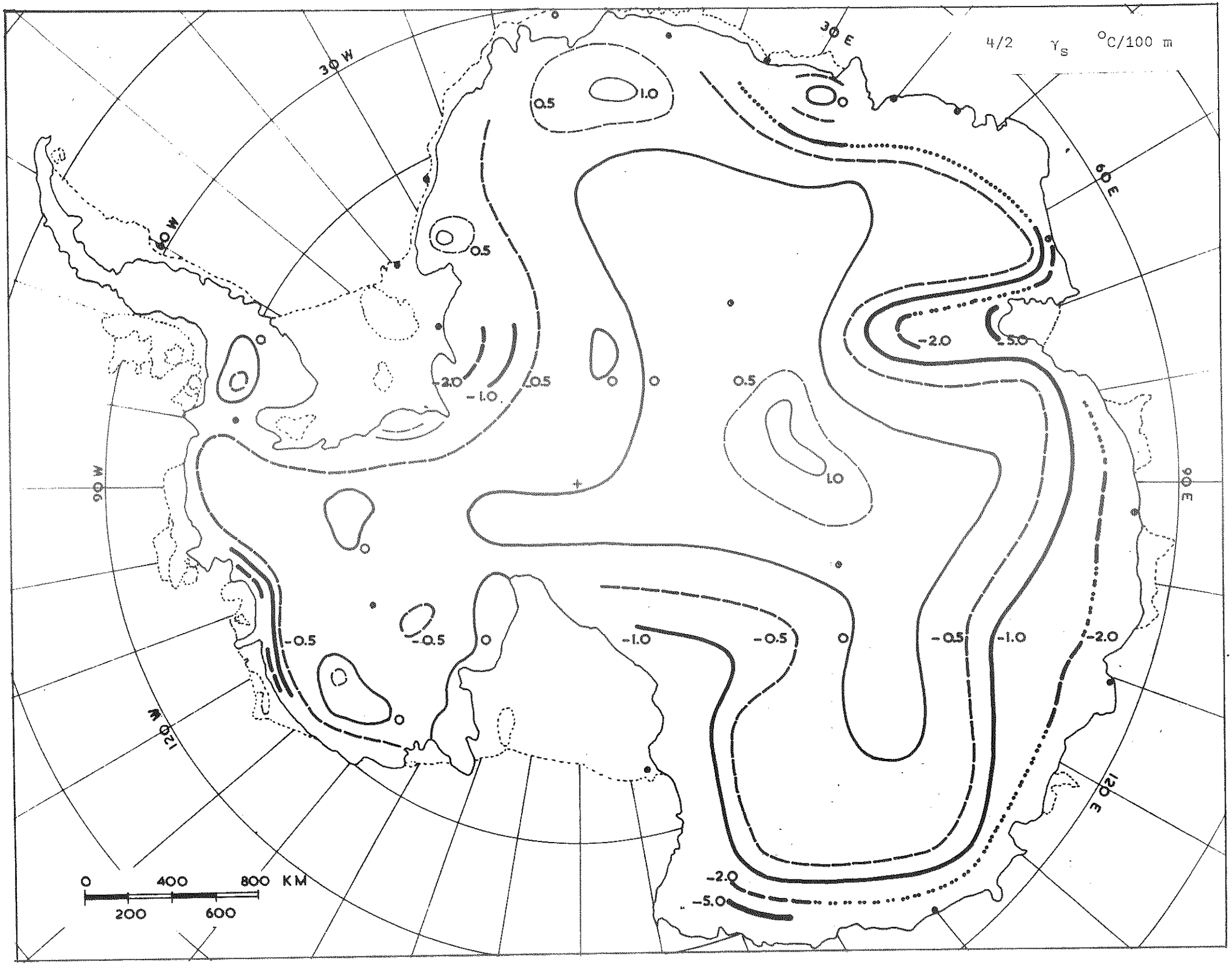
4/2 γ_s °C/100 m
30 W
30 E
60 W
60 E
90 W
90 E
120 W
120 E
0.5
1.0
-2.0
-5.0
-1.0
-0.5
0
0 400 800 KM
200 600

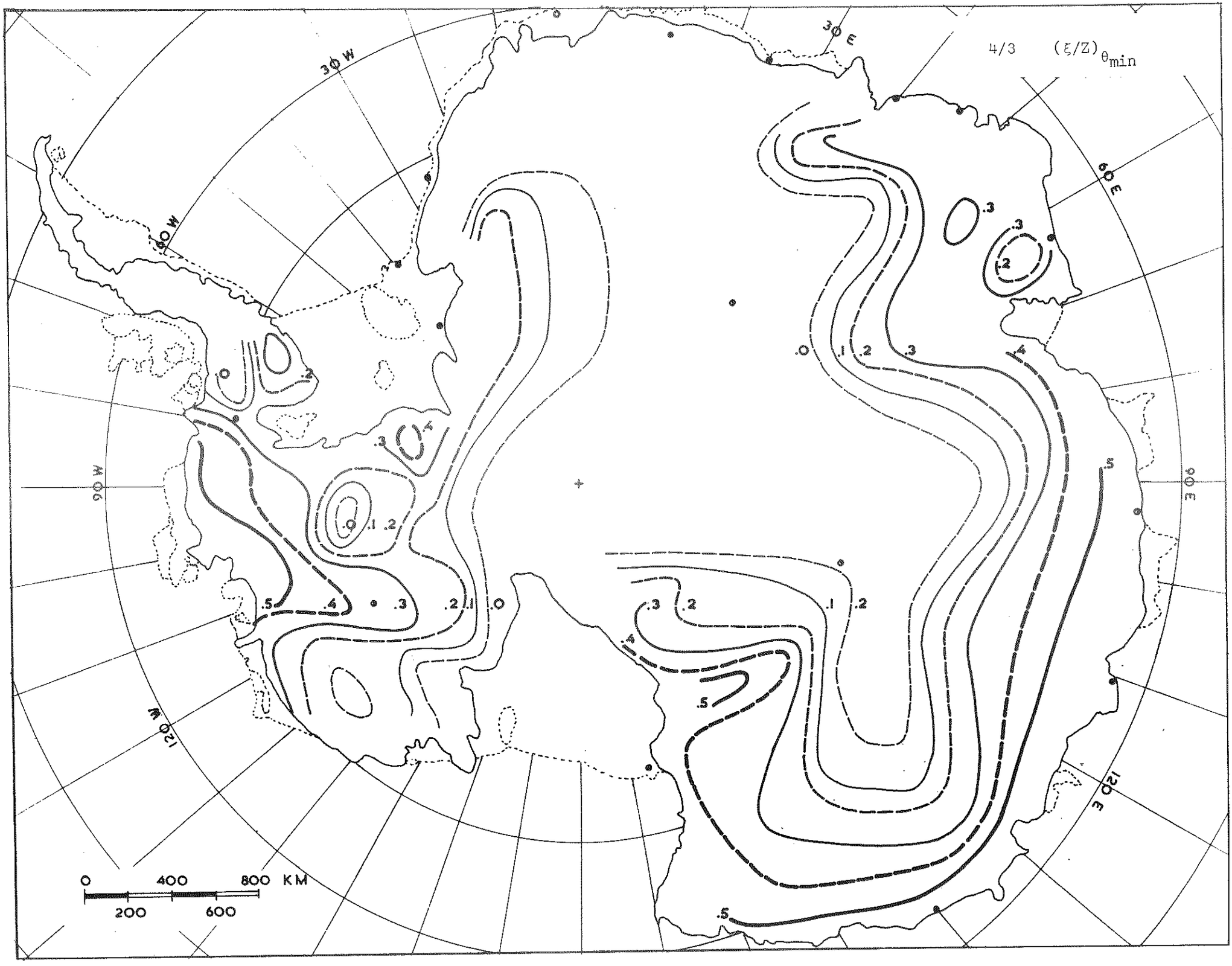
4/3 $(\xi/Z)_{\theta min}$
30 W
30 E
60 W
60 E
90 W
90 E
120 W
120 E
0 400 800 KM
200 600

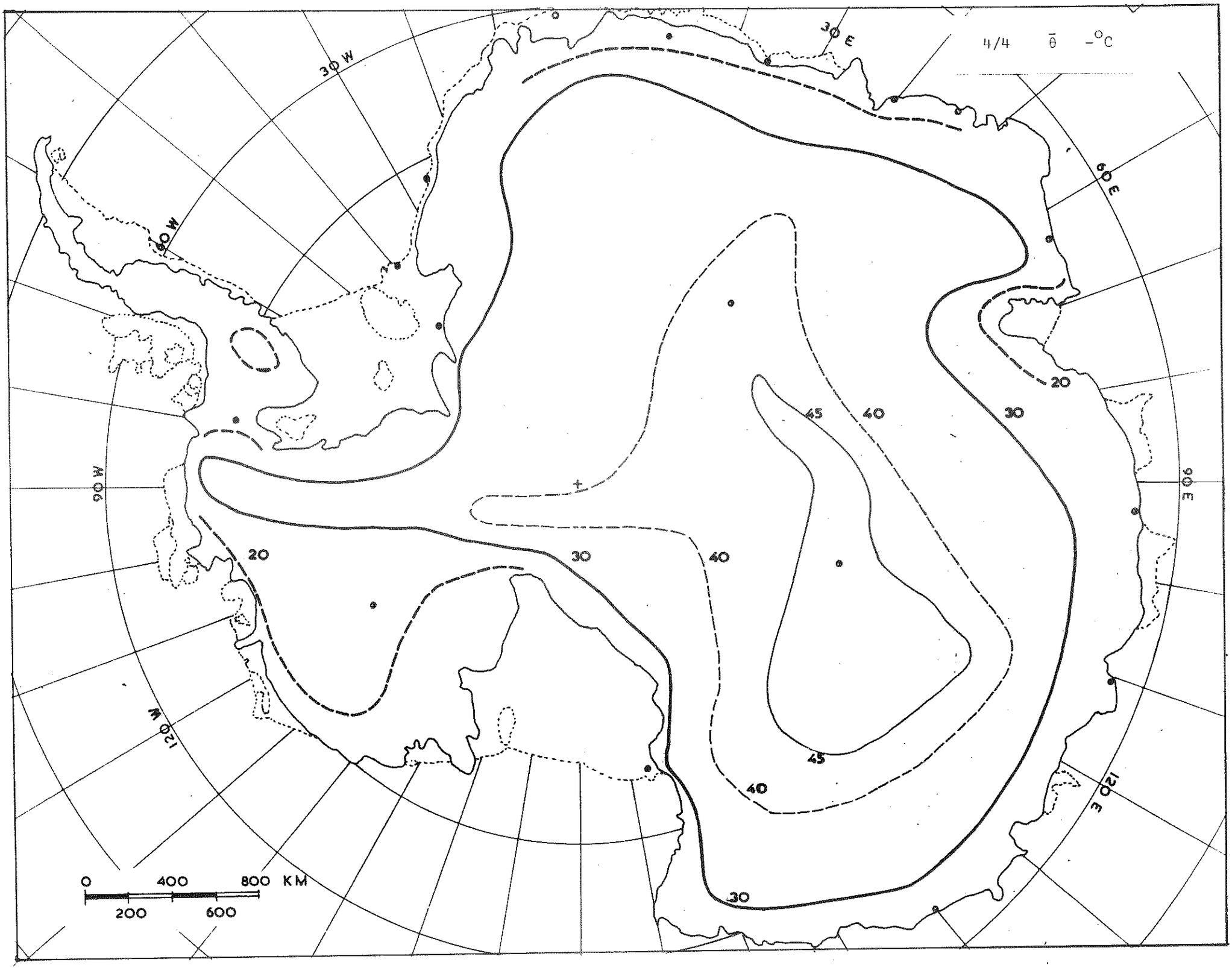
4/4 $\bar{\theta}$ -°C
30 W
30 E
60 W
60 E
90 W
90 E
120 W
120 E
20
30
40
45
0 400 800 KM
200 600

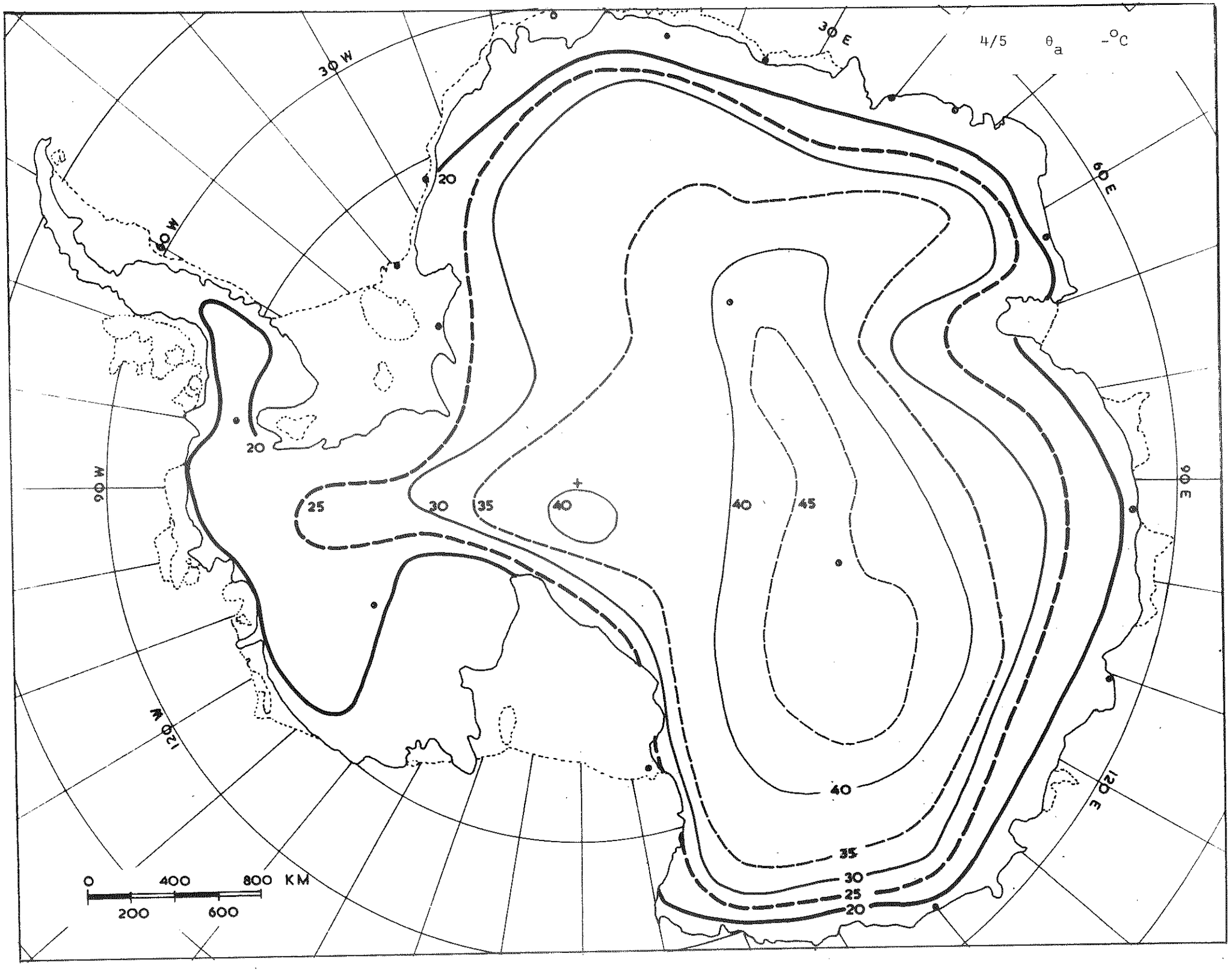
4/5 θa -°C
30 W
30 E
60 W
60 E
90 W
90 E
120 W
120 E
20
20
25
30
35
40
40
45
40
35
30
25
20
0 400 800 KM
200 600

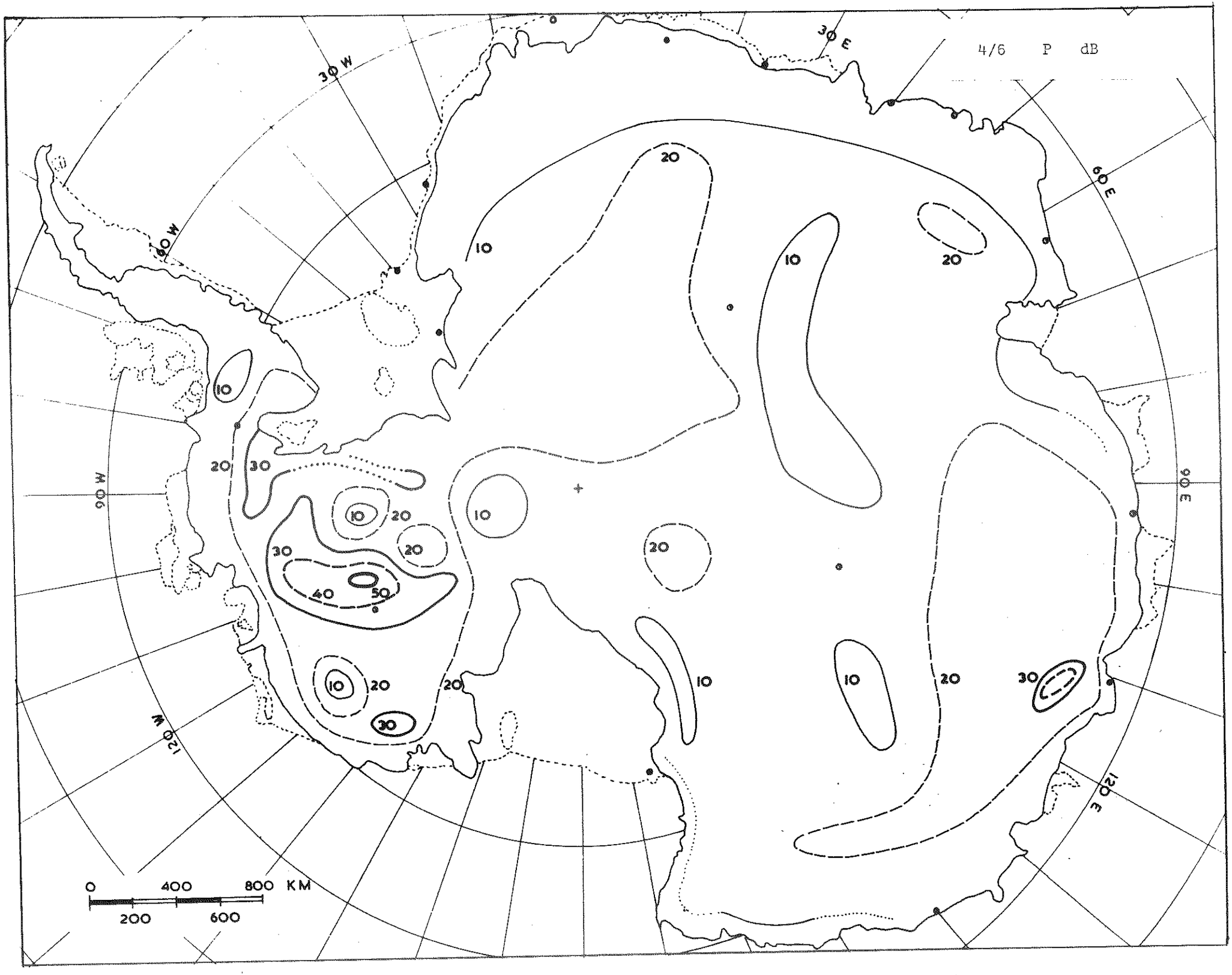
4/6 P dB
30 W
30 E
60 W
60 E
90 W
90 E
120 W
120 E
10
20
30
40
50
0 400 800 KM
200 600

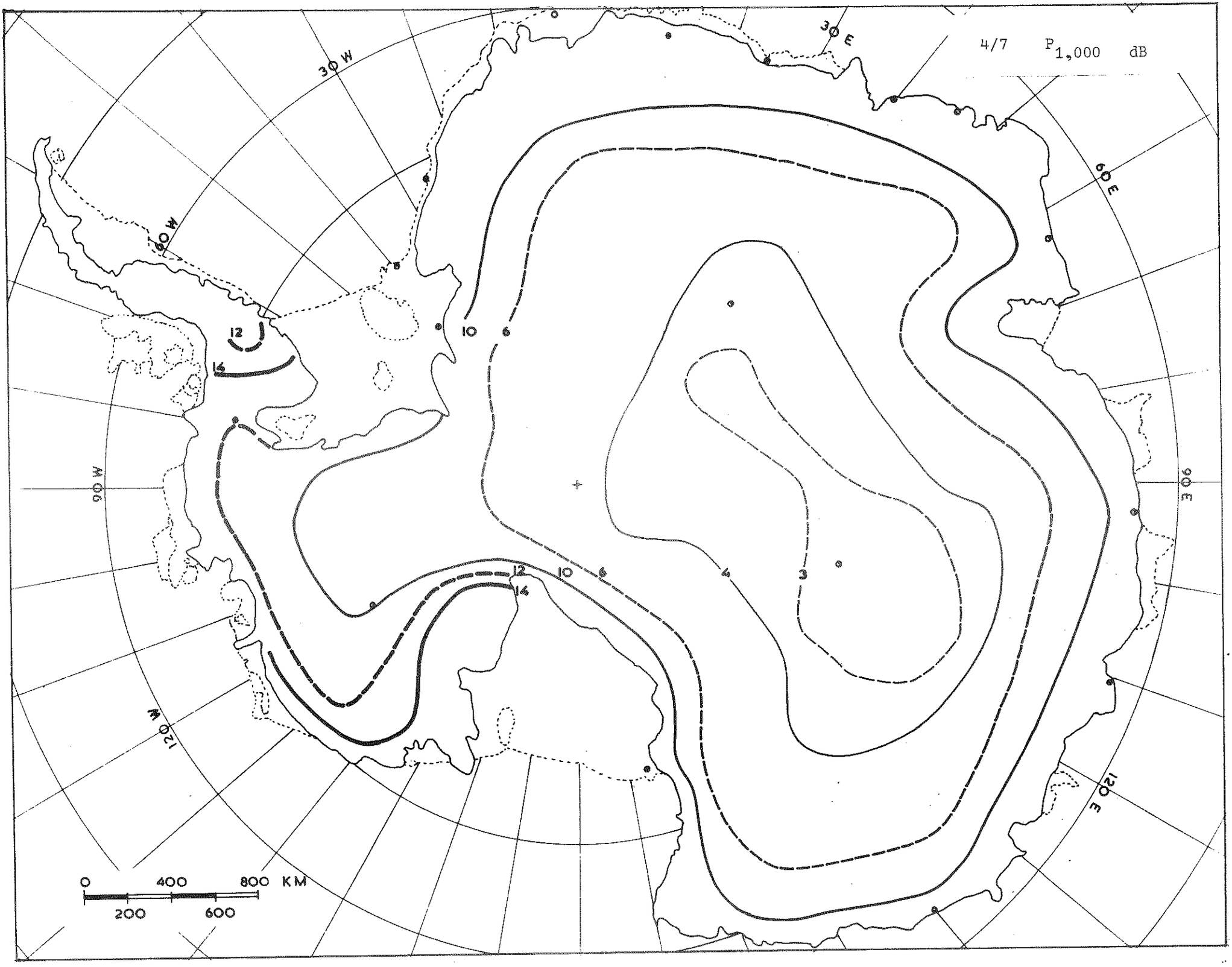
4/7 P 1,000 dB
30 W
30 E
60 W
60 E
90 W
90 E
120 W
120 E
16
14
12
10
6
4
3
0 400 800 KM
200 600

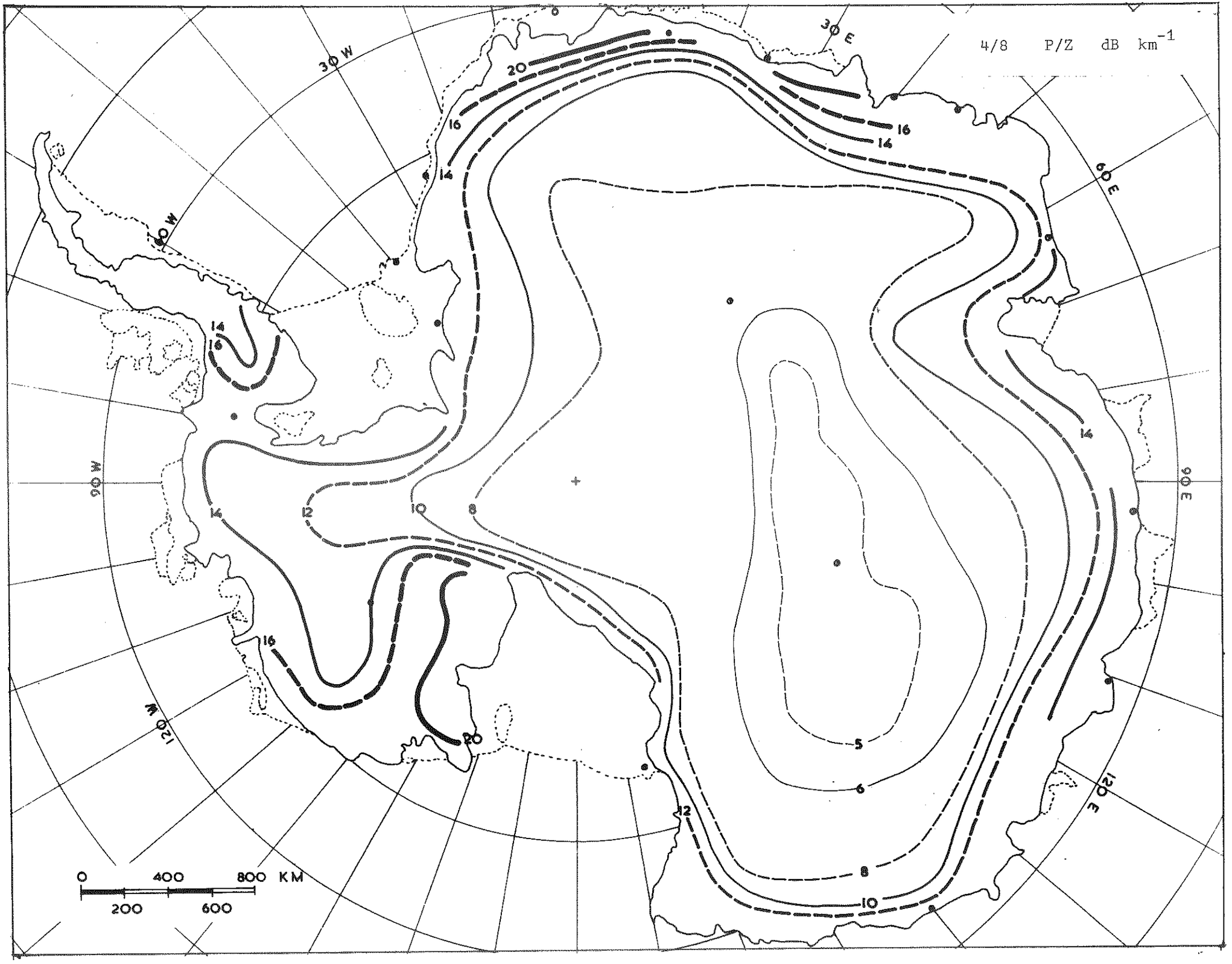
4/8 P/Z dB km^{-1}
30 W
30 E
60 W
60 E
90 W
90 E
120 W
120 E
0 400 800 KM
200 600

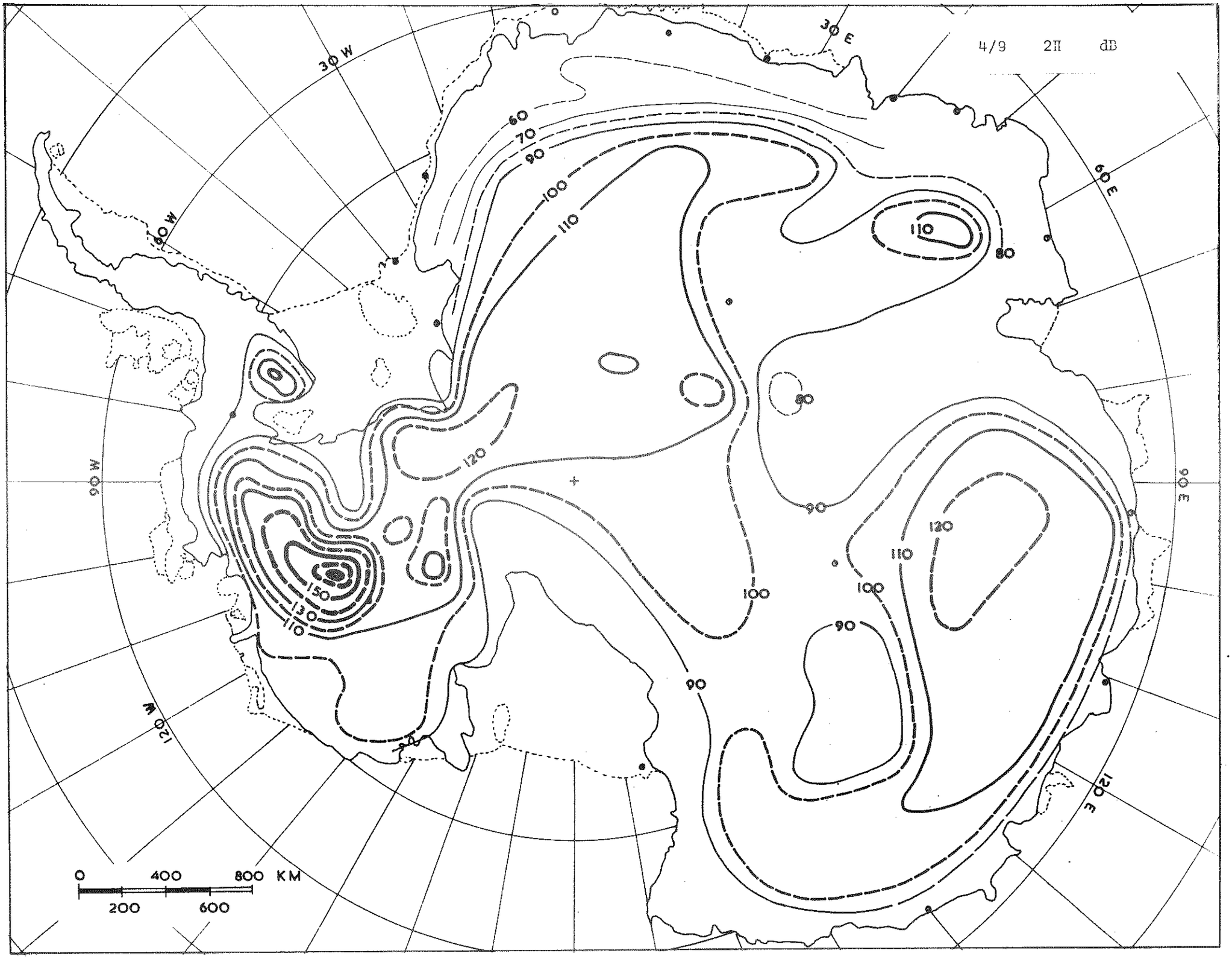
4/9 2Π dB
30 W
30 E
60 W
60 E
90 W
90 E
120 W
120 E
60
70
90
100
110
120
130
150
0 400 800 KM
200 600

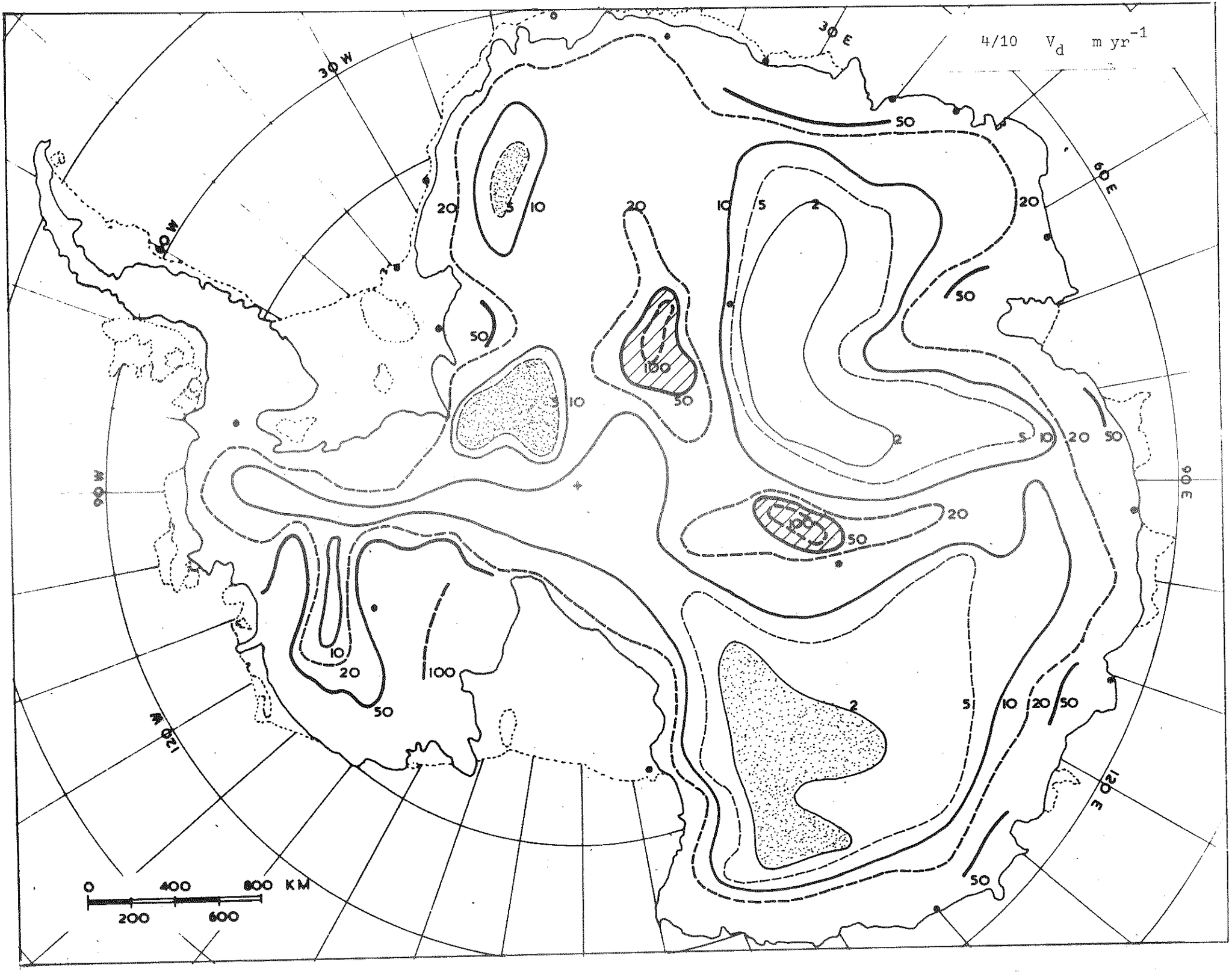
4/10 V_d m yr^{-1}
30 W
30 E
60 W
60 E
90 W
90 E
120 W
120 E
0 400 800 KM
200 600

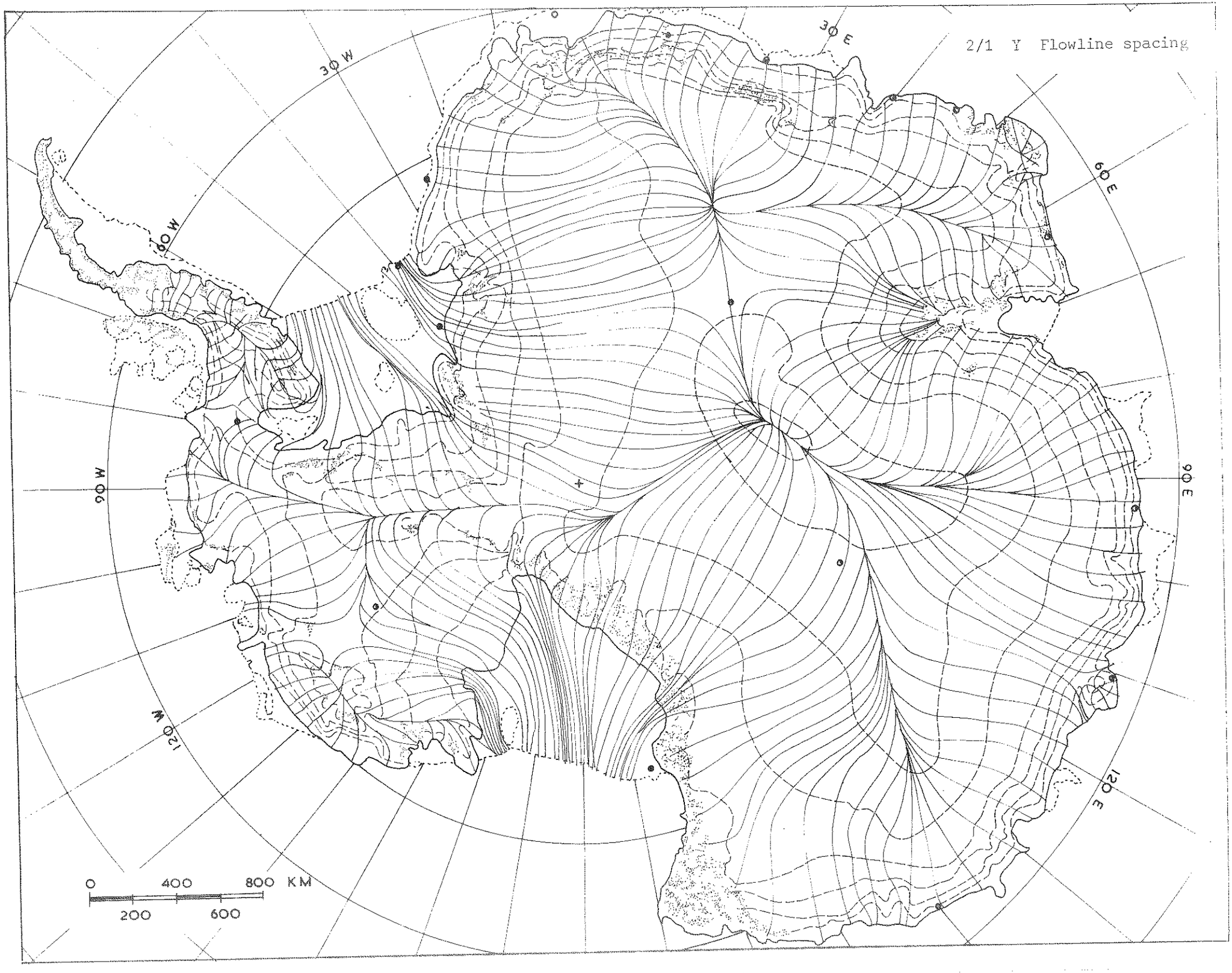
2/1 Y Flowline spacing
0
30 W
30 E
60 W
60 E
90 W
90 E
120 W
120 E
0 400 800 KM
200 600

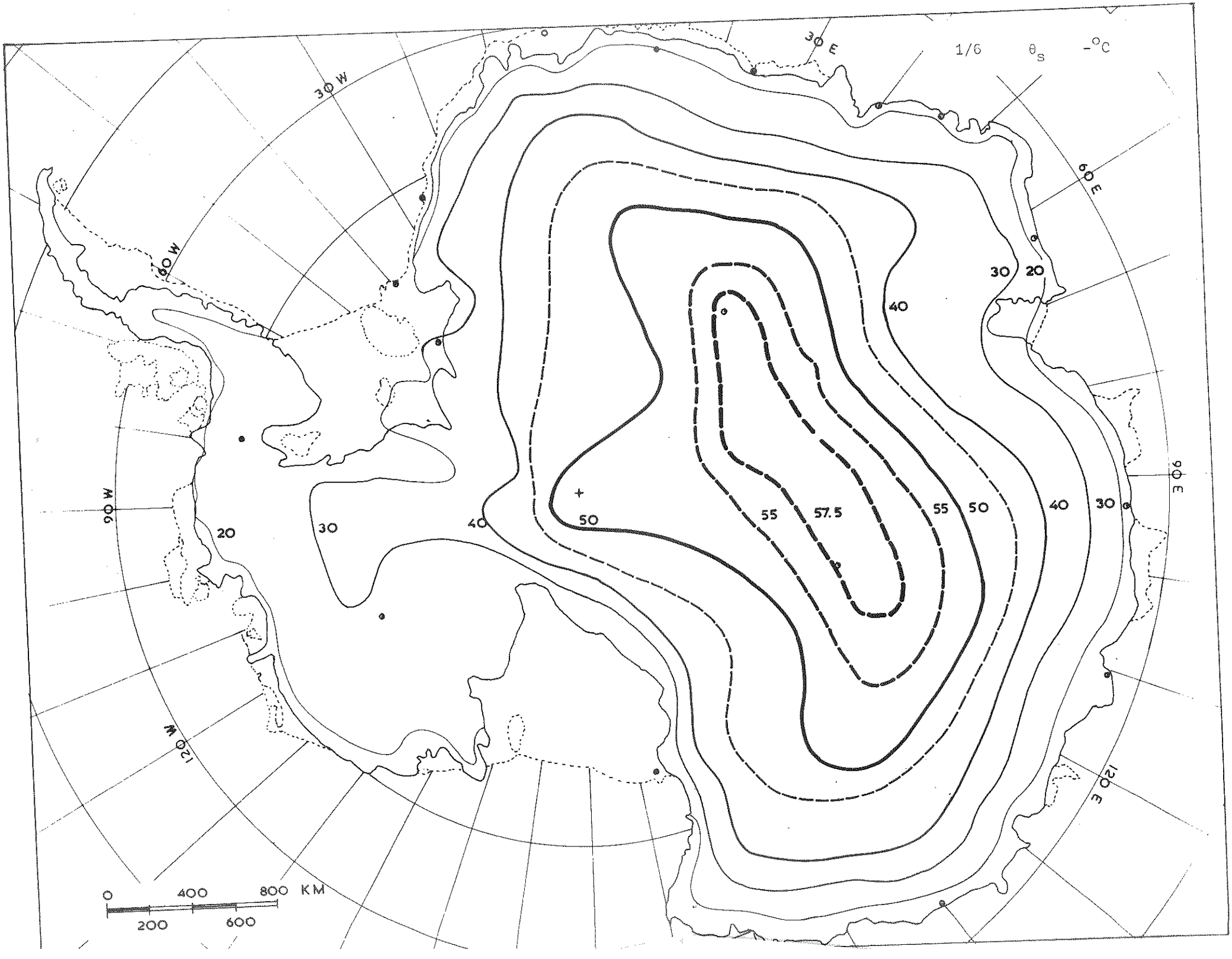
1/6 θs -°C
30 E
60 E
90 E
120 E
150 E
30 W
60 W
90 W
120 W
150 W
20
30
40
50
55
57.5
55
50
40
30
20
0 400 800 KM
200 600